JSCSEN 78(8)1079–1268(2013)

ISSN 1820-7421(Online)

Journal of the Serbian Chemical Society

Electronic Version

VOLUME 78

No 8

BELGRADE 2013

Available on line at

www.shd.org.rs/JSCS/

Journal of the Serbian Chemical Society
JSCS-info@shd.org.rs • www.shd.org.rs/JSCS

J. Serb. Chem. Soc. Vol. 78, No. 8 (2013)

CONTENTS

Published by the Serbian Chemical Society
Karnegijeva 4/III, 11000 Belgrade, Serbia
Printed by the Faculty of Technology and Metallurgy
Karnegijeva 4, P.O. Box 35-03, 11120 Belgrade, Serbia

Journal of the Serbian Chemical Society
JSCS-info@shd.org.rs • www.shd.org.rs/JSCS
J. Serb. Chem. Soc. 78 (8) 1079–1117 (2013) UDC 536.7+53+512.62:541.135.1+54–145.2
JSCS–4482 *Authors' review*

AUTHORS' REVIEW

Prediction of thermophysical and transport properties of ternary organic non-electrolyte systems including water by polynomials

BOJAN D. DJORDJEVIĆ∗#, MIRJANA Lj. KIJEVČANIN#, IVONA R. RADOVIĆ#, SLOBODAN P. ŠERBANOVIĆ# and ALEKSANDAR Ž. TASIĆ

Faculty of Technology and Metallurgy, University of Belgrade, Karnegijeva 4, P. O. Box 35-03, 11120 Belgrade, Serbia

(Received 30 January, revised 4 March 2013)

Abstract: The description and prediction of thermophysical and transport properties of ternary organic non-electrolyte systems including water by polynomial equations are reviewed. Empirical equations of Radojković *et al.* (also known as Redlich–Kister), Kohler, Jacob–Fitzner, Colinet, Tsao–Smith, Toop, Scatchard *et al.* and Rastogi *et al.* are compared with experimental data of available papers that appeared in well know international journals (Fluid Phase Equilibria, Journal of Chemical and Engineering Data, Journal of Chemical Thermodynamics, Journal of Solution Chemistry, Journal of the Serbian Chemical Society, The Canadian Journal of Chemical Engineering, Journal of Molecular Liquids, Thermochimica Acta, *etc*.). The applicability of empirical models to estimate excess molar volumes, V^{E}, excess viscosities, $\Delta\eta$, excess free energies of activation of viscous flow, $\Delta G^{*\mathrm{E}}$, molar refraction changes on mixing, ΔR, changes in the refractive indices on mixing, Δn_{D}, changes of isentropic compressibility, $\Delta\kappa_{\mathrm{s}}$, surface tension deviations, $\Delta\sigma$, speed of sound deviations, Δu, relative permittivity deviations, $\sigma\varepsilon_{\mathrm{r}}$, were checked on the series of ternary mixtures of very complex structure, which is described very shortly. The obtained results of prediction are discussed and some recommendations about the use of symmetric or asymmetric models to the possible application to mixtures are made.

Keywords: prediction; thermophysical properties; transport properties; polynomials; ternary non-electrolyte systems.

CONTENTS

∗Corresponding author. E-mail: bojan@tmf.bg.ac.rs
Serbian Chemical Society member.
doi: 10.2298/JSC130130029D

1. INTRODUCTION

Reliable thermophysical (the term thermodynamic has also been frequently used, especially when enthalpy and phase equilibria were included in the work) and transport properties of binary, ternary and multi-component systems are of primary interest for synthesis, design and process optimization in chemical, petrochemical and other industries. These properties are important not only for a fundamental understanding of mixing processes, but also in many practical problems concerning fluid phase equilibria, excess functions of solutions, fluid flow, *etc*.

The cost of the various process plants could be much higher if the thermochemical and thermophysical data are unreliable, or thermodynamic methods and models for process simulations are inadequate.

Thermophysical and transport properties can be successfully studied using experimental procedures, macroscopic correlations and predictions, molecular theories or computer simulation. However, no general theory has appeared that could adequately describe the composition dependence of the excess and other properties of liquid mixtures. Therefore, these functional forms are frequently presented by various empirical equations.

Experimental measurements of thermophysical properties of binary systems have been performed extensively in the past, and the obtained data and the parameters of the corresponding models are systematized in various Data Banks, but the experimental data for ternary systems are often scarce and could not be adequate. Moreover, these experimental procedures even with modern instrumentation are frequently very complicated and tend to be expensive and time-consuming.

The design of chemical plants requires very accurate data of the considered properties and reliable correlating models or, in the absence of experimental data, accurate predictive methods are necessary. These methods are the most attractive and powerful approaches among the theoretical methods because they are simple and effective and only require binary information that is relatively easy to obtain. On the other hand, experimental data could be applied to verify experimental equations. In addition, it is important to emphasize that accurate prediction of ternary mixtures containing associating and hydrogen-bonding components is traditionally a difficult thermodynamic problem.

This is one of the main reasons for the primary goals of research and the considerable efforts of researchers and process engineers devoted to the development and improvement of traditional models for correlation and prediction of properties for complex mixtures.

This brief review of several polynomial equations can do no more than summarize some recent activities in the prediction of thermodynamic and transport properties of complex ternary systems, using empirical models that are widely employed today as appeared in well known international journals. This text could be treated as continuation of the V^E predictions performed in the work of McCargar and Acree[1] and an extension to other thermodynamic and transport properties, except the prediction of ternary excess enthalpy data reviewed in an article of Prado *et al*.[2]

2. THERMOPHYSICAL AND TRANSPORT PROPERTIES

In order to estimate the utility of empirical equations to describe thermodynamic and transport behaviour of the ternary systems, the excess, changes of mixing, deviation and other properties can be used. Here, these properties are signed as in original papers, bearing in the mind that frequently for the same property different authors use different names.

Excess molar volume. The excess molar volumes V^E are computed using the equation:

$$V^E = \sum_{i=1}^{n} x_i M_i \left[(1/\rho) - (1/\rho_i) \right] = V - \sum_{i=1}^{n} x_i M_i / \rho_i \quad (1)$$

where ρ_i is the density of a pure component and ρ is the density of a mixture. V is a mixture molar volume, while x_i and M_i are the molar fraction and molar mass of component i. n is the number of components in a mixture.

Excess viscosity. The excess viscosities (or viscosity deviations $\Delta\eta$) are evaluated using the expression:

$$\Delta\eta = \eta - \sum_{i=1}^{n} x_i \eta_i \quad (2)$$

where η_i is the pure component dynamic viscosity and η is the dynamic viscosity of the mixture.

Excess free energies of activation of viscous flow. The excess free energies of activation of viscous flow ΔG^{*E} are obtained from the equation:

$$\Delta G^{*E} = RT \left[\ln(\eta V) - \sum_{i=1}^{n} x_i \ln(\eta_i V_i) \right] \quad (3)$$

where R is the universal gas constant, T is the absolute temperature; V and V_i are the molar volumes of a mixture and a component i, respectively.

Molar refraction changes of mixing. The molar refraction changes of mixing ΔR (molar refractivity deviations) are obtained from:

$$\Delta R = R - \sum_{i=1}^{n} x_i R_i = \frac{n_D^2 - 1}{n_D^2 + 2} V - \sum_{i=1}^{n} x_i R_i \quad (4)$$

where R and R_i are molar refractions (molar refractivities) of a mixture and a pure component i, respectively, while n_D is the refractive index of the mixture. ΔR can also be calculated using the volume fraction of component i, ϕ_i:

$$\Delta R = R_m - \sum_{i=1}^{n} \phi_i R_i \quad (5)$$

where

$$R_m = \left(\frac{n_D^2 - 1}{n_D^2 + 1} \right) \left(\frac{\sum_{i=1}^{n} x_i M_i}{\rho_m} \right) \quad (6)$$

$$R_i = \left(\frac{n_{Di}^2 - 1}{n_{Di}^2 + 1} \right) \left(\frac{M_i}{\rho_i} \right) \quad (7)$$

and

$$\phi_i = \frac{x_i V_i}{\sum_{i=1}^{n} x_i V_i} \quad (8)$$

Changes in the refractive indices on mixing. The changes in the refractive indices on mixing, Δn_D, were computed using the equation:

$$\Delta n_D = n_D - \sum_{i=1}^{n} x_i n_{Di} \quad (9)$$

where n_{Di} is a refractive index of the component i, and n_D is the refractive index of a mixture.

Changes of isentropic compressibilities. The changes of isentropic compressibility (excess isentropic compressibility, κ_s^E, or isentropic compressibility changes of mixing) $\Delta\kappa_s$ were calculated by means of the expression:

$$\Delta\kappa_s = \kappa_s - \kappa_s^{id} = \left(\rho u^2 \right)^{-1} - \kappa_s^{id} \quad (10)$$

where κ_s is the isentropic compressibility (determined by means of the Laplace Equation $\kappa_s = \rho^{-1}u^{-2}$) and u is the speed of sound of a mixture, while κ_s^{id} is the isentropic compressibility of an ideal mixture.

Surface tension deviations. The surface tension deviations, $\Delta\sigma$, are computed using the equation:

$$\Delta\sigma = \sigma - \sum_{i=1}^{n} x_i \sigma_i \tag{11}$$

where σ and σ_i are the surface tensions of a mixture and of component i, respectively.

Speed of sound deviations. The speed of sound deviations, Δu, with respect to the ideal behaviour of a mixture are represented using the equation:

$$\Delta u = u - u^{\mathrm{id}} = u - \sum_{i=1}^{n} x_i u_i \tag{12}$$

where u and u_i denote the speed of sound for a mixture and a pure component i, respectively.

The aforementioned properties of experimental data for binary and ternary mixtures incorporated in this study are given in the cited literature. The excess and derived functions of binary mixtures can be given by the Redlich–Kister Equation:[3]

$$Q_{ij} = x_i x_j \sum_{p=0}^{k} A_p (2x_{\mathrm{i}} - 1)^p \tag{13}$$

where Q_{ij} represents any of the aforementioned properties; x_i and x_j are the mole fractions of component i and j, respectively, and A_p denotes the polynomial coefficients.

3. PREDICTING EMPIRICAL MODELS

Although it would be possible to evaluate the thermodynamic and transport properties of ternary and multi-component systems from the properties of their pure components, in many cases in practice such calculations could be very inaccurate due to the complex structure of a non-ideal mixture, which is a consequence of the effects of mixing. A successful approach that limits experimental measurements to binary mixtures is to estimate the properties of multi-component systems using only the corresponding properties of the constituent binary systems. The most essential step seems to be that the data reflecting ternary interactions are very weak. It is clear that in this way enormous experimental effort required for ternary data could be saved.

All models could be regarded as physical or/and mathematical models.[4] A physical model describes information gathered by experiments connected to phenomena which occurs in the chemical and related properties. A mathematical

model is based on parameters generated from experimental data or by examination of a physical model.

The herein considered models treated as physical are transformed to mathematical ones in the form of polynomials. These polynomials can then be applied for predictions. The parameters of these models can be generated using experimental data of the corresponding properties obtained from the physical model. It is important to test the quality of predictions performed with data already available or obtained by new measurements. To solve practical problems, it is almost always necessary to develop corresponding computer programs based on knowledge of thermodynamic and transport properties and models relevant for wide complex mixtures of molecular variety.

No general theory exists that would enable the composition dependence of the various properties of liquid mixtures to be adequately presented. In addition to the work of McCargar and Acree,[1] various empirical methods for the prediction of the properties of ternary systems are reviewed in the work of Hillert[4] as analytical numerical and asymmetric methods, including the polynomials treated in the present review.

During the last few decades, several different empirical equations and polynomials have been developed in order to describe the thermodynamic and transport properties of binary and multi-component systems. Most of them, even the very old, are still popular and suitable for the correlation of most binary mixtures. When their parameters evaluated only from binary mixtures are used to predict ternary or multi-component data, the obtained data are not always satisfactory and comparison must be performed to ascertain which polynomials could be recommended to predict ternary data. Some of the polynomials were originally proposed to predict specific properties; however, they should be applicable to any other property included in the consideration.

Frequently used expressions for empirical models are applied here as follows:

I) The Radojković *et al.* model[5] presents an expression proposed by Redlich and Kister.[3] For a ternary system without ternary effects, the excess properties have the following form:

$$Q_{123} = Q_{12} + Q_{13} + Q_{23} \tag{14}$$

where the binary contributions Q_{12}, Q_{13} and Q_{23} are determined directly with Eqs. (1)–(5) and (9)–(12) using the ternary mole fractions x_1, x_2 and x_3 and the coefficients of corresponding binary systems. Some authors introduce this equation as the Redlich–Kister model. This fact is indicated in the present text.

II) The Kohler model[6] aimed at predicting excess properties of ternary systems is given as:

$$Q_{123} = (x_1 + x_2)^2 Q_{12}(x_1^a, x_2^a) + (x_1 + x_3)^2 Q_{13}(x_1^a, x_3^a) + \\ + (x_2 + x_3)^2 Q_{23}(x_2^a, x_3^a) \quad (15)$$

In this equation Q_{ij} refers to a corresponding property Q calculated by x_i^a and x_j^a in the binary mixtures using the following equation:

$$x_i^a = 1 - x_j^a = x_i / (x_i + x_j)$$

III) The Jacob–Fitzner model[7] for expressing the excess properties of ternary systems takes the form:

$$Q_{123} = \frac{x_1 x_2}{\left(x_1 + \frac{x_3}{2}\right)\left(x_2 + \frac{x_3}{2}\right)} Q_{12}\left(x_1^b, x_2^b\right) + \\ + \frac{x_1 x_3}{\left(x_1 + \frac{x_2}{2}\right)\left(x_3 + \frac{x_2}{2}\right)} Q_{12}\left(x_1^b, x_3^b\right) + \\ + \frac{x_2 x_3}{\left(x_2 + \frac{x_1}{2}\right)\left(x_3 + \frac{x_1}{2}\right)} Q_{23}\left(x_2^b, x_3^b\right) \quad (16)$$

where each binary contribution is evaluated at molar fractions calculated by:

$$x_i^b = 1 - x_j^b = (1 + x_i - x_j)/2$$

IV) The Colinet model[8] can be used for ternary system with six different binary compositions and has the following form:

$$Q_{123} = 0.5\{[x_2/(1-x_1)]Q(x_1, 1-x_1) + [x_1/(1-x_2)]Q(1-x_2, x_2) + \\ + [x_3/(1-x_1)]Q(x_1, 1-x_1) + [x_1/(1-x_3)]Q(1-x_3, x_3) + \\ + [x_3/(1-x_2)]Q(x_2, 1-x_2) + [x_2/(1-x_3)]Q(1-x_3, x_3)\} \quad (17)$$

Equations (14)–(17) are symmetrical in which the three binary mixtures are treated identically.

V) The Tsao–Smith model[9] for ternary system is expressed as:

$$Q_{123} = [x_2/(1-x_1)]Q_{12}(x_1^c, x_2^c) + [x_3/(1-x_1)]Q_{13}(x_1^c, x_3^c) + \\ + (1-x_1)Q_{23}(x_2^c, x_3^c) \quad (18)$$

Bearing in mind that this model is asymmetric, binary contributions are alternatively evaluated in following way:

a) $x_i^c = x_1$ and $x_j^c = 1 - x_i^c$ for binaries 1–2 and 1–3, and $x_2^c = 1 - x_3^c = x_2 / (x_2 + x_3)$ for binary 2–3,

b) $x_i^c = x_2$ and $x_j^c = 1 - x_i^c$ for binaries 2–1 and 2–3, and $x_1^c = 1 - x_3^c = x_1 / (x_1 + x_3)$ for binary 1–3,

c) $x_i^c = x_3$ and $x_j^c = 1 - x_i^c$ for binaries 3–1 and 3–2, and $x_1^c = 1 - x_2^c = x_1 / (x_1 + x_2)$ for binary 1–2.

VI) Toop[10] proposed an equation in the following form:

$$Q_{123} = \left[x_2 / (1 - x_1)\right] Q_{12}(x_1^c, x_2^c) + \left[x_3 / (1 - x_1)\right] Q_{13}(x_1^c, x_3^c) + (1 - x_1)^2 Q_{23}(x_2^c, x_3^c) \quad (19)$$

where binary mole fractions x_i are computed as in the Tsao–Smith model (Eq. (18)). Pelton[11] discussed several models including the Kohler model as a symmetric and the Toop model as an asymmetric model.

VII) The Scatchard *et al.* model[12] is defined by the following expression:

$$Q_{123} = \left[x_2 / (1 - x_1)\right] Q_{12}(x_1^c, x_2^c) + \left[x_3 / (1 - x_1)\right] Q_{13}(x_1^c, x_3^c) + Q_{23}(x_2, x_3) \quad (20)$$

where x_i^c and x_j^c are computed as in the case of the Tsao–Smith model (Eq. (18)). This model presents a modification of Eq. (14) for ternary mixture of polar + two non-polar liquids.

VIII) The Rastogi *et al.* model[13] is expressed as:

$$Q_{123} = 0.5[(x_1 + x_2) Q_{12}(x_1^a, x_2^a) + (x_1 + x_3) Q_{13}(x_1^a, x_3^a) + (x_2 + x_3) Q_{23}(x_2^a, x_3^a)] \quad (21)$$

where each binary contribution are evaluated at molar fractions calculated by:

$$x_i^a = 1 - x_j^a = x_i / (x_i + x_j)$$

In some examined articles, other polynomials such as Lark *et al.*,[14] Hillert,[15] Muggianu *et al.*,[16] Knobeloch–Schwartz,[17] Acree *et al.*,[18] Mathieson–Thynne,[19] *etc.*, were also used, but will not be considered herein. Some authors[20–22] divided polynomials into geometrical models and empirical methods. Some of them extended to calculate physicochemical properties of quaternary systems.[20,21] Polynomials are also used for the calculation other thermodynamic properties, such as for example, vapour–liquid and liquid–liquid equilibria.[23,24] On the other hand, more current empirical models were applied to predict ternary properties of alloys, as can be seen in the literature.[25–31] In addition, it is important to emphasize that alternative forms of the empirical equations given in articles of Atik and Lourdani[32,33] could be used.

Quality of the predictions for particular property was estimated by:

Standard deviation:

$$SD = \left(\sum_{i=1}^{N} \left(Q_{123,i}(\text{exp}) - Q_{123,i}(\text{cal}) \right)^2 \Big/ \left(N - p \right) \right)^{1/2} \quad (22)$$

where N is the number of experimental data and p is the number of parameters of a model.

Root-mean-square-deviation:

$$RMSD = \left(\sum_{i=1}^{N} \left(Q_{123,i}(\text{exp}) - Q_{123,i}(\text{cal}) \right)^2 \Big/ N \right)^{1/2} \quad (23)$$

Average absolute deviation:

$$AAD\ (\%) = \frac{100}{N} \sum_{i=1}^{N} \frac{\left| Q_{123}(\text{exp}) - Q_{123}(\text{cal}) \right|_i}{Q_{123,i}(\text{exp})} \quad (24)$$

4. PREDICTIONS

Alcohol + alcohol + ether ternary systems. Arce *et al.*[34–39] studied excess molar volumes, V^E, isentropic compressibility changes of mixing, $\Delta\kappa_s$, and molar refraction changes of mixing, ΔR. The ternary systems were composed from alcohols: methanol, ethanol and 1-butanol and ethers: 2-methoxy-2-methylpropane (MTBE), 2-methoxy-2-methylbutane (TAME) and 2-ethoxy-2-methylpropane (ETBE).

The ternary systems consisted of TAME or MTBE or ETBE as one of the components and two alcohols: *i*) ethanol + methanol,[34,35] *ii*) 1-butanol + methanol[36,37] and *iii*) 1-butanol + ethanol.[38,39]

The V^E, ΔR and $\Delta\kappa_s$ values for the investigated mixtures were determined from experimental data of densities, refractive indices and speeds of sound at 298.15 K and atmospheric pressure.

All ternary systems exhibited negative values of V^E, while the binary systems containing alcohols showed positive but small values of V^E. These negative V^E data are a consequence of the open-chain molecules with flexible orientation order that increases with increasing chain length of the alkyl group. It is clear that the tendency of interstitial accommodation of alcohols into the ethers leads to negative values of V^E. Properties V^E, ΔR and $\Delta\kappa_s$ were calculated using Eqs. (1), (4) and (10), respectively. The excess molar volumes V^E for the system ethanol + + methanol + TAME[35] had negative values. The minimum values of V^E, around –0.46 $cm^3\ mol^{-1}$ were, also, present at around equimolar mixtures with ether and methanol. The deviations in the molar refractions and in the isentropic compressibility were also negative with minimum values of –0.020 and –24, respectively.

As can be seen from Table I the best prediction of V^E for this ternary system was achieved by the polynomial of Radojković *et al*. Adequate predictions of ΔR were provided with the equations of Radojković *et al*., Jacob–Fitzner and Toop. Radojković *et al*. and Jacob–Fitzner also gave the best predictions of $\Delta\kappa_s$, while the equations of Kohler and of Toop equations functioned somewhat worse. The remaining equations (Colinet, Tsao–Smith, Scatchard *et al*. and Rastogi *et al*.) were unsuitable for the prediction of the $\Delta\kappa_s$ values. It could be concluded that the Scatchard *et al.* and Colinet and Rastogi *et al.* equations were particularly inappropriate for the prediction of V^E, ΔR and $\Delta\kappa_s$ for this ternary system.

TABLE I. The values of standard deviation, *SD*, of V^E / cm^3 mol^{-1}, $\Delta\kappa_s$ / T Pa^{-1} and ΔR / cm^3 mol^{-1} predicted for the ternary systems ethanol + methanol + MTBE, or + TAME or + ETBE at 298.15 K

Model	Property	MTBE[a]	TAME[a]	ETBE[b]
Radojković *et al.*	V^E	0.061	0.009	0.021
	$\Delta\kappa_s$	3	1	3
	ΔR	0.023	0.004	0.008
Rastogi *et al.*	V^E	0.148	0.102	0.210
	$\Delta\kappa_s$	13	5	13
	ΔR	0.024	0.047	0.013
Jacob–Fitzner	V^E	0.049	0.031	0.063
	$\Delta\kappa_s$	2	1	2
	ΔR	0.023	0.004	0.010
Colinet	V^E	0.246	0.177	0.300
	$\Delta\kappa_s$	19	9	17
	ΔR	0.009	0.09	0.018
Toop	V^E	0.029	0.033	0.043[c], 0.047[d], 0.104[e]
	$\Delta\kappa_s$	8	4	9 9 6
	ΔR	0.021	0.004	0.009 0.01 0.006
Kohler	V^E	0.017	0.01	0.023
	$\Delta\kappa_s$	5	3	6
	ΔR	0.022	0.012	0.009
Tsao–Smith	V^E	0.078	0.070	0.092[c], 14[d], 0.007[e]
	$\Delta\kappa_s$	13	6	0.099 13 0.007
	ΔR	0.020	0.015	0.10 6 0.007
Scatchard *et al.*	V^E	0.203	0.170	0.234[c], 25, 0.010[e]
	$\Delta\kappa_s$	24	11	0.264 24 0.013
	ΔR	0.021	0.008	0.131 6 0.008

[a]Arce *et al.*[35]; [b]Arce *et al.*[34]; [c]ethanol was the asymmetric component; [d]methanol was the asymmetric component; [e]ETBE was the asymmetric component

For the system 1-butanol + methanol + TAME[36] (Table II) the minimal values of V^E, $\Delta\kappa_s$ and ΔR were some larger (V^E = –0.56 cm^3 mol^{-1}, $\Delta\kappa_s$ = –34 T Pa^{-1} and ΔR = –0.036 cm^3 mol^{-1}) than the respective values obtained for the system of TAME with ethanol and methanol. The results obtained by polynomials were slightly worse. These equations worked similarly as in the previous

case. The expression of Kohler as the most successful was followed by those of Radojkovic *et al*. and Jacob–Fitzner. The equations of Colinet, Rastogi *et al*. and Scatchard *et al*. produced higher deviations and could not be recommended. However, limitations were achieved by the equations of Toop and Tsao–Smith.

TABLE II. The values of the standard deviation, *SD*, of V^E / cm^3 mol^{-1}, $\Delta\kappa_s$ / T Pa^{-1}, ΔR / cm^3 mol^{-1} predicted for the ternary systems 1-butanol + methanol + MTBE or + TAME at 298.15 K

Model	Property	MTBE[a]			TAME[a]		
Radojković *et al.*	V^E	0.025			0.027		
	$\Delta\kappa_s$	2			1		
	ΔR	0.007			0.010		
Rastogi *et al.*	V^E	0.210			0.165		
	$\Delta\kappa_s$	19			10		
	ΔR	0.011			0.006		
Kohler	V^E	0.023			0.011		
	$\Delta\kappa_s$	3			2		
	ΔR	0.007			0.010		
Jacob–Fitzner	V^E	0.063			0.030		
	$\Delta\kappa_s$	5			2		
	ΔR	0.008			0.009		
Tsao–Smith	V^E	0.092[c]	0.099[d]	0.109[e]	0.063[c]	0.071[d]	0.087[f]
	$\Delta\kappa_s$	11	12	10	5	6	5
	ΔR	0.007	0.006	0.010	0.013	0.014	0.011
Colinet	V^E	0.299			0.231		
	$\Delta\kappa_s$	30			14		
	ΔR	0.013			0.013		
Toop	V^E	0.044 [c]	0.047 [d]	0.104 [e]	0.036[c]	0.037[d]	0.080[f]
	$\Delta\kappa_s$	8	7	10	3	4	5
	ΔR	0.007	0.006	0.010	0.011	0.011	0.011
Scatchard *et al.*	V^E	0.234[c]	0.264[d]	0.131[e]	0.164[c]	0.197[d]	0.111
	$\Delta\kappa_s$	24	21	12	10	10	7
	ΔR	0.011	0.009	0.010	0.017	0.021	0.011

[a]Arce *et al.*[37]; [b]Arce *et al.*[36]; [c]1-butanol was the asymmetric component; [d]methanol was the asymmetric component; [e]MTBE was the asymmetric component; [f]TAME was the asymmetric component

The third ternary system relates to TAME and 1-butanol and ethanol as the two other components.[38] Minimal values of V^E, $\Delta\kappa_s$ and ΔR were similar to those of the two other ternary systems containing TAME (V^E = –0.525 cm^3 mol^{-1}; $\Delta\kappa_s$ = = –30 T Pa^{-1}; ΔR = –0.024 cm^3 mol^{-1}). The empirical equations of Radojković *et al*. and Kohler applied to predict V^E, $\Delta\kappa_s$ and ΔR were the best, followed by Jacob–Fitzner (especially adequate for $\Delta\kappa_s$) and Toop equations. The other equations gave evidently higher deviations.

The ternary system of MTBE with the alcohol components ethanol and methanol[35] (Table I) showed larger deviation from ideal behaviour (V^E = –0.623 cm^3 mol^{-1}) compared to the ternary systems with TAME (–0.455 cm^3 mol^{-1}).

The best prediction of V^E was obtained by the Kohler Equation. The Jacob–Fitzner and the Radojković *et al.* Equations achieved the best predictions of $\Delta\kappa_{s123}$, the Kohler and Toop model gave somewhat poorer results, while the remaining models were unsuitable for the prediction of $\Delta\kappa_s$ values. The models of Rastogi *et al*., Colinet and Scatchard *et al*. are not recommended for the prediction of V^E, $\Delta\kappa_s$ and ΔR for the ethanol + methanol + MTBE system.

The ternary system 1-butanol + methanol + MTBE[37] (Table II) exhibited larger negative values of V^E = –0.735 cm^3 mol^{-1}, $\Delta\kappa_s$ = –68 T Pa^{-1} and ΔR = –0.0376 cm^3 mol^{-1}. The models of Radojković *et al*. and Kohler, followed by the model of Jacob–Fitzner were the most suitable for the prediction of V^E, $\Delta\kappa_s$ and ΔR. Limitations were found when the models of Toop and Tsao–Smith were used. The models of Colinet, Rastogi *et al.* and Scatchard *et al.* produced high deviations and are not recommended.

The same properties V^E, $\Delta\kappa_s$ and ΔR were predicted for the system ethanol + methanol + ETBE[34] (Table I), which also exhibited high non-ideal behaviour with minimal experimental values: V^E = –0.8618 cm^3 mol^{-1}, $\Delta\kappa_s$ = –54 T Pa^{-1} and ΔR = –0.0457 cm^3 mol^{-1}. The best predictions of V^E were obtained using the models of Radojković *et al.* and Kohler. The prediction of the Rastogi *et al.*, Scatchard *et al*. and Colinet models for V^E erred significantly. For $\Delta\kappa_s$, the best predictions were obtained by Radojković *et al.* and Jacob–Fitzner followed by the Kohler model. For the prediction of ΔR, most of the models had similar deviations, although the models of Rastogi *et al.*, Scatchard *et al*. and Colinet were again less successful overall.

In conclusion, it is clear that for all the alcohol + alcohol + ether systems studied by Arce *et al*. the models of Radojković *et al*. and Kohler appear to be valid and could be successfully applied for the prediction of this type of ternary systems.

Alcohol + alcohol + cyclic ether ternary systems. Camacho *et al*.[40] investigated the excess molar volumes and excess refractive indices (changes in the refractive indices on mixing) of the *n*-octanol + 1,4-dioxane + 2-butanol system at 298.15 K and atmospheric pressure.

Systems of alcohols and cyclic components are of interest because of their importance for detecting which molecular and structural effects dominate in liquid mixtures. 1,4-Dioxane with two alcohols exhibited relatively large positive values of V^E with a maximum positive experimental value $V^E = 0.675\times10^{-6}$ m^3 mol^{-1}. It is known that alcohols are self-associated substances and that the addition of another compound results in the rupture of hydrogen bonds and an expansion in volume. Also, differences in the sizes of the molecules present lead to interstitial accommodation of molecules and therefore to a negative contribution in V^E. However, this effect is considerably weaker. The difference in free volume between 1,4-dioxane and alcohols also exists. Bearing in mind that excess refrac-

tive indices for the mixtures of alcohols are positive and negative for two binary systems with 1,4-dioxane, the changes in the refractive indices of the ternary system Δn_{D123} are partially negative in accordance with the data of binary mixtures.

Radojković *et al*., Jacob–Fitzner and Tsao–Smith (with 1,4-dioxane as an asymmetric component, option c of Eq. (18)) gave very satisfactory results in the prediction of V^E and Δn_{D123}.

Alcohol + haloalkane + cyclic ether ternary systems. Postigo *et al*.[41] calculated excess molar volume, V^E, viscosity deviations, $\Delta\eta$, and excess free energies of activation of viscous flow, ΔG^{*E} for the ternary system tetrahydrofuran + + 1-chlorobutane + 1-butanol at 283.15, 298.15 and 313.15 K and atmospheric pressure. The ternary V^E data were small, showing both negative and positive values and changing slightly with temperature change. $\Delta\eta$ and ΔG^{*E} were negative at all investigated temperatures. Some effects that influenced these changes include: *i*) the breaking of hydrogen bonding of alcohols, *ii*) the breaking of dipole–dipole specific interactions of the halogenated compound and *iii*) OH–Cl interactions.

Predictions were performed by equations of Radojkovic *et al*., Jacob–Fitzner, Kohler, Tsao–Smith and Rastogi *et al*. The best results were obtained by the Radojković *et al*., Jacob–Fitzner and Kohler Equations at the three investigated temperatures.

In the paper of Mariano and Postigo,[42] V^E, $\Delta\eta$ and ΔG^{*E} were also calculated by empirical equations for ternary system where the alcohol component 1-butanol was exchanged with 2-butanol under the same temperature and pressure conditions as in the previous case. The values of V^E were positive over the entire composition range and increased slightly with increasing temperature. The values of $\Delta\eta$ and ΔG^{*E} were negative at the three considered temperatures. The increase in temperature considerably changed $\Delta\eta$ while ΔG^{*E} was hardly modified.

The positive V^E values showed that effect (i) was dominant.[41] Namely, breakage of the self-associated 2-butanol molecules influences the final V^E values. This effect differs from the effect present in the previous system tetrahydrofuran + + 1-chlorobutane + 1-butanol where the V^E values were negative in the majority of the composition range for all the investigated temperatures. Negative values of $\Delta\eta$ and ΔG^{*E} are in accordance with (*ii*) and (*iii*), as for the previously investigated system (tetrahydrofuran + 1-chlorobutane + 1-butanol)[38] but higher values are a consequence of the presence of the secondary alcohol (2-butanol) in the ternary system,[42] which reduces the OH–Cl interactions.

The best predictions of the ternary V^E, $\Delta\eta$ and ΔG^{*E} values are given by the model of Jacob–Fitzner, followed by those of Radojković *et al*. and Kohler, which are also adequate for the predictions of these properties. The asymmetric

model of Tsao–Smith and symmetric Rastogi *et al*. model produce very high average absolute deviations, and they cannot be recommended for this system.

Alcohol + amine + hydrocarbon ternary systems. Mixtures of alcohols and amines make highly non-ideal systems having large negative excess properties as a consequence of strong cross-association through complex formation by hydrogen bonds. The third component can be a non-polar inert component which acts as order-breaking molecules when mixed with the associating components.

Gardas and Oswal[43,44] studied the volumetric and transport properties of the following ternary systems: *i*) 1-propanol + triethylamine + *cyclo*-hexane, *ii*) 1-propanol + tri-*n*-butylamine + *cyclo*-hexane, *iii*) 1-butanol + triethylamine + cyclohexane and *iv*) 1-pentanol + triethylamine + cyclohexane, at 303.15 K and atmospheric pressure over the whole range of compositions. The values of V^E could be interpreted by several effects: chemical, structural and physical. In the mixtures under investigation, the authors[43,44] explained the influence of the dominate factors on the results of the experimental measurements of the corresponding properties.

Comparison between the ternary systems (*i*) and (*ii*) with 1-propanol as the alcohol component showed that the V^E values are significantly more negative for system (*i*) (V^E = –1.383 cm^3 mol^{-1}) than system (*ii*) (V^E = –0.463 cm^3 mol^{-1}) indicating that cross-association is more pronounced in the mixture with triethylamine than in the mixture containing tri-*n*-butylamine. However, comparing the values of V^E for the ternaries of triethylamine with different alcohols: 1-propanol (*i*) (V^E = –1.383 cm^3 mol^{-1}), 1-butanol (*iii*) (V^E = –1.535 cm^3 mol^{-1}) and 1-pentanol (*iv*) (V^E = –1.567 cm^3 mol^{-1}), it could be concluded that the V^E values are not much affected by the change in the length of the alcohol from 1-propanol to 1-pentanol. The viscosity deviation, $\Delta\eta$, in these systems were the consequence of molecular interactions as well as of the size and shape of molecules. The ΔG^{*E} values were negative for the three systems containing triethylamine, while the values were both positive and negative for the system containing tri-*n*-butylamine. As pointed out by the authors, the dependence of ΔG^{*E} on composition is complex, depending upon different contributions in the mixture.

Bearing in mind the complex behaviour of the aforementioned systems, it is clear that prediction of V^E, $\Delta\eta$ and ΔG^{*E} by empirical equations was very difficult in all cases, as concluded by the authors. Namely, large standard deviations were obtained when the V^E, $\Delta\eta$ and ΔG^{*E} of viscous flow were predicted by the empirical equations of Kohler, Jacob–Fitzner, Tsao–Smith, Rastogi *et al*. and other applied models containing only binary parameters.

In the work of Kijevčanin *et al.*,[45] excess molar volumes V^E of the ternary system 1-butanol + cyclohexylamine + *n*-heptane were reported at temperatures from 283.15 to 323.15 K. The V^E values of this system are mostly negative

except for the region very close to the binary mixtures of *n*-heptane with 1-butanol or cyclohexylamine, where changes in the V^E values occurred.

In this system, which exhibited large negative values of V^E with a small influence of temperature, the complexes formed by H-bonding between 1-butanol and cyclohexylamine molecules dominate the behaviour.

Calculation of V^E performed by empirical models showed that satisfactory predictions were obtained by the symmetric equations of Radojković *et al*. and Jacob–Fitzner, whereas the most inadequate estimation by this type of model was with the equation of Rastogi *et al*. For all asymmetric models, better results were obtained with *n*-heptane as the asymmetric component (Toop and Scatchard *et al.*), especially with the Tsao–Smith model, while quite poor estimations were achieved when 1-butanol was the asymmetric component. When *cyclo*-hexylamine was used as the asymmetric component, some limitations were obtained in the case of the Tsao–Smith model. Increasing of the temperature had no influence on the predictions by the investigated polynomials.

Dominguez *et al*.[46] measured density of the ternary system 2-butanol + + *n*-hexane + 1-butylamine at 298.15 and 313.15 K. The V^E values were calculated by the Redlich–Kister and other empirical models given in Table II. The V^E values of this ternary system were characterized by (*i*) negative values in the region where interactions between the hydroxyl (–OH) and amino ($–NH_2$) groups dominated (small mole fraction of *n*-hexane), (*ii*) positive values in regions were the rupture of the associated structure of 2-butanol in the mixture with *n*-hexane occurred and (*iii*) when the mole fraction of *n*-hexane increased the brakeage of cross-hydrogen bonding ($OH–NH_2$), leading to positive values of V^E in the region of low fractions of the other two components. As the results of these facts, the V^E values were negative or positive in the corresponding regions of the triangular diagram. The ternary contribution ($V^E–V^E_{bin}$) was very high, conditioning higher standard deviations associated with all the considered empirical models. This means that for this ternary system, ternary contributions are important.

Amine/ester/alcohol/hydrocarbon ternary systems. Kwon *et al*.[47] predicted V^E and ΔR values of ternary mixtures of tridodecylamine (alamine 304-1) with 1-octanol, 2-octanol and 1-decanol at 298.15K using the Radojkivić *et al*. equation. Due to the lack of published ternary V^E and ΔR data, the authors estimated the ternary V^E and ΔR data using possible combinations of the correlated binary Redlich–Kister parameters of given sub-binary systems. The results were plotted as isoclines of V^E and ΔR of the ternary systems : Alamine 304-1 + 1-octanol + + 2-octanol, Alamine 304-1 + 1-octanol + 1-decanol, Alamine 304-1 + 2-octanol + 1-decanol and 1-octanol + 2-octanol + 1-decanol.

Different ternary mixtures formed from alcohols, esters and hydrocarbons have been considerably investigated. All the mentioned mixtures consisted of one

associating component (alcohol), a weakly associating polar component (alkyl alkanoate) and a non-polar inert compound (hydrocarbon).

Some studies[48–52] could be of interest in the context of the present paper, bearing in mind that empirical expressions that predict the ternary properties for binary data were applied. Oswal *et al.*[48] gave excess molar volumes, V^E, viscosity deviations, $\Delta\eta$, and excess free energies of activation of viscous flow ΔG^{*E} for two ternary systems: *i*) 1-propanol + ethyl ethanoate + cyclohexane and *ii*) 1-propanol + ethyl ethanoate + benzene. These properties were determined from density and viscosity measurements of ternaries and binaries at 303.15 K. Ghael *et al.*[49] calculated the same properties (V^E, $\Delta\eta$ and ΔG^{*E}) for the ternary systems of ethyl ethanoate + cyclohexane with higher alcohols as the third component (1-butanol or 1-pentanol or 1-octanol) at 303.15 K. The Equations of Redlich–Kister, Kohler, Rastogi *et al.*, Jacob–Fitzner and Tsao–Smith were applied in some studies.[48,49] Casas *et al.*[50,51] reported V^E, $\Delta\eta$ and Δn_D data for the ternary mixture propyl propanoate + 1-hexanol + benzene at 298.15 and 308.15 K. The prediction was performed by models of Jacob–Fitzner, Kohler, Colinet, Tsao–Smith, Toop and Scatchard *et al.*

Investigations of all the aforementioned systems were performed at atmospheric pressure over the whole composition range.

The values of V^E for all mixtures of 1-alcohols with ($C_4H_8O_2$ + *c*-C_6H_{12}) were large and positive.[48,49] For equimolar composition, the V^E values of the ternary systems C_3H_7OH + $C_4H_8O_2$ + *c*-C_6H_{12}, C_4H_9OH + $C_4H_8O_2$ + *c*-C_6H_{12} , C_5H_9OH + $C_4H_8O_2$ + c-C_6H_{12} and $C_8H_{17}OH$ + $C_4H_8O_2$ + *c*-C_6H_{12} were 0.854, 0.868, 0.832 and 0.812 cm^3 mol^{-1}, respectively. Trend of decreasing V^E values on addition of higher 1-alcohols to the pseudo-binary mixture ($C_4H_8O_2$ + *c*-C_6H_{12}) could be the consequence of specific interactions between the alcohol and alkanoate molecules and the dilution effect on the breakage of the dipolar-structure in the alkanoate.

V^E values were greatly reduced when cyclohexane replaced benzene.[48,50,51] This indicates that the specific interactions between pairs of molecules alcohol, ethanoate and benzene (beside the disruption of alcohol and ethanoate structures) are significant. Namely, the specific interactions of –n···HO–, –HO···π and/or –n···π types lead to decreases in V^E.

The negative values of $\Delta\eta$ are caused by the destruction of hydrogen bonds in 1-alcohols in mixtures with aromatics, decreasing $\Delta\eta$ when cyclohexane is replaced by benzene. Moreover, the $\Delta\eta$ values are negative in mixtures with heptane because dispersion forces are predominant.

The values of ΔG^{*E} are highly negative for both mixtures with *cyclo*-hexane and benzene and are in accordance with corresponding values and sign of V^E and $\Delta\eta$, which arise due to the structure breakage of both 1-alcohols and ethyl ethanoate molecules.

Changes in refractive indices on mixing, Δn_D, for the ternary mixture propyl propanoate + 1-hexanol + benzene were obtained using experimental values of refractive indices at 298.15 and 308.15 K and atmospheric pressure over the entire range of compositions. The values of Δn_D were negative in the whole region of the ternary mixture.

Polynomial examinations[48,49] of the results for the ternary systems 1-alcohols with ($C_4H_8O_2$ + *c*-C_6H_{12}) are given in Table III. It could be concluded that the Redlich–Kister model gave smaller values of *SD* in the prediction of V^E and $\Delta\eta$, while higher values of *SD* were obtained with the equations of Kohler, Rastogi *et al.*, Jacob–Fitzner and Tsao–Smith (Table III). The ternary mixture of 1-propanol with ($C_4H_8O_2$ + *c*-C_6H_{12}) gave higher values for the best *SD* = 0.040 of the Redlich–Kister model, bearing in mind the maximum value of V^E = 1.232 cm^3 mol^{-1} in accordance to corresponding value V^E = 0.249 cm^3 mol^{-1} for the ternary system 1-propanol + $C_4H_8O_2$ with benzene as the third component (*SD* = = 0.012).

TABLE III. The values of standard deviations *SD* of V^E / cm^3 mol^{-1}, $\Delta\eta$ / mPa s and ΔG^{*E} / J mol^{-1} calculated by polynomials for the ternary systems alcohols (A) + ethyl ethanoate (B) + cyclohexane (C) at 303.15 K

Model	Property	1-propanol (A)[a]	1-butanol (A)[b]	1-pentanol (A)[b]	1-octanol (A)[b]
Redlich–Kister	V^E	0.040	0.035	0.016	0.068
	$\Delta\eta$	0.041	0.012	0.033	0.073
	ΔG^{*E}	151	49	112	107
Kohler	V^E	0.055	0.048	0.028	0.068
	$\Delta\eta$	0.087	0.166	0.231	0.579
	ΔG^{*E}	133	178	257	336
Rastogi *et al.*	V^E	0.171	0.187	0.182	0.245
	$\Delta\eta$	0.147	0.206	0.261	0.731
	ΔG^{*E}	248	234	233	218
Jacob–Fitzner	V^E	0.053	0.046	0.026	0.066
	$\Delta\eta$	0.083	0.147	0.205	0.517
	ΔG^{*E}	138	161	239	310
Tsao–Smith	V^E	0.209	0.208	0.222	0.244
	$\Delta\eta$	0.075	0.182	0.250	0.591
	ΔG^{*E}	111	195	277	331

[a]Oswal *et al.*[48]; [b]Ghael *et al.*[49]

The values of *SD* for ΔG^{*E} were in the range 49–336 J mol^{-1} for different polynomials. For the mixture 1-butanol with ($C_4H_8O_2$ + *c*-C_6H_{12}), the smallest value of 49 J mol^{-1} was obtained by the Redlich–Kister model, while in the mixture with benzene, smallest value was 57 J mol^{-1} when the Rastogi *et al*. Equation was applied.

In the mixture propyl propanoate + 1-hexanol + benzene, the ternary contribution,[50,51] given as the difference between the positive and negative experi-

mental value of V^E, and that predicted from the binary mixtures was not large. Bearing in the mind that the influence of this contribution in ternary V^E is insignificant, the prediction performed by the applied polynomials were mostly satisfactory, indicating that for the asymmetric models, the order of the components in the mixtures is essential. A similar conclusion could be reached for the other two properties.

Finally, it could be concluded that predictions with the empirical equations containing only binary parameters gave qualitative representation of V^E, $\Delta\eta$ and ΔG^{*E} for these three ternary systems.

Using different polynomials, Oh *et al.*[52] calculated the standard deviations of V^E and deviations in molar refractivity, ΔR, using measured densities and refractive indices of the ternary mixture dimethyl carbonate + ethanol + 2,2,4-trimethylpentane at 298.15 K. The ternary data showed positive values at all compositions, while deviations in the molar refractivity, ΔR, values were negative. The V^E and ΔR values were predicted using the model of Tsao–Smith, Kohler, Rastogi *et al.* and Radojković *et al.* The Radojkovic *et al.* model provided the best results with standard deviations of 0.0546 and 0.9698 cm^3 mol^{-1} for the ternary V^E and ΔR data, respectively.

Ester + hydrocarbon + aromatic hydrocarbon systems. Pérez *et al.*[53] determined the densities, surface tensions and refractive indices of the ternary system propyl propanoate + hexane + ethylbenzene at 298.15 K and atmospheric pressure over the entire range of composition. The excess molar volume V^E, surface tension deviations $\Delta\sigma_{123}$–$\Delta\sigma_{bin}$ and changes in refractive index of mixing Δn_D were calculated by the polynomials Jacob–Fitzner, Kohler, Colinet, Tsao–Smith, Toop and Scatchard *et al.* Some other empirical equations were also included.

The best results of V^E predictions were obtained with the asymmetric models of Tsao–Smith, Toop and Scatchard *et al.* when hexane was taken as the first component. This ternary system showed a relatively larger ternary contribution $V^E_{123} - V^E_{bin}$ = –0.07 cm^3 mol^{-1}, bearing in the mind that the ternary V^E values were mostly lower over the composition range. Similarly, the models of Toop and Scatchard *et al.* gave satisfactory predictions for $\Delta\sigma_{123}$ when propyl propanoate was taken as the first component. In addition, the ternary contribution $\Delta\sigma_{123}$–$\Delta\sigma_{bin}$ was 0.6 mN m^{-1}. In the study of Casas *et al.*,[54] the densities, kinematic viscosities and refractive indices of the ternary system propyl propanoate + + hexane + benzene were measured at 298.25 K and atmospheric pressure over the whole composition range. The excess molar volumes V^E, viscosity deviations $\Delta\eta$ and changes of refractive indices on mixing Δn_D were estimated from the experimental data by the polynomials proposed by Jacob and Fitzner, Kohler, Colinet, Tsao–Smith, Toop and Scatchard *et al.* The asymmetric models again gave better results in the predictions of V^E when hexane was considered as the first component. The ternary contribution $V^E_{123} - V^E_{bin}$ = –0.155 cm^3 mol^{-1} was

larger than in the case of the system with ethylbenzene. However, the symmetric model of Jacob–Fitzner gave the most accurate predictions of $\Delta\eta$.

Acrylic ester + alcohol + aliphatic/cyclic/aromatic hydrocarbons. Bahadur and Sastry [55] studied densities (ρ), sound speeds (u), excess volumes (V^E) and $\Delta\kappa_s$ of ternary systems composed of methyl acrylate (MA), 1-alcohols (1-propanol and 1-butanol) and inert hydrocarbons (*n*-hexane, *n*-heptane, cyclohexane, benzene and toluene) at 308.15 K. The following mixtures were treated: *i*) five mixtures of MA + 1-propanol + *n*-heptane, or *cyclo*-hexane, or benzene, or benzene, or toluene and *ii*) five mixtures of MA + 1-butanol with the same inert components as in case (*i*). A qualitative analysis of the V^E and $\Delta\kappa_s$ data of these ternary systems showed that in MA + 1-alcohols + *n*-hexane, or *n*-heptane, or cyclohexane, structure disruptions were more predominant, while in MA + 1-alcohols + benzene or toluene, the weak but specific structure making interactions dominated.

The experimental V^E values for mixtures MA + 1-alcohols + cyclohexane were large and more positive than those with the aliphatic hydrocarbons (*n*-hexane or *n*-heptane). Depolymerisation of the 1-alcohols in the presence of *cyclo*-hexane was found to be stronger than in the presence of *n*-hexane or *n*-heptane molecules. The replacement of aliphatic with aromatic hydrocarbons (benzene or toluene) decreased V^E and even resulted in negative values in the ester + 1-alcohol + toluene mixtures. This is also a consequence of the weak specific interactions of –OH···π and n···π types between corresponding molecules of the mixtures. Furthermore, additional dipole-induced dipole interactions in MA + + 1-alcohol + toluene mixtures could be possible. The ternary V^E values were predicted with the models proposed by Redlich and Kister, Kohler and Tsao––Smith.

The difference between the experimental and predicted ternary excess values ΔV^E_{123} by polynomials for the systems MA + 1-propanol + hydrocarbons were found mostly between –0.291 and 0.126 $cm^3\ mol^{-1}$. Similarly, for the systems MA + 1-butanol + hydrocarbons, the ΔV^E_{123} values range mostly from –0.095 and 0.188 $cm^3\ mol^{-1}$. In both cases, for some compositions, ΔV^E_{123} values larger than these limits were found. It is clear that all three polynomials gave only quantitative prediction of V^E for the presented ternary mixtures.

Sastry *et al.*[56] measured densities and speeds of sound for 15 ternary mixtures of methyl methacrylate (MMA) + 1 alcohols (1-butanol, 1-pentanol and 1-heptanol) + organic solvents (benzene, toluene, *p*-xylene, ethylbenzene and cyclohexane) at 298.15 and 308.15 K. The V^E and $\Delta\kappa_s$ values were predicted by the Redlich–Kister, Tsao–Smith and Kohler equations.

Experimental values of V^E show that the ternary mixtures of MMA with (1-alcohols + cyclohexane) have more and large positive values than mixtures with other organic solvents. This is a consequence of the fact that the effective

structure-breaking interactions are predominant between unlike molecules of MMA, 1-alcohols and cyclohexane, while the aromatic solvent interact specifically with either MMA or 1-alcohols, as emphasised by the authors.[54]

The difference between experimental and predicted V^E of the investigated mixtures by polynomials were found to change from 0 to 0.008, 0.006 to 0.15 and 0.001 to 0.093 $cm^3\ mol^{-1}$, respectively. These values were obtained by Redlich–Kister equation as compared to the Tsao–Smith and Kohler models. The difference between experimental excess isentropic compressibilities and predicted $\Delta\kappa_s$ was, also, at a minimum with the Redlich–Kister calculated values as compared to those of the other two models.

Aliphatic esters + glycols + aromatic organic solvents. Sastry *et al.*[57] measured densities, ρ, from 298.15 to 313.15 K, speed of sound, u, and relative permittivity, ε_r, at 298.15 and 308.15 K and atmospheric pressure for ternary mixtures of methyl acetate (MA) + diethylene glycol (DG) + nitrobenzene, MA + + triethylene glycol (TG) + chlorobenzene, MA + TG + bromobenzene, MA + + TG + nitrobenzene, ethyl acetate (EA) + TG + chlorobenzene, EA + TG + bromobenzene, EA + TG + nitrobenzene, EA + DG + nitrobenzene, butyl acetate (BA) + TG + chlorobenzene, BA + TG + bromobenzene and BA + TG + nitrobenzene. V^E, $\Delta\kappa_s$ and relative permittivity deviations, $\delta\varepsilon_r$, were predicted employing the Redlich–Kister, Tsao–Smith and Kohler Equations.

Specific structure interactions between the C- and Br-groups of the organic solvents with the carboxyl oxygen of esters, Cl···H–O complexes and dipole–dipole interactions were probably the main factors for the excess values and deviation functions in these mixtures.

The deviations between the experimental and predicted ΔV^E_{123} by Redlich–Kister, Tsao–Smith and Kohler models changed from –0.006 to 0.001, –0.104 to 0.122 and –0.0002 to 0.127 $cm^3\ mol^{-1}$ for these models at 298.15 and 308.15 K, respectively.

The Redlich–Kister model predicted the V^E and $\Delta\kappa_s$ value of all mixtures very satisfactorily bearing in mind that the deviation between the experimental and calculated values was close to the uncertainty of these properties. Furthermore, the Tsao–Smith model was a better approximation than the Kohler model in predicting $\Delta\kappa_s$. The deviations $\Delta\varepsilon_r$ between the experimental and calculated values for all models were far larger than the uncertainties. It seems that the deviation $\Delta\varepsilon_r$ is different to the other true excess properties.

Aliphatic/cyclic/aromatic hydrocarbons + alcohol ternary systems. Iglesias *et al.*[58] measured the density, refractive index on mixing and speed of sound of ternary mixture benzene + cyclohexane + 2-methyl-2-butanol at 298.15 K and atmospheric pressure over the entire range of compositions. V^E, Δn_D and $\Delta\kappa_s$ were calculated by means of the polynomials: Kohler, Jacob–Fitzner, Colinet, Tsao–Smith, Toop and Scatchard *et al.* The values of V^E were positive over the

entire composition range. The ternary contribution to V^E had the highest value at low concentrations of 2-methyl-2-butanol, with about 15 % of the total ternary excess volume V^E in the maximum. A similar effect was observed for $\Delta\kappa_S$, while for Δn_D, the ternary contribution was almost negligible.

In the calculation of V^E, the asymmetric Toop and Scatchard *et al.* Equation with benzene as the asymmetric component gave lower deviations with respect to the V^E data. For Δn_D, the asymmetric Tsao–Smith Equation with 2-methyl-2--butanol as the asymmetric component and the symmetric Equations of Kohler, Jacob–Fitzner and Colinet gave the best results. It is important to emphasize that in the range with large absolute values of ternary contributions, the ability of calculations using polynomials is worse because the ternary is not adequately represented as the addition of the binaries. Namely, in this case, the zone of low concentrations of 2-methyl-2-butanol presents insignificant simultaneous ternary interactions.

Aromatic ketone + alcohol + aromatic systems. Prasad *et al.*[59] measured the V^E values of five ternary mixtures of acetophenone + 1-propanol + benzene or substituted benzene (toluene, chlorobenzene, bromobenzene and nitrobenzene) at 303.15 K. The ternary V^E values were predicted by the polynomials of Redlich––Kister, Kohler and Tsao–Smith.

The V^E data were negative over the whole composition range for the ternary systems of acetophenone + 1-propanol with chlorobenzene, bromobenzene, or nitrobenzene, while an inversion in sign occurred at low concentrations of acetophenone in mixtures with 1-propanol + benzene or toluene. The V^E data for these mixtures are connected to two opposing contributions: *i*) positive values are a consequence of the rupture of self-associated hydrogen bonds of alcohol and physical dipole–dipole interactions between alcohol monomers and multimers and *ii*) negative values are caused by the formation of –OH$\cdots\pi$ electron hydrogen-bonded complexes, changes in free volume and interstitial accommodations. In the mixtures of acetophenone + 1-propanol with chlorobenzene, bromobenzene or nitrobenzene contributions. Contribution (*ii*) is essential for negative V^E values, while both contributions (*i*) and (*ii*) are responsible for the behaviour of the mixtures with benzene and toluene as the third component. A comparison between experimental V^E data of the ternary mixtures and those calculated by the polynomials of Redlich–Kister, Kohler and Tsao–Smith shows that these polynomials gave only a qualitative estimation of the V^E in the ternary mixtures.

The estimated results for the ternary mixtures with benzene and toluene showed that somewhat poorer predictions were obtained by all polynomials applied to the mixture with toluene. This was expected bearing in mind that absolute difference of maximum and minimum of the V^E values for this system is higher. When the polynomials were used to predict the V^E values of the systems with chlorobenzene, bromobenzene or nitrobenzene, non-adequate results were

achieved in mixtures with bromobenzene, while the polynomials function better for the prediction of V^E for the system with nitrobenzene than with chlorobenzene. This is a consequence of the fact that the order of the maximum values of V^E is bromobenzene > nitrobenzene > chlorobenzene and that differences between the experimental and calculated ternary V^E values are the smallest for the system with chlorobenzene.

Amide + amide + water system. Han *et al.*[60] reported densities and viscosities at 298.15 K for the ternary system *N*,*N*-dimethylformamide (DMF) + + *N*-methylformamide (NMF) + water. The excess molar volumes and viscosity deviations were compared with the predicted values using the models of Tsao–Smith, Kohler, Rastogi *et al.* and Radojković *et al.*

The measured V^E data showed negative values over the entire range of composition. This is a consequence of the strong interactions between DMF and water and between NMF and water. Namely, the breaking of H bonding and specific dipole–dipole interactions of the nitrogen compounds are less important than the interactions between the different molecules. The $\Delta\eta$ values were positive over a wide composition range, except in the DMF + NMF rich region, where the $\Delta\eta$ value were negative.

The Radojković *et al.* Equation gave the best predictions with standard deviation of 0.073 cm^3 mol^{-1} and 0.096 mPa s for V^E and $\Delta\eta$, respectively. The other applied polynomials provided poorer results.

n-*Hexanol + ethanenitrile + dichloromethane system.* Aznares *et al.*[61] measured the densities and refractive indices for the ternary system *n*-hexanol + ethanenitrile + dichloromethane at 298.15 K and determined the excess molar volumes, V^E, and the excess refractive indices (changes in the refractive indices on mixing), Δn_D.

The ternary V^E data were positive. *n*-Hexanol is a self-associated molecule and the addition of the other components resulted in a rupture of hydrogen bonding with concurrent expansion in volume. The polynomials of Radojković *et al.*, Jacob–Fitzner, Kohler and Tsao–Smith were used to predict V^E and Δn_D. The equations of Radojković *et al.* and Kohler gave similar and good results for V^E, while the Tsao–Smith model was unsatisfactory in the prediction of Δn_D.

Acetone + alcohol + water system. Iglesias *et al.*[62,63] presented experimental data of densities and refractive indices at 298.15 K and atmospheric pressure for the systems acetone + methanol + 1-propanol, acetone + methanol + water and acetone + methanol + 1-butanol.

The validity of the estimation of the excess V^E values and the refractive indices on mixing Δn_D were examined by the empirical Equations of Kohler, Jacob–Fitzner, Colinet, Tsao–Smith, Toop and Scatchard *et al.* Values of V^E for the system acetone + methanol with water were negative for the entire composition range, due to the strong interactions between water as a proton donor and

acetone as a proton acceptor. The mixture acetone + methanol with 1-propanol or 1-butanol gave similar effects but with a weaker cross association between 1-propanol or 1-butanol and the other two components. Changes of refractive indices were characterized by positive values for all the ternary systems. For the system acetone + methanol with 1-propanol, the best prediction of V^E were obtained by the asymmetric models of Toop and Tsao–Smith with 1-propanol as the asymmetric component in the equations. The symmetric Equations of Kohler, Jacob–Fitzner and Colinet also gave satisfactory results. Minimal values of standard deviations of Δn_D were obtained with methanol as asymmetric component in the Toop and Tsao–Smith models, bearing in mind that all symmetric models were good accordance with experimental data. The lower standard deviations in V^E for the system acetone + methanol with water were obtained by the model of Jacob–Fitzner, Toop and Scatchard *et al.* with methanol as an asymmetric component. The highest values of deviations were achieved by asymmetric models with water as the asymmetric component (or methanol in the Tsao–Smith model).

Better predictions were obtained for Δn_D using Colinet, Jacob–Fitzner and Scatchard *et al.*, Toop (methanol as the asymmetric component in both cases) and Tsao–Smith (acetone as an asymmetric component).

In the system acetone + methanol with 1-butanol, low standard deviations were obtained with the asymmetric models: for the V^E predictions by the Toop and Scatchard *et al.* models (water as the asymmetric component in both cases) and for Δn_D predictions by the Tsao–Smith, Toop and Scatchard *et al.* models (methanol as the asymmetric component).

Water + fluoroalcohol + alcohol/acetone systems. Atik[64] determined V^E for ternary systems of water + 2,2,2,trifluoroethanol with methanol, ethanol, 1-propanol, 2-propanol or acetone at 298.15 K and 101 kPa. All the molecules are polar having a strong self-associative nature and complex formation. Fluoroalcohol is a better proton donor than the hydrocarbon alcohols.

These ternary systems show regions with both negative and positive values of V^E values. The mixtures of water + alcohol + trifluoroethanol and water + acetone + trifluoroethanol involve the disruption and weakening of self-association occurring in water, alcohols and acetone through hydrogen bonding, attributing a combination of strong (water–water) and weak (alcohol–alcohol) association effects.

Estimations of V^E were performed by the Redlich–Kister, Kohler, Jacob––Fitzner, Colinet and Scatchard *et al.* models and by the Mathieson–Thynne and Muggianu *et al.* models, which are the most included here. In all cases, the Redlich–Kister model gave the best predictions, while the Jacob–Fitzner model works satisfactorily in the systems with methanol, ethanol and 1-propanol. The good results obtained with these symmetric models are the consequence of very small ternary contributions to V^E in both the positive and negative regions.

Hydrocarbon + cyclic hydrocarbon + chloroalkane/alcohol system. Souza *et al.*[65] determined V^E at 298.15 K for ternary mixtures *n*-propyl propanoate with cyclohexane, 1-chloro-*n*-hexane and *n*-hexane, with predictions by the Kohler, Jacob–Fitzner, Colinet and Tsao–Smith models. The deviations from the predictions were 3 to 40 times greater than the standard deviation. The asymmetric Tsao–Smith equation presents better results if component 1 was *n*-propyl propanoate. In addition, from the results of V^E for pseudo-binary mixtures, it could be concluded that the symmetric equations do not predict the existence of a maximum. However, the Tsao–Smith equation gives rise to maximums that did not coincide with those obtained from the fittings.

Menaut *et al.*[66] measured the densities of two ternary systems of *cyclo*-hexane + *n*-hexane with 1-chlorohexane or 1-hexanol at 298.15 K. Experimental values of V^E were compared with the results obtained by the empirical equations of Kohler, Jacob–Fitzner, Colinet, Tsao–Smith, Toop and Scatchard *et al.*

Ternary contributions for both mixtures were small but the forms of the positive and negative curves of constant difference between the ternary and binary contributions were completely different. The system with 1-chlorohexane had isolines of negative values for almost the whole composition diagram except near the sub binary mixture of *n*-hexane and 1-chlorohexane. In the system with 1-chlorohexane, the best results for the standard deviation were obtained by the Toop and Scatchard *et al.* models for the mixtures ordered as *cyclo*-hexane + + *n*-hexane + chlorohexane.

In the case of the ternary system with 1-hexanol, an isoline of zero value divided the composition diagram and the symmetric equations of Jacob–Fitzner, Kohler and Colinet all gave better results.

Alcohol + ester + aromatic ternary systems. Rodriguez *et al.*[67] gave experimental data for the density, refractive index and speed of sound of the ternary system dimethyl carbonate + methanol + benzene at 298.15 K and atmospheric pressure over the entire range of composition. The results were used to calculate V^E, Δn_D and $\Delta\kappa_s$ by the same polynomials as in the previous case. The V^E values of this ternary system were positive over most of the composition range, except in the region close to pure methanol, where the sign changed due to interstitial accommodation of methanol molecules into the molecules of other two components For the prediction of V^E, Δn_D and $\Delta\kappa_s$, the asymmetric equations of Toop and Scatchard *et al.* with methanol as the asymmetric component gave good estimations. Calculations of V^E, Δn_D and $\Delta\kappa_s$ by symmetric Equations of Kohler, Jacob–Fitzner and Colinet were also successful.

Alcohol + chloroform + benzene systems. A review paper of Djordjević *et al.*[68] included the application of the polynomials to V^E prediction of two ternary systems of alcohols (methanol and 1-propanol) with chloroform and benzene. The best results were obtained with the a-type Tsao–Smith Equation when

methanol was treated as an asymmetric component. In addition, two other asymmetric equations, the a-type Toop and the a-type Scatchard *et al*. Equations could be recommended. The Radojković *et al.*, Kohler, Jacob–Fitzner, Colinet, b-type Tsao–Smith, b-type Toop and b-type Scatchard *et al*. expressions were satisfactory when chloroform was the asymmetric component, while the models of Rastogi *et al*. and all c-types with benzene as the asymmetric component (Tsao––Smith, Toop and Scatchard *et al.*) gave higher deviations and could not be recommended.

The best agreements with the experimental V^E data for the system 1-propanol + chloroform + benzene were achieved by the a-type asymmetric models of Scatchard *et al.* and Toop with 1-propanol as the asymmetric compound. Satisfactory predictions were obtained using the symmetric equations of Radojković *et al.*, Kohler, Jacob–Fitzner and Colinet. All other asymmetric models work very poorly, whereas the worst results were obtained with the symmetric Rastogi *et al.* model. It could be concluded that for both the studied ternary systems, the majority of the examined predictive models gave adequate predictions of the ternary V^E from the data of their binary subsystems.

In works of Kijevčanin *et al.*[69] and Smiljanić *et al.*,[70] only the Radojković *et al.* model was applied to the prediction of V^E for the ternary systems ethanol and 1-butanol with chloroform + benzene, respectively, and the obtained results could be treated as acceptable, bearing in the mind that the ternary contribution for both systems was relatively small.

Benzene + cyclohexane + hexane ternary system. Dominguez *et al.*[71] determined the κ_s, $\Delta\kappa_s$ and Δu for the ternary mixture benzene + cyclohexane + + hexane at 298.15 K. The polynomials of Redlich–Kister, Tsao–Smith, Kohler and Colinet were used in order to predict $\Delta\kappa_s$ and Δu of this system.

The $\Delta\kappa_s$ and Δu exhibited similar behaviour but with opposite signs. Namely, the region rich in benzene and hexane and poor in cyclohexane gave the most negative $\Delta\kappa_s$, and the most positive Δu values. Predictions of $\Delta\kappa_s$ performed by the Redlich–Kister and Colinet Equations were satisfactory. On the other hand, only the asymmetric Tsao–Smith model was relatively acceptable in predicting Δu. This is consequence of difference between standard deviations of polynomials and those presented by the fitting to the Cibulka Equation showing the existence of molecular interactions between all the molecules present.

Diethylamine + ethyl acetate + n-*heptane ternary system*. Lillo *et al.*[72] calculated V^E and η^E for the ternary system diethylamine + ethyl acetate + *n*-heptane at 298.15 K. The V^E values were positive over the whole concentration range, indicating that the molecular interactions between the different molecules were weaker than interactions between the molecules in their pure state, showing that repulsive forces dominate in the mixtures. The $\Delta\eta$ values were negative and very small because the dominating repulsive forces decreased the viscosities of the mixtures.

The models of Tsao–Smith, Jacob–Fitzner, Kohler, Rastogi *et al.* and Radojković *et al.* were used to predict V^E and $\Delta\eta$. The Jacob–Fitzner, Radojković *et al.* and Kohler models gave good agreement with the experimental data of this ternary system. The Rastogi *et al.* model exhibited poor results. The Tsao–Smith as an asymmetric model gave lower σ values when diethylamine was the asymmetric component. The other two Tsao–Smith models were not applicable for the prediction of V^E and $\Delta\eta$.

Amine + alcohol + tributylphosphate ternery systems. Kim *et al.*[73] predicted V^E and ΔR for ternary systems tri-octylamine (TOA) + tributylphosphate (TBP) + + 1-octanol, TOA + 1-octanol + 1-decanol, TOA + TBP + 1-decanol and TBP + + 1-octanol + 1-decanol using the Radojković *et al.* model. Prediction for both properties were performed using the correlated Redlich–Kister parameters (Eq. (13)) obtained for the corresponding binary subsystems.

Methyl butanoate + heptane + (octane+cyclooctane + 1-chlorooctane + + 1-octanol). In recent articles,[74–77] presented the results of V^E and $\Delta\eta$ for the ternary systems of (methyl butanoate + heptane) with: *i*) octane, *ii*) cyclooctane, *iii*) 1-chloroctane and *iv*) 1-octanol at four temperatures (283.15, 293.15, 303.15 and 313.15 K) over the whole concentration range and atmospheric pressure were presented.

The obtained results for V^E and $\Delta\eta$ of the ternary systems were used to test the symmetrical (Redlich–Kister, Kohler, Colinet and Rastogi *et al.*) and asymmetrical (Tsao–Smith and Toop) models considered in this work. In addition, the polynomials of Hiller,[15] Muggianu *et al.*,[16] and Acree *et al.*[18] were treated in these papers.[74–77]

In the cases of (*i*)–(*iii*), the authors showed that the maxima and minima for the differences between the ternary properties and the corresponding binary contributions ($V^E_{123} - V^E_{bin}$ and $\Delta\eta_{123}-\Delta\eta_{bin}$) were relatively small, suggesting that the effects due to ternary interactions are of smaller significant.

Binary interactions which dominated in each binaries are the consequence of: *i*) systems of methyl butanoate with *n*-heptane and *n*-octane gave positive V^E values caused by the net rupture of dipole–dipole interactions in methyl butanoate over the molecular packing and heteromolecular dipole–dipole induced interactions, *ii*) in the system *n*-heptane + *n*-octane, molecular packing is the prevalent factor, *iii*) in the system *n*-heptane + cyclooctane, the negative V^E values showed that the packing effect predominated over those due to physical interactions, *iv*) the positive values of V^E for the system methyl butanoate + cyclooctane indicated that the rupture of dipole–dipole interactions between the ester molecules was the predominate factor over the effects of volume contractions and molecular packing, *v*) the negative values of V^E for the system *n*-heptane + 1-chlorooctane showed that the effect of molecular packing was the prevalent factor, *vi*) the positive values of V^E for the system methyl butanoate +

+ 1-chlorooctane suggested that the net rupture of dipole–dipole interactions of the ether molecules prevailed over molecular packing and dipole–dipole interactions of the different molecules, *vii*) for the system methyl butanoate + 1-octanol, the values of V^E were positive and expansive effects connected to the rupture of hydrogen bonds in 1-octanol and dipole–dipole interactions in both components existed and *viii*) the V^E values of the system *n*-heptane + 1-octanol were negative over most of the composition range, indicated that molecular packing was the predominant factor. The breakage of hydrogen bonds at mole fractions of *n*-heptane $x > 0.9$ resulted in positive values of V^E.

Bearing in the mind all these facts, in general, as presented in Table IV, the V^E values for ternary systems with *n*-octane and *cyclo*-octane were predicted reasonably well by all symmetric models, except for the model proposed by Rastogi *et al.* The asymmetric model of Tsao–Smith with the arrangement A + B + + C gave good predictions for both ternary systems, while the Toop model worked satisfactorily only for the mixture with *n*-octane.

TABLE IV. Average percent deviations, *AAD* / %, between the experimental and predicted V^E / cm^3 mol^{-1} and $\Delta\eta$ / mPas values by polynomials for the ternary systems methyl butanoate (A) + *n*-heptane (B) with a third component (C) in the temperature range 283.15 – 313.15 K; for the asymmetrical models, the values depended on the component ordering

Model	*AAD* / %	*n*-Octane(C)[a]	Cyclooctane(C)[b]	1-Chlorooctane(C)[c]	1-Octanol (C)[d]
Redlich–Kister	V^E	1.9	2.0	19.35	45.4
	$\Delta\eta$	6.6	10.95	45	12.35
Kohler	V^E	1.45	5.1	21.35	37.8
	$\Delta\eta$	6.7	14.25	4.1	13.75
Colinet	V^E	1.5	3.45	20.7	38.8
	$\Delta\eta$	6.4	15.15	4.1	15.35
Rastogi *et al.*	V^E	27.2	27.4	65.7	93.5
	$\Delta\eta$	30.05	20.4	33.5	19.6
			Tsao–Smith		
A + B + C	V^E	2.2	5.8	10.4	23.6
	$\Delta\eta$	6.55	45.15	13.75	47.15
C + A + B	V^E	21.5	30.65	146.8	204.75
	$\Delta\eta$	20.75	1.1	4.2	0.8
B + A + C	V^E	19.7	37.6	46.85	62.4
	$\Delta\eta$	15.8	45.5	7.35	45.3
			Toop		
A + B + C	V^E	2.6	10.65	25.65	48.2
	$\Delta\eta$	6.55	23.1	4.45	23.8
C + A + B	V^E	2.5	3.55	28.8	48.65
	$\Delta\eta$	6.9	2.65	6.0	1.05
B + A + C	V^E	3.2	4.85	10.2	18.5
	$\Delta\eta$	6.5	23.85	3.6	21.9

[a]Matos *et al.*[74]; [b]Trenzado *et al.*[75]; [c]Matos *et al.*[76]; [d]Trenzado *et al.*[77]

The prediction of $\Delta\eta$ for ternary system with *n*-octane was accomplished reasonably well by all the considered symmetric models (except for the Rastogi *et al.* model). All asymmetric models of Toop and the arrangement A + B + C of Tsao–Smith model also produced good prediction.

In the case of ternary system with cyclooctane, the most accurate prediction for $\Delta\eta$ was achieved by the models of Tsao–Smith and Toop with the same arrangement (C + A + B).

Less accurate predictions of the V^E values for ternary system with 1-chlorooctane were obtained when compared to the results of systems with *n*-octane and cyclooctane as the third component, as can be seen from Table IV. In the case of the Tsao–Smith (option A + B + C) and Toop option B + A + C) models predicted results that could be treated as less accurate but satisfactory. Good predictions of $\Delta\eta$ were obtained with symmetric models of Kohler and Colinet and the option (C + A + B) of Tsao–Smith and all options of the Toop model. However, these models gave worse predictions of V^E.

As can be seen from Table IV, predicted results of V^E for the ternary system with 1-octanol as the third component were unsatisfactory. Only the Tsao–Smith and Toop models with the disposition C + A + B gave good prediction of $\Delta\eta$.

Dibutylether + ethanol + aromatic ternary systems. V^E and ΔR values the for the ternary systems dibutylether (DBE) + ethanol + toluene or benzene or 2,2,4-trimethylpentane at 298.15 K were reported.[78–80] The interaction between DBE and ethanol molecules gave negative values of V^E and ΔR. The systems of ethanol with toluene or benzene had positive values of V^E at lower concentrations of ethanol, which changed to negative in the alcohol rich region. The systems of DBE + toluene or benzene show negative values of V^E over the entire range of composition. The binary system of 2,2,4-trimethylpentane + ethanol showed positive V^E values, while the system 2,2,4-trimethylpentane + DBE shows negative values of V^E.

The V^E values for the ternary system with toluene were characterized by negative values, while the other two ternaries showed the appearance of both maximum and minimum values of V^E.

Table V shows that the Radojković *et al.* model provided the best estimation results for the ternary V^E and ΔR values in most cases. The models of Tsao–Smith and Kohler can not be recommended, while the Rastogi *et al.* model gave the best results only for the prediction V^E in the ternary system with toluene.

TAME + ethanol + 2,2,4-trimethylpentane system. Hwang *et al.*[81] determined values of V^E and ΔR data of the ternary systems TAME + ethanol + 2,2,4--trimethylpentane at 298.15 K and compared them with the values predicted by the models of Tsao–Smith, Kohler, Rastogi *et al.* and Radojković *et al.* The V^E of binary system TAME + ethanol at 298.15 K showed negative values over the entire ranges of composition, while the other two binary systems had positive

values of V^E. The positive deviations are caused by dispersive interaction forces between two unlike molecules, while the negative deviations are the consequence of the strong polarity of ethanol molecules. The ΔR of all binary system showed negative values. V^E and ΔR were estimated by aforementioned predictive models. The Radojković *et al.* model provided the best results, as in the case of the ternary system DBE + ethanol + 2,2,4-trimethylpentane (Table V). The other applied models could not be recommended for predictions of V^E and ΔR of this ternary system.

TABLE V. The values of the standard deviations *SD* of V^E / cm^3 mol^{-1}, ΔR / cm^3 mol^{-1} calculated by polynomials for the ternary systems DBE (A) + ethanol (B) + third component (C) at 298.15 K

Model	Property	Benzene (C)[a]	Toluene (C)[b]	2,2,4-Trimethylpentane (C)[c]
Tsao–Smith	V^E	0.0837	0.0625	0.1322
	ΔR	1.2977	0.7403	1.7754
Kohler	V^E	0.0524	0.0431	0.0275
	ΔR	0.4779	0.7513	1.7881
Rastogi *et al.*	V^E	0.0624	0.0351	0.0388
	ΔR	1.4336	1.3166	1.2879
Radojković *et al.*	V^E	0.0281	0.0385	0.0273
	ΔR	0.2358	0.0800	0.5962

[a]Han *et al.*[78]; [b]Kwak *et al.*[79]; [c]Lee *et al.*[80]

MTBE + methanol + aromatic hydrocarbon ternary systems. Han *et al.*[82] considered MTBE + methanol in different ternary mixtures with benzene or toluene than the mixtures given in Tables I and II. The V^E and $\Delta\eta$ values at 298.15 K were determined for the ternary systems of MTBE + methanol + benzene and MTBE + methanol + toluene. The values of V^E were negative over the entire range of composition, except for a small region rich of benzene. The $\Delta\eta$ data had small negative values. This is consequence of the molecular interactions between each component which are not very strong in all the binary and ternary systems. The experimental data of V^E and $\Delta\eta$ were compared with the predicted results obtained by the Tsao–Smith, Kohler, Rastogi *et al.* and Radojković *et al.* models. The Kohler and Radojković *et al.* equations provided the best results for both ternary properties.

Formamide + benzene + aromatic amine. In work of Kharat and Nikam,[83] the excess molar volumes and deviations in viscosity of the ternary system aniline + benzene + *N*,*N*-dimethylformamide at 298.15, 303.15, 308.15 and 313.15 K were calculated by several empirical expressions. At all temperatures, the V^E and $\Delta\eta$ values were negative. The main contribution to the negative values of V^E was the interstitial accommodation of non-associated benzene molecules into aggregates of aniline. This also implies that no complex-forming interactions were present in the system, resulting in negative values of $\Delta\eta$.

The Equations of Radojković *et al.*, Kohler and Scachard *et al.* were applied to predict V^E and $\Delta\eta$. Small deviations between the experimental and predicted values were achieved.

Very good predictions[84] were obtained by the same three equations for V^E and $\Delta\eta$ of the ternary system *N*,*N*-dimethylformamide + benzene + chlorobenzene at 298.15, 303.15, 308.15 and 313.15 K.

Arylhalide + ether + alcohol/haloalcohol. Atik and Lourdani[32,33] evaluated the V^E of ternary systems *α*,*α*,*α*-trifluorotoluene and ethanol with diisopropyl ether (DIPE) and fluorobenzene[32] and with 2,2,2-trifluoroethanol (TFE)[33] at 298.15 K at a pressure of 101 kPa. When mixing alcohols and ether with fluorohydrocarbons, the following specific H bonding appeared: H···O–H, OH···O and O–H···F. These types of effects reflect on the magnitudes of V^E. These self- and cross-H bonding along with dipole–dipole interactions especially contribute to the ternary terms and influence the total packing behaviour of the mixtures.

Predictions were performed by symmetrical (Redlich–Kister, Kohler, Colinet and Jacob–Fitzner) and asymmetrical (Scathard *et al.*, Tsao–Smith and Toop) models. It was shown[32] that for ternary system with fluorobenzene where the ternary contribution terms are higher, better results were obtained by the asymmetrical models, while for systems with TFE,[33] higher errors were achieved by asymmetrical V^E with similar ternary contributions, V^E_{123}.

Atik[85] considered ternary mixtures of fluorobenzene + *tert*-butylmethyl ether and *α*,*α*,*α*,-trifluorotoluene + *tert*-butylmethylether + ethanol at 298.15 K and 0.1 MPa. The structure of these systems are similar to those in previous articles[32,33] of the same author, but the results of the predictions by the equations of Scatchard *et al*., Tsao–Smith, Toop, Colinet, Jacob–Fitzner and Hillert were better, bearing in the mind that the ternary contributions of these systems were smaller.

Ether + alcohol + hydrocarbon/ionic liquid. The Radojković *et al.* Equation was applied[86,87] to the isolines of V^E and ΔR for the ternary systems: diisopropyl ether (DIPE) + 1-propanol + trihexyletradecylphosphonium [$P_{666,14}$] [TMPP]; *tert*-amylmethyl ether (TAME) + methanol + [$P_{666,14}$] [TMPP], dimethyl carbonate (DMC) + methanol + 1-ethyl-3-methyl-imiduzolium ethyl sulphate (EMISE); DMC + methanol + 1-butyl-3-methylimiduzolium tetrafluoroborate (B_{mim})(BF_4); 2-propanol + water + EMISE and 2-propanol + water + (B_{mim}) (BF_4) at 298.15 K. For all the systems, these properties were negative over the whole concentration range because of attractive interactions, strong polarity of the components and their difference in size, bearing also in the mind the appearance of the strong polarity of the ionic liquids.

Haloalkane + hydrocarbon systems. Matos *et al.*[88] reported V^E at 25 ºC and atmospheric pressure for four ternary systems methyl ethanoate + 1-chlorooctane + + (*n*-heptane, *n*-octane, *n*-nonane or *n*-decane). The dominant factors in these

mixtures were the breaking of dipole–dipole interactions in the chloroalkanes and methyl ethanoate molecules. Furthermore, the influence of dispersive effects, heteromolecular interactions and packing molecular efficiency as the molecular size of the components increased resulted in higher positive values of V^E. The results of V^E measurement were compared with equations treated in the present article (Tsao–Smith, Toop, Kohler, Colinet, Rastogi *et al.*) and several other polynomials (Muggianu *et al.*, Hillert, Hwang *et al.* and Oracz).

The best results were obtained by the asymmetrical Tsao–Smith and Toop models and the symmetrical Kohler model. In all cases, the values of V^E_{max} were relatively small and with increasing carbon atomic number in the *n*-alkane, these values became smaller; hence, the results obtained by the polynomials became better.

Amide + cyclic ketone + alkanolamine. Iloukhani and Rakhshi[89] used the polynomial Equations of Kohler and Jacob–Fitzner for predictions of V^E, $\Delta\eta$ and Δn_D for the ternary mixture *cyclo*-hexanone + *N*,*N*-dimethylacetamide + *N*,*N*-diethylethanolamine at 298.15, 308.15 and 318.15 K and at ambient pressure over the whole composition ranges. The positive values of the ternary V^E were the consequence of chemical and structural contributions. Negative values of $\Delta\eta$ and Δn_D showed that the forces between pairs of unlike molecules were less than the forces between like molecules, due to the difference in size and shape of component molecules. The results obtained by both polynomial equations were satisfactory.

Haloalcohol + water + polyether. Esteve *et al.*[90] predicted the V^E values of the ternary system water + 2,2,2-trifluoroethanol + 2,5,8,11,14- pentaoxapentadecane at 303.15 K by different symmetric and asymmetric empirical equations. Water with these fluoroalkanol and polyether showed negative values of V^E. As 2,5,8,11,14-pentaoxapentadecane is a stronger proton acceptor than 2,2,2-trifluoroethanol, their molecules would increase the negative ternary V^E, while associations between the molecules of the fluoroalcohol and poly ether are dominant.

Comparison of the predictions of the symmetrical Redlich–Kister (*i.e.*, Radojković *et al.*), Kohler, Muggianuet *et al.* and Colinet and the asymmetrical Tsao–Smith, Toop, Scachard *et al.* and Hillert) models showed that the smallest standard deviation was obtained by the Hiller eEquation with water as the first component. In all cases, the results of the asymmetrical models with water as first component were satisfactory. The Redlich–Kister model was the only symmetrical model that gave similarly good predictions.

The same empirical equations as in the article of Esteve *et al.*,[90] were used in work of Olive *et al.*[91] to predict ternary excess viscosities of the system trifluoroethanol + water + tetraethylene glycol dimethyl ether at 303.15 K. In this case, the Colinet Equation showed the best results with smallest standard deviation. Of the symmetric models, only the Kohler Equation gave satisfactory agreement,

while the asymmetric model of Toop and Hillert could be treated similarly when trifluoroethanol was the first component.

Methyl acetate + methanol + n-alcohols. Rodrigez *et al.*[92] applied the predictive methods (Kohler, Jacob–Fitzner, Colinet, Tsao–Smith, Toop, Scachard *et al.*) to determine V^E and Δn_D for the ternary mixture methyl acetate + methanol + ethanol at 298.15 K. The ternary mixture showed positive values of V^E over most of the triangular diagram, suggesting the different closeness of the packing of the molecules as consequence of the different chain molecular lengths of the *n*-alcohols. In the evaluation of V^E, both types of models (symmetric and asymmetric) showed lower standard deviations. In the prediction of Δn_D, better results were achieved by symmetric and type b asymmetric models, where component b is methanol.

Canosa *et al.*[93] extended their investigation of V^E and Δn_D to ternary mixtures of methyl acetate + methanol with 2-propanol at 298.15 K. The ternary V^E becomes more positive than in the case of the mixture methyl acetate + methanol with ethanol.[92] Namely, molecular packing is more difficult at low amounts of methanol when the *n*-alcohol chain increases due to steric hindrance. In addition, high values of V^E for intermediate regions could appear because of a weakening of the H-bonds between the carboxyl group and the OH group. Finally, in dilute regions of 2-propanol or methyl acetate, the capacity of accommodation is similar as in the case of the smaller ethanol molecules.[92]. The estimations were performed using the same equations as in the previous work.[92]

The best prediction of the ternary V^E was realised with the symmetric Jacob–Fitzner and Tsao–Smith models when methyl ethanoate was the asymmetric component. For Δn_D estimation, better results were obtained with methanol as the asymmetric component. The ternary contribution of V^E is relatively small, and the highest value (–0.04 cm^3 mol^{-1}) was obtained in an approximately equimolar ternary composition. This fact could be the reason for the satisfactory results obtained with all the symmetric models.

Canosa *et al.*,[94] as a continuation of previous articles,[92,93] treated the ternary V^E of the system methyl acetate + methanol with 2-butanol at 298.15 K. The best predictions of V^E were obtained by the symmetric equations[93] and the asymmetric Scatchard *et al.* and Toop Equations with methanol and the Tsao–Smith equation with methyl acetate as the asymmetric component. The highest ternary contribution ΔV^E (–0.030 cm^3 mol^{-1}), detected at approximately equimolar composition, was some what smaller that in system with 2-propanol (0.04 cm^3 mol^{-1}),[93] giving better overall predictions.

Iglesias *et al.*[95] reported experimental densities, refractive indices of mixing and derived properties V^E and Δn_D of the ternary system methyl acetate + methanol + 1-butanol at 298.15 K and 1 atm. over the whole composition range.

These derived properties were predicted by the same models as in the previous studies.[92–94]

The V^E values were positive over the entire range of the calculations. This behaviour could be explained by certain disruptions of the associated alcohol molecules and polar association of the methyl acetate molecules or by rupture of the interaction of the methyl acetate and methanol molecules. Moreover, in accordance with corresponding region of ternary concentrations, the following effects should be taken into consideration: *i*) contractive trend due to the small size of the alcohol molecule and interaction of –OH group and ester groups and *ii*) the steric hindrance caused by the non-polar characteristics of the hydrocarbonated chain.

The good prediction results obtained by the symmetric models of Kohler, Jacob–Fitzner and Colinet, and the asymmetric models of Scatchard *et al.* and Toop (except with methanol as asymmetric component), could be explained by the facts that ternary contribution of V^E was relatively small compared to the binary and ternary values of V^E. Namely, ternary contribution is almost negligible except in the zone of low concentration of 1-butanol, thus the binary interactions determine the final excess value of ternary V^E. Standard deviations of these models are very similar to that obtained by the Cibulka Equation used for correlation of the ternary V^E data.

Amide + cyclic ketone + n*-alcohols*. Venkatesu and Prabhakara Rao[96] measured the V^E values of ternary liquid mixtures of *N*,*N*-dimethylformamide and *cyclo*-hexane with *n*-propanol, *n*-butanol, *n*-pentanol and *n*-hexanol as a function of composition at 303.15 K. The V^E values were positive in all cases except at a lower mole fraction of *N*,*N*-dimethylformamide in the system with *n*-propanol. The positive values of V^E showed that the effect of structure breaking of the components was dominant in the mixtures and increased with increasing chain length of the *n*-alcohols. Analysis of the results indicated good agreement between the measured V^E_{123} values and those predicted from the Redlich–Kister Equation in all ternary systems.

Haloalkane + ester + amine. Iloukhani and Khanlarzadeh[97] applied some geometrical and empirical models to V^E for ternary (1-chlorobutane + 2-chlorobutane + 2-butylamine; 1-chlorobutane + 2-chlorobutane + butyl acetate; 2-chlorobutane + butylamine + butyl acetate) and the quaternary system (1-chlorobutane + 2-chlorobutane + butylamine + butyl acetate) at 298.15 K. Prediction of the ternary systems was realised by different geometrical models (Kohler, Jacob–Fitzner, Rastogi *et al.* and Radojković *et al.*). The best results were obtained by the Kohler and Radojković *et al.* Equations. Estimation of V^E for the quaternary system was achieved by symmetrical (Redlich–Kister, Kohler, Lakhalpan and Colinet) and asymmetrical (Tsao–Smith, Toop, Hilert, Scatchard *et al.* and Knobeloch–Schwartz) models. The best result was obtained by the Tsao–Smith Equation.

5. CONCLUDING REMARKS

1. The choice of liquid mixtures in the present review (organic non-electrolytes and water) was based on their important application in the chemical and other industries. The thermodynamic and transport properties of multicomponent systems and their analysis in terms of various types of models are important for chemical processes. The search for models capable of correlating the molecules structure and macroscopic properties of liquids and predicting the behaviour of multicomponent mixtures are of primary interest for many investigators.

2. Properties considered in this work (ρ, V^{E}, Δn_{D}, Δu, $\Delta \eta$, $\Delta G^{*\mathrm{E}}$, ΔR, $\Delta \kappa_{\mathrm{S}}$ and ε_{r}) are sensitive to different kinds of complexity of liquid mixtures and have often been used to investigate molecular packing, molecular motion and various types of intermolecular interactions and their strength, influenced by the size and chemical nature of different molecules. Assuming that the interactions in a ternary mixture are mostly dependant on the interactions in the binary ones, the use of polynomials was considered to test these methods of predicting ternary properties from binary data.

3. Extensive studies of the current status of the methods for the modelling of the aforementioned properties led to conclusion that, in spite of many years of contribution and development in these fields, there is still no general model that could be capable for the prediction within the accuracy of experimental measurements. Moreover, the success in application of each model is limited to a particular case due to the type and complexity of the systems and the number of their components.

4. The main reason for very extensive application of various polynomials lies not in the theoretical sophistication of this approach, but in the fact that the binary data are more accurately represented in the prediction of multicomponent mixtures. Unlike other approaches frequently used, the polynomials do not require a specific functional form of the equation and do not limit the number of adjustable parameters. The herein treated asymmetric models indicated: *i*) the different contribution of one of the binary constituents, *i.e.*, a pair which does not include a polar component and *ii*) the order of components in the mixture. For symmetric models, all three binary systems were considered identically.

5. Ternary contribution which represents the difference between the experimental value and that predicted from the binary mixtures is the main factor indicating the quality of the polynomial predictions. The following notices are essentials:

– When ternary contributions are relatively small (including positive and negative values), then the effects due to ternary interactions are less important. In these cases, the results obtained by the polynomials are generally very good, particularly when using ordered symmetric models. The standard deviations in

some cases are very close to those obtained by fitting equations, such as the Cibulka, Singh or Nagata equations.

– Larger absolute values of the ternary contribution result in poorer estimations by the polynomials due to the fact that these ternary mixtures are not adequately represented only by the binary sub-systems because stronger ternary molecular interactions exist. Furthermore, unsatisfactory predictions are obtained when the difference in the experimental maximal and minimal ternary values of V^E are large.

– Various factors in connection with position of the ternary contribution (asymmetric, change of sign, magnitude of maximum or minimum) could be important for good predictions. In some cases, asymmetric models gave satisfactory results.

6. The influence of higher temperatures on the calculation by polynomials the errors only slightly. The higher values of the ternary contribution resulting by increasing the temperature lead to poorer prediction. When ternary contribution in ternary diagrams changes sign, the errors of the predictions could be decreased.

7. Results obtained by asymmetric models can be very different:

– For the same ternary system, the best prediction is achieved for one thermodynamic or transport property but the worst for any other.

– Change of temperature changes the quality of the prediction.

– Possible arrangement of the components as the asymmetric one frequently produces results which are completely different. For this reason, it is necessary to use all three components as asymmetric for the prediction.

– Different asymmetric models can give very dissimilar results when the same asymmetric component is applied in testing the same ternary system.

– When the ternary contribution is small, the order of the components in the mixtures could be essential for the asymmetric models.

8. In many cases, the Radojković *et al.* model, or the same model used as the Redlich–Kister model, could be recommended for the prediction of ternary properties as the simplest expression among those presented in this review.

Acknowledgements. The authors gratefully acknowledge the financial support received from the Research Fund of Ministry of Education and Science, Serbia and the Faculty of Technology and Metallurgy, University of Belgrade (project No 172063).

ИЗВОД

ПРЕДСКАЗИВАЊЕ ТЕРМОФИЗИЧКИХ И ТРАНСПОРТНИХ СВОЈСТАВА ТРОЈНИХ ОРГАНСКИХ НЕЕЛЕКТРОЛИТНИХ СИСТЕМА, УКЉУЧУЈУЋИ ВОДУ, ПОМОЋУ ПОЛИНОМА

БОЈАН Д. ЂОРЂЕВИЋ, МИРЈАНА Љ. КИЈЕВЧАНИН, ИВОНА Р. РАДОВИЋ, СЛОБОДАН П. ШЕРБАНОВИЋ и АЛЕКСАНДАР Ж. ТАСИЋ

Технолошко–металуршки факултет, Универзитет у Београду, Карнегијева 4, 11120 Београд

У овом прегледном раду је дат опис и предсказивање термофузичких и транспортних својстава тројних органских неелектролитних система, укључујући и воду помоћу полинома. Емпиријске једначине Радојковића и сар. (односно Redlich–Kister), Kohlera, Jacob–Fitznera, Colineta, Tsao–Smitha, Toopa, Scatcharda и сар. и Rastogia и сар. су поређене са расположивим експерименталним подацима објављеним у познатим међународним часописима (*Fluid Phase Equilibria*, *Journal of Chemical and Engineering Data*, *Journal of Chemical Theromodynamics*, *Journal of Solution Chemistry*, *Journal of the Serbian Chemical Society*, *The Canadian Journal of Chemical Engineering*, *Journal of Molecular Liquids*, *Thermochimica Acta* и др.). Применљивост емпиријских модела на одређивање допунске моларне запремине, V^{E}, допунских вискозности, $\Delta\eta$, допунске слободне енергије активације вискозног тока, $\Delta G^{*\mathrm{E}}$, промене моларне рефракције мешања, ΔR, промене индекса рефракције при мешању, Δn_{D}, промене изентропске компресибилности, $\Delta\kappa_{\mathrm{s}}$, одступање површинског напона, $\Delta\sigma$, одступање брзине звука, Δu, и одступање релативне пермитивности, $\sigma\varepsilon_{\mathrm{r}}$, проверена је на серији тројних смеша врло сложене структуре које су и елементарно описане. Добијени резултати предсказивања су продискутовани и дате су извесне препоруке за коришћење симетричних и несиметричних модела и могућој успешној примени на смеше.

(Примљено 30. јануара, ревидирано 4. марта 2013)

REFERENCES

1. J. W. McCargar, W. E. Acree, *Thermochim. Acta* **149** (1989) 363
2. C. Pando, J. A. R. Renuncio, J. A. G. Calzon, J. J. Christensen, R. M. Izatt, *J. Solution Chem.***16** (1987) 503
3. O. Redlich, A. Kister, *Ind. Eng. Chem.* **40** (1948) 345
4. M. Hillert, *Ber. Bunsenges. Phys. Chem*. **87** (1983) 762
5. N. Radojković, A. Tasić, D. Grozdanić, B. Djordjević, D. Malić, *J. Chem. Thermodyn.* **9** (1977) 349
6. F. Kohler, *Monatsh. Chem*. **91** (1960) 738
7. K. T. Jacob, K. Fitzner, *Thermochim. Acta* **18** (1977) 197
8. C. Colinet, *PhD The*sis, University of Grenoble, France, 1967
9. C. C. Tsao, J. M. Smith, *Chem. Eng. Prog. Symp. Series* **49** (1953) 107
10. G. W. Toop, *Trans. TMS-AIME* **233** (1965) 850
11. A. D. Pelton, *Calphad* **25** (2001) 319
12. G. Scatchard, L. B. Ticknor, J. R. Goates, E. R. McCartney, *J. Am. Chem. Soc.* **74** (1952) 3721
13. R. P. Rastogi, J. Nath, S. S. Das, *J. Chem. Eng. Data* **22** (1977) 249
14. B. Lark, S. Kaur, S. Singh, *Indian. J. Chem., A* **26** (1987) 1109
15. M. Hillert, *Calphad* **4** (1980) 1
16. Y. M. Muggianu, M. Gambino, J. P. Bros, *J. Chim. Phys.* **72** (1975) 83
17. J. B. Knobeloch, C. E. Schwartz, *J. Chem. Eng. Data* **7** (1982) 386

18. W. E. Acree Jr., A. I. Zvaigzne, P. E. Naidu, *Phys. Chem. Liq.* **27** (1994) 69
19. A. R. Mathieson, J. C. J. Thynne, *J. Chem. Soc*. (1956) 3708
20. G.-H. Zhang,L.-J. Wang, K.-C. Chou, *Calphad* **34** (2010) 504
21. H. Ilonkhani, K. Khanlarzadch, *J. Chem. Eng. Data* **56** (2011) 4244
22. H.-D. Kim, I.-C. Hwang, S.-J. Park, *J. Chem. Eng. Data* **55** (2010) 2474
23. P. K. Talley, J. Sangster, A. D. Pelton, Ch. W. Bale, *Calphad* **16** (1992) 93
24. P. K. Talley, J. Sangster, Ch. W. Bale, A. D. Pelton, *Fluid Phase Equilib*. **85** (1993) 101
25. K.-C. Chou, *Calphad* **19** (1995) 315
26. K.-C. Chou, W.-C. Li, F. Li, M. He, *Calphad* **20** (1996) 395
27. X.-M. Zhong, K.-C. Chou, Y. Gao, X. Guo, X. Lan, *Calphad* **25** (2001) 455
28. D. Živković, Ž. Živković, I. Tasić, *Thermochim. Acta* **362** (2000) 113
29. D. Manasijević, D. Živković, Ž. Živković, *Calphad* **27** (2003) 361
30. L. Yan, S. Zheng, G. Ding, G. Xu, Z. Qiao, *Calphad* **31** (2007) 112
31. L. Wang, K.-C. Chou, S. Seetharaman, *Calphad* **32** (2008) 49
32. Z. Atik, K. Lourdani, *J. Solution Chem.* **35** (2006) 1453
33. Z. Atik, K. Lourdani, *J. Chem. Thermodyn.* **39** (2007) 576
34. A. Arce, J. Martinez-Ageitos, E. Rodil, A. Soto, *Fluid Phase Equilib.* **165** (1999) 121
35. A. Arce, E. Rodil, A. Soto, *J. Chem. Eng. Data* **42** (1997) 721
36. A. Arce, E. Rodil, A. Soto, *J. Chem. Eng. Data* **46** (2001) 962
37. A. Arce, E. Rodil, A. Soto, *J. Chem. Eng. Data* **44** (1999) 1028
38. A. Arce, J. Martinez-Ageitos, E. Rodil, A. Soto, *Fluid Phase Equilib.* **187**–**188** (2001) 155
39. A. Arce, E. Pardillo, E. Rodil, A. Soto, *J. Chem. Eng. Data* **44** (1999) 291
40. A. G. Camacho, M. A. Postigo, G. C. Pedrosa, I. L. Acevedo, M. Katz, *Can. J. Chem.* **78** (2000) 1121
41. M. Postigo, A. Mariano, L. Mussari, A. Camacho, J. Urieta, *Fluid Phase Equilib*. **207** (2003) 193
42. A. Mariano, M. Postigo, *Fluid Phase Equilib.* **239** (2006) 146
43. R. L. Gardas, S. Oswal, *Thermochim. Acta* **479** (2008) 17
44. R. L. Gardas, S. Oswal, *J. Solution Chem.* **37** (2008) 1449
45. M. Lj. Kijevčanin, I. R. Radović, S. P. Šerbanović, A. Ž. Tasić, B. D. Djordjević, *Thermochim. Acta* **496** (2009) 71
46. M. Dominguez, I. Gascon, A. Valen, F. M. Royo, J. S. Urieta, *J. Chem. Thermodyn.* **32** (2000) 1551
47. R. K. Kwon, J. I. Kim, S. J. Park, Y. Y. Choi, *Fluid Phase Equilib.* **324** (2012) 44
48. S. L. Oswal, N. Y. Ghael, R. L. Gardas, *Thermochim. Acta* **484** (2009) 11
49. N. Y. Ghael, R. L. Gardas, S. L. Oswal, *Thermochim. Acta* **491** (2009) 447
50. H. Casas, S. Garcia-Garabal, L. Segade, O. Cabeza, C. Franjo, E. Jimenez, *J. Chem. Thermodyn.* **35** (2003) 1129
51. H. Casas, L. Segade, O. Cabeza, C. Franjo, E. Jimenez, *J. Chem. Eng. Data* **46** (2001) 651
52. J. H. Oh, I. C. Hwang, S. J. Park, *Fluid Phase Equilib*. **276** (2009) 142
53. M. D. Pérez, S. Freire, J. Jimenez de Llano, E. Rilo, L. Segade, O. Cabeza, E. Jimenez, *Fluid Phase Equilib*. **212** (2003) 331
54. H. Casas, L. Segade, C. Franjo, E. Jimenez, M. Inmaculada Paz Andrade, *J. Chem. Eng. Data* **43** (1998) 756
55. P. Bahadur, N. V. Sastry, *Inter. J. Thermophys.* **24** (2003) 447
56. N. V. Sastry, S. R. Patel, S. S. Soni, *J. Chem. Eng. Data* **56** (2011) 142

57. N. V. Sastry, M. C. Patel, R. R. Thakor, S. S. Soni, *J. Mol. Liq.* **157** (2010) 25
58. M. Iglesias, M. M. Pineiro, G. Marino, B. Orge, M. Dominguez, J. Tojo, *Fluid Phase Equilib*. **154** (1999) 123
59. K. Prasad, K. S. Kumar, G. Prabhakar, P. Venkateswarlu, *J. Mol. Liq.* **123** (2006) 51
60. K. J. Han, J. H. Oh, S. J. Park, J. Gmehling, *J. Chem. Eng. Data* **50** (2005) 1951
61. S. Aznarez, M. A. Postigo, G. C. Pedrosa, I. L. Acevedo, M. Katz, *J. Solution Chem.* **27** (1998) 949
62. M. Iglesias, B. Orge, J. Tojo, *J. Chem. Eng. Data* **41** (1996) 218
63. M. Iglesias, B. Orge, J. Tojo, *Fluid Phase Equilib.* **126** (1996) 203
64. Z. Atik, *J. Solution Chem.* **33** (2004) 1447
65. M. J. Souza, E. Jimenez, J. L. Legido, J. Fernandez, E. Perez Martell, M. I. Paz Andrade, *J. Chem. Thermodyn.* **24** (1992) 119
66. C. P. Menaut, J. M. Pico, E. Jiménez, C. Franjo, L. Segade, M. I. Paz Andrade, *Fluid Phase Equilib.* **142** (1998) 185
67. A. Rodriguez, J. Canosa, J. Tojo, *J. Chem. Eng. Data* **44** (1999) 1298
68. B. D. Djordjević, S. P. Šerbanović, I. R. Radović, A. Ž. Tasić, M. Lj. Kijevčanin, *J. Serb. Chem. Soc.* **72** (2007) 1437
69. M. Lj. Kijevčanin, S. P. Šerbanović, I. R. Radović, B. D. Djordjević, A. Ž. Tasić, *Fluid Phase Equilib.* **251** (2007) 78
70. J. D. Smiljanić, M. Lj. Kijevčanin, B. D. Djordjević, D. K. Grozdanić, S. P. Šerbanović, *Int. J. Therophys.* **29** (2008) 586
71. M. Dominguez, J. Pardo, J. Santafe, F. M. Royo, J. S. Urieta, *Fluid Phase Equilib.* **118** (1996) 227
72. P. Lillo, L. Mussari, M. A. Postigo, *J. Solution Chem.* **29** (2000) 183
73. J.-I. Kim, Y.-Y. Choi, S.-I. Park, *J. Chem. Eng. Data* **55** (2010) 1179
74. J. S. Matos, J. L. Trenzado, E. Gonzalez, R. Alcalde, *Fluid Phase Equilib.* **186** (2001) 207
75. J. L. Trenzado, J. S. Matos, R. Alcalde, *Fluid Phase Equilib.* **200** (2002) 295
76. J. S. Matos, J. L. Trenzado, R. Alcalde, *Fluid Phase Equilib.* **202** (2002) 133
77. J. L. Trenzado, J. S. Matos, R. Alcalde, *Fluid Phase Equilib.* **205** (2003) 171
78. K.-J. Han, I.-C. Hwang, S.-J. Park, I.-H. Park, *J. Chem. Eng. Data* **52** (2007) 1018
79. H.-Y. Kwak, J.-H. Oh, S.-J. Park, K.-Y. Paek, *Fluid Phase Equilib.* **262** (2007) 161
80. J.-Y. Lee, I.-C. Hwang, S.-J. Park, S.-J. In, *J. Chem. Eng. Data* **55** (2010) 864
81. I.-C. Hwang, J.-Y. Lee, S.-J. Park, *Fluid Phase Equilib.* **281** (2009) 5
82. K.-J. Han, J.-H. Oh, S.-J. Park, *J. Chem. Eng. Data* **51** (2006) 1339
83. S. J. Kharat, P. S. Nikam, *J. Mol. Liq.* **131–132** (2007) 81
84. P. S. Nikam, S. J. Kharat, *J. Chem. Eng. Data* **48** (2003) 1202
85. Z. Atik, *J. Mol. Liq.* **163** (2011) 89
86. H. D. Kim, I. C. Hwang, S. J. Park, *J. Chem. Eng. Data* **55** (2010) 2474
87. J. Y. Lee, S. J. Park, *Can. J. Chem. Eng.* **90** (2012) 396
88. J. S. Matos, J. L. Trenzado, E. Romano, M. N. Caro, M. E. Perez, *J. Solution Chem.* **30** (2001) 263
89. H. Iloukhani, M. Rakhshi, *J. Mol. Liq.* **149** (2009) 86
90. X. Esteve, K. R. Patil, J. Fernandez, A. Coronas, *J. Chem. Thermodyn.* **27** (1995) 281
91. F. Olive, S. K. Chaudhari, K. R. Patil, A. Coronas, *Can. J. Chem. Eng.* **74** (1996) 163
92. A. Rodriguez, J. Canosa, B. Orge, M. Iglesias, J. Tojo, *J. Chem. Eng. Data* **41** (1996) 1446
93. J. M. Canosa, A. Rodriguez, M. Iglesias, B. Orge, J. Tojo, *J. Chem. Thermodyn.* **29** (1997) 907

94. J. Canosa, A. Rodriguez, A. Rodriguez, B. Orge, M. Iglesias, J. Tojo, *J. Chem. Eng. Data* **42** (1997) 1121
95. M. Iglesias, B. Orge, J. M. Canosa, A. Rodriguez, M. Dominguez, M. M. Pineiro, J. Tojo, *Fluid Phase Equilib.* **147** (1998) 285
96. P. Venkatesu, M. V. Prabhakara Rao, *J. Chem. Eng. Data* **42** (1997) 90
97. H. Iloukhani, K. Khanlarzadeh, *J. Chem. Thermodyn.* **48** (2012) 235.

Journal of the Serbian Chemical Society
JSCS-info@shd.org.rs • www.shd.org.rs/JSCS
J. Serb. Chem. Soc. 78 (8) 1119–1125 (2013) UDC 542.913:547.752+547.791+547–304.9
JSCS–4483 *Original scientific paper*

Synthesis of new functionalized derivatives of 1,2,4-triazolo[4′,3′:2,3][1,2,4]triazino[5,6-*b*]indole

SOBHI M. GOMHA[1]* and HATEM A. ABDEL-AZIZ[2]

[1]*Department of Chemistry, Faculty of Science, Cairo University, Giza, Egypt and* [2]*Department of Pharmaceutical Chemistry, College of Pharmacy, King Saud University, P. O. Box 2457, Riyadh 11451, Saudi Arabia*

(Received 14 September, revised 3 October 2012)

Abstract: New functionalized 1,2,4-triazolo[4′,3′:2,3][1,2,4]triazino[5,6-*b*]indole derivatives were synthesized *via* reaction of the hydrazonoyl halides with 2,4-dihydro-3*H*-1,2,4-triazino[5,6-*b*]indole-3-thione or its 3-methylthio derivative. The mechanism and the regioselectivity of the studied reactions are discussed.

Keywords: hydrazonoyl halides; 1,2,4-triazino[5,6-*b*]indole-3-thione; hydrazonothioates.

INTRODUCTION

As a continuation of systematic studies of hydrazonoyl halides devoted to the various aspects of their chemistry,[1–6] it was decided to investigate their use as precursors in the synthesis of the title compounds. In the present contribution, the synthesis is reported of a series of new functionalized derivatives of 1,2,4-triazolo[4′,3′:2,3][1,2,4]triazino[5,6-*b*]indole *via* the reaction of the respective hydrazonoyl halides **5** with either 2,4-dihydro-3*H*-1,2,4-triazino[5,6-*b*]indole-3-thione **3** or its 3-methylthio derivative. The regiochemistry of the reactions studied and the antimicrobial activity of the products isolated from such reactions were investigated.

The interest in synthesis of the target compounds is due to the fact that various derivatives of the 5*H*-1,2,4-triazino[5,6-*b*]indoles have aroused considerable interest as a result of their broad spectrum of antibacterial, antifungal, antiparasitic activities and antihypertensive properties.[7–12] Considerable attention has been drawn to the synthesis of several condensed heterocyclic systems derived from triazoles and triazines.[13–18] Furthermore, some triazolo-1,2,4-triazino[5,6-

* Corresponding author. E-mail: s.m.gomha@hotmail.com
doi: 10.2298/JSC120914013G

-*b*]indoles were reported to have medicinal applications, such as antiviral, antibacterial and antimalarial activities.[19–22]

RESULTS AND DISCUSSION

The starting 2,4-dihydro-3*H*-1,2,4-triazino[5,6-*b*]indole-3-thione **3** or its 3-methylthio derivative **4**[23] were prepared by literature methods (Scheme 1). Reaction of **3** or **4** with **5** was realized in chloroform in the presence of triethylamine under stirring at room temperature. In all cases, hydrogen sulfide was evolved during the course of the reaction and so stirring of the reaction mixture was continued until evolution of hydrogen sulfide ceased. Work-up of the reaction mixture afforded, in each case, one isolable product as evidenced by TLC analysis of the crude product. Elemental analyses and IR, ^{1}H- and ^{13}C-NMR spectroscopy, which showed all the expected signals (see the Supplementary material to this paper), confirmed the structures of the prepared compounds. The regioselectivity of the reaction of **3** with **5** seems consistent with literature reports, which indicated that *N*-2 is the site of preference for cyclization, the isolated products were assigned the structure 1,2,4-triazolo[4′,3′:2,3][1,2,4]triazino[5,6-*b*]indole derivatives **8** rather than the isomeric structure **9**.[24–26]

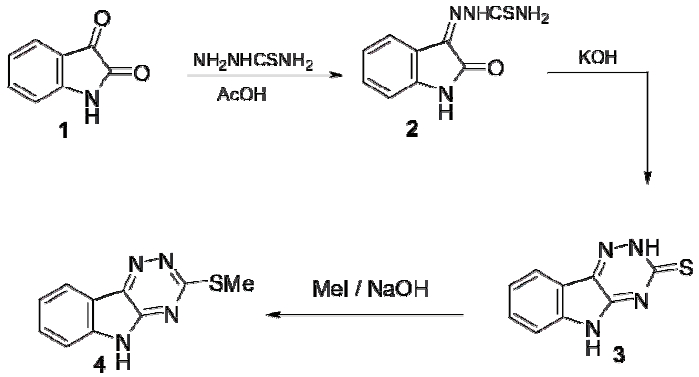

Scheme 1. Synthesis of 5*H*-2,3-dihydro-1,2,4-triazino[5,6-*b*]indole-3-thione (**3**) and its 3-methylthio derivative **4**.

The assignment of structure **8** was further evidenced by an alternate synthesis. Thus, treatment of 2-methylthio derivative **4** with each of the hydrazonoyl halides **5** in chloroform in the presence of triethylamine at room temperature resulted in the evolution of methanethiol and the formation of products that proved identical in all respects (IR, MS, m.p. and mixed m.p.) with **8** (Scheme 2).

Formation of compounds **8** from the thione **3** and hydrazonoyl halides **5** could be accounted for by the hydrazonoylation of **3** to give the hydrazonothioate esters **6**. This is followed by Smiles type rearrangement[27] of the latter esters to form the respective thiohydrazides **6A**, which in turn underwent cyclization to

give **8** as the end products (Scheme 2). Under the employed reaction conditions, it seems that both intermediates **6** and **6A** are consumed immediately after formation since all attempts to isolate them failed.

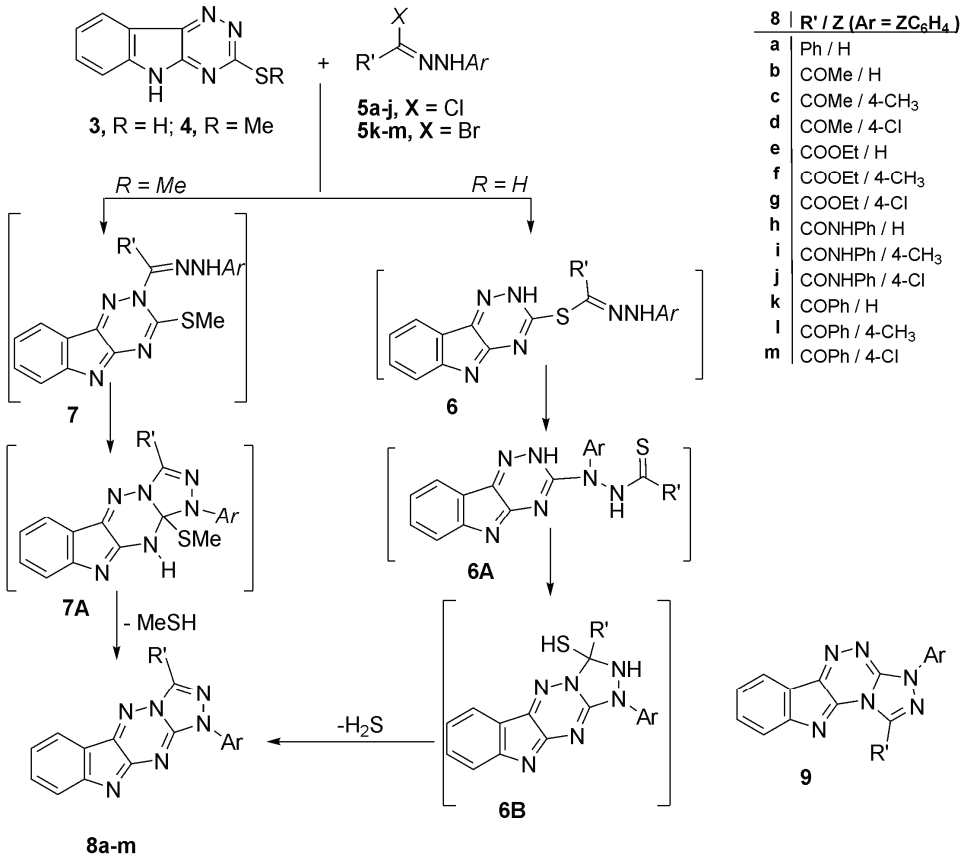

Scheme 2. Synthesis of 1,2,4-triazolo[4′,3′:2,3][1,2,4]triazino[5,6-*b*]indole derivatives **8a**–**m**.

The involvement of **6** and **6A** as intermediates in the formation of **8** was evidenced by alternate synthesis of **8b**, **8e** and **8h** (Scheme 2). Thus, treatment of **3** with each of 3-chloro-2,4-pentanedione, ethyl *α*-chloroacetoacetate and *α*-chloroacetoacetanilide in ethanol in the presence of sodium ethoxide afforded the respective substituted products **11b**, **11e** and **11h**. Coupling of each of the latter with benzenediazonium chloride in ethanol in the presence of sodium acetate yielded the thiohydrazonates **6b**, **6e** and **6h**, respectively (Scheme 3), *via* Japp–Klingemann cleavage of the acetyl group.[28] Treatment of the latter products **7** with sodium ethoxide in ethanol afforded the respective compounds **8b**, **8e** and **8h**, which were identical in all respects with those obtained from the reactions of **3** with each of **5b**, **5e** and **5h**, respectively. These findings indicate that **6** and **6A**

are intermediates in the studied reactions of **3** with **5** and that they are consumed as soon as they are formed under the employed reaction conditions.

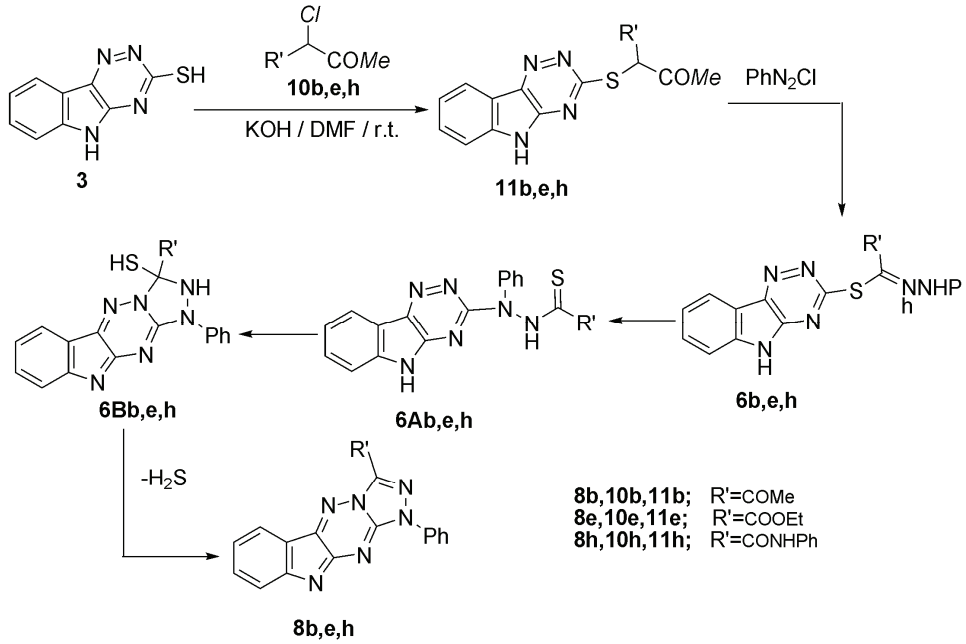

Scheme 3. Alternate synthesis of 1,2,4-triazolo[4′,3′:2,3][1,2,4]triazino[5,6-*b*]indole derivatives **8a**–**m**.

EXPERIMENTAL

Melting points were determined on a Gallenkamp apparatus and are uncorrected. The IR spectra were recorded in potassium bromide using a Pye-Unicam SP300 spectrophotometer. The ^{1}H- and ^{13}C-NMR spectra were recorded in DMSO-d_6 using a Varian Gemini 300 NMR spectrometer (300 MHz for ^{1}H-NMR and 75 MHz for ^{13}C-NMR) and the chemical shifts were related to that of the solvent DMSO-d_6. The mass spectra were recorded on GCMS-Q1000-EX Shimadzu and GCMS 5988-A HP spectrometers, the ionizing voltage was 70 eV. Elemental analyses of the products were performed at the Microanalytical Centre of Cairo University, Giza, Egypt. 2,4-Dihydro-3*H*-1,2,4-triazino[5,6-*b*]indole-3-thione **3** and its 3-methylthio derivative **4**[24] and the hydrazonoyl halides **5**[28–34] were prepared as described in the literature.

*General procedure for the synthesis of 1,2,4-triazolo[4′,3′:2,3][1,2,4]triazino[5,6-*b*]indole derivatives (**8a**–**m**)*

Method A. To a mixture of 2,4-dihydro-3*H*-1,2,4-triazino[5,6-*b*]indole-3-thione **3** (2.02 g, 0.01 mol) and an appropriate hydrazonoyl halide (**5**) (0.01 mol) in chloroform (40 mL), triethylamine (1.4 mL, 0.01 mol) was added. The reaction mixture was stirred at room temperature until cessation of H_2S evolution (4–6 h). The solvent was evaporated and the residue was treated with an ice/ HCl mixture. The solid product was collected, washed with water and crystallized from the appropriate solvent to give the respective derivatives **8**.

Method B. To a solution of 3-(methylthio)-5*H*-1,2,4-triazino[5,6-*b*]indole (**4**) (3.9 g, 0.01 mol) in chloroform (30 mL) containing triethylamine (1.4 mL, 0.01 mol), the appropriate hydrazonoyl halide (**5**) was added (0.01 mol) and the resulting solution was stirred at room temperature overnight. The product was collected, washed with water and crystallized from an appropriate solvent to give the respective products **8**, which are identical in all respects (m.p., mixed m.p. and IR) to those prepared by method A.

Method C. To a stirred ethanolic sodium ethoxide solution, prepared from Na metal (0.23 g, 10 mg atom) and absolute ethanol (20 mL), was added each of the compound **6b**, **6e** and **6h** (10 mmol) and the reaction mixture was stirred at room temperature for 12 h, during which time, the starting reactants **6** dissolved and the crude products precipitated. The latter was filtered, washed with H_2O, dried and finally crystallized from the appropriate solvent to give products, identified as **8b**, **8e** and **8h**, respectively. The latter products proved to be identical in all respects (m.p., mixed m.p. and IR) with those obtained from **3** and the respective hydrazonoyl halides **5**.

*Synthesis of the hydrazonothioates (**6**)*

To a solution of each of **8b**, **8e** and **8h** (10 mmol) in ethanol (40 mL) was added sodium acetate trihydrate (1.38 g, 10 mmol) and the mixture was cooled to 0–5 °C in an ice bath. To the resulting cold solution was added portionwise a cold solution of benzenediazonium chloride, prepared by diazotizing aniline (10 mmol) dissolved in 6 mL HCl (6 M) with a solution of sodium nitrite (0.7 g, 10 mmol) in 10 cm^3 H_2O. After complete addition of the diazonium salt, the reaction mixture was stirred for a further 12 h at room temperature. The solid precipitate was filtered off, washed with water, dried and crystallized from the appropriate solvent to give the respective pure **6b**, **6e** and **6h**.

*Reactions of **3** with active chloromethylene compounds*

To a solution of **3** (2.02 g, 0.01 mol) in chloroform was added triethylamine (1.4 mL, 0.01 mol) and the mixture was stirred for 10 min at room temperature. To the resulting clear solution was added an active chloromethylene compound (0.01 mol) drop-wise under stirring. After complete addition, the reaction mixture was stirred for further 24 h at room temperature. The solid that precipitated was filtered off, washed with H_2O, dried and finally crystallized from the appropriate solvent to give pure **11b**, **11e** and **11h**.

CONCLUSION

In summary, the reactivity of 2,4-dihydro-3*H*-1,2,4-triazino[5,6-*b*]indole-3--thione or its 3-methylthio derivative is a versatile and readily accessible building block for the synthesis of new 1,2,4-triazolo[4′,3′:2,3][1,2,4]triazino[5,6-*b*]indole derivatives.

SUPPLEMENTARY MATERIAL

Analytic and spectral data of the prepared compounds are available electronically from http://www.shd.org.rs/JSCS/, or from the corresponding author on request.

ИЗВОД

СИНТЕЗА НОВИХ ФУНКЦИОНАЛИЗОВАНИХ ДЕРИВАТА 1,2,4-ТРИАЗОЛО[4′,3′:2,3][1,2,4]ТРИАЗИНО[5,6-*b*]ИНДОЛА

SOBHI M. GOMHA[1] и HATEM. A. ABDEL-AZIZ[2]

[1]Department of Chemistry, Faculty of Science, Cairo University, Giza, Egypt и [2]Department of Pharmaceutical Chemistry, College of Pharmacy, King Saud University, P.O. Box 2457, Riyadh 11451, Saudi Arabia

Нови функционализовани деривати 1,2,4-триазоло[4′,3′:2,3][1,2,4]триазино[5,6-*b*]индола синтетисани су реакцијом хидразоноил-халогенида и 2,4-дихидро-3*H*-1,2,4-триазино[5,6-*b*]индол-3-тиона или одговарајућег 3-метилтио деривата. У раду су разматрани механизам и региоселективност испитиваних реакција.

(Примљено 14. септембра, ревидирано 3. октобра 2012)

REFERENCES

1. A. S. Shawali, S. M. Gomha, *J. Pract. Chem.* **342** (2000) 599
2. S. M. Gomha, *Monatsh. Chem.* **140** (2009) 213
3. I. M. Abbas, S. M. Riyadh, M. A. Abdallah, S. M. Gomha, *J. Heterocycl. Chem.* **43** (2006) 935
4. A. S. Shawali, S. M. Gomha, *Tetrahedron* **58** (2002) 8559
5. S. M. Gomha, H. M. E. Hassaneen, *Molecules* **16** (2011**)** 6549
6. S. M. Gomha, S. M. Riyadh, *ARKIVOC* (2009) 58
7. V. J. Ram, *Arch. Pharm.* **313** (1980) 108
8. J. M. Gwaltney, *Proc. Soc. Exp. Biol. Med.* **133** (1970) 1148
9. J. M. Z. Gladych, R. Hornby, J. Hunt, D. Jack, J. J. Boyle, R. J. Ferlauto, R. Haff, C. Kormendy, F. Stanfield, R. Stewart, *J. Med. Chem.* **15** (1972) 277
10. R. F. Haff, J. J. Boyle, R. Stewart, R. Ferlando, J. M. Z. Gladych, J. Hunt, D. Jack, *Nature* **221** (1969) 286
11. J. M. Z. Gladych, R. Hornby, J. H. Hunt, D. Jack, J. J. Boyle, R. J. Ferlauto, R. F. Haff, C. G. Kormendy, F. J. Stanfield, R. C. Stewart, *J. Med. Chem.* **15** (1972) 277
12. J. M. Gwaltney, *Proc. Soc. Exp. Biol. Med.* **133** (1970) 1148
13. R. Mardronero, S. Vega, *J. Heterocycl. Chem.* **15** (1978) 1127
14. S. W. Schneller, D. G. Barthdomew, *J. Heterocycl. Chem.* **15** (1978) 439
15. E. J. Gray, M. F. G. Stevens, *J. Chem. Soc., Perkin Trans. 1* (1977) 1492
16. M. Robba, D. Maume, J. C. Lancelot, *J. Heterocycl. Chem.* **15** (1978) 1209
17. K. C. Joshi, A. Dandi, S. Baweia, *J. Indian Chem. Soc.* **66** (1989) 690
18. M. I. Younes, H. H. Abbas, S. A. Metwally, *Arch. Pharm. (Weinheim)* **320 (**1987) 1191
19. A. Dorn, S. R. Vippagunta, H. Matile, C. Jaquet, J. L. Vennerstrom, R. G. Ridley, *Biochem. Pharmacol.* **55** (1998) 727
20. T. J. Egan, D. C. Ross, P. A. Adams, *Afr. J. Sci.* **92** (1996) 11
21. C. D. Fitch, R. Chevli, H. S. Banyal, G. Phillips, M. A. Pfaller, D. J. Krogstad, *Antimicrob. Agents Chemother.* **21**(1982) 819
22. P. A. Adams, P. A. M. Berman, T. J. Egan, P. J. Marsh, J. J. Silver, *Inorg. Biochem.* **63** (1996) 69
23. J. Mohan, G. S. R. Anjaneyulu, D. Kiran, *Indian J Chem.* **27B** (1988) 346
24. V. J. Ram, V. Dube, A. Vlietinck, *J. Heterocycl. Chem.* **24** (1987) 1435
25. F. F. Abdel-Latif, R. M. Shaker, M. Mahgoub, Z. A. A. Bader, *J. Heterocyl. Chem.* **26** (1989) 769

26. E. S. H. El Ashry, N. Rashed, H. Abdel-Hamid, E. S. Ramadan, *Z. Naturforsch., B* **52** (1997) 873
27. K. Ishii, M. Hatanaka, I. Ueda, *Chem. Pharm. Bull.* **39** (1991) 3331
28. A. S. Shawali, A. O. Abdelhamid *Bull. Chem. Soc. Jpn.* **49** (1976) 321
29. P. Wolkoff, *Can. J. Chem*. **53** (1975) 1333
30. C. Bullow, E. King, *Liebigs Ann.* **439** (1924) 211
31. G. Favrel, *Bull. Soc. Chim. Fr*. **31** (1904) 150
32. W. Dieckmann, O. Platz, *Ber. Dtsch. Chem. Ges*. **38** (1906) 2989
33. H. M. Hassaneen, A. S. Shawali, N. M. Abunada, *Org. Prep. Proced. Int.* **24** (1992) 171
34. T. Curtius, *J. Prakt. Chem.* **51** (1899) 168.

Journal of the Serbian Chemical Society
JSCS@tmf.bg.ac.rs • www.shd.org.rs/JSCS
J. Serb. Chem. Soc. 78 (8) S86–S90 (2013) *Supplementary material*

SUPPLEMENTARY MATERIAL TO

Synthesis of new functionalized derivatives of 1,2,4-triazolo[4′,3′:2,3][1,2,4]triazino[5,6-*b*]indole

SOBHI M. GOMHA[1]* and HATEM A. ABDEL-AZIZ[2]

[1]*Department of Chemistry, Faculty of Science, Cairo University, Giza, Egypt and* [2]*Department of Pharmaceutical Chemistry, College of Pharmacy, King Saud University, P. O. Box 2457, Riyadh 11451, Saudi Arabia*

J. Serb. Chem. Soc. 78 (8) (2013) 1119–1125

ANALYTIC AND SPECTRAL DATA OF THE PREPARED COMPOUNDS

*(2*H*-1,2,4-Triazino[5,6-*b*]indol-3-yl)2-oxo-*N*-phenyl propanehydrazonothioate (**6b**)*. Yield: 75 %; m.p.: 236 °C (EtOH); Anal. Calcd. for $C_{18}H_{14}N_6OS$ (FW: 362): C, 59.32; H, 3.76; N, 22.87 %. Found: C, 59.11; H, 3.56; N, 22.56 %; IR (KBr, cm^{-1}): 3423, 3288 (2NH), 1697 (CO); ^{1}H-NMR (300 MHz, DMSO-d_6, δ / ppm): 2.70 (3H, *s*), 6.76–8.12 (9H, *m*, ArH), 10.34 (1H, *s*), 11.51 (1H, *s*); ^{13}C--NMR (75 MHz, DMSO-d_6, δ / ppm): 178.6 (COPh), 158.2, 155.3, 152.1, 149.2, 143.2, 136.8, 136.2, 134.0, 133.9,131.2, 130.8, 129.6, 125.7, 123.4, 24.3; MS (*m*/*z* (relative abundance, %)): 362 (M^+, 19), 279 (34), 129 (46), 77 (100).

*Ethyl 2-(phenylhydrazono)-2-(2*H*-1,2,4-triazino[5,6-*b*]indol-3-ylthio)-acetate (**6e**)*. Yield: 80 %; m.p.: 218 °C (DMF); Anal. Calcd. for $C_{19}H_{16}N_6O_2S$ (FW: 392): C, 58.01; H, 3.91; N, 21.127 %. Found: C, 57.86; H, 3.87, N; 21.00 %; IR (KBr, cm^{-1}): 3433, 3318 (2NH), 1723 (CO); ^{1}H-NMR (300 MHz, DMSO--d_6, δ / ppm): 1.33 (3H, *t*, *J* = 7.1 Hz), 4.43 (2H, *q*, *J* = 7.1 Hz), 6.87–8.31 (9H, *m*, ArH), 10.31 (1H, *s*), 11.21 (1H, *s*); ^{13}C-NMR (75 MHz, DMSO-d_6, δ / ppm): 164.5 (CONHPh), 155.4, 156.4, 150.3, 146.3, 143.8, 137.6, 136.0, 135.3, 132.5, 131.9, 131.4, 130.4, 128.4, 126.3, 126.1, 123.6, 120.5, 118.9; MS (*m*/*z* (relative abundance, %)): 392 (M^+, 9), 235 (17), 131 (79), 103 (92), 77 (100).

*(2*H*-1,2,4-Triazino[5,6-*b*]indol-3-yl)2-oxo-*N*-phenyl 2-(phenylamino)ethanehydrazonothioate (**6h**)*. Yield: 70 %; m.p.: 254 °C (EtOH); Anal. Calcd. for $C_{32}H_{17}N_7OS$ (FW: 439): C, 62.59; H, 3.78; N, 15.98 %. Found: C, 62.46; H, 3.85; N, 15.77 %; IR (KBr, cm^{-1}): 3440, 3376, 3263 (3NH), 1689 (CO); ^{1}H--NMR (300 MHz, DMSO-d_6, δ / ppm): 6.88–8.18 (14H, *m*, ArH), 10.43 (1H, *s*), 11.04 (1H, *s*), 11.32 (1H, *s*); ^{13}C-NMR (75 MHz, DMSO-d_6, δ / ppm): 178.6

* Corresponding author. E-mail: s.m.gomha@hotmail.com

(COPh), 158.2, 155.3, 152.1, 149.2, 143.2, 136.8, 136.2, 134.0, 133.9, 131.2, 130.8, 129.6, 125.7, 123.4, 24.3; MS (*m*/*z* (relative abundance, %)): 439 (M^+, 100), 237 (33), 118 (26), 77 (45).

*1,3-Diphenyl-1*H-*1,2,4-triazolo[4′,3′:2,3][1,2,4]triazino[5,6-*b*]indole* (***8a***). Yield: 70 %; m.p.: 284 °C (DMF); Anal. Calcd. for $C_{22}H_{14}N_6$ (FW: 362): C, 72.46; H, 3.66; N, 22.89 %. Found: C, 72.26; H, 3.68; N, 22.42 %; ^{1}H-NMR (300 MHz, DMSO-d_6, δ / ppm): 6.64–8.20 (14H, *m*, ArH); ^{13}C-NMR (75 MHz, DMSO-d_6, δ / ppm): 158.5, 156.7, 153.3, 151.2, 149.3, 139.7, 138.7, 138.3, 134.4, 133.2, 133.1, 132.4, 132.1, 130.8, 127.8, 127.1, 125.7, 124.9; MS (*m*/*z* (relative abundance, %)): 362 (M^+, 38), 315 (17), 251 (11.8), 121 (30), 92 (70), 77 (100), 51 (64).

*1-(1-Phenyl-1H-1,2,4-triazolo[4′,3′:2,3][1,2,4]triazino[5,6-*b*]indol-3-yl)ethanone* (***8b***). Yield: 72 %; m.p.: 269 °C (DMF); Anal. Calcd. for $C_{18}H_{12}N_6O$ (FW: 328): C, 65.63; H, 3.59; N, 25.44 %. Found: C, 65.85; H, 3.46; N, 25.03 %; IR (KBr, cm^{-1}): 1693 (CO); ^{1}H-NMR (300 MHz, DMSO-d_6, δ / ppm): 2.74 (3H, *s*), 6.60–8.14 (9H, *m*, ArH); ^{13}C-NMR (75 MHz, DMSO-d_6, δ / ppm): 172.2 ($COCH_3$), 158.8, 155.4, 152.1, 151.2, 148.3, 139.8, 138.3, 134.4, 133.3, 132.4, 130.0, 128.8, 127.1, 124.7, 29.4; MS (*m*/*z* (relative abundance, %)): 328 (M^+, 100), 267 (25), 125 (62), 76 (66), 99 (41), 77 (28).

*1-[1-(4-Methylphenyl)-1H-1,2,4-triazolo[4′,3′:2,3][1,2,4]triazino[5,6-*b*]indol--3-yl]ethanone* (***8c***). Yield: 78 %; m.p.: 254 °C (DMF); Anal. Calcd. for $C_{19}H_{14}N_6O$ (FW: 342): C, 66.45; H, 4.09; N, 24.23 %. Found: C, 66.33; H, 4.02; N, 24.12 %; IR (KBr, cm^{-1}): 1703, (CO); ^{1}H-NMR (300 MHz, DMSO-d_6, δ / / ppm): 2.23 (3H, *s*), 2.57 (3H, s), 6.80–8.16 (4H, *m*, ArH), 7.62 (2H, *d*, J = 8 Hz), 7.81 (2H, *d*, J = 8 Hz); ^{13}C-NMR (75 MHz, DMSO-d_6, δ / ppm): 174.6 ($COCH_3$), 163.4, 158.2, 153.7, 150.8, 149.7, 142.3, 139.6, 137.6, 135.4, 134.2, 133.4, 129.2, 126.7, 122.5, 29.1, 18.4; MS (*m*/*z* (relative abundance, %)): 342 (M^+, 100), 259 (18), 118 (60), 90 (41), 77 (22).

*1-[1-(4-Chlorophenyl)-1H-1,2,4-triazolo[4′,3′:2,3][1,2,4]triazino[5,6-*b*]indol--3-yl]ethanone* (***8d***). Yield: 70 %; m.p.: 276 °C (DMF); Anal. Calcd. for $C_{18}H_{11}ClN_6O$ (FW: 362): C, 59.43; H, 3.17; N, 21.80 %. Found: C, 59.13; H, 3.06; N, 21.83 %; IR (KBr, cm^{-1}): 1693 (CO); ^{1}H-NMR (300 MHz, DMSO-d_6, δ / ppm): 2.64 (3H, s), 6.80–8.29 (4H, *m*, ArH), 7.74 (2H, d, J = 8 Hz), 7.84 (2H, *d*, J = 8 Hz); ^{13}C-NMR (75 MHz, DMSO-d_6, δ / ppm): 174.5 ($COCH_3$), 161.9, 159.8, 154.5, 151.2, 151.0, 139.9, 139.2, 135.7, 133.9, 133.6, 131.0, 129.9, 124.3, 120.4, 30.4; MS (*m*/*z* (relative abundance, %)): 364 (M^++2, 8.5), 363 (M^++1, 17), 362 (M^+, 26), 169 (57), 125 (62), 118 (85), 90 (55), 76 (66), 63 (98), 50 (100).

*Ethyl 1-phenyl-1H-1,2,4-triazolo[4′,3′:2,3][1,2,4]triazino[5,6-*b*]indole-3-carboxylate* (***8e***). Yield: 80 %; m.p.: 234 °C (DMF); Anal. Calcd. for $C_{19}H_{14}N_6O_2$ (FW: 358): C, 63.11; H, 3.68; N, 23.36 %. Found: C, 63.10; H, 3.42; N, 23.23 %;

IR (KBr, cm^{-1}): 1741 (CO); ^{1}H-NMR (300 MHz, DMSO-d_6, δ / ppm): 1.43 (3H, *t*, *J* = 7 Hz), 4.40 (2H, *q*, *J* = 7 Hz), 6.45–8.30 (9H, *m*, ArH); ^{13}C-NMR (75 MHz, DMSO-d_6, δ / ppm): 171.2 (COOEt), 155.1, 148.1, 142.4, 139.2, 138.1, 137.3, 136.0, 135.2, 134.1, 131.5, 130.3, 129.2, 128.1, 119.1, 53.3, 13.4; MS (*m*/*z* (relative abundance, %)): 358 (M^+, 9), 235 (50), 131 (79), 103 (92), 91 (40), 77 (100).

*Ethyl 1-(4-Methylphenyl)-1H-1,2,4-triazolo[4′,3′:2,3][1,2,4]triazino[5,6-*b*]indole-3-carboxylate (**8f**)*. Yield: 78 %; m.p.: 242 °C (DMF / H_2O); Anal. Calcd. for $C_{20}H_{16}N_6O_2$ (FW: 372): C, 64.31; H, 3.68; N, 23.36 %. Found: C, 63.10; H, 4.21; N, 22.30 %; IR (KBr, cm^{-1}): 1751 (CO); ^{1}H-NMR (300 MHz, DMSO-d_6, δ / ppm): 1.44 (3H, *t*, *J* = 7 Hz), 2.4 (3H, *s*), 4.43 (2H, *q*, *J* = 7 Hz), 6.69–8.26 (4H, *m*, ArH), 7.49 (2H, *d*, *J* = 8 Hz), 7.52 (2H, *d*, *J* = 8 Hz); ^{13}C-NMR (75 MHz, DMSO-d_6, δ / ppm): 170.6 (COOEt), 156.5, 148.8, 144.2, 139.9, 139.2, 137.7, 136.4, 136.9, 134.6, 133.1, 132.4, 127.6, 124.8, 119.6, 56.2, 18.8, 13.9; MS (*m*/*z* (relative abundance, %)): 372 (M^+, 100), 260 (50), 220 (17), 158 (12), 104 (14), 91 (40), 77 (32).

*Ethyl 1-(4-Chlorophenyl)-1H-1,2,4-triazolo[4′,3′:2,3][1,2,4]triazino[5,6-*b*]indole-3-carboxylate* (**8g**). Yield: 75 %; m.p.: 248 °C (DMF / H_2O); Anal. Calcd. for $C_{19}H_{13}ClN_6O_2$ (FW: 392): C, 57.92; H, 3.21; N, 21.14 %. Found: C, 57.76; H, 3.32; N, 20.84 %); IR (KBr, cm^{-1}): 1742 (CO); ^{1}H-NMR (300 MHz, DMSO-d_6, δ / ppm): 1.43 (3H, *t*, *J* = 7 Hz), 4.41 (2H, *q*, *J* = 7 Hz), 6.74–8.21 (4H, *m*, ArH), 7.74 (2H, *d*, *J* = 8 Hz), 8.11 (2H, *d*, *J* = 8 Hz); ^{13}C-NMR (75 MHz, DMSO-d_6, δ / ppm): 171.2 (COOEt), 158.8, 149.9, 146.4, 141.0, 139.4, 138.2, 137.6, 136.3, 135.6, 133.5, 133.1, 126.8, 124.8, 118.9, 55.6, 13.9; MS (*m*/*z* (relative abundance, %)): 394 (M^++2, 25), 393 (M^++1, 28), 392 (M^+, 70), 192 (21), 103 (92), 77 (100)

N,*1-Diphenyl-1H-1,2,4-triazolo[4′,3′:2,3][1,2,4]triazino[5,6-*b*]indole-3-carboxylate (**8h**)*. Yield: 75 %; m.p.: 236 °C (AcOH); Anal. Calcd. for $C_{24}H_{17}N_7O$ (FW: 419): C, 68.31; H, 3.87; N, 23.10 %. Found: C, 68.22; H, 3.80; N, 22.89 %; IR (KBr, cm^{-1}): 3256 (NH), 1673 (CO); ^{1}H-NMR (300 MHz, DMSO-d_6, δ / ppm): 6.80–8.20 (14H, *m*, ArH), 11.03 (1H, *s*, NH); ^{13}C-NMR (75 MHz, DMSO-d_6, δ / ppm): 163.2, 155.8, 155.7, 154.2, 149.1, 146.2, 143.3, 139.8, 139.2, 138.3, 129.8, 129.7, 129.1, 128.8, 128.3, 128.1, 125.5, 124.6, 120.5; MS (*m*/*z* (relative abundance, %)): 419 (M^+, 17), 551 (14), 287 (16), 201 (18), 119 (8), 91 (31), 77 (100).

1-(4-Methylphenyl)-N-*phenyl-1H-1,2,4-triazolo[4′,3′:2,3][1,2,4]triazino[5,6-*b*]indole-3-carboxylate (**8i**)*. Yield: 77 %; m.p. 260 °C (DMF); Anal. Calcd. for $C_{24}H_{17}N_7O$ (FW: 419): C, 68.51; H, 4.10; N, 23.10 %. Found: C, 68.31; H, 4.00; N, 22.90 %; IR (KBr, cm^{-1}): 3260 (NH), 1678 (CO); ^{1}H-NMR (300 MHz, DMSO-d_6, δ / ppm): 2.40 (3H, *s*), 6.72–8.28 (9H, *m*, ArH), 7.81 (2H, *d*, *J* = 8 Hz), 8.11 (2H, *d*, *J* = 8 Hz), 11.05 (1H, s); ^{13}C-NMR (75 MHz, DMSO-d_6, δ /

/ ppm): 162.4, 156.5, 156.2, 154.8, 150.3, 148.6, 144.5, 140.3, 139.7, 136.4, 131.8, 129.8, 129.0, 128.8, 128.3, 126.8, 124.6, 122.4, 120.5, 17.9; MS (*m*/*z* (relative abundance, %)): 419 (M^+, 10), 237 (11.4), 152 (13), 118 (100), 91 (43), 77 (93).

1-(4-Chlorophenyl)-N-*phenyl-1H-1,2,4-triazolo[4′,3′:2,3][1,2,4]triazino[5,6-*-b*]indole-3-carboxylate* ***(8j)***. Yield: 65 %; m.p.: 268 °C (DMF); Anal. Calcd. for $C_{23}H_{14}ClN_7O$ (FW: 439): C, 62.58; H, 3.01; N, 22.01 %. Found: C, 62.39; H, 3.23; N, 21.71 %; IR (KBr, cm^{-1}): 3249 (NH), 1662 (CO); ^{1}H-NMR (300 MHz, DMSO-d_6, δ / ppm): 6.72–8.20 (9H, *m*, ArH), 7.59 (2H, *d*, *J* = 8 Hz), 7.61 (2H, *d*, *J* = 8 Hz), 11.05 (1H, *s*); ^{13}C-NMR (75 MHz, DMSO-d_6, δ / ppm): 163.7, 156.8, 155.2, 154.7, 149.9, 147.0, 143.8, 140.1, 139.5, 138.7, 127.6, 126.2, 124.7, 124.3, 124.0, 123.8, 123.5, 120.6, 118.4; MS (*m*/*z* (relative abundance, %)): 441 (M^++2, 6), 440 (M^++1, 8), 439 (M^+, 19), 313 (10), 239 (11), 119 (19), 91 (29), 77 (100).

*Phenyl(1-phenyl-1H-1,2,4-triazolo[4′,3′:2,3][1,2,4]triazino[5,6-*b*]indol-3-yl)methanone* ***(8k)***. Yield: 75 %; m.p.: 282 °C (DMF); Anal. Calcd. for $C_{23}H_{14}N_6O$ (FW: 390): C, 70.44; H, 3.36; N, 21.35 %. Found: C, 63.10; H, 3.42; N, 23.23 %); IR (KBr, cm^{-1}): 1694 (CO); ^{1}H-NMR (300 MHz, DMSO-d_6, δ / / ppm): 6.89–8.30 (14H, *m*, ArH); ^{13}C-NMR (75 MHz, DMSO-d_6, δ / ppm): 176.6 (COPh), 156.3, 154.3, 152.1, 149.3, 146.2, 143.1, 139.8, 139.2, 138.3, 137.1, 134.2, 133.8, 132.8, 132.2, 131.3, 128.8, 127.1, 125.5; MS (*m*/*z* (relative abundance, %)): 390 (M^+, 20), 279 (12), 129 (17), 105 (8.4), 91 (7.1), 77 (100).

*[1-(4-Methylphenyl)-1*H-*1,2,4-triazolo[4′,3′:2,3][1,2,4]triazino[5,6-*b*]indol-3-yl)phenylmethanone* ***(8l)***. Yield: 77 %; m.p.: 276 °C (DMF); Anal. Calcd. for $C_{24}H_{16}N_6O$ (FW: 404): C, 70.89; H, 3.78; N, 20.28 %. Found: C, 63.10; H, 3.42; N, 23.23 %; IR (KBr, cm^{-1}): 1696 (CO); ^{1}H-NMR (300 MHz, DMSO-d_6, δ / / ppm): 2.44 (3H, *s*), 6.89–8.28 (9H, *m*, ArH), 7.88 (2H, *d*, *J* = 8 Hz), 8.18 (2H, *d*, *J* = 8Hz); ^{13}C-NMR (75 MHz, DMSO-d_6, δ / ppm): 175.4 (COPh), 157.6, 154.8, 152.5, 150.6, 147.2, 144.4, 140.4, 139.8, 138.9, 138.5, 134.7, 133.0, 132.6, 132.1, 130.3, 128.2, 122.3, 120.5, 17.9; MS (*m*/*z* (relative abundance, %)): 404 (M^+,16), 341 (31), 192 (23), 118 (43), 91 (33), 77 (53), 63 (100).

*[1-(4-Chlorophenyl)-1*H-*1,2,4-triazolo[4′,3′:2,3][1,2,4]triazino[5,6-*b*]indol-3-yl)phenylmethanone* ***(8m)***. Yield: 65 %; m.p.: 294 °C (DMF); Anal. Calcd. for $C_{23}H_{13}ClN_6O$ (FW: 424): C, 65.50; H, 3.11; N, 19.01 %. Found: C, 65.23; H, 3.03; N, 18.81 %; IR (KBr, cm^{-1}): 1698 (CO); ^{1}H-NMR (300 MHz, DMSO-d_6, δ / ppm): 6.82–8.29 (9H, *m*, ArH), 7.69 (2H, d, *J* = 8 Hz), 7.84 (2H, *d*, *J* = 8 Hz); ^{13}C-NMR (75 MHz, DMSO-d_6, δ / ppm): 176.8 (COPh), 157.7, 154.8, 153.5, 149.8, 147.6, 144.1, 139.6, 139.0, 138.1, 137.6, 134.0, 133.6, 133.5, 132.1, 130.7, 128.2, 123.3, 120.5; MS (*m*/*z* (relative abundance, %)): 426 (M^++2, 6), 425 (M^++1, 8), 424 (M^+, 19), 320 (32), 302 (48), 167 (19), 111 (100), 77 (54).

*3-[(2*H*-1,2,4-triazino[5,6-*b*]indol-3-yl)thio]-2,4-pentanedione* ***(11b)***. Yield: 60 %; m.p.: 198 °C (DMF / EtOH); Anal. Calcd. for $C_{14}H_{12}N_4O_2S$ (FW: 300): C, 55.99; H, 4.03; N, 18.65 %. Found: C, 55.76; H, 4.00; N, 18.43 %; IR (KBr, cm^{-1}): 3410 (NH), 1712, 1702, (2CO); ^{1}H-NMR (300 MHz, DMSO-d_6, δ / / ppm): 2.51 (6H, *s*), 5.4 (1H, *s*), 6.91–7.66 (4H, *m*, ArH), 11.17 (1H, *s*); ^{13}C--NMR (75 MHz, DMSO-d_6, δ / ppm): 187.6, 167.4 (2CO), 156.7, 150.1, 145.6, 132.9, 132.2, 130.4, 124.1, 121.4, 118.6, 66.3, 49.8, 24.8, 14.6; MS (*m*/*z* (relative abundance, %)): 330 (M^+, 21), 202 (100), 65 (63), 50 (18).

*Ethyl 3-oxo-2-[(2*H*-1,2,4-triazino[5,6-*b*]indol-3-yl)thio]butanoate* ***(11e)***. Yield: 75 %; m.p.: 180 °C (DMF / EtOH); Anal. Calcd. for $C_{15}H_{14}N_4O_3S$ (FW: 330): C, 54.53; H, 4.27; N, 16.96 %. Found: C, 54.33; H, 4.43; N, 16.76 %; IR (KBr, cm^{-1}): 3417 (NH), 1743, 1712 (CO); ^{1}H-NMR (300 MHz, DMSO-d_6, δ / / ppm): 1.33 (3H, *t*, *J* = 7.2 Hz), 2.51 (3H, *s*), 4.47 (2H, *q*, *J* = 7.2 Hz), 5.21 (1H, *s*), 6.88–8.15 (4H, *m*, ArH), 11.31 (1H, *s*); ^{13}C-NMR (75 MHz, DMSO-d_6, δ / / ppm): 188.2 (CO), 156.4, 150.9, 145.7, 133.9, 132.8, 130.4, 125.4, 120.8, 118.9, 68.9, 24.8; MS (*m*/*z* (relative abundance, %)): 330 (M^+, 19), 317 (16), 202 (31), 150 (16), 77 (56), 60 (100).

*3-Oxo-*N*-phenyl-2-[(2*H*-1,2,4-triazino[5,6-*b*]indol-3-yl)thio]butanoate* ***(11h)***. Yield: 80 %; m.p.: 215 °C (DMF / EtOH); Anal. Calcd. for $C_{19}H_{15}N_5O_2S$ (FW: 377): C, 60.46; H, 4.01; N, 18.56 %. Found: C, 60.76; H, 3.96; N, 18.28 %; IR (KBr, cm^{-1}): 3417, 3321 (2NH), 1712, 1640 (CO); ^{1}H-NMR (300 MHz, DMSO--d_6, δ / ppm): 2.53 (3H, s), 4.52 (s, 1H), 6.86–8.11 (m, 9H, ArH), 11.04 (s, 1H), 11.32 (s, 1H); ^{13}C-NMR (75 MHz, DMSO-d_6, δ / ppm): 189.8, 166.4 (2CO), 159.4, 154.4, 150.9, 144.2, 136.4, 135.8, 132.9, 131.8, 131.0, 130.4, 127.4, 126.7, 120.8, 117.6, 67.8, 24.6; MS (*m*/*z* (relative abundance, %)): 377 (M^+, 32), 202 (100), 167 (65), 134 (10), 118 (52), 63 (67).

Journal of the Serbian Chemical Society
JSCS-info@shd.org.rs • www.shd.org.rs/JSCS
J. Serb. Chem. Soc. 78 (8) 1127–1134 (2013)
JSCS–4484
UDC 547.78:542.913:615.281:612.064
Original scientific paper

Synthesis, spectroscopic characterization and pharmacological evaluation of oxazolone derivatives

GHULAM FAREED[1,2]*, NIGHAT AFZA[1], MUHAMMAD ALI VERSIANI[2], NAZIA FAREED[2], UZMA RASHEED MUGHAL[3], MAHBOOB ALI KALHORO[1], LUBNA IQBAL[1] and MEHREEN LATEEF[1]

[1]Pharmaceutical Research Center, PCSIR Laboratories Complex Karachi, Shahrah-e-Dr. Salim-uz-Zaman Siddiqui Karachi-75280, Sindh, Pakistan, [2]Department of Chemistry, Federal Urdu University of Arts, Science and Technology, Ghulshan-e-Iqbal, Karachi-75300, Sindh, Pakistan and [3]HEJ Research Institute of Chemistry, ICCBS, University of Karachi, Karachi-75280, Pakistan

(Received 17 September, revised 21 November 2012)

Abstract: A series of six 4-(arylmethylidene)-2-phenyl/methyl-5(4*H*)-oxazolone derivatives were synthesized using a reported method by condensation of aldehydes with *N*-benzoyl/*N*-acetyl glycine in the presence of zinc oxide as a catalyst and acetic anhydride at room temperature in ethanol. Five of the compounds are new derivatives. The structures of the compounds were evaluated based on ^{1}H-NMR, ^{13}C-NMR, EI-MS and FT-IR spectroscopy and elemental analysis. All the compounds were screened for their antibacterial and urease inhibition activity. The antibacterial activity was tested by the agar well diffusion method using Mueller–Hinton agar medium. Compound **2** showed excellent activity against *Staphylococcus aureus* exhibiting 16 mm (80 %) inhibition and above 24 mm (70 %) against *Salmonella typhi*. Compound **6** was the most active compound against *Escherichia coli* having 20 mm (80 %) inhibition followed by compound **5** having above 18 mm (70 %) inhibition. Urease inhibition activity of all the compounds was determined by the indophenol method. Compounds **3**, **6** and **7** showed significant inhibition against Jack bean urease.

Keywords: aldehyde; antibacterial; urease inhibition activities; oxazolones; synthesis; zinc oxide.

INTRODUCTION

For many decades, increasing resistance against human pathogens that cause serious infections is one of the main topics of interest for medicinal chemists. During the last century, many medicines were developed against bacterial infections. However, the available antibacterial drugs could cause undesirable effects

* Corresponding author. E-mail: fareedchm@yahoo.com
doi: 10.2298/JSC120917126F

and might be toxic. In view of these facts, it is important to explore additional drugs that have no adverse effects due to their different mode of action. In recent years, there has also been an increased interest in urease inhibiting drugs. Urease is a major cause of peptic and gastric ulcer. Compounds having urease inhibitory potential play an important role in pharmaceutical companies.[1] Activities of urease (E. C. 3.5.1.5) has been shown to be important virulence determinant in the pathogenesis of many clinical conditions, which are detrimental for human and animal health. Urease is directly involved in the formation of infection stones and contributes to the pathogenesis of urolithiasis, pyelonephritis, ammonia and heptic encephalopathy, hepatic coma and urinary catheter encrustation.[2,3] For the above reasons, a wide range of resistant drugs are important and required to treat patients. Mostly nitrogen-, sulfur- and oxygen-containing five- and six-membered heterocyclic compounds have enormous significance in the field of medicinal chemistry.[4] Oxazolones are five-membered heterocyclic compounds containing nitrogen and oxygen as hetero atoms. The C-2 and C-4 positions of oxazolone are responsible for their various biological activities. Oxazolones perform an important role in the synthesis of several organic molecules, including amino acids,[5] amino alcohols, thiamine[6] and peptides.[7] Certain natural and synthetic oxazolones also possess important biological activities, such as anti-inflammatory,[8] antimicrobial,[9] anticancer,[10] anti-HIV,[11] anti-angiogenic,[12] anticonvulsant,[13] antitumor, antagonistic, sedative[14–16] and cardiotonic activity.[17]. Oxazolone plays a very vital role in the manufacture of various biologically active drugs, such as analgesic, anti-inflammatory, antidepressant, anticancer, antimicrobial, antidiabetic and anti-obesity compounds.[18,19]

In the literature, the syntheses of oxazolone derivatives were achieved by condensation of aldehydes with *N*-benzoyl/*N*-acetyl glycine in the presence of various reagents and catalysts, such as, $ZnCl_2$,[20] KF/NaOAc,[21] Al_2O_3–H_3BO_3,[22] Bi(III) salts[23] and $Pb(OAc)_2$.[24] Herein, the synthesis of a series of 4-(arylmethylidene)-2-phenyl/methyl-5(4*H*)-oxazolone derivatives (**2**–**7**) using a literature method[25] by the condensation of an aldehyde with *N*-benzoyl/*N*-acetyl glycine in the presence of zinc oxide as a catalyst at room temperature in ethanol is reported. Compounds **2**–**6** are new. All the synthesized compounds were tested for their urease inhibition activity and antibacterial activity against *Escherichia coli*, *Bacillus subtilis*, *B. cereus*, *Staphylococcus aureus*, *Pseudomonas aeruginosa*, *Salmonella typhi* and *Proteus mirabilis.*

EXPERIMENTAL

All chemicals were of AR grade. The melting points were measured using Gallen Kemp MF-370 apparatus. The IR spectra were recorded on Nicolet Avatar 300 DTGS instrument. The ^{1}H- and ^{13}C-NMR spectra were recorded on a Bruker AV-300 instrument operating at 300 and 75 MHz, respectively, in dimethyl sulfoxide (DMSO) with trimethylsilane (TMS) as an internal standard. The EI-MS were recorded on a Finnigan MAT-311 A. CHN analysis was

performed on a Carlo Erba Strumentazione-Mod-1106, Italy. Purity of the product was determined by using silica gel $60F_{254}$ TLC, pre-coated cards (0.2 mm thickness) and visualized under UV light (254 and 366 nm) and by iodine vapors.

Antibacterial assay

Antibacterial activity was tested by the agar well diffusion method using Mueller Hinton Agar medium for the assay. The microorganisms were activated by inoculating a loopful of the strains in the nutrient broth (25 mL) and incubating at room temperature on a rotary shaker. Then 0.2 mL of inoculum (inoculum concentration was 10^8 cells mL^{-1} as per the McFarland standard) was inoculated into the molten Mueller–Hinton agar media and after proper homogenization, it was poured into 20 mm×100 mm Petri dishes. For the agar well diffusion, a well was made in the seeded plates with the help of a cup-borer (8.5 mm). The reference standard and test sample (1 %) 0.1 mL was introduced into the well and all the plates were incubated at 37 °C for 24 h. The microbial growth was determined by measuring the zone of inhibition (mm) and the mean values are presented. Percentage inhibitions of the compounds were determined by comparing the zone of inhibition to that of standard drug against each organism.

Urease inhibition assay

Reaction mixtures comprising 25 μL of enzyme (jack bean urease) solution and 55 μL of buffers containing 100 mM urea were incubated with 5 μL of the test compounds (1 mM concentration) at 30 °C for 15 min in 96-well plates. The urease activity was determined by measuring ammonia production using the indophenol method as described by Weatherburn.[26] Briefly, 45 μL each of phenol reagent (1 % w/v phenol and 0.005 % w/v sodium nitroprusside) and 70 μL of alkali reagent (0.5 % w/v NaOH and 0.1 % (w/v) active chlorine NaOCl) were added to each well. The increasing absorbance at 630 nm was measured after 50 min, using a microplate reader (Molecular Device, USA). All reactions were performed in triplicate in a final volume of 200 μL. The results (change in absorbance per min) were processed using Soft Max Pro software (Molecular Device, USA). All the assays were performed at pH 8.2 (0.01 M $K_2HPO_4 \cdot 3H_2O$, 1 mM EDTA and 0.01 M LiCl). The percentage inhibitions were calculated from the formula $100–(OD_{testwell}/OD_{control})\times100$. Thiourea was used as the standard inhibitor of urease.

Synthesis of N*-benzoylglycine (**1a**)*

Glycine (10 g, 133 mmol) was dissolved in 10 % NaOH solution (100 mL) and benzoyl chloride (21.6 ml, 186 mmol) was added in portions to this solution in 500mL conical flask. After each addition, the flask was stoppered and shaken vigorously until all the acid chloride had reacted. The solution was cooled by adding few grams of crushed ice and concentrated hydrochloric acid (pH 2–3) was added. The so-formed precipitates were filtered and washed several times with cold distilled water, dried, and recrystallized from hot water. The required compound was obtained as a crystalline white solid.

*Synthesis of N-acetylglycine (**1b**)*

Glycine (10 g, 133 mmol) and water (30 mL) in a 500 mL conical flask was vigorously stirred until the solid glycine had completely dissolved. Acetic anhydride (25 mL, 266 mmol) was added in portions and stirred vigorously for 20 min. The exothermic reaction produced solid *N*-acetylglycine, which showed the end-point of the reaction. The reaction mixture was then placed in refrigerator overnight for the complete formation of the product. The solid was filtered, washed with ice-cooled water and recrystallized from hot water.

Synthesis of the 4-(arylmethylidene)-2-phenyl/methyl-5-(4H)-oxazolones derivatives (2–7)

A mixture of the required aldehyde (1 mmol), *N*-benzoylglycine/*N*-acetylglycine (1 mmol), acetic anhydride (3 mmol), ZnO as a catalyst (0.05 mmol) and 15 mL ethanol was stirred at room temperature, 25 °C (Scheme 1). After a certain period, the syrupy reaction mixture was solidified and the reaction was completed (Table I). After the final product had been obtained, 20 mL more of cold ethanol was added. The solid was filtered off, dried and washed with hot water before recrystallization of the product.

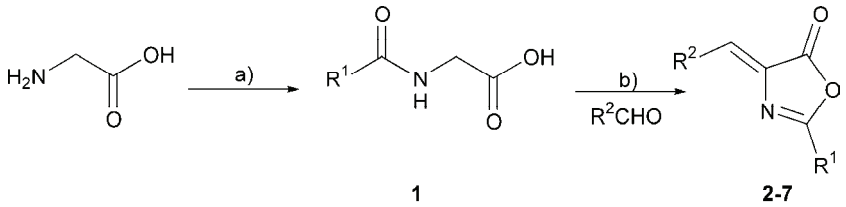

Scheme 1. Synthesis of oxazolones **2**–**7**; a) acetic anhydride or benzoyl chloride, 10 % NaOH, H_2O; b) ZnO, acetic anhydride, C_2H_5OH, reflux under stirring at r.t.

TABLE I. Synthesis of oxazolone derivatives (**2**–**7**) with their physical parameters

Compound	R^1	R^2	Yield %	Molecular weight g mol^{-1}	Reaction time min	M.p. °C
2	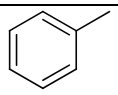	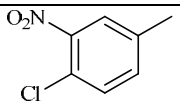	89	328	10	227
3	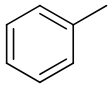	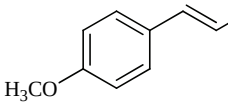	92	305	15	118
4		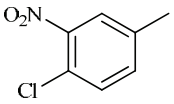	80	266	12	160
5		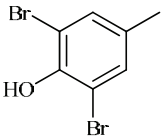	70	360	19	166
6	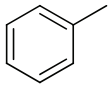	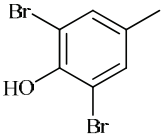	82	423	15	149
7	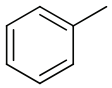	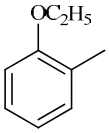	70	293	10	197

RESULTS AND DISCUSSION

Chemistry

Oxazolone derivatives were synthesized by condensation of substituted aromatic aldehydes with *N*-benzoyl/*N*-acetyl glycine using zinc oxide as a catalyst in ethanol at room temperature. All the synthesized compounds were characterized using different spectroscopic techniques. The IR spectrum of compound **3,** as typical, showed characteristic band of carbonyl group at 1781 and C=N at 1652 cm^{-1}. Also, typical ^{1}H-NMR spectrum showed characteristic pattern of peaks. The methyl protons appeared in the region of 3.84 ppm, whereas the aromatic protons appeared at 6.89–8.12 ppm. The electron ionization mass spectrometric fragmentation patterns of the compounds were the same.

The complete analytic and spectral data of the obtained products are given in the Supplementary material to this paper.

Antibacterial activity

All the compounds (**2**–**7**) were tested for their antibacterial activity against *Escherichia coli*, *Bacillus subtilis*, *B. cereus*, *Staphylococcus aureus*, *Pseudomonas aeruginosa*, *Salmonella typhi* and *Proteus mirabilis.* The results were compared with those of the standard 0.3 % gentamycin. The antibacterial activity of compounds **2–7** are shown in Fig 1. The bacterial zones of inhibition values are summarized in Table II. Compounds **5** and **6** showed excellent activities against *E. coli*, which is very difficult to treat with traditionally used antibiotics. The most active compound against *E. coli* was compound **6** having 20 mm inhibition zone (80 % inhibition), followed by compound **5** having above 18 mm inhibition zone (70 %). Thus, compounds **5** and **6** would be the better choice for the treatment of infections caused by *E. coli* than the derivatives **1**–**4** or **7**. All the screened compounds showed low to moderate activities against *B. cereus*, except

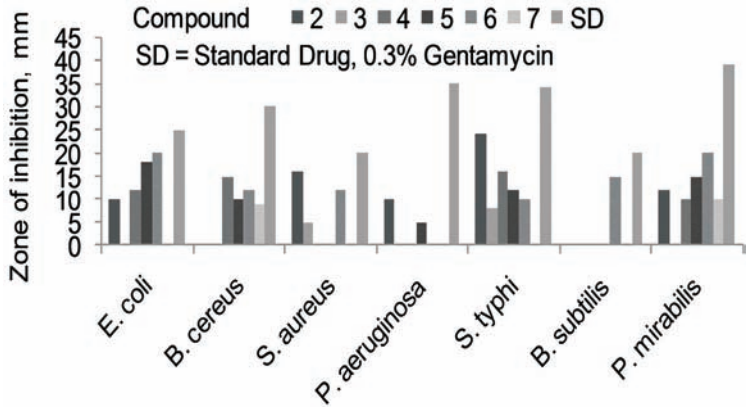

Fig. 1. Antibacterial activity of compounds **2**–**7**.

compound **4** that showed 50 % inhibition. *S. aureus* is responsible for various throat infections and cholic diseases. Therefore, compound **2** would be the best choice to treat infections caused by *S. aureus* as it had a 16 mm inhibition zone (80 %). None of the compounds showed inhibition against *P. aeruginosa* except compound **2** that had less than 30 % inhibition. *S. typhi*, responsible for typhoid, could be inhibited by compound **2**, showing an inhibition zone of 24 mm (70 %). Compound **4** also showed 50 % inhibition followed by compounds **5**–**7**. *B. subtilis* was only inhibited by compound **6**, which showed an inhibition zone of 15 mm (75 %). Compound **6** also showed ≈20 mm inhibition zone (50 %) against *P. mirabilis*, followed by compounds **4**, **5** and **7**.

TABLE II. Antibacterial activity (concentration used: 1 % of each compound); zone of inhibition was measured in mm; SD – standard drug, 0.3 % gentamycin

Bacterium	Compound						SD
	2	**3**	**4**	**5**	**6**	**7**	
E. coli	10	00	12	18	20	00	25
B. cereus	00	00	15	10	12	09	30
S. aureus	16	05	00	00	12	00	20
P. aeruginosa	10	00	00	05	00	00	35
S typhi	24	08	16	12	10	00	34
B. subtilis	00	00	00	00	15	00	20
P. mirabilis	12	00	10	15	20	10	39

Compounds **5** and **6** proved themselves to be very effective antibacterial agents. Compound **5** showed inhibition against four and compound **6** showed inhibitions against six different bacterial strains. The C-2 and C-4 positions of the oxazolones are responsible for their crucial biological activities (Fig. 2). A phenyl group instead of a methyl group at C-2 plays a vital role in the enhancement of the activities, as shown by compounds **5** and **6**. Compared to compound **5**, compound **6** showed a greater tendency of inhibition against different bacterial strains due to the phenyl group at C-2. Electron withdrawing substituents at C-4 position are also a good choice for the enhancement of the activities.

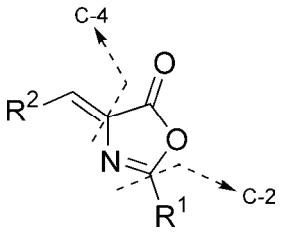

Fig. 2. Structure of oxazolones.

Urease inhibition activity

All the synthesized compounds were screened for their urease inhibition activity. Compounds **3**, **6** and **7** showed strong inhibition against jack bean urease, having IC_{50} values near to the standard inhibitor thiourea as determined by the indophenol method. The results are listed in Table III.

TABLE III. Urease inhibition activity of compounds **2**–**7**; Standard IC_{50} = 21.4 μM

Compound	Urease inhibition, %	IC_{50} / μM
2	21	Not determined
3	85.2	62
4	44	NA
5	49	NA
6	82.5	65.3
7	73.2	58

CONCLUSION

Based on the biological activities of the synthesized oxazolone derivatives, it could be concluded that they are therapeutic antibacterial agents and urease inhibitors.

SUPPLEMENTARY MATERIAL

Analytic and spectral data for the synthesized compounds are available electronically from http://www.shd.org.rs/JSCS/, or from the corresponding author on request.

Acknowledgement. All the authors wish to thank the Pharmaceutical Research Center, PCSIR Laboratories Complex, Karachi, Pakistan, for financial and technical support for this research.

ИЗВОД

СИНТЕЗА, СПЕКТРАЛНА КАРАКТЕРИЗАЦИЈА И ФАРМАКОЛОШКА ИСПИТИВАЊА ДЕРИВАТА ОКСАЗОЛОНА

GHULAM FAREED[1,2], NIGHAT AFZA[1], MUHAMMAD ALI VERSIANI[2], NAZIA FAREED[2], UZMA RASHEED MUGHAL[3], MAHBOOB ALI KALHORO[1], LUBNA IQBAL[1] и MEHREEN LATEEF[1]

[1]*Pharmaceutical Research Center, PCSIR Laboratories Complex Karachi, Shahrah-e-Dr. Salim-uz-Zaman Siddiqui Karachi-75280, Sindh, Pakistan,* [2]*Department of Chemistry, Federal Urdu University of Arts, Science and Technology, Ghulshan-e-Iqbal, Karachi-75300, Sindh, Pakistan и* [3]*HEJ Research Institute of Chemistry, ICCBS, University of Karachi, Karachi-75280, Pakistan*

Синтетисана је серија деривата 4-(арилметилиден)-2-фенил/метил-5(4*H*)-оксазолона (**2**–**7**) од којих су деривати **2**–**6** синтетисани први пут. Једињења су синтетисана кондензацијом алдехида и *N*-бензоил/*N*-ацетил-глицина у присуству цинк-оксида као катализатора и анхидрида сирћетне киселине, на собној температури у етанолу као растварачу. Структура деривата одређена је спектралном (^{1}H-NMR, ^{13}C-NMR, EI-MS и FT-IR) и елементалном анализом. Свим једињењима одређена је антибактеријска активност и инхибиторна активност према уреази. Антибактеријска активност је тестирана према методи дифузије у агару помоћу Mueller–Hinton агар медијума. Једињење **2** показује одличну активност према *Staphylococcus aureus* ≈16 mm (80 %) инхибиције и преко

24 mm (70 %) према *Salmonella typhi*. Према *Escherichia coli* најактивније је једињење **6** са 20 mm (80 %) инхибиције, а затим једињење **5** са преко 18 mm (70 %) инхибиције. Инхибиторна активност према уреази за сва једињења одређена је индофенолном методом. Једињења **3**, **6** и **7** показују значајну активност према уреази пасуља сорте Jack.

(Примљено 17. септембра, ревидирано 21. новембра 2012)

REFERENCES

1. A. Hussain, S. Perveen, A. Malik, N. Afza, L. Iqbl, R. B. Tareen, *Pol. J. Chem.* **83** (2009) 1329
2. H. L. Mobley, M. D. Island, R. P. Hausinger, *Microb. Rev.* **59** (1989) 451
3. H. L. Mobley, R. P. Hausinger, *Microb. Rev.* **53** (1989) 85
4. M. J. Aaglawe, S. S. Dhule, S. S. Bahekar, P. S Wakte, D. B. Shinde. *J. Korean Chem. Soc.* **47** (2003) 133
5. J. Lamb, W. Robson. *Biochem. J.* **25** (1931) 1231
6. M. I. Ismail. *Can. J. Chem.* **69** (1991) 1886
7. M. Palcut. *Acta Chim. Slov.* **56** (2009) 362.
8. U. S. Goksen, N. G. Kelekci, O. Goktas, Y. Koysal, E. Kilic, S. Isik, G. Aktay, M. Ozalp, *Bioorg. Med. Chem.* **15** (2007) 5738
9. G. Brownlee, M. Woodbine. *Br. J. Pharmacol.* **3 (**1948) 305
10. C. Sanchez, C. Mendez, J. A. Salas. *Nat. Prod. Rep.* **23** (2006) 1007
11. M. Witvrouw, C. Pannecouque, E. D. Clercq, E. Fernandez-Alvarez, J. L Marco. *Arch. Pharm. Med. Chem.* **352** (1999) 163
12. F. M. P Sierra, A. Pierre, M. Burbridge, N. Guilbaud. *Bioorg. Med. Chem. Lett.* **12** (2002) 1463
13. H. M. F. Madkour. *Chem. Pap.* **56** (2002) 313
14. K. M. Khan, U. R. Mughal, M. T. H. Khan, Z. Ullah, S. Perveen, M. I. Choudhary. *Bioorg. Med. Chem.* **14** (2006) 6027
15. A. M. Tikdari, S. Fozooni, H. Hamidian. *Molecules* **13** (2008) 3246
16. M. A. Mesaik, S. Rahat, K. M. Khan, Z. Ullah, M. I. Choudhary, S. Murad, Z. Ismail, A. Rahman, A. Ahmad. *Bioorg. Med. Chem.* **12** (2004) 2049
17. R. A. Schnettler, W. D. Jones Jr., G. P. Claxton (Merrell Dow Pharmaceuticals Inc.), United States, Patent No.: US 4698353 (1987)
18. P. A. Conway, K. Devine, F. Paradisi. *Tetrahedron* 65 (2009) 2935
19. V. Taile, K. Hatzade, P. Gaidhane, V. Ingle. *Turk. J. Chem.* **33** (2009) 295
20. P. S. Rao, R. V. Venkataraman. *Indian. J. Chem., B* **33** (1994) 984
21. F. M. Baustista, J. M. Campelo, A. Garcia, D. Luna, J. M. Marinas, A. A. Romero. *J. Chem. Soc., Perkin Trans. 2* (2002) 227
22. H. J. Ringold, B. Loeken, G. Rosenkranz, F. Sondheimer. *J. Am. Chem. Soc.* **78** (1956) 816
23. M. M. Khodaei, A. R. Khosropour, S. J. H. Jomor. *J. Chem. Res. Synop.* **10** (2003) 638
24. H. Hamidian, A. M. Tikari. *Heterocycl. Commun.* **12** (2006) 29
25. M. A. Pasha, V. P. Jayashankara, K. N. Venugopala, G. K. Rao. *J. Pharmacol. Toxicol.* **2** (2007) 264.

Journal of the Serbian Chemical Society
JSCS@tmf.bg.ac.rs • www.shd.org.rs/JSCS
J. Serb. Chem. Soc. 78 (8) S91–S92 (2013) *Supplementary material*

SUPPLEMENTARY MATERIAL TO

Synthesis, spectroscopic characterization and pharmacological evaluation of oxazolone derivatives

GHULAM FAREED[1,2]*, NIGHAT AFZA[1], MUHAMMAD ALI VERSIANI[2], NAZIA FAREED[2], UZMA RASHEED MUGHAL[3], MAHBOOB ALI KALHORO[1], LUBNA IQBAL[1] and MEHREEN LATEEF[1]

[1]Pharmaceutical Research Center, PCSIR Laboratories Complex Karachi, Shahrah-e-Dr. Salim-uz-Zaman Siddiqui Karachi-75280, Sindh, Pakistan, [2]Department of Chemistry, Federal Urdu University of Arts, Science and Technology, Ghulshan-e-Iqbal, Karachi-75300, Sindh, Pakistan and [3]HEJ Research Institute of Chemistry, ICCBS, University of Karachi, Karachi-75280, Pakistan

J. Serb. Chem. Soc. 78 (8) (2013) 1127–1134

ANALYTIC AND SPECTRAL DATA FOR THE SYNTHESIZED COMPOUNDS

4-[(Z)-(4-Chloro-3-nitrophenyl)methylidene]-2-phenyl-5(4H)-oxazolone (***2***). R_f: 0.67 (ethyl acetate: hexane, 2:8); Anal. Calcd. for $C_{16}H_9ClN_2O_4$: C, 58.46; H, 2.76; N, 8.52 %. Found: C, 58.41; H, 2.77; N, 8.50 %; IR (KBr, cm^{-1}): 1799, 1659, 1536, 1451, 1324, 1172, 868, 644; ^{1}H-NMR (300 MHz, $CDCl_3$, δ / ppm): 7.13 (1H, *s*, 6-H), 7.52–7.68 (5H, *m*, Ar-H), 8.15–8.18 (2H, *m*, Ar-H), 8.80 (1H, *s*, Ar-H); ^{13}C-NMR (75 MHz, $CDCl_3$, δ / ppm): 166.70, 164.98, 146.80, 136.57, 135.84, 132.77, 132.03, 129.36, 129.16, 128.68, 127.88, 126.23, 125.60, 125.49; EI-MS (*m*/*z* (relative abundance, %)): 330 (M+2, 12.3), 328 (M^+, 37.5), 105 (100), 77 (71.6), 44 (93.1).

4-[(Z,2E)-3-(4-Methoxyphenyl)-2-propenylidene]-2-phenyl-5(4H)-oxazolone (***3***). R_f: 0.70 (ethyl acetate: hexane, 2:8); Anal. Calcd. for $C_{19}H_{15}NO_3$: C, 74.74; H, 4.95; N, 4.59 %. Found: C, 74.70; H, 4.97; N, 4.57 %; IR (KBr, cm^{-1}): 1781, 1652, 1593, 1328, 1256, 1161, 865; ^{1}H-NMR (300 MHz, $CDCl_3$, δ / ppm): 3.84 (3H, *s*, OCH_3), 7.38 (1H, *d*, *J* = 14.5 Hz, C**H**–CH=CH), 7.42 (1H, *d*, *J* = 9.8 Hz, CH–CH=C**H**), 6.95 (1H, *dd*, *J* = 9.8, 14.5 Hz, CH–C**H**=CH), 7.45–7.58 (5H, *m*, Ar-H), 7.92–8.12 (4H, *m*, Ar-H); ^{13}C-NMR (75 MHz, $CDCl_3$, δ / ppm): 166.03, 162.37, 159.32, 135.13, 134.20, 132.51, 132.03, 129.45, 129.42, 129.36, 129.16, 128.71, 127.81, 114.57, 14.02; EI-MS (*m*/*z* (relative abundance, %)): 305 (M^+, 39.2), 277 (3.0), 105 (100), 77 (29.4), 44 (68.3).

* Corresponding author. E-mail: fareedchm@yahoo.com

*4-[(Z)-(4-Chloro-3-nitrophenyl)methylidene]-2-methyl-5(4H)-oxazolone (**4**).* R_f: 0.77 (ethyl acetate:hexane, 2:8); Anal. Calcd. for $C_{11}H_7ClN_2O_4$: C, 49.55; H, 2.65; N, 10.51 %. Found: C, 49.57; H, 2.61; N, 10.53 %; IR (KBr, cm^{-1}): 3072, 1805, 1661, 1607, 1533, 1360, 1261, 1168, 890, 657, 629; ^{1}H-NMR (300 MHz, $CDCl_3$, δ / ppm): 2.42 (3H, *s*, CH_3), 7.24 (1H, *s*, 6-H), 7.57–8.10 (2H, *m*, Ar-H), 8.70 (1H, *s*, Ar-H); ^{13}C-NMR (75 MHz, $CDCl_3$, δ / ppm): 168.38, 160.19, 146.88, 136.57, 132.77, 129.90, 128.61, 125.64, 125.41, 125.01, 11.12; EI-MS (*m*/*z* (relative abundance, %)): 268 (M^{+2}, 59.4), 266 (M^+, 29), 105 (3.9), 114 (64.5) 77 (35), 44 (100).

*4-[(Z)-(3,5-Dibromo-4-hydroxyphenyl)methylidene]-2-methyl-5(4H)-oxazolone (**5**).* R_f: 0.65 (ethyl acetate:hexane, 2:8); Anal. Calcd. for $C_{11}H_7Br_2NO_3$: C, 36.60; H, 1.95; N, 3.88 %. Found: C, 36.62; H, 1.94; N, 3.85 %; IR (KBr, cm^{-1}): 3071, 1760, 1670, 1580, 1479, 1302, 1139, 876, 646; ^{1}H-NMR (300 MHz, $CDCl_3$, δ / ppm): 2.14 (3H, *s*, CH_3), 7.24 (1H, *s*, 6-H), 7.97 (2H, *s*, Ar-H), 9.88 (1H, *s*, OH); ^{13}C-NMR (75 MHz, $CDCl_3$, δ / ppm): 168.38, 160.19, 151.51, 131.35, 129.02, 126.27, 125.52, 113.41, 14.03; EI-MS (*m*/*z* (relative abundance, %)): 364 (M+4, 10), 362 (M+2, 12), 360 (M^+, 39), 105 (100), 77 (12), 44 (91.8).

*4-[(Z)-(3,5-Dibromo-4-hydroxyphenyl)methylidene]-2-phenyl-5(4H)-oxazolone (**6**).* R_f: 0.72 (ethyl acetate:hexane, 2:8); Anal. Calcd. for $C_{16}H_9Br_2NO_3$: C, 45.42; H, 2.14; N, 3.31 %. Found: C, 45.40; H, 2.15; N, 3.32 %; IR (KBr, cm^{-1}): 3075, 1650, 1541, 1416, 1241, 652, 644; ^{1}H-NMR (300 MHz, $CDCl_3$, δ / ppm): 7.26 (1H, *s*, 6-H), 7.97 (2H, *s*, Ar-H), 7.24–8.32 (5H, *m*, Ar-H) 9.88 (1H, *s*, OH); ^{13}C-NMR (75 MHz, $CDCl_3$, δ / ppm): 166.70, 164.91, 151.51, 134.96, 132.01, 131.31, 129.10, 127.88, 127.11, 126.27, 113.44; EI-MS (*m*/*z* (relative abundance, %)): 427 (M+4, 2) 425 (M+2, 3), 423 (M^+, 2.5), 105 (100), 77 (76.8), 44 (73.5).

*4-[(Z)-(2-Ethoxyphenyl)methylidene]-2-phenyl-5(4H)-oxazolone (**7**).* R_f: 0.72 (ethyl acetate: hexane, 2:8); Anal. Calcd. for $C_{18}H_{15}NO_3$: C, 73.71; H, 5.15; N, 4.78 %. Found: C, 73.70; H, 5.17; N, 4.77 %; IR (KBr, cm^{-1}): 1788, 1768, 1664, 1595, 1557, 1488, 1447, 1248, 1168, 1045; ^{1}H-NMR (300 MHz, $CDCl_3$, δ / ppm): 1.50 (3H, *t*, J = 6.5 Hz, C**H**$_3$CH$_2$O), 4.15 (2H, *q*, J = 6.5 Hz, CH$_3$C**H**$_2$O), 6.88––7.08 (5H, *m*, Ar-H), 7.24 (1H, *s*, 6-H), 7.35–8.87 (4H, *m*, Ar-H); ^{13}C-NMR (75 MHz, $CDCl_3$, δ / ppm): 166.70, 164.98, 157.80, 132.03, 130.96, 129.92, 129.36, 129.16, 128.74, 127.88, 127.69, 122.04, 121.31, 117.24, 64.52, 13.83: EI-MS (*m*/*z* (relative abundance, %)): 293 (M^+, 38.1), 265 (3.7), 105 (100), 77 (77.2).

Journal of the Serbian Chemical Society
JSCS-info@shd.org.rs • www.shd.org.rs/JSCS
J. Serb. Chem. Soc. 78 (8) 1135–1147 (2013)
JSCS–4485
UDC 628.336+66.094.941+628.356+579.852.11
Original scientific paper

Enhancing the hydrolysis of excess sludge using thermophilic *Bacillus* sp. Hnu under different oxygen supply conditions

WEI ZHENG[1]*, XIAO MING LI[2]**, BING ZHENG LI[1], HONG YING XU[1] and YA BING GUO[1]

[1]*School of Environment and Safety, Taiyuan University of Science and Technology, Taiyuan 030024, P. R. China and* [2]*College of Environmental Science and Engineering, Hunan University, Changsha 410082, P. R. China*

(Received 8 October 2012, revised 14 February 2013)

Abstract: A thermophilic *Bacillus* strain was isolated from excess sludge in the present study. A 16S rDNA analysis indicated that this strain was a *Bacillus* sp. that had not been previously reported (named *Bacillus* sp. Hnu). The aim of the present study was to investigate the enhanced efficiency of excess sludge hydrolysis by the addition of thermophilic *Bacillus* sp. Hnu under different oxygen supply conditions. The results indicated that higher temperature and a greater oxygen supply were advantageous for the volatile suspended solid removal ratio, having the same effect to that of protease activity. The maximum volatile suspended solid removal ratio was achieved at 21.5, 42.5 and 54.4 % after 108 h digestion at pH 6.9 and 60 °C and increased by 17.2, 38 and 45.4 % under anaerobic, microaerobic, and aerobic conditions compared with the control test, respectively. The hydrolysis rate constants under anaerobic, microaerobic, and aerobic conditions were 3, 4.8, and 7 times (40 °C), 3.5, 9.8, and 11.8 times (50 °C) and 2.7, 7.2, and 10.3 times (60 °C), respectively. Hydrolysis performance indicated that the *Bacillus* sp. Hnu could accelerate the hydrolysis rate. The kinetic study showed that the hydrolysis of sludge with *Bacillus* sp. Hnu and the control test followed first-order kinetics except at 60 °C.

Keywords: thermophilic; excess sludge; microaeration; hydrolysis; first-order kinetics.

INTRODUCTION

The activated sludge process is the most widely used biological treatment for municipal and industrial wastewater worldwide.[1,2] This process uses microorganisms to transform dissolved and colloidal organic substances in the wastewater into biomass or carbon dioxide and water.[3] The production of the major byproduct, *i.e.*, excess sludge, is a serious disposal problem for treatment plants. The

*,** Corresponding authors. E-mails: (*)zhwstar2008@163.com; (**)xmli@hnu.cn
doi: 10.2298/JSC121008024Z

excess sludge contains considerable amounts of hazardous organic and inorganic materials, such as pathogens, parasite eggs, and a number of heavy metals. The mixture is frequently subjected to treatment prior to disposal to avoid posing a significant threat to ecological systems.[4]

The main treatment of the excess sludge presently employed in China depends on the landfill operation after coagulation filtration. However, the disposal of the excess sludge by this operation is not effective because it occupies a vast area of land. The costs associated with the treatment of excess sludge may cover up to 25 to 65 % of the total plant operational cost.[5,6]

The current technologies for sludge reduction can be roughly classified into the following three major categories: 1) a mechanical method such as mill or ultrasonification,[2,7,8] 2) oxidation using ozone[9–11] or chlorine[12] and 3) hydrolysis with or without enzymes.[13–15] Biological stabilization is considered as one of the most attractive methods for the optimal reduction of the organic fraction in excess sludge. The thermophilic bacteria treatment method is considered particularly advantageous because of its cost-effectiveness.[16,17] This type of treatments has also been reported in other studies,[3,18–22] whereas less information is available regarding the aerobic and anaerobic transition region, which is characterized by low levels of aeration.[23]

The objective of the present study was to investigate the enhanced efficiency of excess sludge hydrolysis by the addition of thermophilic *Bacillus* sp. Hnu under different oxygen supply conditions and analyze the kinetic parameters during this process.

EXPERIMENTAL

Source of excess sludge and culture media

The excess sludge used in the present study was obtained from the secondary sedimentation tank of a municipal wastewater treatment plant in Changsha, China. Concentrated sludge was obtained after the sludge was allowed to settle at 4 °C for 24 h. The supernatant was then removed. The sludge was filtered through a 1 mm×1 mm metal sieve and then stored at 4 °C until use. The main characteristics of the sludge after filtration are given in Table I.

TABLE I. Characteristics of the filtered excess sludge (mg L^{-1})

Parameter	Value
pH	6.9±0.1
Soluble chemical oxygen demand	150±10
Total chemical oxygen demand	14850±287
Concentration of total suspended solid	153840±148
Concentration of volatile suspended solid	71350±69
Concentration of ammonia nitrogen	18±1.5
Concentration of soluble phosphate	16±1

The following culture media were employed: Luria–Bertani (LB) solid medium containing: 10 g tryptone, 5 g yeast extract, 5 g sodium chloride, 30 g agar powder and 1 L distilled

water; starch agar containing: 5 g soluble starch, 1 g yeast extract, 2 g tryptone, 0.003 g calcium chloride, 0.1 g magnesium chloride, 0.36 g monopotassium dihydrogen phosphate, 1.3 g disodium hydrogen phosphate, 20 g agar powder, and 1 L distilled water; casein agar medium containing: 10 g casein, 3 g beef extract, 2 g disodium hydrogen phosphate, 5 g sodium chloride, 15 g agar, 12.5 mL bromothymol blue solution (0.4 %), and 1 L distilled water.

Isolation and identification of the thermophilic strain

Strain isolation. The thermophilic bacteria were isolated from the excess sludge. The fresh sludge was transferred into a 500 mL Erlenmeyer flask covered with a rubber stopper to prevent evaporation. The sludge was cultured at 60 °C in a water-bath with vibrator at a shaking rate of 100 rpm for one week. Then, 2/3 of the old sludge was discharged and replaced with an equal volume of fresh sludge. The same procedure was repeated for 6 months. The cultured sludge was diluted to an appropriate concentration, spread on an LB agar plate, and incubated at 60 °C for 48 h. After the growth of the bacterial colonies, the representative strains of all colony types that could be distinguished on the plates were isolated by sub-culturing onto the same LB agar plates at the same temperature until a single colony was eventually identified to ensure a pure culture. A typical isolated strain was inoculated onto LB agar and LB liquid medium, incubated at 60 °C for 48 h, and then preserved in a refrigerator at 4 °C.

Strain identification. The isolated bacteria were spread onto a standard nutrient agar plate and incubated at 60 °C for 48 h. The morphological characteristics, including: shape, colony, size, color and physiological and biochemical characteristics were determined (Table II).

TABLE II. Characteristics of thermophilic *Bacillus* sp. Hnu

Index	Characteristics	*Bacillus* sp. Hnu
Morphological characteristics	Shape	Bacilliform
	Colony	Smooth
	Size	Moderate
	Color	Semitransparent
Physiological and biochemical characteristics	Motility	+
	Sporiparous	+
	Gram stain	+
	Aerobic	+
	Catalase reaction	+
	Protease-producing	++
	Amylase-producing	+
	pH	5.5–8.5
	Temperature	40–65 °C
	Optimum temperature	60 °C

Casein agar medium and starch agar were used to test the target bacteria for the production of protease and amylase.

Moreover, 16S RNA gene sequence analysis was used to identify the species of the target strain. DNA was extracted from 2 mL of a pure strain solution (LB medium, 60 °C, 48 h), which was concentrated at 12000×*g* for 30 s and then extracted with a DNA extraction kit. The extracted genome was used as the template for 16S RNA amplification with PCR primers 27F (5'-AGAGTTTGATCMTGGCTCAG-3') and 1492R (5'-TACGGYTACCTTGTTACGA-

CTT-3'). The cycle program for the amplification was as follows: 5 min at 95 °C; 24 cycles each for 30 s at 95 °C, 30 s at 55 °C and 1.5 min at 72 °C, followed by a final 10 min extension at 72 °C. The PCR product was detected by agarose gel electrophoresis. The 16S rRNA gene from the isolated bacteria was purified, cloned, and sequenced by Shanghai Majorbio Bio-pharm Technology Co., Ltd. (Shanghai, China).

Bacillus *sp. Hnu-enhanced hydrolysis tests*

Experiments on the influence of *Bacillus* sp. Hnu in the enhanced hydrolysis of excess sludge were performed in four 1000 mL volumetric flasks. The temperature was controlled in each test using a water bath. Distilled water (50 mL) was added to 500 mL concentrated excess sludge in the control test. LB liquid medium (50 mL) was added to the 500 mL concentrated excess sludge in the other three reactors. The control test and anaerobic reactors were sealed with a rubber stopper with an inserted glass tube that reached the sludge, enabling sample withdrawal. Three glass tubes were placed in the rubber plugs of the microaerobic and aerobic reactors. The first tube was for sampling, the second was the air inlet, and the third tube was the gas outlet. The gas outlet was a covered condense pipe to prevent evaporation. Compressed air was allowed to pass through the microaerobic and aerobic reactors at ventilation rates of 20 and 70 mL min^{-1}, respectively. Under these aerating conditions, the dissolved oxygen (*DO*) ranged from 0.4 to 0.6 mg L^{-1} and 1.5 to 2.5 mg L^{-1}, respectively.

Using these experimental techniques, the effect of temperature on excess sludge digestion was investigated under control, anaerobic, microaerobic and aerobic conditions at 40, 50 and 60 °C with no pH adjustment (pH 6.9). The effect of pH on excess sludge digestion was investigated under control, anaerobic, microaerobic and aerobic conditions at pH values of 6.0, 7.0, 8.0 and 9.0, adjusted using 2 M NaOH or 2 M HCl. All flasks were mechanically stirred at 100 rpm.

The parallel experiments were performed simultaneously, and all experiments were repeated.

Analytical methods

The values of soluble chemical oxygen demand, total chemical oxygen demand, total suspended solid, volatile suspended solid, ammonia nitrogen and soluble phosphate were determined according to standard methods.[24] The pH was determined using a Multiline 330i pH meter standardized using buffer solutions of different pH values.

The protease activity was measured according to a universal protease activity assay (GB/T23527-2009): 1 mL of sample and 1 mL casein solution (10.00 mg mL^{-1}) were incubated for 10 min at 40 °C. The reaction was stopped by the addition of 2 mL 0.4 M trichloroacetic acid, and after standing for 10 min, the mixture was filtered though filter paper. 5 mL of sodium carbonate (0.4 M) and 1 mL of Folin reagent were added to 1 mL of the filtrate and the absorbance was detected at 680 nm. One unit of absorbance is expressed as one enzyme unit per milliliter (EU mL^{-1}) protease activity.

RESULTS AND DISCUSSION

Effect of temperature and oxygen supply on excess sludge digestion

Temperature influences the metabolic activities of microbial populations and characterizes the hydrolysis rates. The mesophilic temperature (40 °C) and thermophilic temperatures (50 and 60 °C) were chosen as target temperatures to determine the volatile suspended solid removal ratio as well as the presence of

protease activity with and without the incubation of the *Bacillus* sp. Hnu under different oxygen supply conditions. The temperature remarkably influenced the volatile suspended solid removal ratio in the *Bacillus* sp. Hnu-inoculated sample (Figs. 1a and 1b). The highest volatile suspended solid removal ratio (54.4 %) was obtained at 60 °C after 108-h cultivation, whereas only 30 and 45.6 % were obtained under aerobic condition at 40 and 50 °C, respectively. The volatile suspended solid removal ratios for the microaerobic process were 22, 37.4 and 42.5 % at 40, 50 and 60 °C, respectively, whereas corresponding values for the anaerobic process were 14.6, 18.3 and 21.5 %. These effects were attributed to the autolysis of the mesophilic organisms, a major group in the excess sludge caused by the temperature shock. The protease exo-enzymatic activity produced by thermophilic processes can cause simultaneously lysis. The volatile suspended solid removal ratio, as seen in the control test (no *Bacillus* sp. Hnu inoculation and no oxygen supply), was 4.6 % at 60 °C after 6 h and only 0.8 % at 30 °C. In addition, the results demonstrated that 33.6 % of the volatile suspended solid were removed in the first 24 h at 60 °C under the thermophilic aerobic condition, which accounted for 66.7 % of the total removals. However, only 50.7 and 58.3 % of the total removals were obtained at 40 and 50 °C, similar to the anaerobic and microaerobic excess sludge processes.

Protease activity was important in the depolymerization of the excess sludge, lysis and hydrolysis of proteins. The variations in protease activity were evaluated during the volatile suspended solid degradation ratio test. The results of the protease activity at 50 and 60 °C are shown in Fig. 1c. The increase in the digestion temperature from 50 and 60 °C resulted in an increase of the protease activity in the supernatant. The protease activity increased with digestion time and the amount of oxygen supply (Fig. 1c). This activity reached 0.6 EU mL^{-1} at 60 °C under aeration after 24 h, and the highest activity reached 0.79 EU mL^{-1}, whereas the protease activities were only 0.354 and 0.396 EU mL^{-1} at 50 and 60 °C under anaerobic condition after 24 h. However, the amount of protease activity under the microaerobic condition was almost the same as that under the aerobic condition and increased to 0.58 EU mL^{-1} at 60 °C after 24 h. According to the equation $(K_d)_T = (K_d)_{20}q^{(T-20)}$, where K_d is reaction rate, T is temperature and q is reaction rate constant, an increase in the temperature of the reactor results in an increase in the reaction rate constant, which implies an increase in the digestion rate. A higher temperature leads to more bacteria lysis and release of endo-enzyme, resulting in an increased digestion rate. The aerobic digestion of the excess sludge could be considered as a continuation of the activated sludge process. The cell tissue is oxidized aerobically to carbon dioxide, water, and ammonia. The microaerobic oxidation, *i.e.*, a limited oxygen supply, could also produce gases, including carbon dioxide.[15] The supply of oxygen in the thermophilic excess sludge process could affect a decrease of the volatile suspended solid (Figs. 1a and 1b) compared with the anaerobic condition, as oxygen can increase

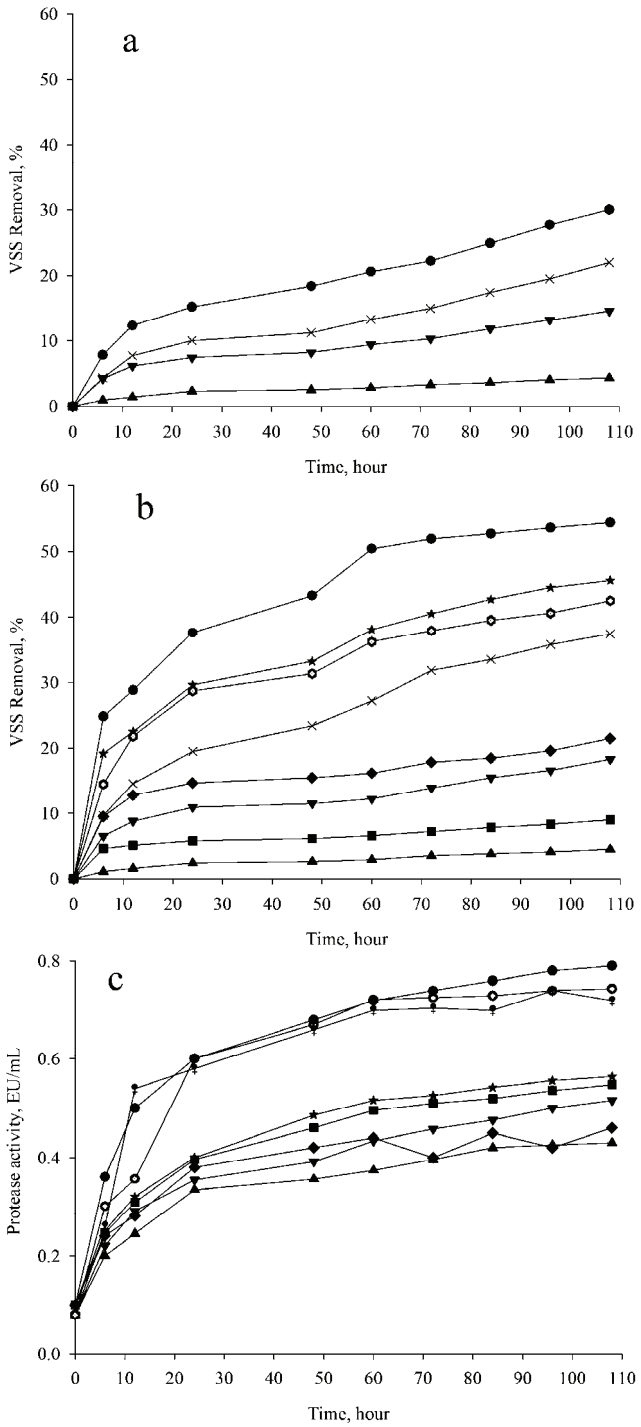

Fig. 1. Effect of temperature on anaerobic, microaerobic and aerobic digestion of waste activated sludge with and without inoculation of *Bacillus* sp. Hnu. a) Removal ratio of volatile suspended solid at 40 °C (▲ – control, ▼ – anaerobic, ✕ – microaerobic, ● – aerobic); b) removal ratio of volatile suspended solid at 50 and 60 °C (▲ – 50 °C, control, ▼ – 50 °C, anaerobic, ✕ – 50 °C, microaerobic, ★ – 50 °C, aerobic, ■ – 60 °C, control, ◆ – 60 °C, anaerobic, ○ – 60 °C, microaerobic, ● – 60 °C, aerobic); c) variations of protease activity (▲ – 50 °C, control, ▼ – 50 °C, anaerobic, ★ – 50 °C, microaerobic, ○ – 50 °C, aerobic; ◆ – 60 °C, control, ■ – 60 °C, anaerobic, ✕ – 60 °C, microaerobic, ● – 60 °C, aerobic).

increase the activity of the microorganism and accordingly increase the enzymatic activity. The above results demonstrate that protease activity has an important effect on the sludge digestion. The optimum temperature is 60 °C because *Bacillus* sp. Hnu cannot survive temperatures in excess of 65 °C.

Effect of pH on thermophilic excess sludge digestion

Bacillus sp. Hnu was inoculated into the excess sludge at pH values ranging from 6 to 9, which were adjusted with 0.1 M HCl or 0.1 M NaOH, and the effects of pH on the volatile suspended solid removal rate and protease activity were investigated. The volatile suspended solid removal rate and protease activity under different pH levels and oxygen supplies are shown in Figs. 2a and 2b, respectively. As can be seen from Fig. 2, within the range studied, the volatile suspended solid solubilization ratio was high at pH 7 and 8. The highest volatile suspended solid solubilization ratio (55 %) was obtained at pH 7 under aerobic

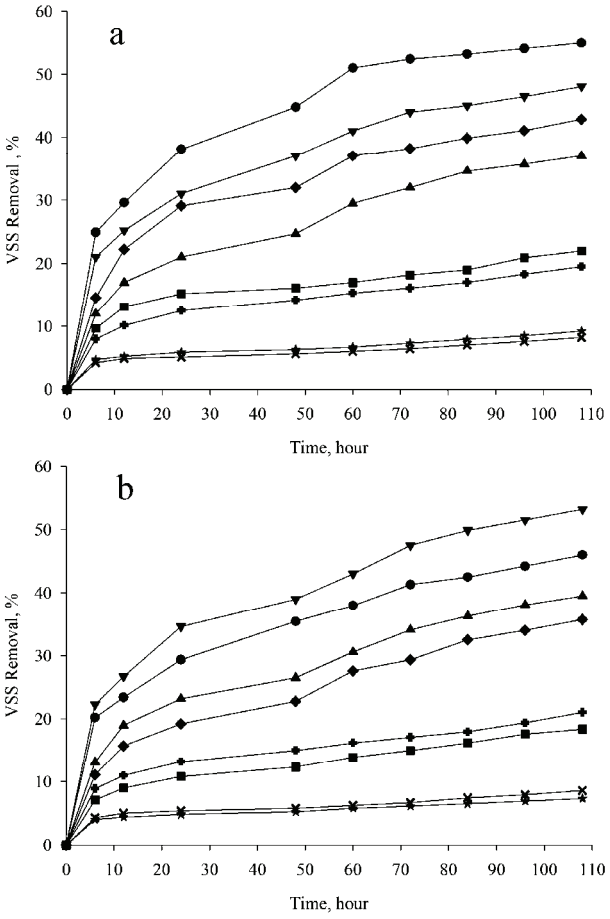

Fig. 2. Effect of pH on the volatile suspended solid removal under anaerobic, microaerobic and aerobic digestion of waste activated sludge with and without inoculation of *Bacillus* sp. Hnu at 60°C. a) pH 6 and 7 (– pH 6, control, – pH 6, anaerobic, – pH 6, microaerobic, – pH 6, aerobic, – pH 7, control, – pH 7, anaerobic, – pH 7, microaerobic, – pH 7, aerobic); b) pH 8 and 9 (– pH 8, control, – pH 8, anaerobic, – pH 8, microaerobic, – pH 8, aerobic; – pH 9, control, – pH 9, anaerobic, – pH 9, microaerobic, – pH 9, aerobic).

condition after 108 h. Moreover, the solubilization ratios of the volatile suspended solid were 42.9 and 22 % at pH 7 after 108 h under microaerobic and anaerobic conditions, respectively. These phenomena indicate that the oxygen supply is an important factor in volatile suspended solid degradation primarily because of the notable DO effect on the protease activity.

Bacterial life, *i.e.*, metabolism, growth and cellular division, is closely related to pH. The effect of pH on the transport of nutrients and organic components through the cytomembrane determines its toxicity action on bacteria. This condition also activates the hydrolytic enzyme alkaline phosphatase. The pH range suitable for the existence of most biological life is quite narrow and critical (typically 6 to 9).[25] The effects of pH on the protease activity were studied in the range of 6 to 9 under anaerobic, microaerobic, and aerobic digestions of the excess sludge with and without *Bacillus* sp. Hnu inoculation at 60 °C. The results are shown in Fig. 3. The protease activity increased with time under all sludge

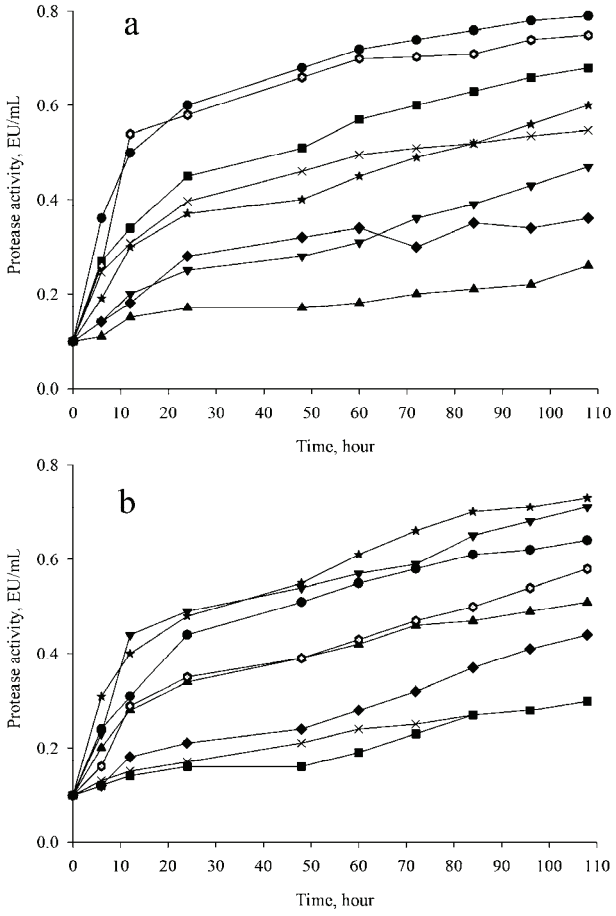

Fig. 3. Effect of pH on the protease activity under anaerobic, microaerobic and aerobic digestion of waste activated sludge with and without inoculated *Bacillus* sp. Hnu at 60 °C. a) pH 6 and 7 (▲ – pH 6, control, ▼ – pH 6, anaerobic, ★ – pH 6, microaerobic, ■ – pH 6, aerobic; ◆ – pH 7, control, × – pH 7, anaerobic, ◇ – pH 7, microaerobic, ● – pH 7, aerobic); b) pH 8 and 9 (× – pH 8, control, ▲ – pH 8, anaerobic, ▼ – pH 8, microaerobic, ★ – pH 8, aerobic; ■ – pH 9, control, ◆ – pH 9, anaerobic, ◇ – pH 9, microaerobic, ● – pH 9, aerobic).

conditions and the highest activity of 0.79 EU mL^{-1} was reached at pH 7 under aerobic conditions. The activity of the sludge without inoculated *Bacillus* sp. Hnu at pH 7 was only 0.36 EU mL^{-1}. At the same pH, the protease activity increased with the increasing supply of oxygen. Thus, the inoculation of *Bacillus sp.* Hnu and the oxygen supply helped accelerate the hydrolysis rate.

Kinetic analysis of sludge hydrolysis

Different rates of hydrolysis, k_h, values were reported because the hydrolysis process was affected by various factors, such as pH, temperature, particle size and its distribution pattern, and sludge source.[26] Therefore, a comparison of the k_h values obtained in the present study with those in previous publications is quite challenging.

Feng *et al.*[27] analyzed excess sludge hydrolysis and short-chain fatty acids (SCFAs) production at pH 10, and observed that the hydrolysis of excess sludge particulate chemical oxygen demand (*COD*), as well as the accumulation of SCFAs followed first-order kinetics. Thus, the hydrolysis of volatile suspended solid in the present study could also be assumed to follow first-order kinetics. The first-order kinetic equation of the hydrolysis (volatile suspended solid reduction) can be described as:

$$\frac{dM}{dt} = -k_h M \quad (1)$$

$$\ln M = -k_h t + b \quad (2)$$

where dM/dt is the rate of change of the volatile suspended solid per unit time and b is the integration constant. By plotting ln M *versus* t, the slope and the intercept, corresponding to the values of $-k_h$ and b, respectively, could be obtained. The regression curves are illustrated in Fig. 4, and a summary of the values of the volatile suspended solid hydrolysis rate constants are given in Table III.

The goodness of fit values for the different types of treatment at the temperature 40 °C were generally good within the range 0.9169–0.9523 (Fig. 4a and Table III). At a temperature 50 °C, the correlation coefficients were in the range from 0.8660–0.9505 (Fig. 4b and Table III). However, the correlation coefficients of 60 °C at different oxygen supply were not high, only 0.7608–0.8460 (Fig. 4c and Table III). This phenomenon may be due to thermophilic bacteria exhibiting higher protease activity at higher temperatures (optimum temperature 60 °C) resulting in faster degradation of the volatile suspended solid, while at high temperatures partially mesophilic bacteria are killed and the organic particles rupture, which results in the sludge hydrolysis that does not follow the first-order kinetic model at the highest temperature (60 °C). The hydrolysis rate constants (k_h) for the anaerobic, microaerobic, and aerobic conditions were 3, 4.8, and 7 times (40 °C), 3.5, 9.8, and 11.8 times (50 °C) and 2.7, 7.2, and 10.3 times (60 °C)

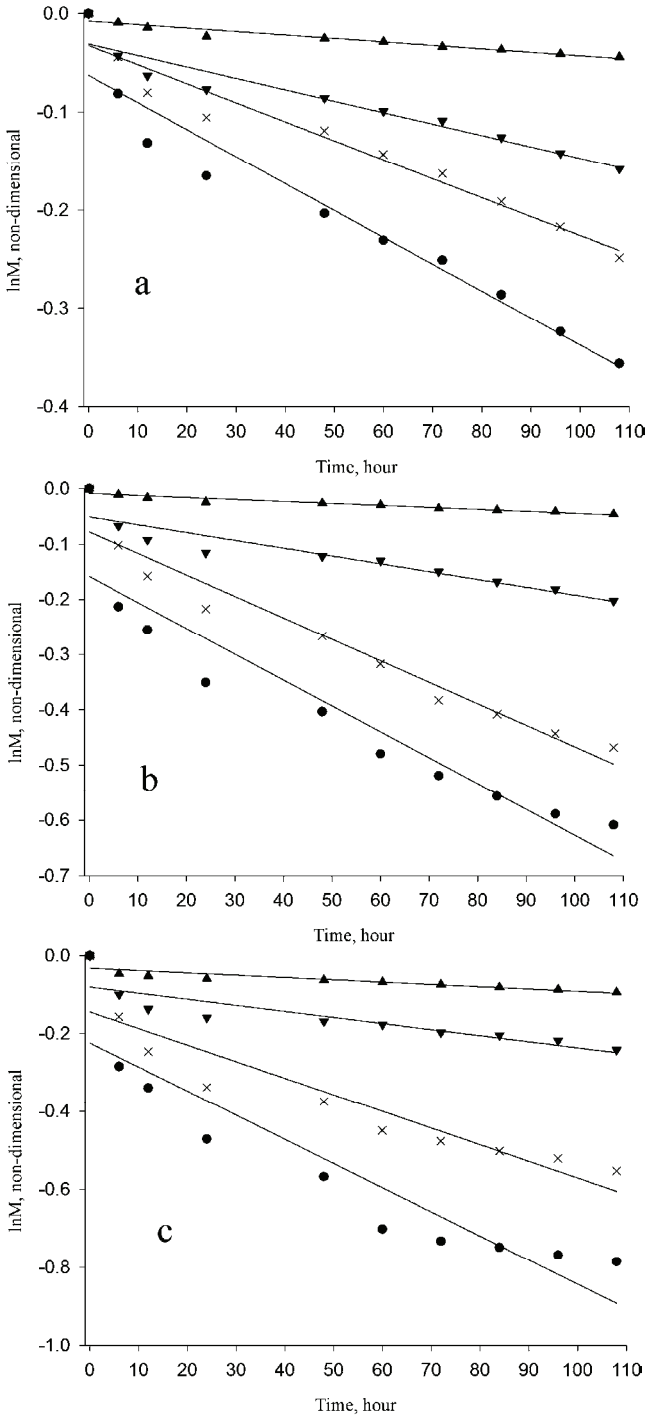

Fig. 4. Relation between ln *M* and time during sludge hydrolysis. a) 40 °C (▲ – control, ▼ – anaerobic, × – microaerobic, ● – aerobic); b) 50 °C (▲ – control, ▼ – anaerobic, × – microaerobic, ● – aerobic); c) 60 °C (▲ – control, ▼ – anaerobic, × – microaerobic, ● – aerobic).

higher, respectively, than that of the control test, indicating that the *Bacillus* sp. Hnu and the oxygen supply helped accelerate the hydrolysis rate.

TABLE III. Hydrolysis rate constants under different temperature and oxygen supply conditions

Temperature, °C	Type of treatment	Dynamic equation	Rate constant k_h / h^{-1}	R^2
40	Control	$y = -0.0004x - 0.0075$	0.0004	0.9344
	Anaerobic	$y = -0.0012x - 0.0308$	0.0012	0.9169
	Microaerobic	$y = -0.0019x - 0.0324$	0.0019	0.9523
	Aerobic	$y = -0.0028x - 0.0626$	0.0028	0.9392
50	Control	$y = -0.0004x - 0.0087$	0.0004	0.9268
	Anaerobic	$y = -0.0014x - 0.0359$	0.0014	0.8660
	Microaerobic	$y = -0.0039x - 0.0778$	0.0039	0.9505
	Aerobic	$y = -0.0047x - 0.1584$	0.0047	0.8839
60	Control	$y = -0.0006x - 0.0324$	0.0006	0.7608
	Anaerobic	$y = -0.0016x - 0.0808$	0.0016	0.7676
	Microaerobic	$y = -0.0043x - 0.1444$	0.0043	0.8640
	Aerobic	$y = -0.0062x - 0.2243$	0.0062	0.8493

CONCLUSION

A thermophilic strain was isolated from excess sludge and identified as a new species of *Bacillus* by 16S rRNA gene sequence analysis, named *Bacillus* sp. Hnu. *Bacillus* sp. Hnu was able to release a protease that could dissolve sludge. The results indicated that temperature and oxygen supply affect the volatile suspended solid removal ratio and protease activity, and higher temperature and greater oxygen supply were advantageous to the volatile suspended solid removal ratio and protease activity. The maximum volatile suspended solid removal ratios of 21.5, 42.5 and 54.4 % were obtained after 108 h digestion at pH 6.9 and 60 °C under anaerobic, microaerobic and aerobic conditions, respectively. Volatile suspended solid removal ratio and protease activity were only slightly affected by the pH. The kinetic study showed that the hydrolysis of sludge with *Bacillus* sp. Hnu and the control test followed the first-order kinetics except at the highest employed temperature (60 °C). The hydrolysis rate constants (k_h) for the anaerobic, microaerobic, and aerobic conditions were 3, 4.8, and 7 times (40 °C), 3.5, 9.8, and 11.8 times (50 °C) and 2.7, 7.2, and 10.3 times (60 °C) higher, respectively, than that of the control test, indicating that *Bacillus* sp. Hnu and oxygen supply helped accelerate the hydrolysis rate.

Acknowledgment. This research was supported financially by the Doctorate Science Fund of Taiyuan University of Science & Technology (No. 20122056) and the University

Innovation and Training Program Fund of Taiyuan University of Science & Technology (No. xj2013036).

И З В О Д

УБРЗАВАЊЕ ХИДРОЛИЗЕ ОТПАДНИХ НАСЛАГА ПРИМЕНОМ ТЕРМОФИЛНЕ БАКТЕРИЈЕ *Bacillus* sp. Hnu У ПРИСУСТВУ РАЗЛИЧИТИХ КОНЦЕНТРАЦИЈА КИСЕОНИКА

WEI ZHENG[1], XIAO MING LI[2], BING ZHENG LI[1], HONG YING XU[1] и YA BING GUO[1]

[1]*School of Environment and Safety, Taiyuan University of Science and Technology, Taiyuan 030024, P. R. China* и [2]*College of Environmental Science and Engineering, Hunan University, Changsha 410082, P. R. China*

Термофилна бактерија је изолована из отпадних наслага у води и 16S рДНК анализом је констатовано да припада роду *Bacillus*. Идентификована је као нова и названа је *Bacillus* sp. Hnu. Циљ рада је био да испита ефикасност хидролизе отпадних наслага овом бактеријом у присуству различитих концентрација кисеоника. Резултати су показали да је боље уклањање испарљивих састојака при већим температурама и више кисеоника, као и да је повећана протеазна активност. Највећи удео уклањања испарљивих супстанци суспендованих у чврстом талогу постигнут је после 108 сати дигестије на pH 6,9 и 60 °C и повећавао се за 17,2, 38,0 и 45,4 % у анеробним, микроаеробним и аеробним условима, редом, у односу на контролни тест. Константе брзине хидролизе за анаеробне, микроаеробне и аеробне услове су биле 3,0; 4,8 и 7 пута (40 °C), 3,5; 9,8 и 11,8 пута (50 °C), односно 2,7; 7,2 и 10,3 пута (60 °C) веће од оних у контролним условима. Може се закључити да је *Bacillus* sp. Hnu способна да убрза хидролизу отпадних наслага. Кинетичка испитивања су показала да хидролиза отпада бактеријом *Bacillus* sp. Hnu, као и контролни тест, прате кинетику првог реда, осим на 60 °C.

(Примљено 8. октобра 2012, ревидирано 14. фебруара 2013)

REFERENCES

1. Y. S. Wei, R. T. V. Houten, A. R. Borger, D. H. Eikelboom, Y. B. Fan, *Water Res*. **37** (2003) 4453
2. G. M. Zhang, P. Y. Zhang, J. M. Yang, Y. M. Chen, *J. Hazard. Mater*. **145** (2007) 515
3. Y. K. Kim, M. S. Kwak, W. H. Lee, J. W. Choi, *Biotechnol. Bioprocess Eng.* **5** (2000) 469
4. X. S. Li, H. Z. Ma, Q. H. Wang, S. Matsumoto, T. Maeda, H. Ogawa, *Bioresour. Technol*. **100** (2009) 2475
5. E. W. Low, H. A. Chase, M. G. Milner, T. P. Curtis, *Water Res.* **34** (2000) 3204
6. Y. S. Wei, R. T. V. Houten, A. R. Borger, D. H. Eikelboom, Y. B. Fan, *Environ. Sci. Technol.* **37** (2003) 3171
7. J. Müller, G. Lehne, J. Schwedes, S. Battenberg, R. Näveke, J. Kopp, N. Dichtl, A. Scheminski, R. Krull, D. C. Hempel, *Water Sci. Technol.* **38** (1998) 425
8. G. M. Zhang, J. G. He, P. Y. Zhang, J. Zhang, *J. Hazard. Mater*. **164** (2009) 1105
9. J. L. Campos, L. Otero, A. Franco, A. Mosquera-Corral, E. Roca, *Bioresour. Technol.* **100** (2009) 1069
10. L. B. Chu, J. L. Wang, B. Wang, X. H. Xing, S. T. Yan, X. L. Sun, B. Jurcik, *Chemosphere* **77** (2009) 269
11. S. T. Yan, H. Zheng, A. Li, X. Zhang, X. H. Xing, L. B. Chu, G. J. Ding, X. L. Sun, B. Jurcik, *Bioresour. Technol.* **100** (2009) 5002

12. Y. Liu, *Chemosphere* **50** (2003) 1
13. L. Thomas, G. Jungschaffer, B. Sprossler, *Water Sci. Technol.* **28** (1993) 189
14. Q. Yang, K. Luo, X. M. Li, D. B. Wang, W. Zheng, G. M. Zeng, J. J. Liu, *Bioresour. Technol.* **101** (2010) 2924
15. L. Guo, J. Zhao, Z. L. She, M. M. Lu, Y. Zong, *Bioresour. Technol.* **117** (2012) 368
16. S. Hasegawa, N. Shiota, K. Katsura, A. Akashi, *Water Sci. Technol.* **41** (2000) 163
17. H. Q. Ge, P. D. Jensen, D. J. Batstone, *J. Hazard. Mater.* **187** (2011) 355
18. P. Burt, S. F. Morgan, B. N. Dancer, J. C. Fry, *Appl. Microbiol. Biotechnol.* **33** (1990) 725
19. E. Neyens, J. Baeyens, *J. Hazard. Mater., B* **98** (2003) 51
20. T. Forster-Carneiro, M. Pérez, L. I. Romero, D. Sales, *Bioresour. Technol.* **98** (2007) 3195
21. S. G. Liu, N. W. Zhu, L. Y. Li, H. P. Yuan, *Water Res.* **45** (2011) 5959
22. S. G. Liu, N. W. Zhu, L. Y. Li, *Bioresour. Technol.* **104** (2012) 266
23. J. E. Johansen, R. Bakke, *Water Sci. Technol.* **53** (2006) 43
24. L. S. Clescerl, A. E. Greenberg, A. D. Eaton, *Standard Methods for the Examination of Water and Wastewater*, American Public Health Association, Washington DC, USA, 1999, p. 100
25. G. Tchobanoglous, F. L. Burton, H. D. Stensel, *Wastewater Engineering: Treatment and Reuse*, McGraw-Hill, New York, USA, 2003, p. 100
26. I. S. Turovskiy, P. K. Mathai, *Wastewater sludge processing*, Wiley, Hoboken, NJ, 2006, p. 100
27. L. Y. Feng, Y. Y. Yan, Y. G. Chen, *J. Environ. Sci.* **21** (2009) 589.

Journal of the Serbian Chemical Society
JSCS-info@shd.org.rs • www.shd.org.rs/JSCS
J. Serb. Chem. Soc. 78 (8) 1149–1160 (2013) UDC **Arabidopsis thaliana*+664.8.047+66–973
JSCS–4486 *Original scientific paper*

Dehydrins (LTI29, LTI30, and COR47) from *Arabidopsis thaliana* expressed in *Escherichia coli* protect thylakoid membranes during freezing

VLADAN BOZOVIC[1]*, JAN SVENSSON[2], JÜRGEN SCHMITT [3] and CARSTEN KOHN[3]

[1]University of Montenegro, Biotechnical Faculty, Mihajla Lalića 1, 20000 Podgorica, Montenegro, [2]Uppsala Genetic Center, Swedish University of Agricultural Sciences, Uppsala S-750 07, Sweden and [3]Institute for Plant Physiology and Microbiology – Department of Biology, Chemistry and Pharmacy - FU Berlin, Schwendenerstrasse 1, 14195 Berlin, Germany

(Received 27 November 2012, revised 5 February 2013)

Abstract: As the name dehydrins implies, these proteins are typically expressed in response to dehydration, which can be caused by drought, osmotic stress, or freezing temperatures.[1] In general, dehydrins occur in plants as multi-gene families. Four arabidopsis dehydrins (LTI29, ERD14, COR47 and RAB18) were tested for protection of thylakoid membranes during freeze–thaw cycles *in vitro*.[2,3] The first reported results showed that dehydrins LTI29, ERD14, COR47 have cryoprotective activity while RAB18 did not protect the thylakoid membranes at low temperatures. The cryoprotective activity reached a maximum of 50–60 % at a protein concentration of 140–250 μg mL^{-1} in the assay. A contribution of dehydrins to freezing tolerance *in vivo* is supported by the observation of Nylander *et al.*[4] that LTI29 and COR47 are cold induced at the mRNA and protein expression level.

Keywords: *Arabidopsis thaliana*; dehydrins; freezing tolerance; thylakoid; cold acclimation.

INTRODUCTION

Dehydration is a common process during seed maturation, which is realized by programmed expression of specific genes.[5] Nowadays, genes encoding dehydrins have been cloned from numerous plant species belonging to diverse groups such as angiosperms, gymnosperms, mosses and lycopods.[6] Dehydrins are widely distributed in plants. They significantly vary in amino acid composition (from 100 to 600 amino acid residues) and in molecular mass. The amino acid composition of these proteins is characterized by a high content of charged and polar residues, which determine their biochemical properties, including thermostat-

* Corresponding author. E-mail: vladan.bozovic@yahoo.com
doi: 10.2298/JSC121127017B

bility.[7,8] The features of dehydrin proteins have recently been summarized in a review by Kosova *et al.*[9]

Structure of Arabidopsis thaliana *dehydrins (RAB18, LTI29, LTI30, and COR47)*

Isolation and purification of native arabidopsis dehydrins[10] allowed an investigation of their biochemical properties *in vitro*. Generally, arabidopsis dehydrins are enriched in glycine and lysine residues, but lack cysteine and tryptophan.[11] For example, in arabidopsis LTI30 dehydrin with a molecular mass of 21 kD, glycine, histidine, lysine, and threonine represent 56 % of the total amino acids, whereas cysteine, tryptophan, arginine, and valine are not found. This explains the highly hydrophilic nature of this protein. Dehydrins are not very likely to form oligomers and they are intrinsically unstructured proteins.

Cryoprotective activity of dehydrins

Many studies reported a positive correlation between the accumulation of dehydrin transcripts or proteins and the tolerance to freezing, drought, and salinity.[12] Puhakainen *et al.*[1] provided data that overexpression of multiple Arabidopsis dehydrin genes, such as LTI29 and LTI30, resulted in an increased freezing tolerance and improved survival under exposure to low temperatures, demonstrating that dehydrins do contribute to freezing tolerance.

One of the proteins with proved cryoprotective activity is a plant lipid-transfer protein called cryoprotectin (CPP).[13] This protein was isolated from cold acclimated spinach and cabbage leaves that prevented inactivation of cyclic photophosphorylation in spinach thylakoid membranes during freeze–thaw cycles to –25 °C.[14] In addition, treatment of the extracts with a protease confirmed that the cryoprotective activity is indeed due to the presence of protein and not to the presence of contaminants such as sugars.[15] In the present study, cryoprotectin from cabbage (*Brassica oleracea*) was used as a positive control regarding cryoprotective activity.[16] The aim of the study was to test the cryoprotective activity of *Arabidopsis thaliana* dehydrins LTI29, ERD14, COR47 and RAB 18 on isolated spinach thylakoid membranes during freeze–thaw cycles.

MATERIALS AND METHODS

Spinach (*Spinacia oleracea* L. cv Monnopa) was grown under non-hardening conditions in a growth chamber at 25/15°C (day/night) temperature and 50 % of relative humidity. Cabbage *(Brassica oleracea* L. cv Grüfiwi) was grown in the garden for several months and then transferred to pots. The plants were harvested and the leaves used directly for protein extraction.

Bacterial strain: Escherichia coli *M15[pREP4], SG13009[pREP4] Qiagen*

For regulated high-level expression with pQE vectors, the cells contained pREP4 plasmid encoding lac repressor in trans, ensuring strictly regulated expression.

Expression vector

The analyzed proteins were expressed using the expression vector pJTS1. This vector was a pQE-60 vector modified by Jan Svensson (Uppsala University, Sweden).[10] Expression vector pQE-60 containing genes for analyzed proteins were transferred to *E. coli* M15 [pREP4], SG13009[pREP4] strain.

Colony screening by PCR

PCR (Table I) was used to screen colonies with the genes of the analyzed proteins. A list of the primers used in this study is shown in the Table II.

TABLE I. PCR conditions

Number of cycle	Temperature, °C	Duration, s
1	94	60
	94	30.
35	–[a]	30
	72	60.

[a]Different annealing temperatures were used for the amplification of the dehydrins genes: LTI29, 56 °C; ERD14, 50 °C; COR47, 63 °C; RAB18, 63 °C

TABLE II. List of primers used for amplification of dehydrins genes

Primer	Dehydrins gene
PQE F1	5'CCCGAAAAGTGCCACCTG3'
PQE F2	5'CGGATAACAATTTCACACAG3'
PQE R	3'GGTCATTACTGGAGTCTTG5'
LTI29	5'GAAAAGAATGGCAGAAGAGTACAAGAACACC3'
LTI29	3'TTAATCAGACACTTTTTCTTTCTTCTCT5'
ERD14	5'CCGCTCGAGAAAAGAATGGCTGAGGAAATCAAGAATG3'
ERD14	3'GCTCTAGATTATTCTTTATCTTTCTTCTCC5'
COR47	5'GAAAAGAATGGCTGAGGAGTACAAGAACAACG3'
COR47	3'TTAATCATCAGACTCTTTTTCTTTCTTCACTTCC5'
RAB18	5'CCGCTCGAGAAAAGAATGGCGTCTTACCAGAACCGTCCGTCCAGG3'
RAB18	3'GCTCTAGATTAACGGCCACCACCGGGAAGCTTTTCC5'

Protein extraction from E. coli

Dehydrin genes were cloned in a bacterial vector that allowed IPTG-inducible expression of His6-tagged fusion proteins. Bacterial cells were grown in LB medium until an OD_{600} of 0.6 was reached. The cultures were cooled to the induction temperature in ice water. Harvesting of the cells was realized by centrifugation (20 min at 6000 g). The cell pellets were stored at –20 °C.

Cells were lysed by lysozyme treatment followed by sonication.[16] The supernatant and solubilized cell debris were analyzed for the presence of inclusion bodies by sodium dodecyl sulfate-polyacrylamide gel electrophoresis (SDS-PAGE).

The proteins were separated on a 16.5 % polyacrylamide resolving gel following the Laemmli procedure.[17] The resolving gel was 7 cm×8 cm×0.1 cm in size and was run at 200 V (constant voltage) for 60–70 min at room temperature. A 10X running buffer according to Laemmli was used. The gel was stained with Coomassie Brilliant Blue R250. Standard

Mark12™ with 12 polypeptides resolved into bands in the range from 2.5 to 200 kDa was used as the standard marker.

Protein purification

The recombinant proteins were efficiently purified with a two-step purification protocol: heat fractionation and immobilized metal ion affinity chromatography (IMAC).[18] Protein concentration was measured using Bradford method.[19] Bovine serum albumin (BSA) was used as the standard. A stock standard solution of 10 mg mL^{-1} was used to construct a calibration curve by measuring OD_{595} for different BSA concentrations.

Cryoprotectin extraction

Cryoprotectin extraction was performed according to the protocol modified by Hincha and Schmitt.[19]

Thylakoid isolation

Thylakoids are sensitive to elevated temperatures, therefore all solutions and glassware should be cooled to 4 °C before use. Isolated membranes should always be kept on ice, preferably in dim light. All centrifugation steps should take place at 4 °C.

Spinach leaves (50 g) were homogenized with 100 mL of homogenization buffer in a blender for approx 10 s. Immediately after, 125 µL of 1 M Na-ascorbate and 340 µL of 1 M cysteine were added to the buffer as these substances are unstable in solution. The homogenate was filtered through a nylon mesh to remove coarse particles. After filtration, the filtrate was centrifuged for 5 min at 2000 g. The pellets were resuspended in approximately 50 mL of washing solution. This was most easily performed using a Pasteur pipette. Centrifugation at 7000*g* for 5 min was performed with the aim of washing the thylakoid pellet; this procedure was repeated twice. The pellets from the last centrifugation step were resuspended in a minimum volume of washing solution. 10 µL of the thylakoid suspension was mixed with 990 µL of 80 % (v/v) acetone and centrifuged for 2 min in a bench-top centrifuge. The absorbance of the supernatant at 663 and 645 nm with 80 % (v/v) was measured using acetone as the reference. Chlorophyll content is calculated as follows:

$$0.1(8.02A_{663} + 20.2A_{645}) = \text{mg chlorophyll mL}^{-1} \quad (1)$$

Freeze–thaw cycle

Thylakoid suspension was diluted with washing buffer to a concentration of at least 1 mg chlorophyll mL^{-1}. The thylakoid suspension (0.5 mL) was mixed with an equal volume of proteins suspension in Eppendorf tubes. The suspension was placed in a freezer at –20 °C for 2 h.

Samples are most conveniently thawed in a water bath at room temperature and should be transferred to an ice bath immediately when the ice in the tubes has melted.

Thylakoid volume measurements

Hematocrit capillaries (Fig. 1) were loaded with diluted thylakoid suspensions after thawing and the capillaries were sealed at one end. Capillaries were centrifuged for 15 min in a hematocrit centrifuge and pellet heights were measured (Fig. 1) with a magnifying glass on a 0.1 mm scale.

The cryoprotective activity (in %) was calculated using the equation:

$$TKV(\text{PP–20 °C}) - TKV(\text{–20 °C})/TKV(\text{0 °C}) - TKV(\text{–20 °C}) = X/100 \quad (2)$$

where TKV(PP–20 °C) is the thylakoid volume in presence of analyzed protein at –20 °C, TKV(–20 °C) is the thylakoid volume without protein at –20 °C and TKV(0 °C) is the thylakoid volume without protein at 0 °C.

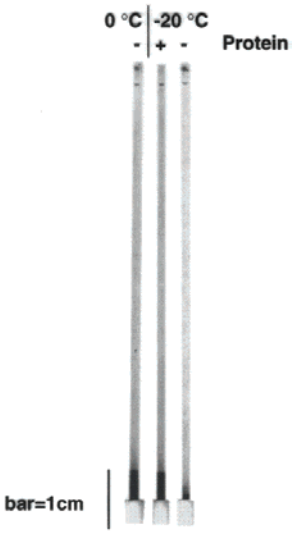

Fig 1. Volumetric test. Hematocrit capillaries were used to measure the cryoprotective activity. The controls at 0 and –20 °C show the total volume of the thylakoids at these temperatures after centrifugation; + – the thylakoid volume at –20 °C in the presence of dehydrins; - – the thylakoid volume at –20 °C without any dehydrin.

Immunoblot analysis

The antibodies for LTI29 and RAB18 dehydrins were developed by J. Svensson (Uppsala University). It was possible to obtain a LTI29 antibody that was specific to LTI29 and the previously made RAB18 antibodies were only recognized by RAB18.[20] Both antibodies were directed against the conservative K-segment of the dehydrins. The analyzed protein (10 μg) was subjected to 16.5 % SDS–PAGE and transferred onto nitrocellulose membranes (Amersham Biosciences Inc.). The nitrocellulose membranes were incubated with primary antibody (diluted 1:250 to 1:1000 in blocking buffer) for 2 h in blocking buffer at room temperature, and 1:2000 dilution for affinity-purified rabbit polyclonal to green fluorescent protein (GFP) antibody (Abcam). Blots were then probed with peroxidase-labeled anti-rabbit secondary antibodies (Dako) at 1:2000 dilution. The signals were visualized using an enhanced chemiluminescence reagent (ECL, Amersham Biosciences Inc.) and exposed onto an ECL Hyperfilm (Amersham Biosciences Inc.).

RESULTS AND DISCUSSION

Transformation and checking by colony PCR

Escherichia coli M15 strain was transformed and screened for positive clones by PCR constructed primers for each gene individually. Previously, a PCR program was designed (suitable annealing temperatures) for all the analyzed sequences (Table II).

The PCR products were analyzed by 2 % agarose gel electrophoresis (Fig. 2). For each analyzed gene, the corresponding PCR product in base pairs length was confirmed.

Dehydrins expression

The highest production of soluble dehydrins was obtained by inducing expression of the cloned dehydrin genes with IPTG (isopropylthio-*β*-galactoside)

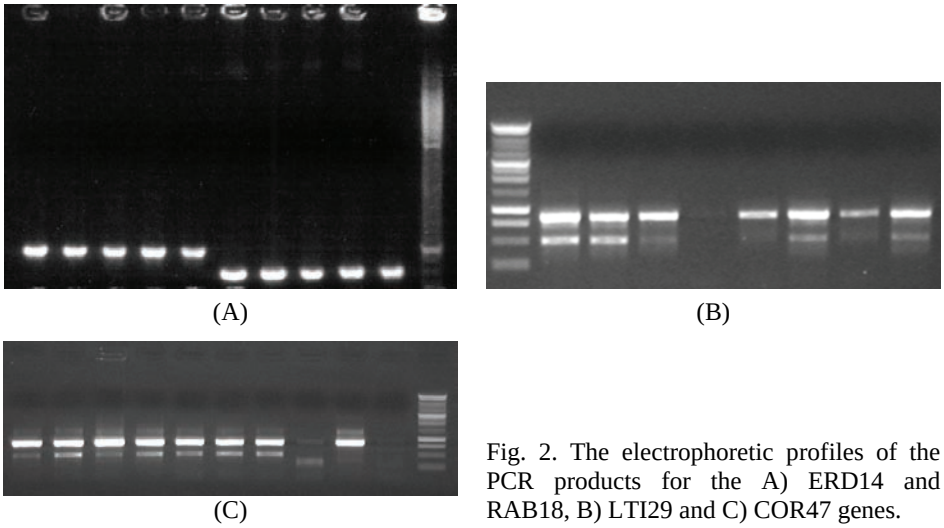

(A) (B) (C)

Fig. 2. The electrophoretic profiles of the PCR products for the A) ERD14 and RAB18, B) LTI29 and C) COR47 genes.

when the cells reached an OD_{600} of 0.5–0.7. Overproduction of recombinant proteins in *E. coli* often results in the formation of insoluble inclusion bodies. After resuspension in 20 mM NaH_2PO_4, pH 6.0, it was clear that the recombinant proteins were localized in the supernatant and did not form inclusion bodies. For heat fractionation, the lysate was placed in a water bath at 90 °C for 8 min. Approximately 80 % of the contaminating proteins precipitated during the heat fractionation, while the dehydrins remained heat stable. Using concentration filters (Promega), the final concentration of the analyzed proteins was doubled (Figs. 3 and 4). Heat treatment was followed by immobilized metal ion affinity chromatography (IMAC).[18] Purification according to this procedure showed additional bands (Figs. 3 and 4) originating from crude bacterial proteins which had no cryoprotective activity (negative control). The yields of purified proteins were between 4 and 15.5 mg L^{-1} of bacterial culture, which was sufficient for further biochemical studies. The estimated molecular mass values for the analyzed proteins according to SDS–PAGE were the following: LTI29, 47 kDa; ERD14, 34 kDa; COR47, 54 kDa; RAB18, 25 kDa.

Protein desalting

The analyzed proteins were desalted using PD10 desalting columns (Promega). Protein concentration and conductivity from small aliquots (50 μL) were measured simultaneously. It was shown that proteins LTI 29 and COR 47 (Fig. 5) flowed through the column after 1.5 mL eluting buffer and the highest concentration of the proteins was reached at 2.5–3.5 mL. Elution kinetics for all proteins were different because of their different size (Fig. 5).

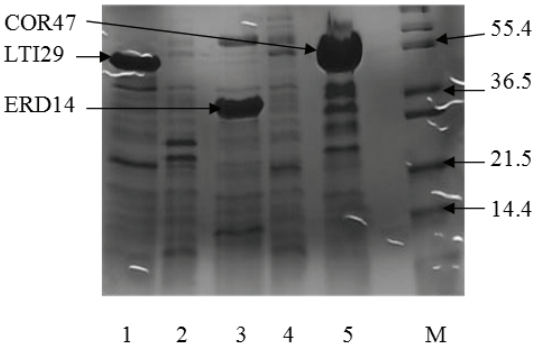

Fig 3. SDS–PAGE profile for the three cryoprotective dehydrins (LTI29, ERD14 and COR47) after the purification and concentration procedure. The differences in the expressed yields of the analyzed proteins are caused by induction during the expression procedure using IPTG. 1 – LTI29 induced; 2 – LTI29 not induced; 3 – ERD14 induced; 4 – ERD14 not induced; 5 – COR47 induced; M – protein marker "Mark 12^{TM} Unstained Standard".

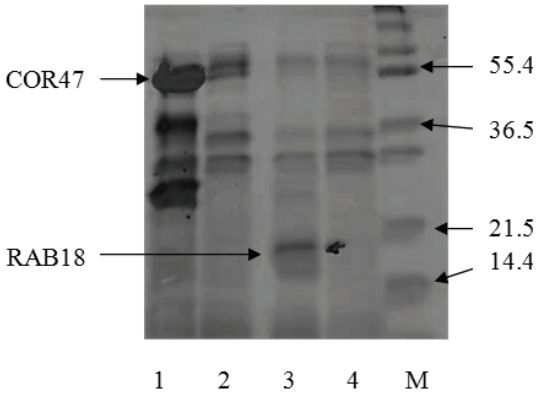

Fig 4. SDS–PAGE profile for the cryoprotective dehydrins COR47 and RAB18 after purification and concentration procedure. The differences in the expressed yields of analyzed proteins were caused by induction during expression procedure using IPTG. 1 – COR47 induced; 2 – COR47 not induced; 3 – RAB18 induced; 4 – RAB18 not induced; M – protein marker "Mark 12^{TM} unstained Standard".

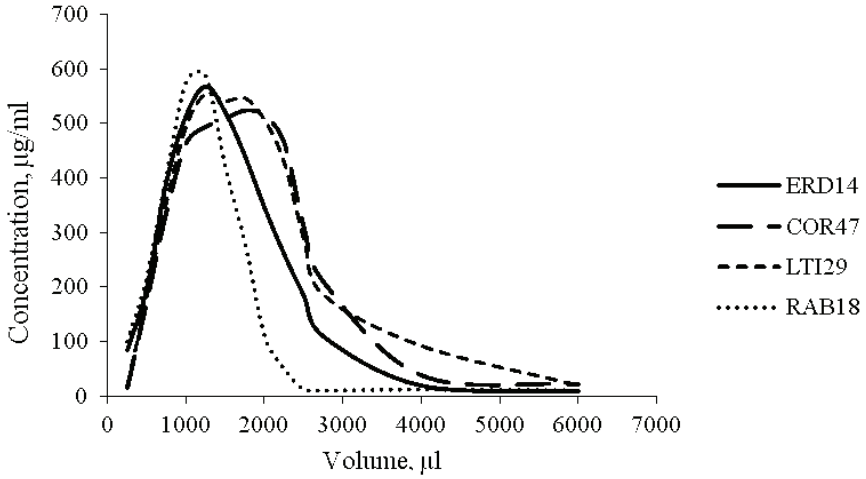

Fig 5. Protein desalting using desalting PD 10 columns. Using desalting columns, ammonium sulfate was removed from the solutions containing the analyzed proteins. It was shown that proteins LTI 29, COR 47 and ERD 14 had different elution kinetics to that of RAB18 because of the different dimensions of the analyzed proteins.

Cryoprotective activity

During the period of plant acclimatization to low temperatures, it was shown[12] that the dehydrins were expressed, which indicates a possible cryoprotective activity of these proteins. A freezing test, which was based on measuring the ability of proteins to protect thylakoids during a freeze–thaw cycle, was used in this study.[19] As a result, cryoprotective activity was evidenced in three out of four analyzed dehydrins. (Table III).

In addition to these results, dehydrin RAB18 had a small percentage of cryoprotective activity over the level of the negative control. As a negative control, a non-induced crude bacterial extract boiled, purified and concentrated using the previously described procedure, which showed no cryoprotective activity, was used. As a positive control, a CPP (cryoprotectin) was used.[13] In this study, it was found that the analyzed dehydrins (LTI29, ERD14, and COR47) from *Arabidopsis thaliana* have cryoprotective activity in various percentages (Fig. 6). Cryoprotective activity was individually measured 10 times per each dehydrin.

TABLE III. Cryoprotective activity of the analyzed dehydrins and CPP protein in %; SD – standard deviation; AV – average value; Cont. 0 °C and Cont –20 °C – measured cryoprotective activity at 0 and –20 °C without added proteins in the suspension

Dehydrin/protein	1	2	3	4	*SD*	*AV*
ERD 14	47.4	43.6	56.8	53.1	5.89	49.3
RAB 18	7.6	15.2	3.8	5.7	4.99	8.1
LTI 29	47.4	36	43.6	45.5	4.9	43.1
COR 47	41.7	45.5	43.6	30.3	6.8	40.2
Cont. 0 °C	115.6	94.8	96.7	92.9	10.5	100
Cont. –20 °C	0.0	1.9	0.0	1.9	1.55	0.95
CPP	59.4	55	62	60.8	4.94	59.3

The protein concentration is a relevant factor for the level of cryoprotective activity (Fig. 7). With increasing initial protein concentration, the cryoprotective activity increased. Saturation was reached at an activity of 50–60 %.

The possible mechanism of dehydrin cryoprotection is still unknown. Some authors reported that dehydrins have a binding ability to lipid vesicles,[20] therefore, the binding ability of dehydrins LTI29 and RAB18 to thylakoid membranes was analyzed. Thylakoids from non-hardened spinach leaves were incubated with dehydrins LTI29 and RAB18 and then subjected to three rounds of centrifugation and resuspension in a protein-free solution.

Immunoblot analyses of supernatant after several washing steps are shown in Fig. 8. After several washing steps, it was shown that the supernatant was free of dehydrins, while dehydrin with binding ability to thylakoid membrane was assumed to be found.

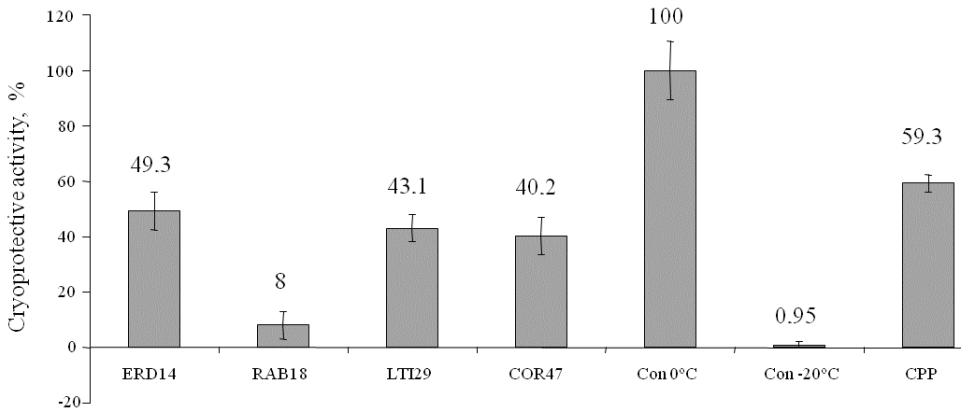

Fig 6. Cryoprotective activity of four analyzed dehydrins. Using the "freezing test", the results showed that the four dehydrins had different cryoprotective activities. It was also revealed that dehydrin RAB18 had a smaller percentage of cryoprotective activity. A crude extract of cold hardened *Brassica oleracea* containing cryoprotectin[16] was used as the positive control (CPP). As a negative control, a non-induced crude bacterial extract boiled, purified and concentrated using the standard procedure, which showed no cryoprotective activity, was used (Con –20 °C).

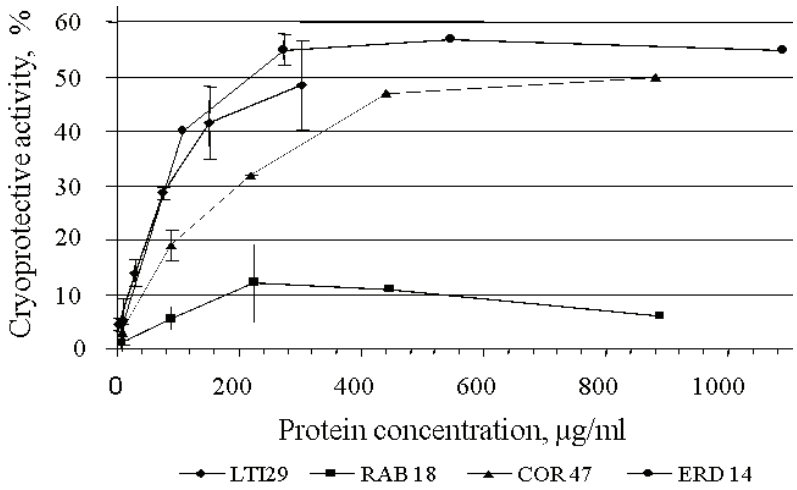

Fig 7. The cryoprotective activity as a function of protein concentration. The dependences of cryoprotective activities on the concentration of the protein are linear only for low protein concentrations; at higher protein concentrations, there are clear saturation points for the cryoprotective activities of the proteins.

Immunoblot analyses showed (Fig. 8, line 4) that the protein LTI29 was still detected after several washing steps. In the parallel experiment with protein RAB18 (no cryoprotective activity), the protein was not visible. The result of this experiment clearly shows the presence of binding ability of LTI29 protein to the

thylakoid membranes, which could be linked to the cryoprotective activity of the protein. Immunoblot analysis of thylakoid membranes showed that there was no protein present that could react with the antibody.

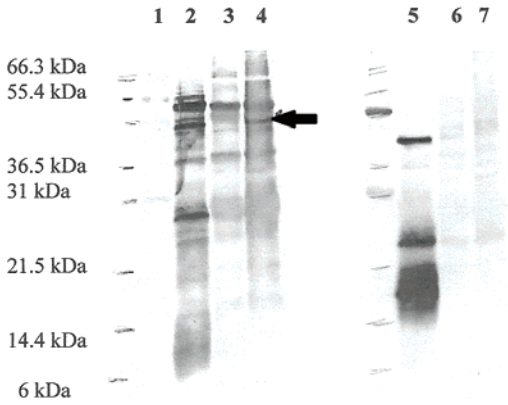

Fig 8. Binding ability of dehydrins LTI29 and RAB18. Immunoblot analyses indicated to binding abilities of dehydrins to the thylakoid membrane, which were in correlation with their cryoprotective activity. 1. PM – protein marker; 2. LTI29 – expressed protein LTI29 from *E. coli*; 3. Thyl. thylakoid proteins; 4. Thyl.+ LTI29 (after washing); 5. RAB18 – expressed protein RAB18 from *E. coli*; 6. Thyl. thylakoid proteins; 7. Thyl+ +RAB18 (after washing). The arrow shows the position of dehydrin LTI29 after several washing steps.

CONCLUSIONS

The results show, for the first time, that three out of four analyzed proteins from *Arabidopsis thaliana* expressed in *Escherichia coli* protect thylakoid membranes during a freeze–thaw cycle *in vitro* (cryoprotective activity), which indicates the possible function of these proteins under stress conditions. The highest cryoprotective activity was shown by the ERD14 dehydrin (49 %), while dehydrins LTI29 and COR47 showed similar levels of cryoprotective activity (43 and 40 %, respectively). In this study, no cryoprotective activity for the protein RAB18 was evidenced. It was also demonstrated that most of the proteins from the bacterial supernatant become denatured due to the heat treatment process, while dehydrins remained stable. This was taken to be an important step in the purification of the dehydrins. In addition, the yield of the proteins was satisfactory although differences in the yields among the analyzed proteins were found. Immunoblot analyses indicated that the binding ability of dehydrins to the thylakoid membrane was in correlation with their cryoprotective activity. Dehydrin RAB18, which showed no cryoprotective activity, did not bind to the thylakoid membranes, according to the present results. This suggests that the binding of analyzed proteins to the cell membrane is an important prerequisite for cryoprotective activity. The protein concentration is a relevant factor for the level of cryoprotective activity since cryoprotective activity increases with increasing initial protein concentration. Further studies should be performed with the aim of investigating the possible mechanism of cryoprotective activity of the dehydrins used in this study.

ИЗВОД

ДЕХИДРИНИ (LTI29, LTI30, COR47) ИЗ *Arabidopsis thaliana* ЕКСПРИМИРАНИ У *Escherichia coli* ШТИТЕ ТИЛАКОИДНЕ МЕМБРАНЕ ТОКОМ СМРЗАВАЊА

VLADAN BOZOVIC[1], JAN SVENSSON[2], JURGEN SCHMITT[3] И CARSTEN KOHN[3]

[1]*University of Montenegro, Biotechnical Faculty, Podgorica, Montenegro,* [2]*Uppsala Genetic Center, Swedish University of Agricultural Sciences, Uppsala, Sweden и* [3]*Institute for Plant Physiology and Microbiology – Department of Biology, Chemistry and Pharmacy – FU Berlin, Berlin, Germany*

Као што им само име говори, дехидрини су протеини који се експримирају као одговор на дехидратацију изазвану сушом, осмотским стресом или замрзавањем. Дехидрини су у биљкама кодирани мултигенским фамилијама. Заштитна улога четири дехидрина биљке *Arabidopsis* (LTI29, ERD14, COR47 и RAB18) приликом замрзавања тилакоидних мембрана је испитана *in vitro*. Наши резултати су показали да дехидрини LTI29, ERD14 и COR47 имају криопротективно дејство, док тај ефекат нема RAB18. Максимална криопротективна активност (50 до 60 %) је постигнута при концентрацији протеина од 140–250 μg mL^{-1} у тесту. О утицају дехидрина говоре и литературни подаци, према којима је експресија LTI29 и COR47, на РНК и протеинском нивоу, подстакнута ниским температурама.

(Примљено 27. новембра 2012, ревидирано 5. фебруара 2013)

REFERENCES

1. T. Puhakainen, M. V. Hess, P. Mäkela, J. Svenson, P. Heino, E. T. Palva, *Plant Mol. Biol.* **54** (2004) 743
2. D. K. Hincha, J. M. Schmitt, *Plant Physiol*. **140** (1992) 236
3. D. K. Hincha, U. Heber, J. M. Schmitt, *Planta* **180** (1990*)* 416
4. M. Nylander, J. Svensson, E. T. Palva, B. V. Welin, *Plant Mol. Biol.* **45** (2001) 263
5. J. F. Carpenter, J. H. Crowe, *Cryobiology* **25** (1988) 244
6. S. A. Campbell, T. J. Close, *New Phytol.* **137** (1997) 25
7. T. J. Close, *Physiol. Plant.* **97** (1996) 795
8. T. J. Close, *Physiol. Plant.* **100** (1997) 291
9. K. Kosova, P. Vitamvas, I. T. Prasil, *Biol. Plantarum* **51** (2007) 601
10. J. Svensson, A. M. Ismail, E. T. Palva, T. J. Close, in: *Cell and Molecular Response to Stress*, Vol. 3, *Sensing, Signaling and Cell Adaptation*, K. B. Storey, J. M. Storey, Eds., Elsevier Press, Amsterdam, 2002, p. 155
11. M. Wisniewski, R. Webb, R. Balsamo, T. J. Close, X. M. Yu, M. Griffith, *Physiol Plant.* **105** (1999) 600
12. M. F. Thomashow, *Plant Mol. Biol.* **50** (1999) 571
13. F. Sieg, W. Schröder, J. M. Schmitt, D. K. Hincha, *Plant Physiol*. **111** (1996) 215
14. D. K. Hincha, B. Neukamm, H. A. M. Sror, F. Sieg, W. Weckwarth, M. Rückels, V. Lullien-Pellerin, W. Schröder, J. M. Schmitt, *Plant Physiol*. **125** (2001) 835
15. D. K. Hincha, J. M. Schmitt, in: *Water and Life: Comparative analysis of water relationships at the organismic, cellular, and molecular levels*, G. N. Somero, C. B. Osmond, C. L. Bolis, Eds., Springer, Berlin, 1992, p. 316
16. D. K. Hincha, J. M. Schmitt, *Plant Cell Environ.* **11** (1989) 47
17. U. K. Laemmli, E Molbert, M. Showe, E. Kellenberger, *J. Mol. Biol.* **49** (1970) 99
18. J. Svensson, E. T. Palva, B. Welin, *Protein Expr. Purif.* **20** (2000) 169
19. M. M. Bradford, *Anal. Biochem.* **72** (1976) 248

20. D. K. Hincha, F. Sieg, I. Bakaltcheva, H. Köth, J. M. Schmitt, in: *Advances in low-temperature Biology*, Vol. 3, P. L. Steponkus, Ed., JAI Press, London, 1996, p. 141
21. M. C. Koag, S. Wilkens, R. D. Fenton, J. Resnik, E. Vo, T. J. Close, *Plant Physiol.* **150** (2009) 1503.

Journal of the Serbian Chemical Society
JSCS-info@shd.org.rs • www.shd.org.rs/JSCS
J. Serb. Chem. Soc. 78 (8) 1161–1170 (2013)
JSCS–4487
UDC 546.881.5–31+547.821'461.2'
288.2'495.9:548.7:535.33
Original scientific paper

Dioxidovanadium(V) complexes with pyridoxal aminoguanidine derivative: synthesis and spectral and structural characterization

MIRJANA M. LALOVIĆ#, VUKADIN M. LEOVAC*#, LJILJANA S. VOJINOVIĆ-JEŠIĆ#, MARKO V. RODIĆ#, LJILJANA S. JOVANOVIĆ# and VALERIJA I. ČEŠLJEVIĆ#

Faculty of Sciences, University of Novi Sad, Trg D. Obradovića 3, 21000 Novi Sad, Serbia

(Received 26 March 2013)

Abstract: Three square–pyramidal complexes of dioxidovanadium(V) with {[(3-hydroxy-5-(hydroxymethyl)-2-methyl-4-pyridyl)methylene]amino}guanidine (PLAG), of the formulas $NH_4[VO_2(PLAG{-}2H)]\cdot H_2O$ (**1**), $VO_2(PLAG{-}H)$ (**2**) and $K[VO_2(PLAG{-}2H)]\cdot H_2O$ (**3**) were synthesized and characterized by IR and electronic spectra, and in case of **1** and **3** by X-ray crystallography as well. The reaction of aqueous ammoniacal solution of NH_4VO_3 and PLAG resulted in formation of **1**, which in MeOH undergoes spontaneous transformation into **2**, which, in turn, in the reaction with KOH transforms into **3**. In these complexes, PLAG is coordinated in a common tridentate ONN mode, *via* the phenoxide oxygen atom and the nitrogen atoms of the azomethine and imino groups of the aminoguanidine fragment. In all previously characterized complexes, PLAG was coordinated in the neutral form. However, here it was proven that this ligand could be coordinated in both mono- (**2**) and doubly-deprotonated forms (**1** and **3**) as well.

Keywords: pyridoxalaminoguanidine derivative, dioxidovanadium(V), complexes, crystal structure, spectra.

INTRODUCTION

The great interest in vanadium coordination chemistry[1] in the context of medical applications has arisen from the ability of vanadium complexes to promote the insulin-mimetic activity in the treatment of human *Diabetes mellitus*.[2,3] Other studies involving potential applications of some oxidovanadium(IV) and dioxidovanadium(V) complexes have also been performed in the context of their antitumor, antibacterial and anti-inflammatory activities.[4–7]

* Corresponding author. E-mail: vukadin.leovac@dh.uns.ac.rs
# Serbian Chemical Society member.
doi: 10.2298/JSC130326038L

Concerning the fact that pyridoxal (PL) is a co-enzyme in a large number of enzymatic systems that catalyze biochemical transformations of amino acids, it is not surprising that a large number of vanadium complexes with the Schiff bases of PL have been synthesized and characterized.[8]

Despite the wide range of pharmacological activity[9–13] of aminoguanidine (AG), vanadium complexes with its Schiff bases are still unknown. Considering the biological importance of vanadium and both ligand precursors, as well as the fact that only a few complexes of pyridoxal aminoguanidine derivative, {[(3-hydroxy-5-(hydroxymethyl)-2-methyl-4-pyridyl)methylene]amino}guanidine (PLAG)[14–17], have been synthesized, it seemed worthwhile to examine the synthesis and characteristics of new ones. Herein, a synthesis and spectral study of three dioxidovanadium(V) complexes with PLAG, *viz*. $NH_4[VO_2(PLAG–2H)]\cdot H_2O$ (**1**), $VO_2(PLAG-H)$ (**2**) and $K[VO_2(PLAG-2H)]\cdot H_2O$ (**3**), is presented together with the structural characterization of two of the complexes.

EXPERIMENTAL

Reagents

All employed chemicals were commercial products of analytical reagent grade, except for the ligand pyridoxal aminoguanidine derivative, which was obtained in the reaction of aqueous solutions of pyridoxal hydrochloride and aminoguanidine hydrogencarbonate in the presence of $Na_2CO_3\cdot 10H_2O$.[17]

Synthesis of the complexes

A mixture of NH_4VO_3 (0.12 g, 1.0 mmol) and PLAG (0.22 g, 1.0 mmol) was heated in ccNH_3(aq) (5 cm^3) under reflux for 3 h. After 2 days, from the orange solution, orange single crystals of $NH_4[VO_2(PLAG-2H)]\cdot H_2O$ (**1**) precipitated, which were filtered off and washed with EtOH and Et_2O. When the reaction, with the same quantities of reactants, was performed in MeOH, yellow microcrystals of $VO_2(PLAG-H)$ (**2**) were formed. The same product could be obtained by the dissolution of **1** in MeOH. The reaction of **2** with KOH resulted in formation of orange single crystals of $K[VO_2(PLAG-2H)]\cdot H_2O$ (**3**).

Analytical methods

Elemental analyses (C, H, N) of air-dried complexes were performed by standard micromethods in the Center for Instrumental Analyses, ICTM in Belgrade.

Molar conductivities of freshly prepared complex solutions ($c = 1\times10^{-3}$ mol dm^{-3}) were measured on a Jenway 4010 conductivity meter.

IR spectra were recorded using KBr pellets on a NEXUS 670 FTIR spectrophotometer (Thermo Nicolet) in the range of 4000–400 cm^{-1}.

Electronic spectra of DMF solutions were recorded on a T80+ spectrometer (PG Instruments Ltd.) from 270 to 1100 nm.

Single crystal X-ray diffraction

Single crystals of the complexes **1** and **3** were selected, glued on glass fibers and mounted on a Gemini S κ-geometry diffractometer (Agilent Technologies), equipped with Sapphire3 CCD area detector, for diffraction measurements at room temperature. Data were collected in the ω scan mode using graphite-monochromated Mo $K\alpha$ X-radiation (λ = 0.71073 Å) for **1** and Cu $K\alpha$ X-radiation (λ = 1.54184 Å) for **3**. Data collection, reduction and cell

refinement were performed with CRYSALISPRO. The structures were solved by direct method using SIR92[18] and refined on F^2 with SHELXL-97 program.[19] Hydrogen atoms bonded to carbon atoms were introduced in idealized positions and refined as riding with U_{iso} fixed as 1.2–1.5 U_{eq} of the parent atoms. Position of hydrogen atoms bonded to heteroatoms were taken from ΔF map and refined isotropically as riding on their parent atoms, since their free refinement did not lead to the most satisfactory geometry. The programs used to prepare material for publication were WINGX[20] and ORTEP-3.[21] Crystal data and refinement parameters are listed in Table I.

TABLE I. Crystallographic data for the $NH_4[VO_2(PLAG{-}2H)]\cdot H_2O$ (**1**) and $K[VO_2(PLAG{-}2H)]\cdot H_2O$ (**3**)

Parameter	**1**	**3**
Molecular formula	$C_9H_{17}N_6O_5V$	$C_9H_{13}KN_5O_5V$
Formula weight	340.23	361.28
Temperature, K	298(2)	294(2)
Wavelength, Å	0.71073	1.54184
Crystal system	Triclinic	Triclinic
Space group	$P\bar{1}$	$P\bar{1}$
a / Å	8.5563(11)	8.5478(9)
b / Å	9.1477(13)	9.1738(8)
c / Å	9.9439(15)	9.7808(9)
α / °	78.943(12)	79.865(8)
β / °	86.305(11)	85.467(8)
γ / °	63.426(14)	62.052(10)
V / Å^3	682.97(19)	666.94(13)
Z	2	2
D_c / g cm^{-3}	1.654	1.799
μ / mm^{-1}	0.76 (Mo $K\alpha$)	9.33 (Cu $K\alpha$)
F(000)	352	368
Crystal size, mm	0.33×0.20×0.05	0.77×0.25×0.23
Color/shape	Orange/prism	Orange/prism
θ range, °	3.3–29.2	4.6–72.3
No. reflections measured	5006	4205
No. unique reflections	3106	2573
R_{int}	0.024	0.024
No. reflections with $I > 2\sigma I$	2429	2390
No. restraints	0	0
No. refined parameters	201	198
Goodness-of-fit on F^2	1.084	1.054
R / wR [$F_o > 4\sigma F_o$]	0.038 / 0.105	0.034 / 0.098
R / wR [all data]	0.052 / 0.110	0.036 / 0.100
$\Delta\rho_{max}$ and $\Delta\rho_{min}$, e Å^{-3}	0.39 and −0.38	0.34 and –0.44

RESULTS AND DISCUSSION

Synthesis

Orange single crystals of the monoanionic complex $NH_4[VO_2(PLAG{-}{-}2H)]\cdot H_2O$ (**1**) were obtained in the reaction of warm ammoniacal solutions of

NH_4VO_3 and PLAG in the mole ratio 1:1. The MeOH solution of **1** is unstable, thus the dissolution of **1** in MeOH resulted in the formation of a yellow neutral microcrystalline complex of the formula VO_2(PLAG−H) (**2**). Compound **2** could also be obtained in the reaction of MeOH solutions of NH_4VO_3 and PLAG in the mole ratio 1:1. The mixture of complexes **1** and **2** could be obtained in the reaction of ammoniacal solutions of $VOSO_4$ and PLAG, which indicates that, under these conditions, the oxidation of V(IV) to V(V) occurred. The identities of the complexes obtained in this reaction were proved by X-ray analysis data (for complex **1**) and by elemental analysis data and IR spectrum identical to those obtained in other two ways of synthesis (for complex **2**). In the reaction with KOH in MeOH, complex **2** transforms into K[VO_2(PLAG−2H)]·H_2O (**3**). Details of the synthetic procedure to the complexes are summarized in Scheme 1.

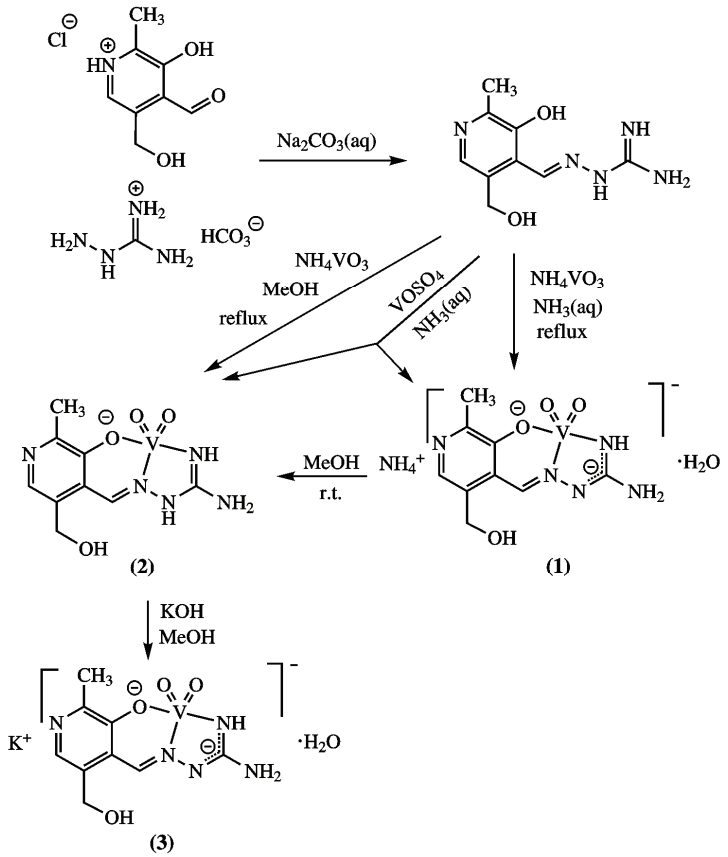

Scheme 1. Reaction scheme of the syntheses of the ligand and the complexes.

In all previously described complexes,[14–17] PLAG was coordinated in the neutral but dipolar zwitter-ionic form, which was the result of prototropic tauto-

merism, *i.e.*, the migration of an H-atom from the phenolic OH-group to pyridine nitrogen of the pyridoxal moiety. However, complexes **1** and **3** are the first two examples of metal complexes in which PLAG is coordinated as a dianionic ligand, because of deprotonation of both the pyridinium and hydrazine nitrogen atoms. As was already mentioned, in these complexes PLAG is coordinated as tridentate ONN ligand, *via* the oxygen atom of the deprotonated OH-group and the nitrogen atoms of the azomethine and imino groups of the aminoguanidine fragment, forming one six-membered (pyridoxylidene) and one five-membered (aminoguanidine) metallocycle.

The complexes are stable in air. Complexes **1** and **3** are soluble in H_2O, MeOH and DMF, and partially in EtOH, whilst **2** is soluble in DMF. The molar conductivity of **1** and **3** in H_2O suggest a 1:1 type of electrolyte,[22] which is in accordance with the coordination formulas, whilst the conductivity of **1** in MeOH and DMF had slightly lower values. This can be explained by the lower mobility of the voluminous complex anion as well as the gradual transformation into **2**. The value for the molar conductivity of **2** in DMF indicates its non-electrolyte nature.

It should be mentioned that, concerning the similar reactions in analogous complexes with similar ligands,[23] the transformation of **1** into **2** is expected to be reversible. It was experimentally shown that neutral complex **2** cannot be deprotonated by NH_3(aq) as those with similar ligands,[23] but by strong bases only. Thus, dissolution of complex **2** in warm MeOH in the presence of equimolar amount of KOH gives an orange solution, from which the orange single crystals of **3** were formed.

Analytic and spectral characteristics

*$NH_4[VO_2(PLAG-2H)]\cdot H_2O$ (**1**)*. Yield: 67 %; Anal. Calcd. for $C_9H_{17}N_6O_5V$: C, 31.77; H, 5.04; N, 24.70 %. Found: C, 31.75; H, 4.98; N, 24.41 %; FTIR (KBr, cm^{-1}): 3384, 3187, 3010, 1655, 1597, 1542, 1499, 1398, 920, 890; UV–Vis (DMF) (λ_{max} / nm (log (ε / dm^3 mol^{-1} cm^{-1}))): < 270 (≈4.15), 353 (3.76), 404 (3.82); Molar conductivity, Λ_M (S cm^2 mol^{-1}): 120 (H_2O), 55 (MeOH), 35 (DMF).

*$VO_2(PLAG-H)$ (**2**)*. Yield: 96 %; Anal. Calcd. for $C_9H_{12}N_5O_4V$: C, 35.42; H, 3.96; N, 22.95 %. Found: C, 35.58; H, 4.02; N, 22.77 %; FTIR (KBr, cm^{-1}): 3271, 3132, 1659, 1592, 1563, 1372, 1319, 953, 925, 897; UV–Vis (DMF) (λ_{max} / / nm (log (ε / dm^3 mol^{-1} cm^{-1}))): <270 (≈4.15), 373 (3.67); Molar conductivity, Λ_M (S cm^2 mol^{-1}): 18 (DMF).

*$K[VO_2(PLAG-2H)]\cdot H_2O$ (**3**)*. Yield: 42 %; Anal. Calcd. for $C_9H_{13}KN_5O_5V$: C, 29.89; H, 3.60; N, 19.37 %. Found: C, 30.25; H, 3.73; N, 19.65 %; FTIR (KBr, cm^{-1}): 3366, 3319, 3133, 1658, 1598, 1540, 1501, 1396, 922, 885; Molar conductivity, Λ_M (S cm^2 mol^{-1}): 110 (H_2O).

IR spectra

Using a comparative analysis of the IR spectra of the ligand and the complexes, a tridentate ONN coordination mode of PLAG could be established. The positive shift of the ν(C–O) band from 1290 cm^{-1} in the spectrum of the ligand to 1370 cm^{-1} in the spectra of the complexes indicates the coordination of the oxygen atom of the deprotonated phenolic OH-group.[14–17,24] In contrast to this band, bands originating from the vibrations of guanidino and azomethine group, which were observed at 1631 and 1697 cm^{-1}, respectively, in the spectrum of the ligand were shifted toward the lower energy region by 35 and 40 cm^{-1}, respectively, due to the coordination of nitrogen atoms of the imino and azomethine groups of the aminoguanidine fragment.[14–17] The broad bands in the region 2700–3000 cm^{-1}, which can be ascribed to ν(NH^+) vibrations, were observed in all previously characterized complexes with PLAG.[14–17] However, the absences of these bands in the IR spectra of the complexes **1**–**3** confirmed the deprotonation of the nitrogen atom of PL-residue, *i.e.*, the anionic form of the ligand.[25,26] Apart from these, in the spectra of complexes **1**–**3**, very strong bands characteristic for $\nu_{sym/asym}$ (VO_2^+) vibrations were observed at 920 and 890 cm^{-1}, 925 and 897 cm^{-1}, and 922 and 885 cm^{-1}, respectively.[23]

Electronic spectra

Electronic spectra of the complexes **1** and **2** in DMF (available wavelength range 270–1100 nm) were, similarly to previous reports on alike complexes,[17,23,27] rather simple. The observed strong band with λ_{max} < 270 nm is due to intraligand π→π* transitions. The other bands of medium intensity at 353–404 nm were ascribed to L→M charge transfer. No d–d transitions were recorded, as expected for VO_2^+ complexes.

*Crystal structure of **1** and **3***

Molecular structures of the complexes **1** and **3** are shown in Fig. 1 whilst selected bond distances and angles for the complexes are given in Table II. The asymmetric unit of the complexes contained a mono cation (NH_4^+ for **1** and K^+ for **3**), a complex anion consisting of PLAG chelating VO_2^+, and one water molecule. The vanadium atom is pentacoordinated in a slightly distorted square-pyramidal arrangement (τ = 0.109 for **1** and τ = 0.044 for **3**). The complexes **1** and **3** are isomorphous and isostructural, which was expected considering the tolerant difference in the radius of NH_4^+ and K^+ ($r(NH_4^+)/r(K^+)$ = 1.48 Å/1.33 Å). The basal plane of the pyramid is defined by two nitrogen atoms (N1 and N3) and one oxygen atom (O1) of the tridentate Schiff base and one oxygen atom (O3) of dioxido-group. The apex of the pyramid is occupied by the other oxygen atom (O4) of dioxido moiety. The vanadium atom is displaced from the basal plane toward the apical oxygen by 0.529(1) and 0.524(1) Å in **1** and **3**, respecti-

vely. The VO_2-group is in the *cis*-configuration with the usual value of O–V–O angle (108.79(9)° for **1** and 109.53(10)° for **3**).

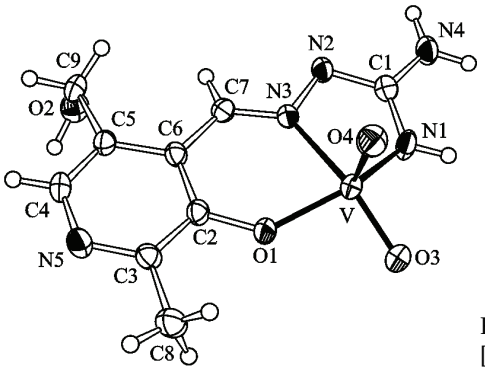

Fig. 1. The structure of the complex anion $[VO_2(PLAG{-}2H)]^-$.

TABLE II. Selected bond lengths and valence angles for **1** and **3**

Bond(s)	Complex	
	1	**3**
	Distance, Å	
V–O1	1.8851(17)	1.8960(17)
V–N1	1.972(2)	1.965(2)
V–N3	2.1816(19)	2.1935(19)
V–O3	1.6536(17)	1.6490(17)
V–O4	1.6292(19)	1.6379(18)
C1–N1	1.331(3)	1.325(3)
C1–N2	1.350(3)	1.345(3)
C1–N4	1.339(3)	1.348(3)
C7–N3	1.296(3)	1.288(3)
N2–N3	1.395(3)	1.394(3)
C2–O1	1.338(3)	1.332(3)
	Angle, °	
N1–V–N3	71.90(8)	71.99(8)
O1–V–N3	81.58(7)	81.65(7)
O4–V–N1	103.31(10)	102.13(10)
O3–V–O4	108.79(9)	109.53(10)
O1–V–N1	141.44(9)	143.47(8)
O3–V–N3	148.02(9)	146.08(9)
C3–N5–C4	118.4(2)	118.7(2)

As can be seen in Table II, the chelate ligand donors–vanadium distances in **1** and **3** vary systematically in the expected fashion. Due to the deprotonation of the phenolic OH-group, the negative charge associated with the formed phenoxide group makes it the best electron donor among the PLAG ligators, which is why the V–O1 bond is the shortest. This fact is in concordance with all the earlier characterized complexes with this ligand.[14–17] The significantly longer (0.21 Å

for **1** and 0.23 Å for **3**) V–N3 bond compared to the V–N1 distance can be correlated with the presence of multiple-bonded O3 and single-bonded O1 atoms in the basal plane, *i.e.*, the stronger *trans* influence of the O3 oxygen atom compared to O1.[27,28]

It should be noted that C2–O1 bond is slightly longer (1.338(3) and 1.332(3) Å for **1** and **3**, respectively) compared with the C–O^- bond in the zwitter-ion of a similar ligand, *i.e.*, pyridoxal thiosemicarbazone (1.29 Å),[29] which could be explained by means of the excess electron density transfer from the phenoxide oxygen to the metal ion *via* coordinative bonding. The intraligand bond distances fall within the expected values based on mentioned structural reports.[14–17] Accordingly, C7–N3 bond length corresponds to pure Csp^2–Nsp^2 azomethine double bond, whilst C1–N1, C1–N2 and C1–N4 bond lengths have values between those characteristic for pure single and double C–N bonds due to extensive delocalization of the electron density within the aminoguanidine moiety. Although the deprotonation of pyridinic (N5) and hydrazine nitrogen (N2) atoms is evident from difference electron density maps calculated during structural analysis, additional confirmation is given by the following facts. The deprotonation of N2 and N5 is unambiguously proved by the fact that these nitrogen atoms are acceptors in strong H–bonds, and the value of C3–N5–C4 angle, which is lower than 120° (118.4(2)° for **1** and 118.7(2)° for **3**) is another proof for the deprotonation of the PL residue.[26]

SUPPLEMENTARY MATERIAL

Fig. S-1, showing the crystal packing, as well as Tables S-I and S-II with hydrogen bonding descriptions are available electronically at http://www.shd.org.rs/JSCS/, or from the corresponding author on request.

Crystallographic data reported for the complex $NH_4[VO_2(PLAG{-}2H)]\cdot H_2O$ (**1**) and $K[VO_2(PLAG{-}2H)]\cdot H_2O$ (**3**) have been deposited with the CCDC, No. CCDC-870175 and 926853. Copies of the data can be obtained free of charge *via* www.ccdc.cam.ac.uk.

Acknowledgement. This work was supported by the Provincial Secretariat for Science and Technological Development of Vojvodina and the Ministry of Education, Science and Technological Development of the Republic of Serbia (Grant No. 172014).

ИЗВОД

КОМПЛЕКСИ ДИОКСИДОВАНАДИЈУМА(V) СА АМИНОГВАНИДИНСКИМ ДЕРИВАТОМ ПИРИДОКСАЛА— СИНТЕЗА, СПЕКТРАЛНА И СТРУКТУРНА КАРАКТЕРИЗАЦИЈА

МИРЈАНА М. ЛАЛОВИЋ, ВУКАДИН М. ЛЕОВАЦ, ЉИЉАНА С. ВОЈИНОВИЋ-ЈЕШИЋ, МАРКО В. РОДИЋ, ЉИЉАНА С. ЈОВАНОВИЋ и ВАЛЕРИЈА И. ЧЕШЉЕВИЋ

Природно–математички факултет, Универзитет у Новом Саду, Трг Д. Обрадовића 3, 21000 Нови Сад

Три комплекса диоксидованадијума(V) са {[(3-хидрокси-5-(хидроксиметил)-2-метил-4-пиридил)метилен]амино}гванидином (PLAG), формула $NH_4[VO_2(PLAG{-}2H)]\cdot H_2O$ (**1**), $VO_2(PLAG{-}H)$ (**2**) и $K[VO_2(PLAG{-}2H)]\cdot H_2O$ (**3**), су синтетисана и спектрално

окарактерисана, а за комплексе **1** и **3** урађена је и рендгенска структурна анализа. Реакцијом амонијачног раствора NH_4VO_3 и PLAG добијен је комплекс **1**, који у MeOH подлеже спонтаној трансформацији у комплекс **2**. Комплекс **2** у реакцији са KOH даје комплекс **3**. У овим комплексима PLAG је координован на уобичајен тридентатни ONN начин, преко атома кисеоника депротоноване OH-групе и атома азота азометинске и имино групе аминогванидинског фрагмента. У свим до сада окарактерисаним комплексима нађена је координација PLAG у неутралној форми, док је у комплексима описаним у овом раду лиганд по први пут координован у моно- (**2**) и двоструко депротонованој (**1** и **3**) форми.

(Примљено 26. марта 2013)

REFERENCES

1. M. R. Maurya, *Coord. Chem. Rev.* **237** (2003) 163
2. H. Sakurai, Y. Kojima, Y. Yoshikawa, K. Kawabe, H. Yasui, *Coord. Chem. Rev.* **226** (2002) 187
3. M. Nakai, M. Obata, F. Sekiguchi, M. Kato, M. Shiro, A. Ichimura, I. Kinoshita, M. Mikuriya, T. Inohara, K. Kawabe, H. Sakurai, C. Orvig, S. Yano, *J. Inorg. Biochem.* **98** (2004) 105
4. G. Verquin, G. Fontaine, M. Bria, E. Zhilinskaya, E. Abi-Aad, A. Aboukais, B. Baldeyrou, C. Bailly, J. L. Bernier, *J. Biol. Inorg. Chem.* **9** (2004) 345
5. N. Raman, A. Kulandaisamy, K. Jeyasubramanian, *Synt. React. Inorg. Met-Org. Chem.* **34** (2004) 17
6. K. H. Thompson, C. Orvig, *Coord. Chem. Rev.* **219**–**221** (2001) 1033
7. M. R. Maurya, A. Kumar, M. Abid, A. Azam, *Inorg. Chim. Acta* **359** (2006) 2439
8. J. S. Casas, M. D. Couce, J. Sordo, *Coord. Chem. Rev.* **256** (2012) 3036
9. B.-O. Nilsson, *Inflammation Res.* **48** (1999) 509
10. C. Scaccini, G. Chiesa, I. Jialal, *J. Lipid Res.* **35** (1994) 1085
11. P. C. Burcham, L. M. Kaminskas, F. R. Fontaine, D. R. Peterson, S. M. Pyke, *Toxicology* **181**–**182** (2002) 229
12. I. Jedidi, P. Therond, S. Zarev, C. Cosson, M. Couturier, C. Massot, D. Jore, M. Gardès-Albert, A. Legrand, D. Bonnefont-Rousselot, *Biochemistry* **42** (2003) 11356
13. S. Atasayar, H. Gürer-Orhan, H. Orhan, B. Gürel, G. Girgin, H. Özgünes, *Exp. Toxicol. Pathol.* **61** (2009) 23
14. V. M. Leovac, M. D. Joksović, V. Divjaković, Lj. S. Jovanović, Ž. Šaranović, A. Pevec, *J. Inorg. Biochem.* **101** (2007) 1094
15. V. M. Leovac, Lj. S. Vojinović-Ješić, V. I. Češljević, S. B. Novaković, G. A. Bogdanović, *Acta Crystallogr., C* **65** (2009) m337
16. M. M. Lalović, Lj. S. Vojinović-Ješić, Lj. S. Jovanović, V. M. Leovac, V. I. Češljević, V. Divjaković, *Inorg. Chim. Acta* **388** (2012) 157
17. M. M. Lalović, Lj. S. Jovanović, Lj. S. Vojinović-Ješić, V. M. Leovac, V. I. Češljević, M. V. Rodić, *J. Coord. Chem.* **65** (2012) 4217
18. A. Altomare, G. Cascarano, C. Giacovazzo, A. Gualardi, *J. Appl. Crystallogr.* **26** (1993) 343
19. G. M. Sheldrick, *Acta Crystallogr., A* **64** (2008) 112
20. L. J. Farrugia, *J. Appl. Crystallogr.* **32** (1999) 837
21. L. J. Farrugia, *J. Appl. Crystallogr.* **30** (1997) 565
22. W. J. Geary, *Coord. Chem. Rev.* **7** (1971) 81

23. Lj. S. Vojinović-Ješić, V. M. Leovac, M. M. Lalović, V. I. Češljević, Lj. S. Jovanović, M. V. Rodić, V. Divjaković, *J. Serb. Chem. Soc.* **76** (2011) 865
24. P. Kalaivani, R. Prabhakaran, E. Ramachandran, F. Dallemer, G. Paramaguru, R. Renganathan, P. Poornima, V. Vijaya Padma, K. Natarajan, *Dalton Trans.* **41** (2012) 2486
25. V. M. Leovac, V. S. Jevtović, L. S. Jovanović, G. A. Bogdanović, *J. Serb. Chem. Soc.* **70** (2005) 393, and references therein
26. S. Floquet, M. C. Muños, R. Guillot, E. Rivière, G. Blain, J. A. Real, M.-L. Boillot, *Inorg. Chim. Acta* **362** (2009) 56
27. V. M. Leovac, V. Divjaković, M. D. Joksović, Lj. S. Jovanović, Lj. S. Vojinović-Ješić, V. I. Češljević, M. Mlinar, *J. Serb. Chem. Soc.* **75** (2010) 1063
28. T. Ghosh, S. Bhattacharya, A. Das, G. Mukherjee, M. G. B. Drew, *Inorg. Chim. Acta* **358** (2005) 989
29. M. Belicchi Ferrari, F. Bisceglie, E. Leporati, G. Pelosi, P. Tarasconi, *Bull. Chem. Soc. Jpn.* **75** (2002) 781.

Journal of the Serbian Chemical Society
JSCS@tmf.bg.ac.rs • www.shd.org.rs/JSCS
J. Serb. Chem. Soc. 78 (8) S93–S94 (2013) *Supplementary material*

SUPPLEMENTARY MATERIAL TO

Dioxidovanadium(V) complexes with pyridoxal aminoguanidine derivative: synthesis and spectral and structural characterization

MIRJANA M. LALOVIĆ, VUKADIN M. LEOVAC*, LJILJANA S. VOJINOVIĆ-JEŠIĆ, MARKO V. RODIĆ, LJILJANA S. JOVANOVIĆ and VALERIJA I. ČEŠLJEVIĆ

Faculty of Sciences, University of Novi Sad, Trg D. Obradovića 3, 21000 Novi Sad, Serbia

J. Serb. Chem. Soc. 78 (8) (2013) 1161–1170

TABLE S-I. Hydrogen-bonding geometry parameters in compound **1**

Bond (*D*–H···*A*)	Distances, Å		Angle, °
	H···*A*	*D*···*A*	
O2–H2···O4[a]	1.95	2.851(3)	163.7
N1–H1···O2[b]	2.34	3.105(3)	144.9
N4–H4A···O4[c]	2.25	3.136(3)	168.3
N4–H4B···O5[d]	1.99	2.870(3)	170.9
O5–H5B···N2[e]	1.99	2.861(3)	170.1
O5–H5A···N5	1.85	2.772(3)	168.4
N6–H6A···O3[f]	2.15	2.862(3)	162
N6–H6B···O3	1.94	2.850(3)	161.2
N6–H6C···N2[b]	2.02	3.003(3)	175.7
N6–H6D···O5[g]	2.09	2.835(3)	144.3

[a]*x*–1, *y*, *z*; [b]–*x*+1, –*y*, –*z*+2; [c]–*x*+2, –*y*, –*z*+2; [d]*x*+1, *y*–1, *z*+1; [e]–*x*+1, –*y*, –*z*+1; [f]–*x*+1, –*y*+1, –*z*+2; [g]–*x*, –*y*+1, –*z*+1, are the equivalent positions

TABLE S-II. Hydrogen-bonding geometry parameters in compound **3**

Bond (*D*–H···*A*)	Distances, Å		Angle, °
	H···*A*	*D*···*A*	
O2–H2···O4[a]	2.03	2.885(3)	164.4
N1–H1···O2[b]	2.33	3.071(3)	149.4
N4–H4B···O5[c]	1.98	2.813(3)	165.2
N4–H4A···O4[d]	2.31	3.121(3)	175.6
O5–H5B···N2[e]	1.88	2.776(3)	172.6
O5–H5A···N5	1.89	2.782(3)	167

[a]*x*–1, *y*, *z*; [b]–*x*+1, –*y*, –*z*+2; [c]*x*+1, *y*–1, *z*+1; [d]–*x*+2, –*y*, –*z*+2; [e]–*x*+1, –*y*, –*z*+1, are the equivalent positions

* Corresponding author. E-mail: vukadin.leovac@dh.uns.ac.rs

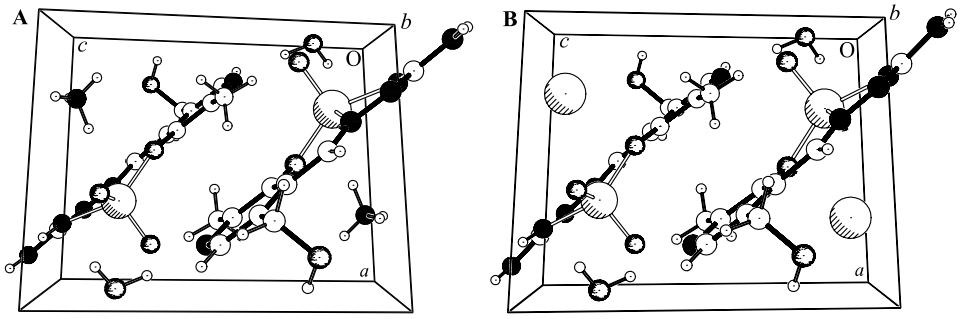

Fig. S-1. Unit cell packing for the complexes **1** (A) and **3** (B).

Journal of the Serbian Chemical Society
JSCS-info@shd.org.rs • www.shd.org.rs/JSCS
J. Serb. Chem. Soc. 78 (8) 1171–1176 (2013) UDC 546.982+547.313.2+546.131:542.913
JSCS–4488 *Short communication*

SHORT COMMUNICATION

Palladium(II) complexes with R_2edda derived ligands. Part VI. *O,O′*-Diisopropyl ester of *N,N′*-1,2-ethanediylbis-L-leucine, dihydrochloride dihydrate and its palladium(II) complex: synthesis and characterization

BOJANA B. ZMEJKOVSKI[1], TIBOR J. SABO[2] and GORAN N. KALUĐEROVIĆ[3,4]*

[1]*Department of Chemistry, Institute of Chemistry, Technology and Metallurgy, University of Belgrade, Njegoševa 12, 11000 Belgrade, Serbia,* [2]*Faculty of Chemistry, University of Belgrade, P. O. Box 158, 11001 Belgrade, Serbia,* [3]*Institut für Chemie, Martin-Luther-Universität Halle-Wittenberg, Kurt-Mothes-Straße 2, D-06120 Halle, Germany and* [4]*Faculty of Pharmacy, European University, Trg mladenaca 5, 21000 Novi Sad, Serbia*

(Received 23 January, revised 15 February 2013)

Abstract: A new R_2edda-type ester, *O,O′*-diisopropyl ester of *N,N′*-1,2-ethanediylbis-L-leucine, dihydrochloride dihydrate, [(*S,S*)-H_2*i*Pr_2eddl]Cl_2·2H_2O, **1**, and its palladium(II) complex, dichlorido(*O,O′*-diisopropyl-*N,N′*-1,2-ethanediylbis-L-leucinate)palladium(II) hemihydrate, [$PdCl_2${(*S,S*)-*i*Pr_2eddl}]·0.5H_2O, **2**, were synthesized and characterized by elemental analysis, and IR and NMR spectroscopy. As expected, the palladium(II) complex was found in two from three possible diastereoisomeric forms (*R,R*), (*S,S*) and (*R,S*) ≡ (*S,R*).

Keywords: palladium complexes; R_2edda-type ligands; diastereoisomers.

INTRODUCTION

Palladium(II) complexes containing the EDTA ligand represent interesting fields in terms of synthesis and characterization.[1–3] In these complexes, the potentially hexadentate EDTA acts as a tetradentate or a bidentate ligand when competing ligands are present (*e.g.*, chlorides), forming mono- or even dimeric species. A significant part of previous research was focused on complexes with branched-chain esters of chiral edda-type acids, *N,N′*-1,2-ethanediylbis-L-alanine hydrochloride, [(*S,S*)-H_3eddip]Cl, and *N,N′*-1,2-ethanediylbis-L-leucine dihydrochloride, [(*S,S*)-H_4eddl]Cl_2, and a large amount of structural information was obtained, as well as interesting findings related to the antiproliferative activity of platinum(II), platinum(IV) and palladium(II) complexes.[4–10]

* Corresponding author. E-mail: goran.kaluderovic@chemie.uni-halle.de
doi: 10.2298/JSC130113021Z

Palladium(II) complexes with branched-chain R_2edda-type esters, previously described in literature,[7–9] are represented in Fig. 1, including the complex **2** from the present study (Fig. 1, complex **C**).

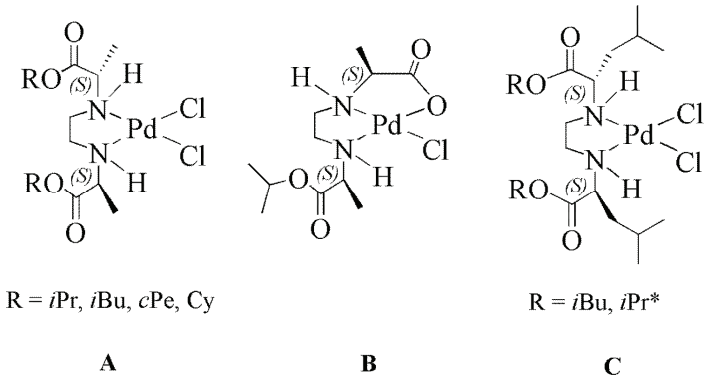

Fig. 1. Palladium(II) complexes with branch-chained R_2edda-type esters (* – complex **2** reported in this work).

Palladium(II) complexes **A** presented in Fig. 1 were obtained as a mixture of two diasteroisomers, as (*R*,*R*) and (*R*,*S*) isomers, as verified by ^{1}H- and ^{13}C--NMR spectroscopy and supported by DFT calculations.[7,8] However, three diastereoisomers can be formed in theory, (*R*,*R*), (*S*,*S*) and (*R*,*S*) ≡ (*S*,*R*), due to the formation of chiral centers on the coordinated nitrogen atoms. In a recent study a palladium(II) complex with a partially hydrolized isopropyl ester of *N*,*N*′-1,2-ethanediylbis-L-alanine (Fig. 1, **B**) was isolated and its structure was confirmed by X-ray analysis. It was found that the (*R*,*R*)–*N*,*N*′ configured isomer with a κ^2*N*,*N*′,κ*O* coordination mode was obtained, and that this is the most stable isomer of four theoretically possible ones.[7] All of the other complexes mentioned here have a κ^2*N*,*N*′ coordination mode of the ligand.

Herein, the synthesis and characterization of two new compounds, branched-chain R_2edda-type ester [(*S*,*S*)-H_2*i*Pr_2eddl]Cl_2·2H_2O, **1**, and corresponding palladium(II) complex [$PdCl_2${(*S*,*S*)-*i*Pr_2eddl}]·0.5H_2O, **2**, (Fig. 1, **C**, complex **2**) are described.

EXPERIMENTAL

Materials and methods

[(*S*,*S*)-H_4eddl]Cl_2 was prepared using a method described in the literature.[11] $K_2[PdCl_4]$ was purchased from Merck and used without further purification. The infrared spectra were recorded on a Nicolet 6700 FT-IR spectrophotometer using the ATR technique (4000–400 cm^{-1}). The ^{1}H- and ^{13}C-NMR spectra were recorded on Varian Gemini 2000 (200 MHz) spectrometer in DMSO-d_6 using tetramethylsilane as an internal standard. Elemental analyses for C, H and N were realized on a Vario EL III C, H, N, S elemental analyzer.

*Synthesis of [(S,S)-H$_2$iPr$_2$eddl]Cl$_2$·2H$_2$O (**1**)*

The ligand **1** was prepared using a modified previously described esterification reaction.[9,10,12,13] Thionyl chloride (4.0 cm^3, 55 mmol) was introduced into a flask containing 50 ml of ice cooled 2-propanol (anhydrous conditions) during 1 h. Then, 2 g (5.54 mmol) of *N*,*N*´-1,2-ethanediylbis-L-leucine dihydrochloride, [(*S*,*S*)-H$_4$eddl]Cl$_2$, was added into the flask and the suspension was refluxed for 16 h. The mixture was filtered and the filtrate was stored for a few days at 4 °C. A white crystalline solid was obtained. The ester was purified by recrystallization from methanol.

*Synthesis of [PdCl$_2${(S,S)-iPr$_2$eddl}]·0.5H$_2$O (**2**)*

Complex **2** was prepared by dissolving K$_2$[PdCl$_4$] (0.167 g, 0.512 mmol) in water (10 ml) and 0.247 g (0.512 mmol) of [(*S*,*S*)-H$_2$*i*Pr$_2$eddl]Cl$_2$·2H$_2$O (**1**) was added. During 2 h of stirring, 10 ml of a 0.1 M solution of LiOH (1.02 mmol) was added in small portions to the reaction mixture. A pale yellow precipitate was obtained, which was filtered off, and the crude product dissolved in 5 ml of CHCl$_3$ and filtered. A crystalline solid of the pure complex was obtained from the CHCl$_3$ solution.

RESULTS AND DISCUSSION

Synthesis and characterization

[(*S*,*S*)-H$_2$*i*Pr$_2$eddl]Cl$_2$·2H$_2$O (**1**) was prepared using an appropriate modification of known methods.[5–10,12,13] This compound is not soluble in chloroform, poorly soluble in water, but fairly soluble in methanol and dimethyl sulfoxide.

[PdCl$_2${(*S*,*S*)-*i*Pr$_2$eddl}]·0.5H$_2$O (**2**) was synthesized by combining aqueous solutions of K$_2$[PdCl$_4$] and **1**. The obtained complex is soluble in chloroform and dimethyl sulfoxide, partially soluble in methanol, but not soluble in water. The preparations of the ester and the complex are shown in Scheme 1.

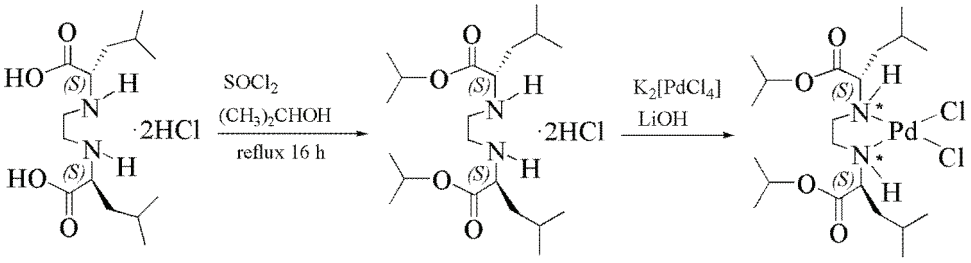

1 **2**

Scheme 1. Synthesis of the ester **1** and the palladium complex **2** (✶ – N atoms configured (*R*,*R*) or (*S*,*S*) or (*S*,*R*) ≡ (*R*,*S*)).

The analytic and spectral data for **1** and **2** are as follows:

Compound **1**. Yield: 1.25 g (47 %); Anal. Calcd. for C$_{20}$H$_{42}$Cl$_2$N$_2$O$_4$·2H$_2$O: C, 49.89; H, 9.13; N, 5.82 %. Found: C, 49.56; H, 8.86; N, 6.17 %; IR (cm^{-1}): 3395, 2959, 2620, 2404, 1728, 1468, 1217, 1103, 913, 802; ^{1}H-NMR (200 MHz,

DMSO-d_6, δ / ppm): 0.92 (12H, *d*, $^3J_{H,H}$ = 4.40 Hz, 4 C**H**$_3$–*i*Pr), 1.26 (12H, *d*, $^3J_{H,H}$ = 6.20 Hz, 4 C**H**$_3$), 1.75 (6H, *m*, 2 C**H**$_2$, 2 C**H**(CH$_3$)$_2$), 3.42 (4H, *m*, 2 C**H**$_2$–(en)), 4.05 (2H, *m*, 2 C**H**), 5.04 (2H, *m*, 2 C**H**–*i*Pr), 9.80–10.40 (4H, *s*, 2 N**H**$_2^+$); ^{13}C-NMR (50 MHz, DMSO-d_6, δ / ppm): 21.5 (**C**H$_3$), 21.6 (**C**H$_3$–*i*Pr), 23.2 (**C**H(CH$_3$)$_2$), 24.5 (**C**H$_2$), 41.6 (**C**H$_2$–(en)), 57.9 (**C**H), 70.4 (**C**H–*i*Pr), 168.5 (**C**OO–*i*Pr).

Compound **2**. Yield: 0.145 g (51 %); Anal. Calcd. for $C_{20}H_{40}Cl_2N_2O_4Pd{\cdot}0.5H_2O$: C, 42.98; H, 7.39; N, 5.01 %. Found: C, 42.80; H, 7.32; N, 5.23 %; IR (cm^{-1}): 3086, 2958, 2873, 1733, 1371, 1198, 1104, 936, 824; ^{1}H-NMR (200 MHz, DMSO-d_6, δ / ppm): Isomer **A**: 0.93 (12H, *d*, $^3J_{H,H}$ = 6.60 Hz, 4 C**H**$_3$–*i*Pr), 1.21 (12H, *d*, $^3J_{H,H}$ = 5.60 Hz, 4 C**H**$_3$), 1.68 (2H, *m*, 2 C**H**(CH$_3$)$_2$), 2.24 (4H, *m*, 2 C**H**$_2$), 2.58 and 2.77 (4H, *m*, 2 C**H**$_2$–(en)), 4.03 (2H, *m*, 2 C**H**), 4.92 (2H, *m*, 2 C**H**–*i*Pr), 6.20–6.80 (2H, *bs*, 2 N**H**); Isomer **B**: 0.88 (12H, *d*, $^3J_{H,H}$ = 6.00 Hz, 4 C**H**$_3$–*i*Pr), 1.28 (12H, *d*, $^3J_{H,H}$ = 6.60 Hz, 4 C**H**$_3$), 1.88 (2H, *m*, 2 C**H**(CH$_3$)$_2$), 2.34 (4H, *m*, 2 C**H**$_2$), 2.69 and 2.85 (4H, *m*, 2 C**H**$_2$–(en)), 3.72 (2H, *m*, CH), 5.02 (2H, *m*, 2 C**H**–*i*Pr), 5.80–6.10 (2H, *bs*, 2 N**H**); ^{13}C-NMR (50 MHz, DMSO-d_6, δ / ppm): Isomer **A**: 21.6 (**C**H$_3$), 22.1 (**C**H$_3$–*i*Pr), 23.1 (**C**H(CH$_3$)$_2$), 25.6 (**C**H$_2$), 38.2 and 47.0 (**C**H$_2$–(en)), 58.6 (**C**H), 68.6 (**C**H–*i*Pr), 169.3 (**C**OO–*i*Pr); Isomer **B**: 22.3 (**C**H$_3$), 22.6 (**C**H$_3$–*i*Pr), 23.7 (**C**H(CH$_3$)$_2$), 24.6 (**C**H$_2$), 40.9 and 50.0 (**C**H$_2$–(en)), 53.3 (**C**H), 63.8 (**C**H–*i*Pr), 170.5 (**C**OO–*i*Pr); Ratio of isomers: A/B = 5/1.

IR spectrum of **2** shows specific absorption bands: ν(C=O) at 1733 cm^{-1} (strong), ν(C–O) at 1198 cm^{-1} (strong), and ν(CH$_3$) at 2958 cm^{-1} (medium); (for comparison, **1** shows: ν(C=O) at 1728 cm^{-1} (strong), ν(C–O) at 1217 cm^{-1} (strong), and ν(CH$_3$) at 2959 cm^{-1} (medium)). Indication of nitrogen coordination was proved by the presence of a band for secondary amino group (3086 cm^{-1}), contrary to the IR spectrum of **1**, for which the absorption of the secondary ammonium group was observed at 3395 cm^{-1}.

In ^{1}H-NMR spectrum of **2**, the chemical shifts of hydrogen atoms belonging to secondary amino groups appeared at 8.55 ppm (compared with the ammonium groups of **1** at 9.9–10.4 ppm).[7–9] Coordination induced shifts in **2** related to the proton atoms from the ethylenediamine moiety were observed (≈0.7 ppm upfield), thus confirming nitrogen coordination to the palladium atom. Chemical shifts for the hydrogen atom bonded to the chiral carbon atom of **1** and **2** were observed at 4.05 ppm as a multiplet.

The ^{13}C-NMR spectra of **1** and **2** have resonances for the carbon atom of the COO moiety at similar positions, indicating that oxygen atoms did not coordinate and that the ester function remained intact.[7–9] The chiral carbon atom shows a chemical shift at 57.9 ppm for **1**, but two signals for the same carbon atom in corresponding palladium(II) complex were observed at 58.3 and 58.8 ppm, indi-

cating the presence of two isomers. Selected ^{1}H- and ^{13}C-NMR data for **1** and **2** are given in Table I.

TABLE I. Selected ^{1}H- and ^{13}C-NMR data (δ in ppm) of [(*S,S*)-H$_2$*i*Pr$_2$eddl]Cl$_2$·2H$_2$O (**1**) and [PdCl$_2${(*S,S*)-*i*Pr$_2$eddl}]·0.5H$_2$O (**2**)

Compound		C**H**$_3$ [*i*Pr]	C**H**$_3$ [Leu]	C**H** [*i*Pr]	**C**H$_3$ [Leu]	**C**H$_3$ [*i*Pr]	**C**OO–*i*Pr	**C**H [*i*Pr]
1	[(*S,S*)-H$_2$*i*Pr$_2$eddl]Cl$_2$·2H$_2$O	0.92	1.26	5.04	21.5	21.6	168.5	70.4
2	[PdCl$_2${(*S,S*)-*i*Pr$_2$eddl}]·0.5H$_2$O							
	Isomer **A**	0.93	1.21	4.92	21.6	22.1/	169.3	68.6
	Isomer **B**	0.88	1.28	5.02	22.3	22.6	170.5	63.8

As expected,[5–8] two sets of signals were found upon coordination of the ligand to the PdCl$_2$ moiety because of the formation of two extra chiral centers at the ligating *N* atoms. Thus, at least two from three diastereoisomers might be formed in the reaction of K$_2$[PdCl$_4$] and **1**. This is in agreement with earlier performed DFT calculations for similar compounds.[7,8]

CONCLUSION

Two novel compounds, R$_2$edda-type ester [(*S,S*)-H$_2$*i*Pr$_2$eddl]Cl$_2$·2H$_2$O, and its corresponding palladium(II) complex [PdCl$_2${(*S,S*)-*i*Pr$_2$eddl}]·0.5H$_2$O, were synthesized and characterized by IR and NMR spectroscopy and elemental analysis. Potassium tetrachloridopalladate(II) reacts with [(*S,S*)-H$_2$*i*Pr$_2$eddl]Cl$_2$·2H$_2$O forming two out of three possible diasteroisomers (*R,R*), (*S,S*) and (*R,S*) ≡ (*S,R*), as evidenced by NMR spectroscopy, which is in agreement with previous DFT calculations.

Acknowledgements. The authors are grateful to the Ministry of Education, Science and Technological Development of the Republic of Serbia for financial support (Grant No. 172035).

ИЗВОД

КОМПЛЕКСИ ПАЛАДИЈУМА(II) СА ЛИГАНДИМА R$_2$EDDA ТИПА. ДЕО VI. *O,O′*-ДИИЗОПРОПИЛ ЕСТАР *N,N′*-1,2-ЕТАНДИИЛБИС-L-ЛЕУЦИНА, ДИХИДРОХЛОРИД ДИХИДРАТ И ЊЕГОВ КОМПЛЕКС СА ПАЛАДИЈУМОМ(II): СИНТЕЗА И КАРАКТЕРИЗАЦИЈА

БОЈАНА Б. ЗМЕЈКОВСКИ[1], ТИБОР. Ј. САБО[2] и ГОРАН Н. КАЛУЂЕРОВИЋ[3,4]

[1]*Институт за хемију, технологију и металургију – Центар за хемију, Универзитет у Београду, Студентски трг 14, 11000 Београд,* [2]*Хемијски факултет, Универзитет у Београду, п.пр. 158, 11001 Београд,* [3]*Institut für Chemie, Martin-Luther-Universität Halle-Wittenberg, Kurt-Mothes-Straße 2, D-06120 Halle, Germany и* [4]*Фармацеутски факултет, Европски Универзитет, Трг младенаца 5, 21000 Нови Сад*

Нов естар R$_2$edda-типа *O,O′*-диизопропил естар *N,N′*-1,2-етандиилбис-L-леуцина, дихидрохлорид дихидрат [(*S,S*)-H$_2$*i*Pr$_2$eddl]Cl$_2$·2H$_2$O (**1**) и његов комплекс паладијума(II), дихлоридо(*O,O′*-диизопропил-*N,N′*-1,2-етандиилбис-L-леуцинат)паладијум(II)-

-хемихидрат $[PdCl_2\{(S,S)\text{-}iPr_2eddl\}]\cdot 0.5H_2O$ (**2**) су синтетисани и окарактерисани уз помоћ елементалне анализе, IR и NMR спектроскопије. Калијум-тетрахлоридопаладат(II), реагујући са $[(S,S)\text{-}H_2iPr_2eddl]Cl_2\cdot 2H_2O$, очекивано даје паладијумов комплекс **2** у облику два од могућа три дијастереоизомера, (*R*,*R*), (*S*,*S*) и (*R*,*S*) ≡ (*S*,*R*), што је потврђено уз помоћ NMR спектроскопије, а у сагласности је са раније урађеним DFT прорачунима.

(Примљено 23 јануара, ревидирано 15. фебруара 2013)

REFERENCES

1. M. Kaplun, M. Sandström, D. Boström, A. Shchukarev, P. Peresson, *Inorg. Chim. Acta* **358** (2005) 527
2. D. J. Robinson, C. H. L. Kennard, *J. Chem. Soc., A* (1970) 1008
3. X.-M. Luo, X.-H. Chen, S. S. S. Raj, H.-K. Fun, L.-G. Zhu, *Acta Crystallogr., C* **55** (1999) 1220
4. G. P. Vasić, V. V. Glodjović, G. N. Kaluđerović, F. W. Heinemann, S. R. Trifunović, *Transition Met. Chem.* **36** (2011) 331
5. G. N. Kaluđerović, H. Schmidt, D. Steinborn, T. J. Sabo, in: *Inorganic Biochemistry: Research Progress*, J. G. Hughes, A. J. Robinson, Eds., Nova Science Publishers, Hauppauge, NY, 2008, p. 305
6. B. B. Krajčinović, G. N. Kaluđerović, D. Steinborn, H. Schmidt, C. Wagner, Ž. Žižak, Z. D. Juranić, S. R. Trifunović, T. J. Sabo. *J. Inorg. Biochem.* **102** (2008) 892
7. B. B. Krajčinović, G. N. Kaluđerović, D. Steinborn, C. Wagner, K. Merzweiler, S. R. Trifunović, T. J. Sabo, *J. Serb. Chem. Soc.* **74** (2009) 389
8. B. B. Zmejkovski, G. N. Kaluđerović, S. Gómez-Ruiz, Ž. Žižak, D. Steinborn, H. Schmidt, R. Paschke, Z. D. Juranić, T. J. Sabo, *Eur. J. Med. Chem.* **44** (2009) 3452
9. B. B. Zmejkovski, G. N. Kaluđerović, S. Gómez-Ruiz, T. J. Sabo, *J. Serb. Chem. Soc.* **74** (2009) 1249
10. J. Vujić, M. Cvijović, G. N. Kaluđerović, M. Milovanović, B. B. Zmejkovski, V. Volarević, N. Arsenijević, T. J. Sabo, S. R. Trifunović, *Eur. J. Med. Chem.* **45** (2010) 3601
11. L. N. Schoenberg, D. W. Cooke, C. F. Liu, *Inorg. Chem.* **7** (1968) 2386
12. G. N. Kaluđerović, T. J. Sabo, *Polyhedron* **21** (2002) 2277
13. D. B. Haydock, T. P. C. Mulholland, *J. Chem. Soc., C* (1971) 2389.

Journal of the Serbian Chemical Society
JSCS-info@shd.org.rs • www.shd.org.rs/JSCS
J. Serb. Chem. Soc. 78 (8) 1177–1188 (2013)
JSCS–4489
UDC 547.431.4+66.094.3:544.4+541.124:544.452
Original scientific paper

A criterion based on computational singular perturbation for the construction of a reduced mechanism for dimethyl ether oxidation

ZUOZHU WU, XINQI QIAO* and ZHEN HUANG

Key Laboratory of Power Machinery and Engineering, Ministry of Education, Shanghai Jiao Tong University, Shanghai 200240, China

(Received 22 November 2012, revised 9 February 2013)

Abstract: A criterion based on the computational singular perturbation (CSP) method is proposed in order to determine the number of quasi-steady state (QSS) species. This criterion is employed for the reduction of a detailed chemical kinetics mechanism for the oxidation of dimethyl ether (DME), involving 55 species and 290 reactions, leading to a 20-step reduced mechanism that involves 26 species. A software package, named I-CSP, was developed to make the reduction process algorithmic. The input to the I-CSP includes: a) the detailed mechanism, b) the numerical solution of the problem for a specific set of operating conditions and c) the number of quasi steady state (QSS) species. The resulting reduced mechanism was validated both in homogenous reactor, including auto-ignition and a perfectly stirred reaction (PSR), over a wide range of pressures and equivalence ratios, and in a one-dimensional, unstretched, premixed, laminar steady DME/air flame. Comparison of the results calculated with the detailed and the reduced mechanisms shows excellent agreement in the case of a homogenous reactor, but discrepancies could be observed in the case of a premixed laminar flame.

Keyword: I-CSP; auto-ignition; perfectly stirred reaction; premixed flame; ignition delay; combustion.

INTRODUCTION

Dimethyl ether (DME) has drawn much attention because of its low emissions of nitrogen oxides (NO_x), reduction of engine noise, and high diesel thermal efficiency[1,2] and soot-free combustion.[3,4] However, making full use of its advantages or further improvement of these favorable results requires a thorough understanding of the underlying combustion chemistry. Simulations with detailed chemical kinetics are useful methods to explore combustion pro-

* Corresponding author. E-mail: qiaoxinqi@sjtu.edu.cn
doi: 10.2298/JSC121122023W

cesses. However, even for the simplest fossil fuels, combustion simulation with detailed mechanisms still involves hundreds of species and thousands of reactions, which causes large amount of CPU times and low economic efficiency. The simulation is further complicated by the existence of highly reactive radicals, which induce significant rigidity to the governing equations due to the dramatic differences in the time scales of the species. Consequently, it is necessary to develop reduced mechanisms of a few detailed mechanisms.

Skeletal mechanisms are derived from detailed mechanisms by the removal of unimportant species and reactions. The methods that are used to develop skeletal mechanisms include sensitivity analysis performed by multiplying the rate constant of a reaction by a factor of 2 (both forward and reverse rate constants)[5] or by solving sensitivity equations, principal component analysis,[6] path flux analysis (PFA),[7] directed related graph (DRG),[8–10] and directed relation graph with error propagation (DRGEP)[11] methods, DRG-aided sensitivity analysis (DRGASA)[12] and DRGEP with sensitivity analysis (DRGEPSA).[13] The PFA method analyses the formation and consumption fluxes of each species for multiple reaction path generations and uses the fluxes to identify the important reaction pathways and the associated species. The DRG algorithm maps species to a graph and consequently identifies the species strongly coupled to the major species, thus solving successively strongly connected components (SCC) group by group. The DRG method uses absolute reaction rates, which makes the relation index not conservative (the interaction coefficient or relation index is the ratio of species flux). The DRGEP method which employs net reaction rates fails to identify all of the reaction paths when more than one intermediate species exist and to identify the relation between the species that have both fast production and consumption rates, such as species having catalytic effects.[7,14]

The skeletal mechanisms can be further reduced by time-scale reduction methods, which are based on the concept that fast time-scale species are in equilibrium state when related fast time-scale modes are exhausted and will result in algebraic relations of the species. Such methods include the partial-equilibrium approximation and the quasi-steady state approximation (QSSA),[15–21] intrinsic low-dimensional manifold (ILDM)[22,23], *in situ* adaptive tabulation (ISAT)[24,25] and computational singular perturbation (CSP).[26–31]

The CSP method using a programmable computational algorithm generates CSP data, such as radical pointer and fast reaction pointer, without the need of intuition and experience. The CSP data can then be used to identify quasi-steady state (QSS) species and fast reactions (using the fast reaction pointer) that are essential for the construction of reduced mechanisms. Valorani *et al.*[30] developed an automatic procedure based on CSP to generate skeletal mechanisms, which could replicate the dynamics of a user-specified set of species at sampling points. J. Prager *et al.*[32] used this method[30] to develop skeletal mechanisms for pre-

mixed *n*-heptane flames. A reduced mechanism can be called "global" if it is developed based on global QSS species that do not vary according to time and space.

Massias *et al.*[26] used a concentration-weighted CSP pointer to derive a 7-step reduced mechanism for CH_4/air that accounted for both thermal and prompt NO_x production. Lu *et al.*[33] extended the CSP method to complex eigensystems and employed a complex CSP to generate a 4-step and a 10-step reduced mechanism for the high-temperature oxidation of H_2/air and CH_4/air, respectively.

DME oxidation process contains both low and high temperature oxidation. Curran *et al.*[34] studied the low temperature oxidation of DME over the temperature range 550–850 K and formic acid was observed as the major intermediate. It was found that dimethyl ether exhibits a negative temperature coefficient (NTC) behavior. The high temperature oxidation of DME was studied by Fischer et al.[35.] It was found that the most important initiation reaction for the oxidation of dimethyl ether was its unimolecular decomposition to form methoxy and methyl radicals. Much emphasis has been placed on the development of a reduced mechanism for DME. Yamada *et al.*[36] developed a reduced mechanism consisting of 23 species and 23 reactions by extracting essential elementary reactions from the detailed mechanism of DME. Chin *et al.*[37] constructed a 28-species reduced mechanism for DME combustion using the QSSA method based on the detailed mechanism given by Zhao *et al.*[38] Ryu *et al.*[39] deduced a 44-species and 166-reaction reduced mechanism for DME from a detailed 79-species and 351-reaction mechanism using sensitivity analysis.

In this manuscript, a criterion based on computational singular perturbation is presented and applied to the detailed mechanism for DME oxidation given by Zhao *et al.*[38] for the construction of a 20-step reduced mechanism.

METHODOLOGIES

A thorough description of the CSP method may be found in the literature.[27,28,40] Herein, an overview of the CSP method is given. A general chemical reaction system that contains R elementary chemical reactions and N species can be expressed as:

$$g(y) \equiv \frac{\mathrm{d}y}{\mathrm{d}t} = \mathbf{S}F(y) \tag{1}$$

where y is the $N\times1$ concentration vector of all the species, $\mathbf{S}$ the $N\times R$ stoichiometric coefficients matrix and $F(y)$ is the $R\times1$ species production rates vector of the elementary reactions. By taking the time derivative of Eq. (1), one obtains:

$$\frac{\mathrm{d}g}{\mathrm{d}t} = \mathbf{J}g \tag{2}$$

where:

$$\mathbf{J} = \frac{\partial g}{\partial y} \tag{3}$$

is the time-dependent Jacobian matrix. **J** depends only on the state of reaction system at every time step. By undertaking eigen-decomposition of the matrix **J**, **J** can be decomposed as:

$$\mathbf{J} = \mathbf{A}\mathbf{\Lambda}\mathbf{B} \tag{4}$$

where **A** is the matrix of the basis vectors and **B** is the inverse matrix of **A**. If an ideal base vector **A** (eigenvectors) exists, then **Λ** reduces to a diagonal matrix and its diagonal elements are the eigenvalues of **J**. Supposing there are *M* fast modes and that $\mathbf{A}_m$ and $\mathbf{B}^m$ correspond to the *N*×*M* and the *M*×*N* fast base matrix, respectively, then the matrix:

$$\mathbf{Q}_m \equiv \mathbf{A}_m \mathbf{B}^m \tag{5}$$

is called the fast projection matrix. The diagonal elements of $\mathbf{Q}_m$:

$$D = \mathrm{diag}\left[\mathbf{Q}_m\right] \tag{6}$$

are radical pointers that identify the locally optimal QSS species, where *D* is an *N*-dimensional vector. A larger diagonal element suggests a better CSP radical candidate, namely a QSS specie.

By defining the participation and importance index as:[30]

$$P_r^i \equiv \frac{b^i s_r F^r}{\sum_{r=1}^{R}\left|b^i s_r F^r\right|}, \quad i = 1,\ 2,\ ...,\ M,\quad r = 1,\ 2,\ ...,\ R \tag{7}$$

$$I_r^i \equiv \frac{s_r^i F^r}{\sum_{r=1}^{R}\left|s_r^i F^r\right|}, \quad i = 1,\ 2,\ ...,\ M,\quad r = 1,\ 2,\ ...,\ R \tag{8}$$

where P_r^i and I_r^i are the participation index and importance index, b^i is the *i*-th row vector in B^m, s_r (column vector) is the stoichiometric vector of the *r*-th reaction, F^r the reaction rate of the *r*-th reaction and s_r^i is the *i*-th element of the stoichiometric vector of the *r*-th reaction, one can estimate: a) where the major cancellations occur and b) the contribution of each step in the production of the *i*-th species. The fast reactions for each QSS species can be identified by the importance index. The largest I_r^i in the *i*-th row means the *r*-th reaction is the fast reaction for the *i*-th specie.

Massias *et al.*[26] used the following algorithm to integrate the radical pointers through the computational domain:

$$I^i \equiv \frac{1}{L}\int_0^L D^i \frac{1}{X^i + \varepsilon_1}\frac{q^i}{q_{\max}^i + \varepsilon_2}\mathrm{d}x. \tag{9}$$

where D^i is the *i*-th radical pointer in *D*, X^i the *i*-th species concentration, q^i the net production rate of the *i*-th species, $q_{\max}^i$ is the maximum production rate for the *i*-th species throughout the computational domain *D*, ε_1 and ε_2 are small positive numbers that are used to avoid numerical problems when X^i and $q_{\max}^i$ equal zero. The values of ε_1 and ε_2 must be chosen with care. Their order must be much lower than X^i and $q_{\max}^i$ so that their influence to I^i can be neglected.

For transient reaction systems:

$$I^i \equiv \frac{1}{T}\int_0^L D^i \frac{1}{X^i + \varepsilon_1}\frac{q^i}{q_{\max}^i + \varepsilon_2}\mathrm{d}t \tag{10}$$

To apply the CSP method, a prior *M* needs to be determined. A possible way to realize this is to calculate the errors between the detailed and the reduced mechanisms and then choose *M* with the specified error. Considering the importance of ignition delay in a closed homogenous reaction system, it is chosen as the target variable of which the errors are calculated.

The following discussion is based in the context of developing a reduced mechanism for DME, which consists of 55 species and 290 reactions.[38] The results of the ignition delay with respect to M in a closed homogeneous transient reactor (constant pressure and variable volume), is shown in Fig. 1. As can be seen, the errors become larger with increasing *M*. Numerical difficulties occur when *M* increases to a certain number. In this manuscript, the specified error for ignition delay will be chosen as 5 %. Consequently, the number of QSS species *M* will be 29 and non-QSS species will be 26. The steps of the reduced mechanism will be 20 as there are 6 elements.[26]

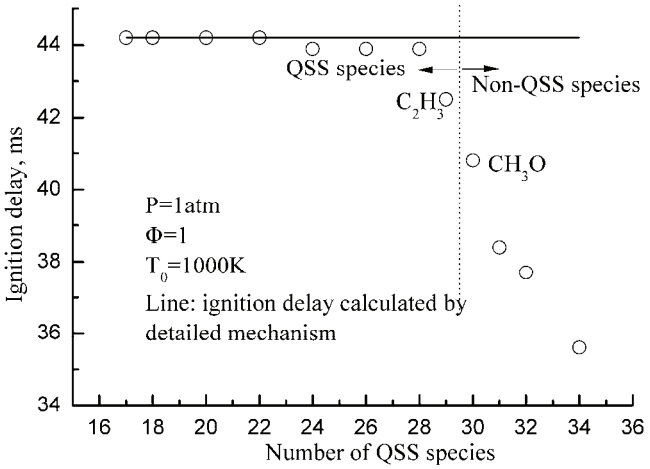

Fig. 1. Errors in the calculation of the ignition delay as a function of number of QSS species.

Radical pointers were calculated with Eq. (10). The 29 species with largest integrated radical pointers are considered as QSS species and the remaining 26 species are non-QSS species (in the same order as appearing in the detailed mechanism): H_2, CH_2, $CH_2(S)$, CH_3, CH_4, OH, H_2O, CH_2O, C_2H_6, CH_3O, O_2, CH_3OH, HO_2, H_2O_2, CH_2HCO, CO_2, OCHO, HCOOH, CH_3OCH_3, CH_3OCHO, H, O, CO, N_2, Ar and He.

The fast reactions can be determined by Eqs. (7) and (8). These two equations reflect the contribution of each reaction to the production of QSS species:

$$\frac{\mathrm{d}[C_2H_5]}{\mathrm{d}t}=s_{94}^{13}F^{94}+s_{105}^{13}F^{105}+s_{117}^{13}F^{117}+s_{238}^{13}F^{238}+s_{109}^{13}F^{109}+s_{111}^{13}F^{111}+s_{103}^{13}F^{103}+$$
$$+s_{115}^{13}F^{112}=-0.268204+0.19623+0.15421-0.141398-0.052505-\quad(11)$$
$$-0.047145+0.044899-\,-0.028644-0.018679+0.016272$$
$$\frac{\mathrm{d}[HCCO]}{\mathrm{d}t}=s_{143}^{22}F^{143}+s_{149}^{22}F^{149}+s_{145}^{22}F^{145}+s_{135}^{22}F^{135}+s_{144}^{22}F^{144}+s_{146}^{22}F^{146}=\quad(12)$$
$$=-0.327922-0.195474-0.152123+0.14655-0.114665-0.027255$$

$$\frac{\mathrm{d}[CH_3HCO]}{\mathrm{d}t} = s_{174}^{28}F^{174} + s_{115}^{28}F^{115} + s_{220}^{28}F^{220} + s_{176}^{28}F^{176} + s_{181}^{28}F^{181} + s_{180}^{28}F^{180} = \\ = -0.642532 + 0.122233 + 0.080127 - 0.077731 - 0.032477 - 0.015273 \quad (13)$$

where d[C]/dt is the derivative of the concentration of species C over time, s_k^i is the stoichiometric coefficient of i-th specie in the k-th reaction, F^k the reaction rate of the k-th reaction. The first item on the right side of equal mark in Eq. (11) refers to the contribution of the 94-th reaction to the consumption of C_2H_5. The number below is the specific value that is calculated by Eqs. (7) and (8). Sufficient terms are kept so that the total error of the omitted terms is below a user-defined error criterion. It can be seen from Eq. (13) that the 174th reaction contributes the most to the destruction of CH_3HCO, it is therefore deemed a fast reaction for CH_3HCO. By the same method, the fast reactions for the 29 QSS species could be calculated, as shown in Table I.

TABLE I. 29 QSS species and the corresponding fast reactions

QSS species	Fast reactions	QSS species	Fast reactions	QSS species	Fast reactions
CH_3OCH_2OH	267	$CH_3OCH_2O_2$	264	C_2H	152
HO_2CH_2OCHO	274	CH_3OCO	261	CH_3HCO	174
$O_2CH_2OCH_2O_2H$	273	HCCOH	139	HCO	31
$CH_3OCH_2O_2H$	268	$HOCH_2O$	280	C_2H_4	117
OCH_2OCHO	276	C_2H_5OH	203	C_2H_2	126
CH_3OCH_2O	251	CH_3OCH_2	240	CH_2OH	64
$HOC_2H_4O_2$	235	CH_3CO	176	C_2H_5	94
$CH_2OCH_2O_2H$	272	C_2H_4OH	237	HCCO	143
CH_3CHOH	227	CH_3CH_2O	238	C_2H_3	131
$HOCH_2OCO$	277	CH_2CO	127		

The reduced mechanism could be constructed after the QSS species and fast reactions had been determined. In order to make the process more efficient, a software package called Integral CSP (I-CSP) was developed. The I-CSP is written in C++ language and uses the interface functions provided by CHEMKIN-PRO[43] to read the reaction solutions generated in Chemkin. The I-CSP first reads temperatures, heat release rates and species concentrations and then calculates the Jacobian matrix and generates radical pointers and fast reaction pointers automatically. The outputs of the program contain three files. The first is the copied file with file extension asc. The second is a .inp file containing all elements, species and reduced mechanism. The third is a .dat file containing a (N–M–E)×(R–M) dimension matrix, which indicates the reaction rate of each step. Finally, the I-CSP uses the method developed by Goussis[42] to construct a reduced mechanism compatible with Chemkin and is convenient for validation, which is the content of next part of this manuscript.

RESULTS AND VALIDATION

A reduced mechanism that consists of 26 species and 20 steps was constructed with the help of I-CSP. The 20-step reduced mechanism was first validated over a closed homogeneous transient reactor with the same conditions as the reduced mechanisms being conducted. The results of the ignition delay over a wide range of equivalence ratios and with three different pressures, calculated with the detailed and the 20-step reduced mechanisms are shown in Fig. 2.

Excellent agreements can be observed, which demonstrate the high accuracy of the reduced mechanism in predicting ignition delay. Results calculated with the detailed and the reduced mechanisms under various initial temperatures, pressures, and equivalence ratios in auto-ignition are shown in Fig. 3. It can be seen that the results calculated with the reduced mechanism are quite consistent with those calculated with the detailed mechanism.

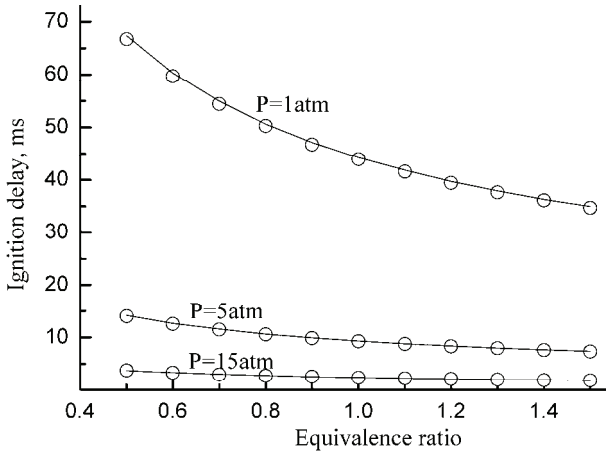

Fig. 2. Ignition delay as a function of equivalence ratio, in a constant pressure auto-ignition process, calculated for both the detailed and the reduced mechanisms.

To demonstrate further the ability of the reduced mechanism in predicting species concentrations, the results of calculation in a constant pressure auto-ignition reactor are displayed in Fig. 4 and no discrepancy could be found. The results of the calculation of temperature in a perfectly stirred reactor (PSR) over a wide range of equivalence ratios and pressures are shown in Fig. 5 and excellent agreements were found. The results of the variations of the mole fractions of H_2, O_2, H_2O in a PSR, calculated with the detailed and the 20-step reduced mechanisms, are presented in Fig. 6. Good agreements were observed therefore demonstrating the ability of the 20-step reduced mechanism in predicting the species concentrations in a PSR.

In order to demonstrate the validity of the reduced mechanism in predicting the profiles of the species in a premixed flame, the mole fractions of five species calculated in a steady, one-dimensional, burner-stabilized freely propagating premixed laminar flame are presented in Fig, 7. Obvious discrepancies could be observed for O_2 and H. Small discrepancies could be found for H_2 and CO. From Fig. 7, it could be learnt that the 20-step reduced mechanism shows limited accuracy in the prediction of species profiles in a freely propagating premixed laminar flame.

In this section, the reduced mechanism was validated over several reactors. Excellent agreements could be found in a homogenous reactor, such as auto-

ignition and PSR. However, in an inhomogeneous reactor, the reduced mechanism exhibited limited accuracy.

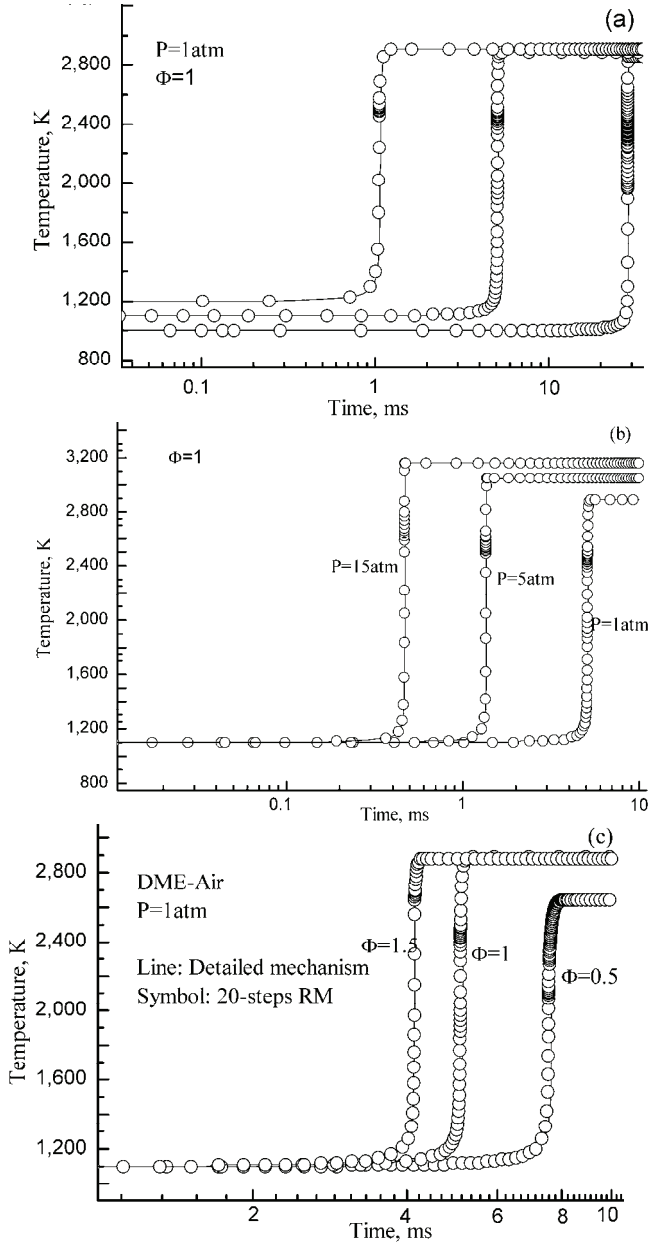

Fig. 3. Comparison of the temperature profiles in auto-ignition, calculated with the detailed and the reduced mechanisms under various a) initial temperatures, b) pressures and c) equivalence ratios.

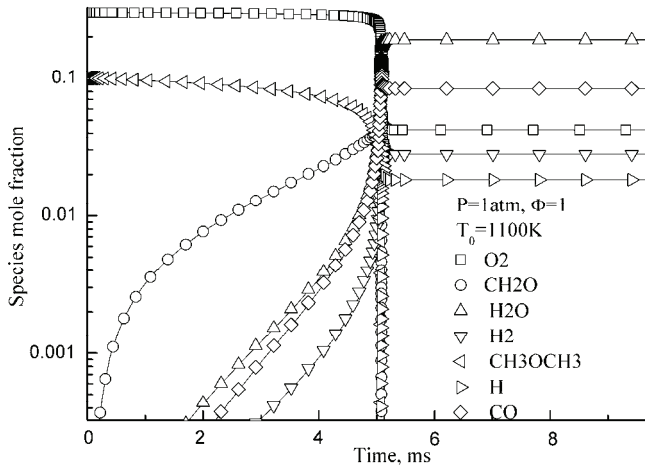

Fig. 4. Comparison of the mass fractions of the species in a constant pressure auto-ignition process, calculated with the detailed (lines) and the reduced (symbols) mechanisms.

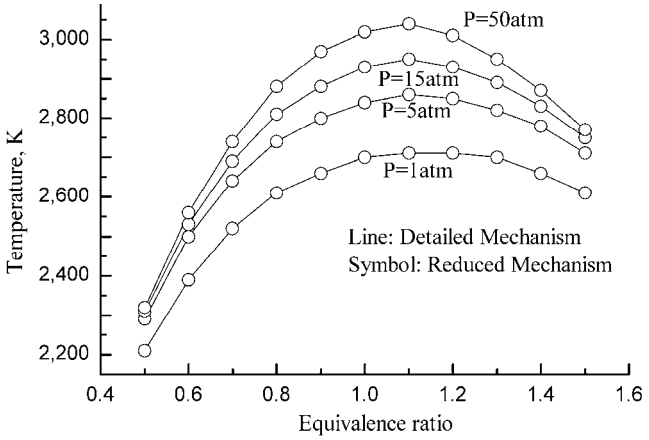

Fig. 5. Comparison of the temperature in a PSR, at 4 different pressures, calculated with the detailed and the reduced mechanisms.

CONCLUSIONS

In the present study, a criterion for determining the number of QSS species *M* was presented. A software package named Integral CSP (I-CSP) was developed to construct the reduced mechanism. The input to I-CSP includes the detailed mechanism, the numerical solution of the problem on a specific set of operating conditions, under which the reduced mechanism is expected to be valid, and the number of QSS species. The I-CSP can be obtained by mailing to: zuozhuwu@gmail.com. The output of I-CSP is three files that describe the reduced mechanism and the numerical relations between the QSS species and

non-QSS species. These files are compatible with Chemkin, which makes the validation of the reduced mechanism easier.

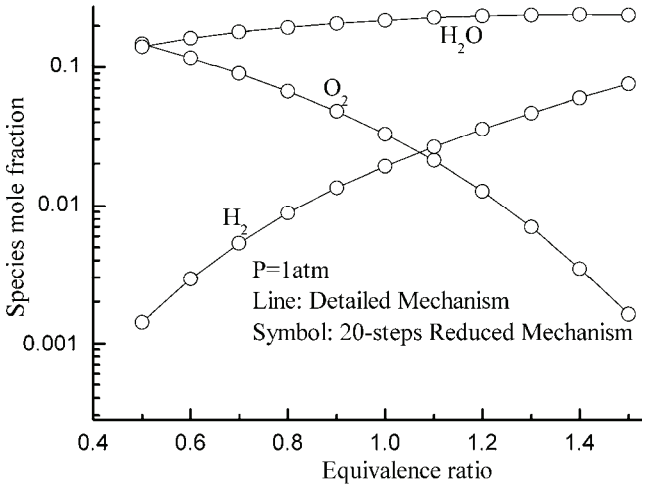

Fig. 6. Comparison of mole fraction of the species H_2, O_2, H_2O in a PSR, calculated with the detailed and the reduced mechanisms.

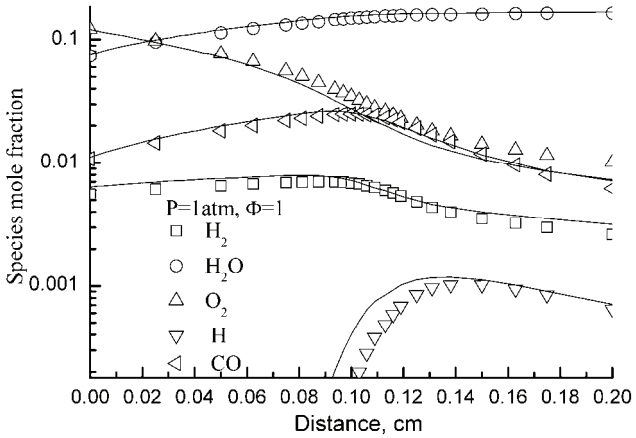

Fig. 7. Comparison of the mole fractions of species in a freely propagating premixed laminar flame, calculated with the detailed (lines) and the reduced (symbols) mechanisms.

To construct global reduced mechanism, the following four steps need to be performed. First, the QSS species require to be identified with the help of the CSP-pointer. These species will not appear in the reduced mechanism and their concentrations are calculated by the non-QSS species. Second, fast elementary reactions need to be determined. Reactions consuming most QSS species are deemed as “fast”. The fast reactions must be unique which means that one reac-

tion cannot be chosen twice as a fast reaction. The third step is the construction of global reduced mechanism. The purpose of the final step, which is called “simplification” or “truncation”, is to enable faster computation of the solution to problems where the reduced mechanism is implemented. The “simplification” or “truncation” is realized with the help of an importance index and a participation index.

The I-CSP was implemented over auto-ignition calculation with DME and conducted using a 20-step reduced mechanism. The reduced mechanism was validated first in a homogenous reactor including auto-ignition and PSR over a wide range of equivalence ratios and pressures, and then in a steady, one-dimensional, burner-stabilized freely propagating premixed laminar flame. Good agreements were observed therefore demonstrating the validity of the reduced mechanism, especially in homogenous reactors.

И З В О Д

КРИТЕРИЈУМ ЗАСНОВАН НА РАЧУНСКОЈ СИНГУЛАРНОЈ ПЕРТУБАЦИЈИ ЗА ОДРЕЂИВАЊЕ РЕДУКОВАНОГ МЕХАНИЗМА ОКСИДАЦИЈЕ ДИМЕТИЛ-ЕТРА

ZUOZHU WU, XINQI QIAO и ZHEN HUANG

Key Laboratory of Power Machinery and Engineering, Ministry of Education, Shanghai Jiao Tong University, Shanghai 200240, China

Предложен је критеријум заснован на методу рачунске сингуларне пертурбације за одређивање броја квази-равнотежних врста. Овај критеријум је коришћен за редукцију детаљног кинетичког механизма за оксидацију диметил-етра (ДМЕ), који укључује 55 врста и 290 реакција, а који доводи до редукованог механизма од 20 корака који укључује 26 врста. Софтверски пакет I-CSP је развијен да би редукциони процес постао алгоритмичан. Улазни подаци за I-CSP укључују: 1) детаљни механизам, 2) нумеричко решење проблема за одређени скуп радних услова и 3) број квази равнотежних врста. Добијени редуковани механизам је проверен у хомогеном реактору са аутоматским паљењем и савршеним мешањем у широком опсегу притисака и еквивалентних односа, и такође у једнодимензионалном, неизduженом, помешаном, ламинарном, равнотежном DME/ваздух пламену. Поређење резултата добијених са детаљним и редукованим механизмом показује одлично слагање у случају хомогеног реактора док се одступања примећују у случају помешаног ламинарног пламена.

(Примљено 22. новембра 2012, ревидирано 9. фебруара 2013)

REFERENCES

1. T. Fleisch, C. McCarthy, A. Basu, C. Udovich, P. Charbonneau, W. Slodowske, S.-E. Mikkelsen, J. McCandless, *A New Clean Diesel Technology: Demonstration of ULEV Emissions on a Navistar Diesel Engine Fueled with Dimethyl Ether*, SAE Technical Paper 950061, 1995, doi:10.4271/950061
2. S. Sorenson, S. Mikkelsen, *Performance and Emissions of a 0.273 Liter Direct Injection Diesel Engine Fuelled with Neat Dimethyl Ether*, SAE Technical Paper 950064, 1995, doi:10.4271/950064
3. T. A. Semelsberger, R. L. Borup, H. L. Greene, *J. Power Sources* **156** (2006) 497

4. C. Acroumanis, C. Bae, R. Crookes, E. Kinoshita, *Fuel* **87** (2008) 1014
5. A. S. Tomlin, T. Turanyi, M. J. Pilling, in *Comprehensive Chemical Kinetics*, Vol. 35, *Low-Temperature Combustion and Autoignition*, M. J. Pilling, Ed., Elsevier, Amsterdam, 1997, p. 293
6. S. Vajada, P. Valko, T. Turanyi, *Int. J. Chem. Kinetics* **17** (1985) 55
7. W. Sun, Z. Chen, X. Gou, Y. Ju, *Combust. Flame* **157** (2010) 1298
8. T. F. Lu, C. K. Law, *Proc. Combust. Inst.* **30** (2005) 1333
9. T. F. Lu, C.K. Law, *Combust. Flame* **144** (2006) 24
10. T. F. Lu, C. K. Law, *Combust. Flame* **146** (2006) 472
11. P. Pepiot, H. Pitsch, *Combust. Flame* **154** (2008) 67
12. X. L. Zheng, T. F. Lu, C. K. Law, *Proc. Combust. Inst.* **31** (2007) 367
13. K. Niemeyer, C. Sung, M. Raju, *Combust. Flame* **157** (2010) 1760
14. T. Ombrello, Y. Ju, A. Fridman, *AIAA J.* **46** (2008) 2424
15. N. Peters, in, *Numerical Simulations of Combustion Phenomena*, *Lecture Notes in Physics*, Vol. 241, R. Glowinsky, B. Larrouturou, R. Temum, Eds., Springer Verlag, Berlin, 1985, p. 90
16. N. Peters, R. J. Kee, *Combust. Flame* **68** (1987) 17
17. J.Y. Chen, *Combust. Sci. Technol.* **57** (1988) 89.
18. M. D. Smooke, V. Giovangigli, in *Reduced Kinetic Mechanisms and Asymptotic Approximations for Methane–Air Flames*, *Lecture Notes in Physics*, Vol. 384, M. D. Smooke, Ed., Springer Verlag, Berlin, 1991, p. 1
19. Y. Ju, T. Niioka, *Combust. Flame* **99** (1994) 240
20. C. J. Sung, C. K. Law, J. Y. Chen, *Proc. Combust. Inst.* **27** (1998) 295
21. T. Lovas, D. Nilsson, F. Mauss, *Proc. Combust. Inst.* **28** (2000) 1809
22. U. Maas, S. B. Pope, *Combust. Flame* **88** (1992) 239
23. Z. Ren, S. B. Pope, *Combust. Flame* **147** (2006) 243
24. S. B. Pope, *Combust. Theor. Model.* **1** (1997) 41
25. B. Yang, S. B. Pope, *Combust. Flame* **112** (1998) 85
26. A. Massias, D. Diamantis, E. Mastorakos, D. A. Goussis, *Combust. Flame* **117** (1999) 685
27. S. H. Lam, D.A. Goussis, *Proc. Combust. Inst.* **22** (1989) 931
28. S. H. Lam, D. A. Gousis, *Int. J. Chem. Kinet.* **26** (1994) 461
29. M. Valorani, H. N. Najm, D. A. Goussis, *Combust. Flame* **134** (2003) 35
30. M. Valorani, F. Creta, D. A. Goussis, J. C. Lee, H. N. Najm, *Combust. Flame* **146** (2006) 29
31. S. H. Lam, in *Proceedings of 11th International Conference on Numerical Combustion*, Granada, Spain, 2006
32. J. Prager, H. N. Najm, M. Valorani, D. A. Goussis, *Proc. Combust. Inst.* **32** (2009) 507
33. T. F. Lu, Y. Ju, C. K. Law, *Combust. Flame* **126** (2001) 1445
34. H. J. Curran, S. L. Fischer, F. L. Dryer, *Int. J. Chem. Kinetics* **32** (2000) 741
35. S. L. Fischer, F. L. Dryer, H. J. Curran, *Int. J. Chem. Kinetics* **32** (2000) 713
36. H. Yamada, H. Sakanashi, N. Choi, A. Tezaki, *Simplified Oxidation Mechanism of DME Applicable for Compression Ignition*, SAE Technical Paper 2003-01-1819, 2003, doi: 10.4271/2003-01-1819
37. G. T. Chin, J. Y. Chen, V. H. Rapp, R. W. Dibble, *J. Combust.* **2011** (2011) 630580
38. Z. Zhao, M. Chaos, A. Kazakov, F. L. Dryer, *Int. J. Chem. Kinet.* **40** (2007) 1
39. B. W. Ryu, S. W. Park, C. S. Lee, *Trans. Korean Soc. Mech. Eng., B* **35** (2011) 75
40. D. A. Goussis, S. H. Lam, *Proc. Combust. Inst.* **24** (1992) 113
41. CHEMKIN-PRO Release, Reaction Design, San Diego, CA, 2008
42. D. A. Goussis, *J. Comput. Phys.* **128** (1996) 261.

Journal of the Serbian Chemical Society
JSCS-info@shd.org.rs • www.shd.org.rs/JSCS
J. Serb. Chem. Soc. 78 (8) 1189–1202 (2013)
JSCS–4490
UDC 547.291:541.138.2:544.478:
544.6.076–32–546.92'87
Original scientific paper

Electrocatalytic properties of Pt–Bi electrodes towards the electro-oxidation of formic acid

JELENA D. LOVIĆ#, DUŠAN V. TRIPKOVIĆ#, KSENIJA Đ. POPOVIĆ#, VLADISLAVA M. JOVANOVIĆ# and AMALIJA V. TRIPKOVIĆ*#

ICTM – Institute of Electrochemistry, University of Belgrade, Njegoševa 12, P. O. Box 473, 11000 Belgrade, Serbia

(Received 12 October, revised 16 November 2012)

Abstract: Formic acid oxidation was studied on two Pt–Bi catalysts, *i.e.*, Pt_2Bi and polycrystalline Pt modified by irreversible adsorbed Bi (Pt/Bi_{irr}) in order to establish the difference between the effects of Bi_{irr} and Bi in the alloyed state. The results were compared to pure Pt. It was found that both bimetallic catalysts were more active than Pt with the onset potentials shifted to more negative values and the currents at 0.0 V *vs.* saturated calomel electrode (under steady state conditions) improved by up to two order of magnitude. The origin of the high activity and stability of Pt_2Bi was increased selectivity toward formic acid dehydrogenation caused by the ensemble and electronic effects and suppression of Bi leaching from the surface during formic acid oxidation. However, although Pt/Bi_{irr} also showed remarkable initial activity compared to pure Pt, dissolution of Bi was not suppressed and poisoning of the electrode surface induced by the dehydration path was observed. Comparison of the initial quasi-steady state and potentiodynamic results obtained for these two Pt–Bi catalysts revealed that the electronic effect, existing only in the alloy, contributed to the earlier start of the reaction, while the maximum current density was determined by the ensemble effect.

Keywords: formic acid; electrochemical oxidation; Pt_2Bi catalyst; Pt/Bi_{irr} catalyst; fuel cell.

INTRODUCTION

The electrocatalytic oxidation of small organic molecules, such as methanol, ethanol and formic acid, has been extensively studied because such molecules can potentially be used as fuel in fuel cell applications.[1] Pt is an excellent catalyst for the dehydrogenation of small organic molecules but, on the other hand, has several significant disadvantages, such as high cost and extreme susceptibility to

* Corresponding author. E-mail: amalija@tmf.bg.ac.rs
# Serbian Chemical Society member.
doi: 10.2298/JSC121012138L

poisoning by CO. To improve its catalyst performance and minimize its amount in catalysts, Pt has been modified by the addition of other metals, such as Ru, Rh, Pd, Sn, Pb, *etc*.[2–5]

The electrochemical oxidation of formic acid has been comprehensively investigated as the anodic reaction in direct formic acid fuel cells (DFAFC) and as a model reaction important for the understanding the electro-oxidation of other small organic molecules.[6,7] Mechanistic studies of formic acid electro-oxidation suggested that the reaction on Pt proceeds through two parallel paths:[8] dehydrogenation with direct oxidation to CO_2 and a path consisting of a dehydration step, to yield water and adsorbed CO (CO_{ad}), as a poisoning intermediate, and the subsequent oxidation of CO_{ad} to CO_2. Since the potential of CO_{ad} formation is lower than the dehydrogenation potential, the poison remains on electrode surfaces until it is oxidized by oxygen-containing species at positive potentials.[9] Thus, the Pt atoms covered with poison are not available for dehydrogenation and the catalytic efficiency of the Pt surface decreases.

Therefore, practical application of Pt for formic acid oxidation requires some modification of the surface. This is commonly realized by alloying or by alteration of the Pt surface with adsorbed foreign metals in amounts less than a full monolayer. As the CO_{ad} poison require an ensemble of Pt surface atoms to adsorb on, modification of the local distribution of surface domains is achieved by adsorption of different ad-atoms, such as Bi. Irreversibly adsorbed Bi.[10–13] inhibits poison formation and simultaneously enhances dehydrogenation,[13] *i.e*., this modification is an efficient way to hinder the dehydration path (CO-intermediate pathway) in favor of the direct path.[14] This increased selectivity for dehydrogenation has been proposed as an "ensemble effect"[15,16] in which the adsorbed Bi divides the Pt surface into small domains where only dehydrogenation can occur. A correlation between ensemble size and formic acid oxidation activity was also established.[17] According to literature data, the activity of a Pt catalyst modified with Bi depends on the shape of the Pt nanocrystals,[18] the size of the particles[19] and Pt catalyst loading.[14]

Ordered intermetallic PtBi or $PtBi_2$ alloys[20–23] and PtBi alloy nanoparticles[24–29] were proposed as good catalysts for formic acid oxidation. The onset potential of the reaction is significantly shifted to more negative values (by over 300 mV) and the current density is remarkably enhanced over the whole potential range compared to Pt.[30] Moreover, the PtBi surface appears to have a considerably lower sensitivity to poisoning by CO according to DEMS,[22,30] FTIR[22,31] and DFT calculations.[22,23,32] The origin of its catalytic activity was related to electronic effects. The formation of the PtBi ordered intermetallic phase results in a charge redistribution, enhancing the affinity of PtBi for formic acid adsorption and producing surface oxides at low potentials,[25,33] as well as to geometric effects reducing the affinity for CO poisoning. In addition, the excellent catalytic

properties of PtBi nanoparticles can be attributed to the occurrence of the ensemble effect on the nanoscale level.[29]

In previous studies, the oxidation of formic acid was investigated on single phase PtBi alloy,[34] as well as on Pt_2Bi catalyst, a two-phase material consisting of PtBi alloy and pure Pt.[35] A huge increase in catalytic activity on the PtBi electrode relative to polycrystalline Pt was observed and discussed in terms of electrochemically detected UPD phenomena of Bi re-adsorbed on Pt. Additionally, based on the analysis of X-ray photoelectron spectra, it was proposed that the bifunctional action of hydroxylated Bi species may contribute to the enhanced activity of PtBi alloys.[34] Pt_2Bi was found to be powerful catalyst for formic acid oxidation, exhibiting high activity and stability. The high activity originates from the fact that formic acid oxidation proceeds entirely through the dehydrogenation path, while the high stability of Pt_2Bi surface is induced by the suppression of Bi leaching in the presence of formic acid.[35] It is difficult to separate the contributions of the ensemble and the electronic effect since both of them could be present in the Pt–Bi surfaces.

In the present study, formic acid oxidation was studied on two types of Pt–Bi surfaces: polycrystalline Pt modified by irreversibly adsorbed Bi (designated as Pt/Bi_{irr}) and a Pt_2Bi catalyst. In order to investigate the promotional role of Bi in formic acid oxidation, as well as the difference between the effect of irreversibly adsorbed Bi and Bi in the alloyed state, Pt was modified with ≈30 % Bi_{irr}, which correspond to the nominal content of Bi in the Pt_2Bi catalyst. The comparative investigation based on the effects influencing the catalytic properties of these electrodes enabled a better understanding of the difference in the activities between the Pt_2Bi catalyst and the Bi_{irr} modified Pt.

EXPERIMENTAL

Polycrystalline Pt and Pt_2Bi electrodes in the form of discs were used in this study. Pt_2Bi catalyst was prepared and characterized at the Institute of Catalysis and Surface Chemistry, Polish Academy of Sciences, Krakow, Poland.[35] Briefly, the catalyst was fabricated by melting the pure elements in an inert atmosphere in the proportion of Bi to Pt of 1:2 and characterized by X-ray diffraction (XRD) analysis. Diffraction pattern for Pt_2Bi sample revealed two crystal phases: platinum (*fcc*) and platinum bismuth PtBi (*hcp*). The phase composition of the sample was calculated using the Rietveld refinement as 45 % and 55 % for Pt and PtBi phases, respectively.

Prior to each experiment, the electrodes were mirror polished (1–0.05 μm Buehler alumina). The surfaces were rinsed with high purity water (Millipore, 18 MΩ cm resistivity), sonicated for 2–3 min and rinsed again with ultrapure water.

All experiments were performed on the as-prepared catalysts. Three-compartment electrochemical glass cells with a Pt wire as the counter electrode and a saturated calomel electrode (SCE) as the reference electrode were used. All the potentials are expressed on the SCE scale. The electrolyte containing 0.1 M H_2SO_4 as a supporting electrolyte and 0.125 M HCOOH was prepared with high purity water and *p.a.* grade chemicals (Merck). The electrolyte was de-aerated by bubbling with nitrogen. Upon addition of HCOOH at –0.20 V,

potentiodynamic (v = 50 mV s^{-1}), quasi steady-state measurements (v = 1 mV s^{-1}) or chronoamperometric measurements were performed. The electrode was rotating at 2000 rpm in all the experiments.

Modification of the Pt electrode was performed from 1×10^{-5} M Bi_2O_3 in 0.1 M H_2SO_4 at the open circuit potential during 45 s. After modification, the electrode (denoted Pt/Bi_{irr}) was rinsed with water and transferred into a cell containing the supporting electrolyte. The fraction of the sites covered by Bi was estimated from the decrease in the charge for the desorption of hydrogen, assuming a charge of 210 μC cm^{-2} for hydrogen monolayer adsorption.

The real surface area of all the as-prepared catalysts was calculated from CO stripping voltammetry. For the CO stripping measurements, pure CO was bubbled through the electrolyte for 20 min while keeping the electrode potential at –0.20 V *vs*. SCE. After purging the electrolyte by N_2 for 30 min to eliminate the dissolved CO, the adsorbed CO was oxidized in an anodic scan at 50 mV s^{-1}. Two subsequent voltammograms were recorded to verify the completeness of the CO oxidation. The real surface area of all the employed electrodes was estimated by calculation of the charge from the CO_{ad} stripping voltammograms corrected for background currents. Assuming a charge of 420 μC cm^{-2} for a CO monolayer adsorption on the Pt electrode, a roughness factor of 1.4±0.1 was estimated. The real surface area of the Pt_2Bi electrode was estimated assuming the same roughness factor as for the Pt electrode, which is to be expected since both electrodes were polished in the same way. The specific activity of Pt and Pt_2Bi electrodes for formic acid oxidation were normalized using these values of the surface area.

The experiments were conducted at 295±0.5 K employing a VoltaLab PGZ 402 (Radiometer Analytical, Lyon, France).

RESULTS AND DISCUSSION

Electrochemical characterization

The initial voltammograms of the as-prepared Pt and Pt/Bi_{irr} catalysts are presented in Fig. 1. The cyclic voltammogram for the polycrystalline Pt electrode is characterized by a defined region of hydrogen adsorption/desorption (E < 0.05 V), separated by a double layer from the region of surface oxide formation (E > 0.45 V). The absence of well-developed peaks at the polycrystalline Pt in hydrogen adsorption/desorption region arises from the employed preparation procedure.

In Fig. 1, the typical voltammograms recorded in the supporting electrolyte before and after Pt modification with adsorbed bismuth are compared. Distinctive characteristics for the presence of bismuth ad-atoms on the platinum surface are the diminution of the hydrogen adsorption/desorption charge due to the fact that hydrogen does not adsorb on Bi[36] and the appearance of peaks “a” and “a′”, as a result of the irreversible oxidation/reduction of Bi adsorbed onto the Pt surface, which superimpose those corresponding to Pt oxide formation/reduction. Since only the Pt sites not blocked by Bi are available for hydrogen adsorption, the fractional coverage by Bi ad-atoms, evaluated from the decrease in charge involved in the hydrogen desorption before and after adsorption of Bi on the Pt electrode

surface, was set to be about 30 %, corresponding to the nominal content of Bi in the Pt_2Bi catalyst.

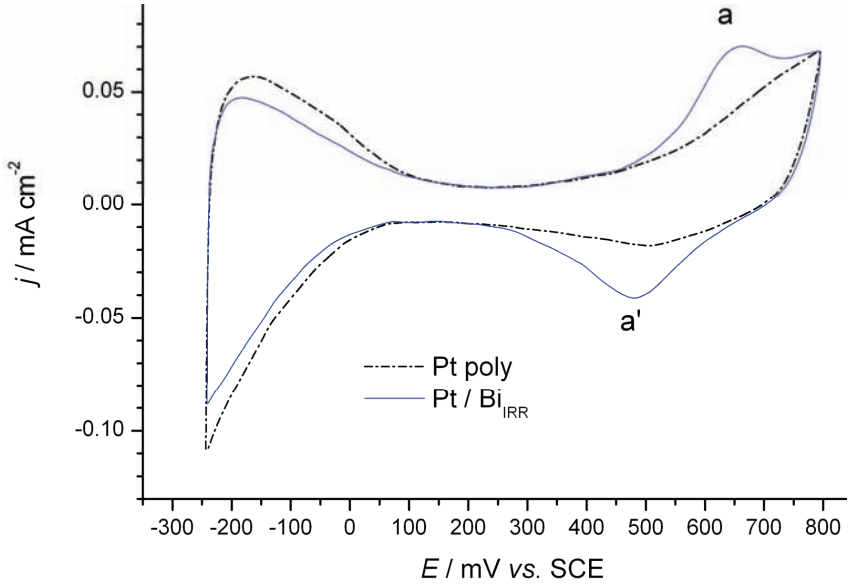

Fig. 1. Initial basic voltammograms for Pt/Bi_{irr} and Pt catalysts in 0.1 M H_2SO_4 solution. Scan rate: 50 mV s^{-1}.

Oxidation of pre-adsorbed CO

Oxidation of pre-adsorbed CO was examined on Pt, Pt_2Bi and Pt/Bi_{irr} electrodes and the stripping voltammograms after subtraction of the background current are given in Fig. 2. As can be seen, the oxidation of CO_{ad} started earlier on the Pt_2Bi catalyst than on pure Pt. The difference in the onset and peak potential of CO_{ad} oxidation could be ascribed to some electronic modification of the Pt surface atoms by Bi[10,17,37,38] resulting in weaker bonding of CO_{ad}. This statement is consistent with literature data based on theoretical calculations.[39,40] However, the difference in onset and peak potentials between Pt/Bi_{irr} and Pt catalysts was insignificant.

The CO stripping charge was also determined for the Pt_2Bi electrode and corrected for the background currents to eliminate the contribution of the double layer charge, as well as Bi oxidation charge. Since Bi[37] and PtBi[23,30] are inactive for CO adsorption, the oxidation of CO occurs only on the Pt domains. Therefore, the charge under the CO_{ad} peak at Pt_2Bi reflects a process at the Pt parts and could be used for determining the contribution of pure Pt in the surface composition of Pt_2Bi catalyst.[35]

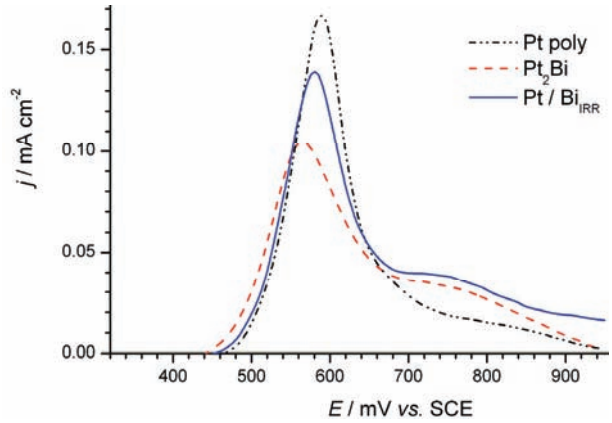

Fig. 2. CO stripping voltammograms on Pt_2Bi, Pt/Bi_{irr} and Pt catalysts (first positive going sweeps) in 0.1 M H_2SO_4 solution corrected for background current. Scan rate: 50 mV s^{-1}.

Oxidation of formic acid

Activity of the catalysts. The activities of Pt_2Bi, Pt/Bi_{irr} and Pt electrodes (first sweeps) towards formic acid oxidation are compared in Fig. 3. The cyclic voltammogram for the Pt electrode shows well established features for the oxidation of formic acid.[8] In the positive scan, the current slowly increased reaching a plateau at ≈0.25 V followed by ascending current starting at 0.5 V that attains a maximum at ≈0.62 V. This behavior could be explained by considering the dual path mechanism, *i.e.*, dehydrogenation assigned as the direct path, based on the oxidation of formate,[41,42] and dehydration, indirect path, assumes the formation of CO_{ad}, both of which generate CO_2 as the final reaction product. At low potentials, HCOOH is oxidized through the direct path with the simultaneous formation of CO_{ad}. Increasing coverage with CO_{ad} reduces the number of Pt sites available for the direct path and the current slowly increases reaching a plateau. Subsequent formation of oxygen-containing species on the Pt enables the oxi-

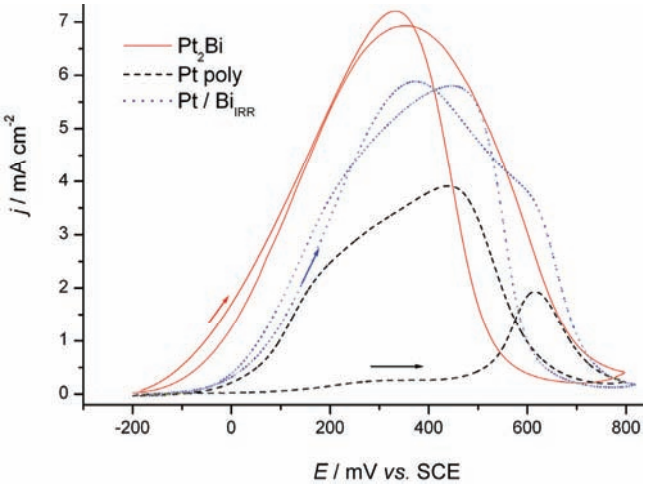

Fig. 3. Cyclic voltammograms for the oxidation of 0.125 M HCOOH in 0.1 M H_2SO_4 solution on Pt, Pt_2Bi and Pt/Bi_{irr} catalysts. Scan rate: 50 mV s^{-1}.

dative removal of CO_{ad} and more Pt sites become available for HCOOH oxidation whereby the current increases until Pt oxide, inactive for HCOOH oxidation, is formed, which results in the current peak at ≈0.62 V. In the backward scan, the sharp increase of HCOOH oxidation current coincides with reduction of Pt oxide. The currents are much higher than in the forward sweep because the Pt surface is freed of CO_{ad}.

The polarization curves for bimetallic surfaces indicate a quite different behavior. Figure 3 shows that the onset potential for the reaction on Pt/Bi_{irr} was about 0.1 V less positive than on the Pt electrode. The current increases up to 0.35 V and reaches a peak, which corresponds to the oxidation of HCOOH to CO_2 in the direct path, occurring on Pt sites that are not blocked by CO_{ad}. On the descending part of the curve, a shoulder appears at almost the same potential as the peak on the curve for the bare Pt electrode. The currents recorded in the backward direction are slightly higher, so the difference between forward and backward scan is not as large as on the bare Pt. Since the peak at ≈0.62 V arises from HCOOH oxidation on the Pt sites being freed by CO_{ad} oxidation, its height is an indication of the degree of Pt poisoning at lower potentials. Accordingly, the amount of CO_{ad} formed in the indirect path on Pt/Bi_{irr} is much lower than that formed on the pure Pt electrode.

The oxidation of formic acid on Pt_2Bi electrode starts at ≈ –0.2 V, which is 0.1 V less positive than on Pt/Bi_{irr} and ≈0.2 V less positive than on the Pt electrode. The current increases up to 0.35 V and reaches a peak about 15 times higher than the plateau on the curve for Pt. At more positive potentials, the reaction currents decrease due to surface oxide formation. The absence of a shoulder on the descending part of the curve, recorded on Pt/Bi_{irr}, indicating that no poisoning of the alloy by CO_{ads} occurred.

Well-shaped voltammogram clearly suggests that oxidation of HCOOH on Pt_2Bi proceeds through dehydrogenation path.[35] Since Bi does not adsorb HCOOH,[34,40] oxidation of HCOOH occurs on the Pt sites in the pure Pt and Bi alloyed Pt domains. As is shown in Fig. 3, the lower activity of Pt/Bi_{irr} compared to Pt_2Bi and the appearance of a shoulder on the curve of Pt/Bi_{irr} could suggest a low coverage by CO_{ad} at the Pt sites on Pt/Bi_{irr}, *i.e.*, incomplete suppression of the dehydration path although these two electrodes contained almost the same (nominal) amount of Bi. Thus, HCOOH oxidation on Pt/Bi_{irr} proceeded predominantly by the dehydrogenation path with some minor degree of dehydratation occurring a well. The increased selectivity toward the dehydrogenation path on Pt_2Bi as well as on Pt/Bi_{irr} compared to Pt was mainly the result of an ensemble effect caused by Bi reducing the continuous Pt sites necessary for dehydration. However, the ensemble effect on the Pt/Bi_{irr} catalyst was enabled by adsorbed Bi having practically no influence on the neighboring free Pt atoms. Whereas in the Pt_2Bi alloy, the ensembles were created by alloyed Bi atoms incorporated into

the Pt lattice, causing a shift in the d-band center of the adjacent Pt atoms. Therefore, Bi in the alloy also exhibited an electronic effect that could have been the reason for the better performance of this catalyst, resulting in higher currents and a lower onset potential.

Stability of catalysts. Cyclic voltammograms (first and 20th sweep) recorded on Pt_2Bi and Pt/Bi_{irr} catalysts in a formic acid containing solution are shown in Fig. 4. On potential cycling up to 0.8 V, the activity of the Pt_2Bi electrode (Fig. 4a) slowly decreased during the first 5–7 cycles, reaching values of 90 and 82 % of the initial currents at the potential of the maximum current and at the potential of 0.0 V in the low current region, respectively. After these first few sweeps, the currents remain unchanged with further cycling (Inset in Fig. 4a). Since cycling of Pt_2Bi in the supporting electrolyte leads to enhancement of the currents related to the oxidation of Bi species, indicating some surface decomposition caused by Bi leaching/dissolution processes,[35] the stability of Pt_2Bi during oxidation of formic acid could be induced by the presence of HCOOH in the electrolyte. Abruna and co-workers[43] explained that the stability of Pt–Bi intermetallic surface originates from the competition between the oxidation of formic acid at the electrode/solution interface and Bi leaching, *i.e.*, corrosion/oxidation processes of the electrode surface itself. Accordingly, the main reason for high stability of formic acid oxidation current on the Pt_2Bi catalyst was inhibition of the dehydration path, as well as, suppression of Bi leaching. This statement was confirmed by STM imaging before and after electrochemical treatment in formic acid-containing solution, which did not indicate any significant change of surface morphology and roughness after that procedure.[35]

Contrary to the Pt_2Bi alloy, as can be seen in Fig. 4b, the Pt/Bi_{irr} electrode showed significant changes with continuous cycling in a solution containing formic acid (Inset in Fig. 4b). Repetitive cycling up to 0.8 V shifted the onset potential for formic acid oxidation to more positive values, decreased the reaction currents, while anodic peak diminishes and a new peak starts to emerge and grow at ≈0.6 V. These transformations of the cyclic voltammograms indicate continuous Bi dissolution and modification of the surface composition. Upon prolonged cycling, the electrode surface became enriched in platinum and exhibited a Pt-like electrochemical behavior in the acid electrolyte containing formic acid. Apparently, re-adsorption of Bi species from the solution is rather low, so the initial voltammogram was never restored, which is in accordance with results obtained for formic acid oxidation on bismuth-coated mesoporous Pt microelectrodes.[44]

Finally, it could be concluded that the initial activities at the two Bi–Pt catalysts originate from the ensemble effect, but the activity of the Pt/Bi_{irr} in the reaction is diminished due to leaching of Bi. An electronic effect contributes to the early start of the reaction on the alloy.

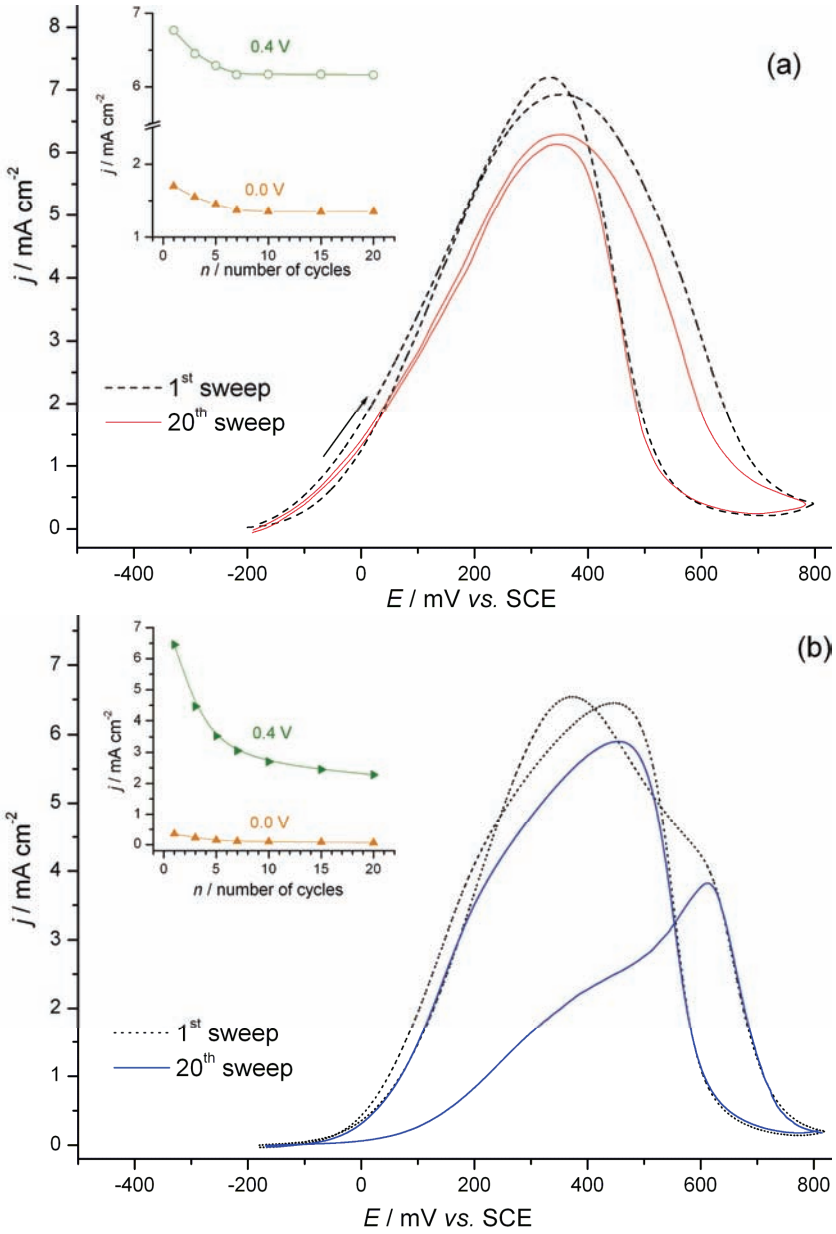

Fig. 4. First and 20th sweep for the oxidation of 0.125 M HCOOH in 0.1 M H_2SO_4 solution on a) Pt_2Bi and b) Pt/Bi_{irr} catalysts. Insets: Effect of cycling – plots of the current density *vs.* number of cycles. Scan rate 50 mV s^{-1}.

Chronoamperometric measurements. Chronoamperometric experiments were performed to prove the activity and stability of the investigated catalysts. The

current density of formic acid oxidation was recorded as a function of time at 0.20 V over 30 min (Fig. 5). The highest initial current density at 0.20 V on Pt_2Bi compared to the other two catalysts is in accordance with the potentiodynamic measurements (Fig. 3). The initial currents at Pt_2Bi electrode decreases slightly and in observed period of time attain a value which was about 3.5 times higher than at the Pt/Bi_{irr} catalyst and almost 20 times higher than at the Pt electrode. The chronoamperometic results confirmed the high activity and stability of the Pt_2Bi catalyst.

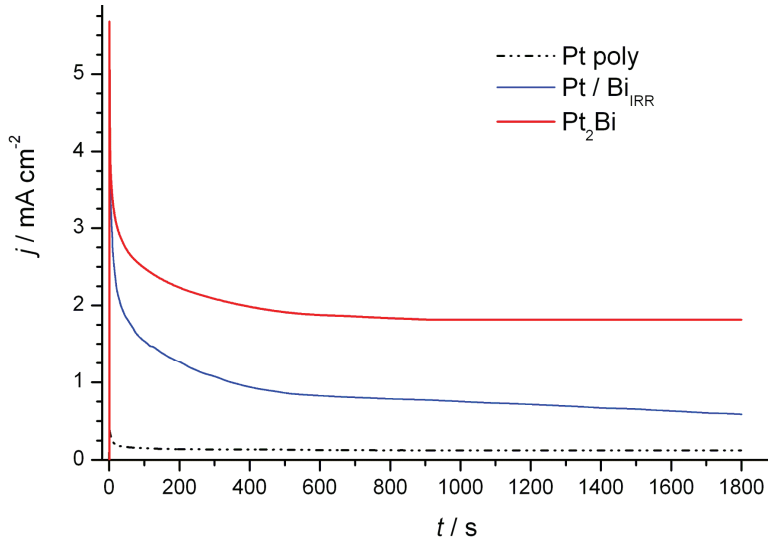

Fig. 5. Chronoamperometric curves for the oxidation of 0.125 M HCOOH at 0.20 V in 0.1 M H_2SO_4 solution on Pt_2Bi, Pt/Bi_{irr} and Pt catalysts.

Quasi-steady state measurements. The results of the quasi-steady state measurements for formic acid oxidation at all the investigated electrodes are presented in Fig. 6. The data obtained under the slow sweep conditions corroborated the differences in the activities of pure Pt, Pt modified by Bi and Pt_2Bi alloy that were found in the potentiodynamic measurements.

The Tafel slope on the Pt_2Bi electrode was about 120 mV dec^{-1}, indicating that the first electron transfer is the rate-determining step, with the transfer coefficient being about 0.5. This means that C–H bond cleavage, to form $COOH_{ad}$, is the slow step and determines the rate of formic acid oxidation on Pt_2Bi electrodes.

The Tafel slope of about 150 mV dec^{-1} obtained during formic acid oxidation on bare Pt indicates that the formed CO was adsorbed and collected on the surface, thereby slowing down the reaction rate. The same value of Tafel slope was obtained for formic acid oxidation on carbon-supported high surface area

platinum.[45] A Tafel slope of 135 mV dec^{-1} was found at Pt/Bi$_{irr}$, which implies moderate surface coverage by CO$_{ad}$.

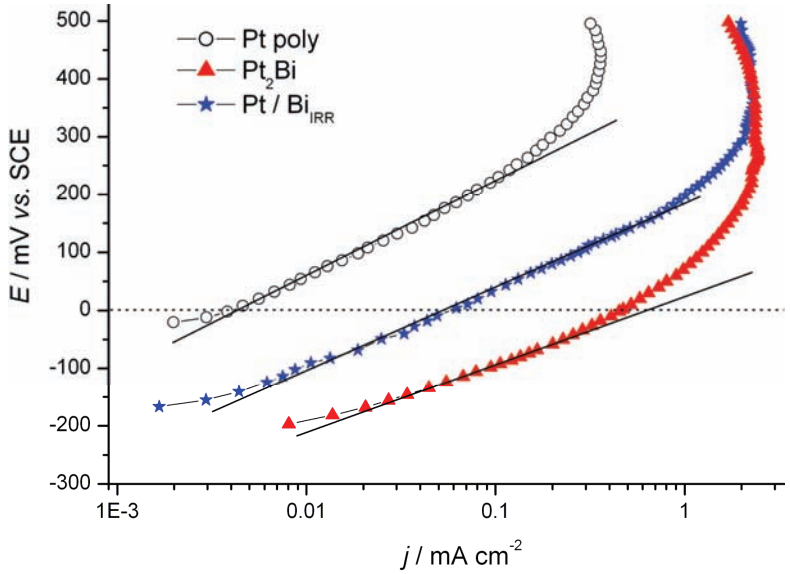

Fig. 6. Tafel plots for the oxidation of 0.125 M HCOOH in 0.1 M H_2SO_4 solution on Pt_2Bi, Pt/Bi$_{irr}$ and Pt catalysts. Scan rate: 1 mV s^{-1}.

Comparing the activities of the investigated electrodes at 0.0 V, it can be seen that the current densities were enhanced 15 times at Pt/Bi$_{irr}$ and up two orders of magnitude at the Pt_2Bi catalyst with respect to the Pt electrode.

CONCLUSIONS

Pt_2Bi and Pt/Bi$_{irr}$ electrodes were investigated in the oxidation of formic acid and the results were compared to those of a Pt electrode. The presented results indicate that Bi in alloy and irreversibly adsorbed Bi exhibit different effects on the catalytic activity of these materials.

Pt_2Bi is highly active for formic acid oxidation because the dehydrogenation path is predominant in the overall reaction. Bi in the alloy not only that facilitates the ensemble effect, but also has an electronic effect that could be the reason for better performance of this catalyst, resulting in higher currents and a lower onset potential. The main reason for the high stability of the Pt_2Bi catalyst is the inhibition of dehydration path in the reaction, as well as suppression of Bi leaching, indicated by the insignificant change in the surface morphology and roughness.

On the contrary, the Pt/Bi$_{irr}$ electrode was not stabilized by formic acid oxidation, since the desorption of Bi was not suppressed in the presence of formic acid, and a poisoning effect induced by the dehydration path was present. Since

Bi_{irr} does not provoke any significant modification of the electronic environment, the modified Pt catalysts were less active than corresponding alloy.

Comparing the results obtained for these two Pt–Bi catalysts, the role of the ensemble effect and electronic effect in the oxidation of formic acid on Pt–Bi electrodes could be distinguished. The electronic effect, existing only on the alloy, contributes to an earlier start of the reaction, while the maximum current density is determined by the ensemble effect. During potential cycling of the Pt/Bi_{irr} electrode, Bi was leached from the electrode surface and the ensemble effect was reduced over time, or lost. Insight into the chronoamperometric curves confirmed the advantage of the alloys, *i.e.*, the necessity of alloying Pt with Bi to obtain a corrosion stable catalyst.

Acknowledgement. This work was financially supported by the Ministry of Education, Science and Technological development of the Republic of Serbia, Contract No. H-172060.

И З В О Д

ЕЛЕКТРОКАТАЛИТИЧКА СВОЈСТВА Pt–Bi ЕЛЕКТРОДА У ОКСИДАЦИЈИ МРАВЉЕ КИСЕЛИНЕ

ЈЕЛЕНА Д. ЛОВИЋ, ДУШАН В. ТРИПКОВИЋ, КСЕНИЈА Ђ. ПОПОВИЋ, ВЛАДИСЛАВА М. ЈОВАНОВИЋ и АМАЛИЈА В. ТРИПКОВИЋ

ИХТМ – Центар за електрохемију, Универзитет у Београду, Његошева 12, п. пр. 473, 11000 Београд

Оксидација мравље киселине испитивана је на два типа Pt–Bi катализатора: Pt_2Bi електроди и на поликристалној Pt електроди модификованој иреверзибилно адсорбованим Bi (Pt/Bi_{irr}). Активности су упређене са резултатима добијеним на чистој поликристалној Pt електроди. Циљ је био да се објасни разлика у деловању иреверзибилно адсорбованог Bi (Bi_{irr}) и Bi у легираном стању. Показано је да су оба биметална катализатора активнија од поликристалне Pt, почетак реакције је померен ка негативнијим вредностима и у поређењу са чистом Pt при стационарним условима добијене су до два реда величине веће густине струје. Разлог за велику активност и стабилност Pt_2Bi електроде у оксидацији мравље киселине је одигравање реакције по главном реакционом путу (дехидроганација мравље киселине), што је изазвано ефектом трећег тела и електронским ефектом, као и спречавање излуживања Bi из елецтроде. С друге стране, иако Pt/Bi_{irr} показује значајну почетну активност у односу на Pt, ова електрода није стабилна током реакције оксидације HCOOH због континуалног растварања Bi са површине електроде, као и тровања површине изазваног током реакције по индиректном, дехидратационом путу. Поређењем резултата добијених на ове две Pt–Bi електроде може се објаснити улога ефекта трећег тела и електронског ефекта у оксидацији HCOOH. Наиме, електронски ефекат, који постоји само код легуре, доприноси ранијем почетку реакције, док је максимална струја одређена ефектом трећег тела. Током циклизирања Pt/Bi_{irr} електроде Bi одлази са површине и ефекат трећег тела се губи током времана. Хроноамперометријска мерења указују на предност легуре, односно неопходност легирања Bi са Pt да би се добио корозионо стабилан катализатор.

(Примљено 12. октобра, ревидирано 16. новембра 2012)

REFERENCES

1. R. Parsons, T. Vander Noot, *J. Electroanal. Chem.* **257** (1988) 9
2. A. V. Tripković, J. D. Lović, K. Dj. Popović, *J. Serb. Chem. Soc*. **75** (2010) 1559
3. J. D. Lović, K. Dj. Popović, A. V. Tripković, *J. Serb. Chem. Soc*. **76** (2011) 1523
4. S. Stevanović, D. Tripković, D. Poleti, J. Rogan, A. Tripković, V. M. Jovanović, *J. Serb. Chem. Soc*. **76** (2011) 1673
5. X. Xia, T. Iwasita, *J. Electrochem. Soc*. **140** (1993) 2559
6. X. Wang, J.-M. Hu, I.-M. Hsing, *J. Electroanal. Chem.* **562** (2004) 73
7. A. V. Tripković, K. Đ. Popović, J. D. Lović, *J. Serb. Chem. Soc.* **68** (2003) 849
8. A. Capon, R. Parsons, *J. Electroanal. Chem*. **44** (1973) 1
9. J. M. Feliu, E. Herrero, *Formic acid oxidation*, in *Handbook of Fuel Cells-Fundamentals Technology and Applications*, Vol. 2, W. Vielstich, A. Lamm, H. A. Gasteiger, Eds., Wiley, New York, 2003, Ch. 42, p. 625
10. E. Herrero, A. Fernandez-Vega, J. M. Feliu, A. Aldaz, *J. Electroanal. Chem*. **350** (1993) 73
11. J. Clavilier, A. Fernandez-Vega, J. M. Feliu, A. Aldaz, *J. Electroanal. Chem*. **258** (1989) 89
12. J. Clavilier, A. Fernandez-Vega, J. M. Feliu, A. Aldaz, *J. Electroanal. Chem.* **261** (1989) 113
13. B.-J. Kim, K. Kwon, C. K. Rhee, J. Han, T.-H. Lim, *Electrochim. Acta* **53** (2008) 7744
14. A. Sáez, E. Expósito, J. Solla-Gullón, V. Montiel, A. Aldaz, *Electrochim. Acta* **63** (2012) 105
15. A. Lopez-Cudero, F. J. Vidal-Iglesias, J. Solla-Gullon, E. Herrero, A. Aldaz, J. M. Feliu, *Phys. Chem. Chem. Phys*. **11** (2009) 416
16. J. Clavilier, J. M. Feliu, A. Aldaz, *J. Electroanal. Chem*. **243** (1988) 419
17. J. Kim, C. K. Rhee, *Electrochem. Comm*. **12** (2010) 1731
18. Q.-S. Chen, Z.-Y. Zhou, F. J. Vidal-Iglesias, J. Solla-Gullon, J. M. Feliu, S.-G. Sun, *J. Am. Chem. Soc.* **133** (2011) 12930
19. C. Jung, T. Zhang, B.-J. Kim, J. Kim, C. K. Rhee, T.-H. Lim, *Bull. Korean Chem. Soc.* **31** (2010) 1543
20. D. Volpe, E. Casado-Rivera, L. Alden, C. Lind, K. Hagerdon, C. Downie, C. Korzniewski, F. J. DiSalvo, H. D. Abruna, *J. Electrochem. Soc.* **151** (2004) A971
21. E. Casado-Rivera, D. J. Volpe, L. Alden, C. Lind, C. Downie, T. Vazquez-Alvarez, A. C. D. Angelo, F. J. DiSalvo, H. D. Abruna, *J. Am. Chem. Soc*. **126** (2004) 4043
22. H. Wang, L. Alden, F. J. DiSalvo, H. D. Abruna, *Phys. Chem. Chem. Phys*. **10** (2008) 3739
23. M. Oana, R. Hoffmann, H. D. Abruna, F. J. DiSalvo, *Surf. Sci*. **574** (2005) 1
24. C. Roychowdhury, F. Matsumoto, V. B. Zeldovich, S. C. Warren, P. F. Mutolo, M. J. Ballesteros, U. Wiesner, H. D. Abruna, F. J. DiSalvo, *Chem. Mater*. **18** (2006) 3365
25. Y. Liu, M. A. Lowe, F. J. DiSalvo, H. D. Abruna, *J. Phys. Chem., C* **114** (2010) 14929
26. L. M. Magno, W. Sigle, P. A. van Aken, D. G. Angelescu, C. Stubenrauch, *Chem. Mater*. **22** (2010) 6263
27. X. Yu, P. G. Pickup, *Electrochim. Acta* **56** (2011) 4037
28. Y. Liu, M. A. Lowe, K. D. Finkelstein, D. S. Dale, F. J. DiSalvo, H. D. Abruna, *Chem. Eur. J*. **16** (2010) 13689.
29. X. Ji, K. T. Lee, R. Holden, L. Zhang, J. Zhang, G. A. Botton, M. Couillard, L. F. Nazar, *Nat. Chem*. **2** (2010) 286
30. E. Casado-Rivera, Z. Gal, A. C. D. Angelo, C. Lind, F. J. DiSalvo, H. D. Abruna, *ChemPhysChem* **4** (2003) 193
31. N. de-los-Santos-Alvarez, L. R. Alden, E. Rus, H. Wang, F. J. DiSalvo, H. D. Abruna, *J. Electroanal. Chem.* **626** (2009) 14

32. I. Pašti, S. Mentus, *Phys. Chem. Chem. Phys*. **11** (2009) 6225
33. D. R. Blasini, D. Rochefort, E. Fachini, L. R. Alden, F. J. DiSalvo, C. R. Cabrera, H. D. Abruna, *Surf. Sci*. **600** (2006) 2670
34. A. V. Tripković, K. Dj. Popović, R. M. Stevanović, R. Socha, A. Kowal, *Electrochem. Comm.* **8** (2006) 1492
35. J. D. Lović, M. D. Obradović, D. V. Tripković, K. Dj. Popović, V. M. Jovanović, S. Lj. Gojković, A. V. Tripković, *Electrocatalysis* **3** (2012) 346
36. R. Gomez, J. M. Feliu, A. Aldaz, *Electrochim. Acta* **42** (1997) 1675
37. T. J. Schmidt, B. N. Grgur, R. J. Behm, N. M. Markovic, P. N. Ross, Jr., *Phys. Chem. Chem. Phys.* **2** (2000) 4379
38. B. E. Hayden, A. J. Murray, R. Parsons, D. J. Pegg, *J. Electroanal. Chem*. **409** (1996) 51
39. L.-L. Wang, D. D. Johnson, *J. Phys. Chem., C* **112** (2008) 8266
40. N. Kapur, B. Shan, J. Hyun, L. Wang, S. Yang, J. B. Nicholas, K. Cho, *Mol. Simul.* **37** (2011) 648
41. A. Miki, S. Ye, M. Osawa, *Chem. Commun*. (2002) 1500
42. G. Samjeske, A. Miki, S. Ye, M. Osawa, *J. Phys. Chem., B* **110** (2006) 16559
43. Y. Liu, M. A. Lowe, F. J. DiSalvo, H. D. Abruna, *J. Phys. Chem., C* **114** (2010) 14929
44. S. Daniele, C. Bragato, D. Battistel, *Electroanalysis* **24** (2012) 759
45. J. D. Lović, A. V. Tripković, S. Lj. Gojković, K. Dj. Popović, D. V. Tripković, P. Olszewski, A. Kowal, *J. Electroanal. Chem.* **581** (2005) 294.

Journal of the Serbian Chemical Society
JSCS-info@shd.org.rs • www.shd.org.rs/JSCS
J. Serb. Chem. Soc. 78 (8) 1203–1212 (2013)
JSCS–4491
UDC 54–32+53.085.4:544.6.076.32–546.11'98:543.554
Original scientific paper

The application of hydrogen–palladium electrode for potentiometric acid–base determinations in tetrahydrofuran

ANJA B. JOKIĆ[1], RADMILA M. DŽUDOVIĆ[2#], LJILJANA N. JAKŠIĆ[3#] and SNEŽANA D. NIKOLIĆ-MANDIĆ[4*#]

[1]*Faculty of Science, Kosovska Mitrovica, University of Priština, Lole Ribara 29, Kosovska Mitrovica, Serbia,* [2]*Faculty of Science, University of Kragujevac, R. Domanovića 12, Kragujevac, Serbia,* [3]*University of Belgrade, Faculty of Mining and Geology, Đušina 7, Belgrade, Serbia and* [4]*University of Belgrade, Faculty of Chemistry, Studentski trg 16, Belgrade, Serbia*

(Received 27 September 2012, revised 9 February 2013)

Abstract: The application of the hydrogen–palladium electrode (H_2/Pd) as an indicator electrode for the determination of the relative acidity scale (E_s, mV) of tetrahydrofuran (THF) and potentiometric titrations of acids in this solvent were investigated. The relative acidity scale of THF was determined from the difference between the half-neutralization potentials of perchloric acid and tetrabutylammonium hydroxide (TBAH), which were measured using both H_2/Pd–SCE and glass–SCE electrode pairs. The experimentally obtained value of the E_s scale of THF with the H_2/Pd–SCE electrode pair was 1155 mV, while that obtained with the glass–SCE electrode pair was 880 mV. By using an H_2/Pd indicator electrode, the individual acids (benzoic acid, palmitic acid, maleic acid, acetyl acetone and α-naphthol) and two component acid mixtures (benzoic acid + α-naphthol, palmitic acid + α-naphthol, maleic acid + α-naphthol and maleic acid + phthalic acid) were titrated with a standard solution of TBAH. In addition, sodium methylate and potassium hydroxide proved to be very suitable titrating agents for the titrations of the individual acids and the acids in mixtures, respectively. The relative error of the determination of acids in the mixtures was less than 3 %. The results are in agreement with those obtained using a conventional glass electrode. The advantages of the H_2/Pd electrode over a glass electrode in the potentiometric acid–base determinations in THF lie in the following: this electrode gives a wider relative acidity scale for THF, larger potential jumps at the titration end-point and relatively fast response times. Furthermore, it is very durable, simple to prepare and can be used in the titrations of small volumes.

Keywords: relative acidity scale; hydrogen–palladium electrode; potentiometry; acid mixtures; tetrahydrofuran.

* Corresponding author. E-mail: snezananm@chem.bg.ac.rs
# Serbian Chemical Society member.
doi: 10.2298/JSC120927018J

INTRODUCTION

Tetrahydrofuran (THF) is a dipolar aprotic protophilic solvent with a low relative permittivity (ε_r = 7.39 at 298.15 K), a dipole moment of 5.4×10^{-30} C m and a large acidity scale (34.7 pK_S). It is a colorless, water-miscible organic liquid with low viscosity (0.48 cP at 25 °C) and a wide liquid range (165 to 339 K).[1] THF is an excellent solvent for dissolving a wide variety of substances, such as ionic species, organometallic compounds and many polymeric materials.[2–4] The solvatochromic properties of THF (hydrogen-bond donor capacity, α = 0, polarity, π = 0.58, and low hydrogen-bond acceptor capacity, β = 0.55), and autodissociation constant of the solvent determine the high resolution of acids strength in THF. Based on the dissociation constants of series of acids and their tetrabutylammonium salts in THF, it was shown that the resolution of acid strengths in THF is higher than that in water and methanol and similar to those in acetone, dimethyl sulfoxide and 4-methylpentan-2-one.[5–9]

From analytical point of view, THF is a suitable medium for the titrations of substances exhibiting acidic characteristics in this solvent. Numerous organic compounds, such alcohols, acetophenones, esters, anilides, carbamates and lactams, can be titrated as very weak acids.[10] The determination of carbamates, lactams and ureas is important since these compounds are often the active ingredients in many pesticides and pharmaceutical chemical. Champion and Bush[4] determined coulometrically the weak acrylic acid content incorporated in a copolymer with electrically generated tetrabutylammonium hydroxide (TBAH) in THF. Meng-Liang and Chang-Yi[11] reported the potentiometric micro-titration of *p*-phthalic acid and Barron and Barbosa[6] performed differential potentiometric titrations of acids in THF medium.

A glass electrode in most frequently used indicator electrode for potentiometric acid–base titrations, both in aqueous and non-aqueous media. However, the potential response of a glass electrode in non-aqueous solutions is often slow; in same cases, one hour is required for the establishment of the equilibrium potential. In addition, the electrode has a limited useful life when employed in non-aqueous titrations because the solvents dehydrate the glass membrane, thereby reducing its response to hydrogen ions. These properties of glass electrodes have led to intensive research of new indicator electrodes for potentiometric acid–base titrations in non-aqueous media. As alternatives to a glass electrode, metal and metalloid indicator electrodes, metallic electrodes coated with layer of hydroxide or oxide and some natural minerals have been employed.[12–21]

Mihajlović *et al.*[22–28] proposed hydrogen–palladium (H_2/Pd) and deuterium–palladium (D_2/Pd) electrodes as new indicator electrodes for the potentiometric titrations acids and bases in ketones, nitriles, cyclic esters and alcohols. Similar behavior of the H_2/Pd and D_2/Pd indicator electrodes was observed in titrations acids and bases in some non-aqueous solvents (propylene carbonate,

ketones and nitriles).[23–25] Taking into account these facts, as well the simplicity of preparing an H_2/Pd electrode (does not require deuterium oxide) and the good properties of tetrahydrofuran as a solvent for the titrations of acids, it was thought that an investigation of the possibility of applying a H_2/Pd electrode as indicator electrode for determination of relative acidity scale of tetrahydrofuran and potentiometric titrations acids in this solvent could be useful.

EXPERIMENTAL

Reagents

All employed chemicals were of analytical grade from Merck or Fluka. Tetrahydrofuran (THF, Fluka) with water content 0.03 % was used as the solvent without further purification. The acids used were benzoic acid, acetyl acetone, α-naphthol, palmitic acid, maleic acid, phthalic acid and perchloric acid. Due to the instability of perchloric acid in THF, their solution was prepared in dioxane. Solutions of acids were used as primary standard (benzoic acid) or their concentrations were previously determined by titrating them against a standard solution of TBAH using visual (Thymol Blue indicator) or potentiometric end-point detection by means a glass-modified saturated calomel electrode (SCE) couple. Methanolic potassium hydroxide solutions were prepared according to Kreshkov.[29] TBAH (0.10 M) in a 2-propanol––methanol (10:1, v/v) was potentiometrically standardized against benzoic acid using a glass––SCE electrode pair. A Thymol Blue solution (0.1 %) in THF was used as an indicator.

Apparatus

The employed apparatus was described previously.[27] The potential changes during the titrations were followed with a Digital 870 pH meter, Dresden, Germany.

Electrodes

The hydrogen–palladium electrode was a spiral of 0.5 mm diameter palladium wire (99.9% pure; Johnson Matthey Metals, London) with surface area of 30 mm^2 saturated with hydrogen obtained by electrolysis of dilute sulfuric acid at a current 2 mA. The potential of the H_2/Pd electrode prepared in this manner was measured as a function of time (Fig. 1).

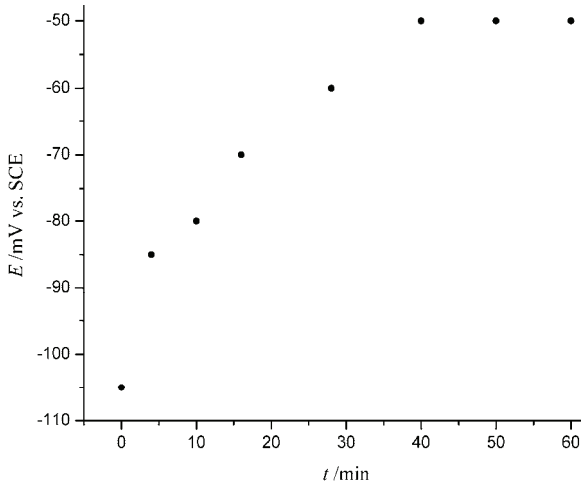

Fig. 1. Dependence of the H_2/Pd electrode potential on time in THF medium.

As can be seen, if the H_2/Pd electrode was used 40 min after saturation with hydrogen, a stable potential was established within a few minutes. The response time of the indicator H_2/Pd electrode was determined by measuring the time that elapsed to reach a stable potential value after the H_2/Pd electrode and the reference electrode were immersed in solutions from highly acidic (0.01 mol L^{-1} perchloric acid) to highly basic (0.01 mol L^{-1} TBAH). The H_2/Pd electrode showed a relatively fast response time in the investigated solvent (less than 15 s). If the electrode was used frequently and for a long time, it was necessary to refill the H_2/Pd electrode with hydrogen by electrolysis.

The glass electrode, type G-202C (Radiometer, Copenhagen, Denmark) was conditioned in THF before use. The electrode was stored in water when not in use and soaked for 30 min in THF before potentiometric measurements.

A modified saturated calomel electrode (modified SCE), type K201 (Radiometer, Copenhagen, Denmark) with potassium chloride in methanol was used as the reference electrode.

Procedures

Determination of the relative acidity scale. The relative acidity scale of THF was determined from the difference in the half-neutralization potentials of perchloric acid and TBAH.[30] Two electrode pairs, glass–SCE and H_2/Pd–SCE, were used for the measurement of the half-neutralization potentials of the acid and base.

Determination of the half-neutralization potential of perchloric acid. THF (12.0 mL) was placed in the titration vessel and a measured volume of a standard solution of $HClO_4$ (1.00 mL) was added. The electrode pair, H_2/Pd–SCE or glass–SCE, was immersed in the investigated solution and connected to a pH-meter. The solution of acid was then titrated to half neutralization with the standard solution of TBAH (0.1 M). The potential of half-neutralization of perchloric acid was read 15 min after thermostating (25±1 °C).

The determination of the half-neutralization potential of TBAH. THF (12.0 mL) was placed in the titration vessel and a measured volume of TBAH (1.00 mL) was added. The electrode system (H_2/Pd–SCE or glass–SCE) was immersed in the solution and base was than titrated to half neutralization with a standard solution of perchloric acid (0.1 M). The half-neutralization potential of the base was also measured after thermostating of the solution.

Potentiometric titrations. THF (12.0 mL) was placed in the titration vessel and the required volume of the investigated acid and two drops of the indicator solution were added. The indicator electrode, either H_2/Pd or glass electrode and a SCE as the reference one were immersed in the investigated solution and connected to a pH-meter. The solution was then titrated with standard solution of TBAH (potassium hydroxide or sodium methylate) and the potential was read after each addition of titrant. The test solution was stirred magnetically under a continuous stream of dry nitrogen.

RESULTS AND DISCUSSION

The choice of the optimal conditions for potentiometric acid–base titrations in a non-aqueous medium can be made based on the relative acidity scale of the solvent. The relative acidity scale of a solvent, E_S, has no physical meaning, as does the acidity scale pK_S, which is calculated from the autoprotolysis constant of the solvent. The value of the E_S scale is calculated from the difference between the half-neutralization potentials of a strong acid and a strong base in the given solvent. The E_S scale of a solvent defines the approximate potential ranges that could be used for potentiometric acid–base titrations under the determined expe-

rimental conditions (electrode pair, titrant, *etc.*). With increasing range of the E_s scale, the possibility of the titration of weak acids (bases) and differentiating titrations of mixtures acids (bases) in the solvent is increased.

The relative acidity scale of tetrahydrofuran (THF) was determined potentiometrically from the difference between the half-neutralization potentials of solutions of perchloric acid and TBAH of the same concentration.

$$E_s = E_{1/2}(\mathrm{HClO_4}) - E_{1/2}(\mathrm{TBAH}) \quad (1)$$

The half-neutralization potentials of perchloric acid and TBAH were measured using a glass–SCE and H_2/Pd–SCE electrode pair. When a H_2/Pd–SCE electrode pair was used for measuring the half-neutralization potentials, a wider acidity scale of the solvent was obtained than when a glass–SCE electrode couple was applied (Table I).

TABLE I. Determination (n = 6) of the relative acidity scale of THF. The potentials were measured using a glass–SCE and a H_2/Pd–SCE electrode pair at 25.0±0.1 °C

Electrode pair	$E_{1/2(\mathrm{HClO_4})}$ / mV	$E_{1/2(\mathrm{TBAH})}$ / mV	E_s / mV
Glass–SCE	465±5	–415±0	880±5
(H_2/Pd)–SCE	455±5	–700±5	1155±7

Water lowered the range of the relative acidity scales. The addition of small amounts of water to the titrated solution had a large effect on the E_s scale of THF. Thus, after the addition of 1 % water, the relative acidity scale of THF was narrowed by 300 mV.

Based on the obtained experimental data for the relative acidity scale of the solvent, it is to be expected that the higher potential jumps at the end-point would be obtained if a H_2/Pd indicator electrode were used for the detection end-point in potentiometric titrations of acids in THF medium.

Potentiometric titrations of acids

The behavior of the H_2/Pd electrode as an indicator electrode in THF was investigated by potentiometric titration of acids of different strengths and various structures with standard solutions of TBAH and sodium methylate. The titrations of acids with TBAH can be represented by the following equations:

$$\mathrm{C_4H_8O + HA \rightleftarrows C_4H_8OH^+ + A^-} \quad (2)$$

$$\mathrm{(C_4H_9)_4NOH \rightleftarrows (C_4H_9)_4N^+ + OH^-} \quad (3)$$

$$\mathrm{C_4H_8OH^+ + OH^- \rightleftarrows C_4H_8O + H_2O} \quad (4)$$

$$\mathrm{(C_4H_9)_4N^+ + A^- \rightleftarrows (C_4H_9)_4NA} \quad (5)$$

Summary:

$$\mathrm{HA + (C_4H_9)_4NOH \rightleftarrows (C_4H_9)_4NA + H_2O} \quad (6)$$

and with sodium methylate by:

$$HA + C_4H_8O \rightleftarrows C_4H_8OH^+ + A^- \quad (7)$$

$$CH_3ONa \rightleftarrows CH_3O^- + Na^+ \quad (8)$$

$$C_4H_8OH^+ + CH_3O^- \rightleftarrows C_4H_8O + CH_3OH \quad (9)$$

$$Na^+ + A^- \rightleftarrows NaA \quad (10)$$

Summary:

$$HA + CH_3ONa \rightleftarrows CH_3OH + NaA \quad (11)$$

As can be seen from the above equations, in the titration of an acid with TBAH, water, which has negative effect on the titration of weak acids in THF, is produced. In the titrations acids with a standard solution of sodium methylate, the presence of water in the titration solution is avoided.

The titration curves of the very weak acid *α*-naphthol (pK_a in water is 9.30) in THF with sodium methylate and TBAH as titrants by applying the electrode couples H_2/Pd–SCE and glass–SCE are shown in Fig. 2. When a H_2/Pd electrode was used for the titration end-point (TEP) detection, the potential jumps with sodium methylate and TBAH as titrants amounted to 125 and 105 mV per 0.30 mL, respectively. In addition, it can be seen that the potential jumps were smaller when a glass electrode was applied (35 mV per 0.30 mL with sodium methylate and 75 mV per 0.30 mL with TBAH as titrants). The more significant decrease of the potential jump in the titration with sodium methylate as the titrant can be explained by the effect of the sodium ions on the glass electrode.

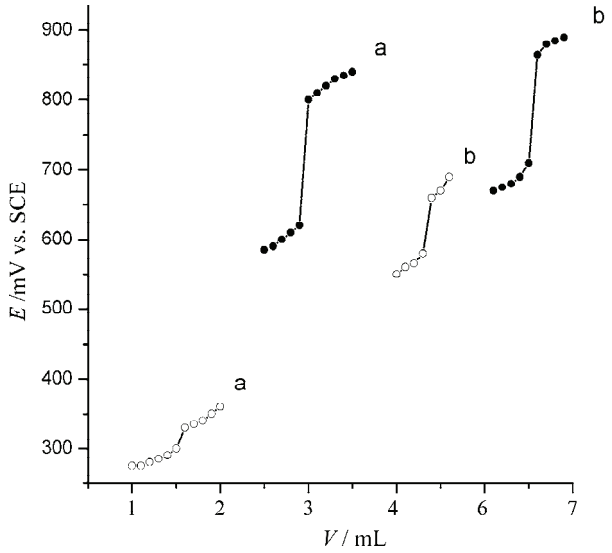

Fig. 2. The effect of the indicator electrode on the shape of the end-point in the potentiometric titration of *α*-naphthol in THF. Electrode: empty circles – glass electrode; full circles – H_2/Pd electrode. Titrant: sodium methylate (a); TBAH (b).

The experimental results obtained in the titrations of the investigated acids are summarized in Table II. In all titrations, the potential jumps with a H_2/Pd electrode were larger than those obtained with a glass electrode, which is in accordance with the experimentally determined range of the E_s scale of THF. The potentials during the titration and at the equivalence point were rapidly established (within a couple of minutes), and the change of the potential at the TEP coincided with that of the applied indicator color.

TABLE II. Potentiometric titration of acids in THF by application of the H_2/Pd–SCE and glass–SCE electrode pairs

Titrated acid	Taken mg	Titration agent	Found (n = 5), %		Potential jump, mV per 0.30 mL	
			H_2/Pd–SCE	Glass–SCE	H_2Pd–SCE	Glass–SCE
Benzoic acid	12.21	Na methylate	100.00±0.45	99.64±0.35	383	25
		TBAH	100.01±0.08	100.02±0.02	405	390
Acetyl acetone	7.84	Na methylate	100.71±0.20	100.63±0.37	210	86
		TBAH	99.44±0.29	99.77±0.22	150	130
α-Naphthol	12.03	Na methylate	103.11±0.25	103.69±0.15	125	35
		TBAH	100.40±0.40	100.50±0.19	105	75
Palmitic acid	22.14	Na methylate	99.77±0.10	99.93±0.64	305	50
		TBAH	97.78±0.04	97.21±0.26	120	107

Water lowered the potential jumps at the equivalence point in the applied solvent. A more significant decrease of the potential jump was obtained when the content of water was increased by 1 %. The impact of water on the decrease of the potential jumps was much stronger in the titration of very weak acids.

The results obtained in the determination of the investigated acids (Table II) using a H_2/Pd indicator electrode deviated on average by ±0.02–0.50 % in relation to those obtained with a glass electrode.

Differential titrations of acids

The differential titration of acids in mixture is possible if the difference between in the pK_a values of the acids in the employed solvent is sufficiently large. In cases where the pK_a values have not been reported, the choice can be made by comparing the titration curves of individual acids present in the mixture.

For differential titrations of acids in mixture in non-aqueous solvents, TBAH and alcoholic potassium hydroxide were recommended as suitable titrants.[29] Potassium hydroxide is advantageous over the other titration agents in the titrations of dicarboxylic acids. In a titration with alcoholic potassium hydroxide, the carboxylic groups of the dicarboxylic acid are neutralized separately due to the different solubility of the corresponding salts formed in the course of the titration. Therefore, the solvolysis of the potassium salts is considerably decreased and the sharpness of the end-point enhanced.

The potentiometric titrations of mixed acids in THF media were performed with methanolic potassium hydroxide as titrant using H_2/Pd indicator electrode. The potentiometric titrations curves for the acid mixtures palmitic acid + α-naphthol, maleic acid + α-naphthol, maleic acid + phthalic acid and benzoic acid + + α-naphthol are shown in Fig. 3.

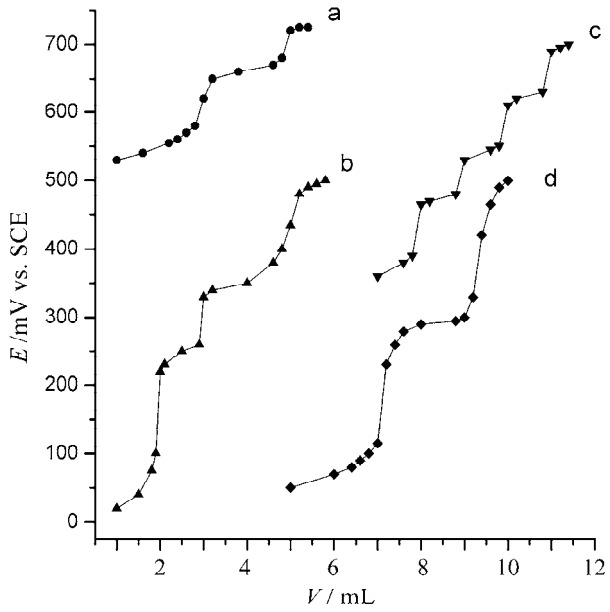

Fig. 3. Potentiometric titration curves acid mixtures in THF using an H_2/Pd electrode: a) palmitic acid + α-naphthol; b) maleic acid + α-naphthol; c) maleic acid + phthalic acid; d) benzoic acid + α-naphthol. Titrant: KOH (a, b and c); TBAH (d).

The titration curve of the mixture palmitic acid + α-naphthol has two potential jumps. The first jump corresponds to the neutralization of the palmitic acid and the second to the neutralization of α-naphthol (Fig. 3, curve a). The titration curve of the mixture dicarboxylic maleic acid and α-naphthol shows three potential jumps (Fig. 3, curve b); the first and second correspond to the neutralizations of the two carboxylic groups of maleic acid whereas the third corresponds to the neutralization of α-naphthol. The potentiometric titration curve for a mixture of maleic acid and phthalic acid (Fig. 3, curve c) proves that the successive titration of a two dicarboxylic acids in a mixture is possible in this solvent.

The results of the potentiometric titrations of two component mixtures of acids under optimum experimental conditions are listed in Table III. The relative error of these determinations with respect to the individual determinations was less than 3 %.

CONCLUSIONS

Based on the presented results, it may be concluded that a H_2/Pd indicator electrode is very suitable for the potentiometric titrations of acids both indi-

vidually and as mixtures in tetrahydrofuran medium. In accordance with the range and position of the relative acidity scale of THF determined using an H_2/Pd–SCE electrode pair, the proposed electrode gives larger potential jumps at the titration end-point than a glass electrode. The advantages of the hydrogen–palladium electrode are rapid attainment of stable potential values, fast response, reproducibility and easy preparation.

TABLE III. The results of the potentiometric titration of acid mixtures in tetrahydrofuran using an H_2/Pd indicator electrode

Acid mixture	Titrant	Taken mg	Found (n = 5) %	Potential jump, mV per 0.30 mL
Benzoic acid + α-naphthol	TBAH	12.8	100.33±0.10	155
		13.41	99.43±0.32	80
Palmitic acid + α-naphthol	KOH	26.67	98.65±0.13	75
		13.84	100.62±0.02	30
Maleic acid + α-naphthol	KOH	11.03	100.00±0.03	125
		13.84	103.11±0.03	40
Maleic acid + phthalic acid	KOH	11.03	100.00±0.10	60
		15.70	102.48±1.20	70

Acknowledgement. The authors are grateful to the Ministry of Education, Science and Technological Development of the Republic of Serbia for financial support (Project No. 172051).

ИЗВОД

ПРИМЕНА ВОДОНИК/ПАЛАДИЈУМОВЕ ЕЛЕКТРОДЕ ЗА ПОТЕНЦИОМЕТРИЈСКА КИСЕЛИНСКО–БАЗНА ОДРЕЂИВАЊА У ТЕТРАХИДРОФУРАНУ

АЊА Б. ЈОКИЋ[1], РАДМИЛА М. ЦУДОВИЋ[2], ЉИЉАНА Н. ЈАКШИЋ[3] и СНЕЖАНА Д. НИКОЛИЋ-МАНДИЋ[4]

[1]*Природно–математички факултет, Косовска Митровица, Универзитет у Приштини, Лоле Рибара 29, Косовска Митровица,* [2]*Природно–математички факултет, Универзитет у Крагујевцу, Радоја Домановића 12, 34000 Крагујевац,* [3]*Универзитет у Београду, Рударско–геолошки факултет, Ђушина 7, 11000 Београд, и* [4]*Хемијски факултет, Универзитет у Београду, Студентски трг 16, 11000 Београд*

Испитана је примена водоник–паладијумове индикаторске електроде (H_2/Pd) за одређивање релативне скале киселости тетрахидрофурана (THF) и потенциометријске титрације киселина у овом растварачу. Релативна киселинска скала (E_s, mV) је одређена из полунеутрализационих потенцијала перхлорне киселине и тетрабутиламонијум-хидроксида (TBAH) применом електродних парова H_2/Pd–ЗКЕ и стаклена електрода–ЗКЕ. Експериментално добијена вредност E_s скале THF употребом H_2/Pd–ЗКЕ електродног пара износи 1155 mV, а употребом електродног пара стаклена електрода–ЗКЕ 880 mV. H_2/Pd индикаторска електрода је употребљена за потенциометријске титрације киселина (бензоева киселина, палмитинска киселина, малеинска киселина, ацетил-ацетон и α-нафтол) и смеше киселина (бензоева киселина + α-нафтол, палмитинска киселина + α-нафтол, малеинска киселина + α-нафтол и малеинска + фтална киселина) стандардним раствором TBAH. Поред TBAH, натријум-метилат и калијум-хидроксид су се показали веома погодним титрантима за титрацију појединачних киселина и смеше киселина. Релативна грешка одређивања киселина у смеши је мања од 3 %. Резултати одре-

ђивања су у сагласности са оним добијеним применом конвенционалне стаклене електроде. Предности водоник–паладијумове електроде у потенциометријским киселинско–базним одређивањима у односу на стаклену електроду су у следећем: ова електрода даје већи опсег релативне скале киселости THF, веће скокове потенцијала на завршној тачки титрације и брз одговор. Поред тога, електрода има мали отпор, једноставно се припрема и може бити коришћена за титрацију раствора малих запремина.

(Примљено 27. септембра 2012, ревидирано 9. фебруара 2013)

REFERENCES

1. I. M. Kolthoff, *Anal. Chem*. **46** (1974) 1992
2. S. Mah, D. You, H. Cho, S. Choi, J.-H. Shin, *J. Appl. Polym. Sci.* **69** (1998) 611
3. S. Hanesian, N. Moitessier, S. Wilmouth, *Tetrahedron* **56** (2000) 7643
4. C. E. Champion, D. G. Bush, *Anal. Chem.* **45** (1973) 640
5. J. Barbosa, D. Barron, E. Bosch, M. Roses, *Anal. Chim. Acta* **265** (1992) 157
6. D. Barron, J. Barbosa, *Anal. Chim. Acta* **403** (2000) 339
7. J. Barbosa, D. Barron, E. Bosch, M. Roses, *Anal. Chim. Acta* **264** (1992) 229
8. G. Garrido, E. Koort, C. Rafols, E. Bosch, T. Radima, I. Leito, M. Roses, *J. Org. Chem.* **71** (2006) 9062
9. G. Garrido, M. Roses, C. Rafols, E. Bosch, *J. Solution Chem.* **37** (2008) 689
10. D. D. Clyde, *Anal. Chem.* **52** (1980) 1308
11. W. Meng-Liang, W. Chang-Yi, *Anal. Chim. Acta* **198** (1987) 325
12. C. J. Lintner, R. F. Schleif, T. Higuchi, *Anal. Chem.* **22** (1950) 534
13. E. J. Greenhow, B. F. Al Mudarris, *Talanta* **22** (1975) 417
14. K. Izutsu, T. Nakamura, T. Arai, M. Ohmaki, *Electroanalysis* **7** (1995) 884
15. K. Izutsu, M. Ohmaki, *Talanta* **43** (1996) 643
16. K. Izutsu, H. Yamamoto, *Anal. Sci.* **12** (1996) 905
17. M. Antonijević, B. Vukanović, R. Mihajlović, *Talanta* **39** (1992) 809
18. Lj. V. Mihajlović, R. P. Mihajlović, M. M. Antonijević, B. V. Vukanović, *Talanta* **64** (2004) 879
19. Lj. Mihajlović, S. Nikolić-Mandić, B. Vukanović, R. Mihajlović, *Anal. Sci.* **25** (2009) 437
20. Lj. Mihajlović, S. Nikolić-Mandić, B. Vukanović, R. Mihajlović, *J. Solid State Electrochem.* **13** (2009) 895
21. R. P. Mihajlović, Z. D. Stanić, *J. Solid State Electrochem.* **9** (2005) 558
22. V. J. Vajgand, R. P. Mihajlović, R. M. Džudović, Lj. N. Jakšić, *Anal. Chim. Acta* **202** (1987) 231
23. R. Mihajlović, V. Vajgand, R. Džudović, *Talanta* **38** (1991) 673
24. R. P. Mihajlović, Lj. N. Jakšić, R. M. Džudović, *J. Serb. Chem. Soc.* **61** (1996) 689
25. R. Mihajlović, Z. Simić, Lj. Mihajlović, A. Jokić, M. Vukašinović, N. Rakićević, *Anal. Chim. Acta* **318** (1996) 287
26. R. Mihajlović, Z. Stanić, M. Antonijević, *Anal. Chim. Acta* **497** (2003) 143
27. Lj. V. Mihajlović, S. D. Nikolić-Mandić, R. P. Mihajlović, *J. Appl. Electrochem.* **39** (2009) 1917
28. Lj. V. Mihajlović, S. D. Nikolić-Mandić, I. Đ. Pantić, R. P. Mihajlović, *J. Solid State Electrochem.* **14** (2010) 123
29. A. P. Kreshkov, L. N. Bykova, N. A. Kazaryan, *Kislotno-osnovnoe titrovanie v nevodnikh rastvorakh*, Khimiya, Moscow, 1967, p. 37
30. A. P. Kreshkov, *Analiticheskaya khimiya nevodnykh rastvorov*, Khimiya, Moscow, 1982, p. 183.

Journal of the Serbian Chemical Society
JSCS-info@shd.org.rs • www.shd.org.rs/JSCS
J. Serb. Chem. Soc. 78 (8) 1213–1223 (2013) UDC 678.84–261+62–405.8:546.261.000.57+
JSCS–4492 536.421.5:539.24
Original scientific paper

Conversion of a wood flour–SiO_2–phenolic composite to a porous SiC ceramic containing SiC whiskers

ZHONG LI[1]*, TIEJUN SHI[2] and DEXIN TAN[1]

[1]*School of Chemical Engineering, Anhui University of Science & Technology, Huainan 232001, China and* [2]*School of Chemical Engineering, Hefei University of Technology, Hefei 230009, China*

(Received 1 December 2012, revised 5 February 2013)

Abstract: A novel wood flour–SiO_2–phenolic composite was chosen for conversion into a porous SiC ceramic containing SiC whiskers *via* carbothermal reduction. At 1550 °C, the composite was converted into porous a SiC ceramic, with pore diameters of 10–40 μm, consisting of *β*-SiC located at the position of former wood cell walls. *β*-SiC wire-like whiskers of less than 50 nm in diameter and several tens to over 100 μm in length form within the pores. The surface of the resulting ceramic was coated with *β*-SiC necklace-like whiskers with diameters of 1–2 μm.

Keywords: porous silicon carbide; biocarbon; sintering; microstructure.

INTRODUCTION

In the past decades, conversion of wood to porous ceramics with peculiar microstructures has attracted much interest.[1–4] The as-prepared high porosity ceramics, inheriting the microstructure of the wood template, exhibit an interpenetrating pore structure in the micrometer range, high internal surface area and respectable strength, which showed great potential applications in industrial catalysis, separation technology, membranes, sensors, and optical devices.[5–7] Simultaneously, the development of a technology for the synthesis of porous ceramics with wood as the raw material and template was driven by environmental and economical issues, as wood serves as a renewable and relatively inexpensive carbon source.[8,9]

To date, different sorts of ceramic materials have been produced by the conversion of wood. Among them, porous SiC is particularly attractive because of its unique physical, mechanical and chemical properties. For example, Sieber *et al.*[10] used pyrolyzed carbon preforms from different wood structures as templates

* Corresponding author. E-mail: zhongli-91@163.com; stjhfut@163.com
doi: 10.2298/JSC121201014L

for infiltration with gaseous or liquid Si to form SiC- and SiSiC-ceramics. Ota *et al.*[11] produced wood-like SiC by firing oak charcoal infiltrated with tetra-ethyl orthosilicate (TEOS) at 1400 °C under Ar. Esposito *et al.*[12] prepared porous SiC by infiltration of pyrolyzed hard woods with Si at $T > T_{\text{Si melting}}$. Shin *et al.*[13] synthesized SiC ceramics consisting of crystalline SiC nanoparticles as well as some whiskers by carbothermal reduction of mineralized wood with silica at 1400 °C. Herzog *et al.*[14] utilized the carbothermal reduction of the carbonized wood-based material and an infiltrated silica sol to produced porous wood-derived SiC. Qian *et al.*[15] fabricated porous SiC ceramics by carbonizing and sintering phenolic resin–charcoal–SiO_2 composites at elevated temperatures, which were prepared by infiltrating a phenolic resin–SiO_2 sol mixture into pine charcoal *via* the vacuum/pressure impregnation procedure.

Generally, a two-step process is adopted for the conversion. That is, first, bulk wood is pyrolyzed to obtain a porous carbon preform and second, the preform is infiltrated by a Si source-containing reactant and sintered. Although bulk wood offers a highly aligned porosity and interconnected cell network, twist and shrinkage is inevitable during carbonization, and a perfectly infiltrated sample thickness is limited irrespective of the applied infiltration technique.[14,16,17] To overcome these problems, a wood flour–SiO_2–phenolic composite could offer an alternative. For preparing a wood flour–SiO_2–phenolic composite, wood flour is obtained by grinding bulk wood that is subsequently infiltrated by a silicon-precursor and then integrated by a phenolic resin. Finally, a porous SiC ceramics is produced directly from the wood flour–SiO_2–phenolic composite by the carbothermal reduction without a previous carbonization step. Simultaneously, SiC whiskers could be self-assembled within the space of the highly porous ceramics.

EXPERIMENTAL

Material preparation

Fir wood (*Cunninghamia lanceolata*) was ground into flour of size ≈200 μm and dried at 105 °C for 24 h. To extend the pore volume and increase the inclusion of the Si precursor, the flour was treated with NaOH treatment. Thus, the wood flour was washed by 15 wt. % NaOH solution for 2 h at 30 °C and subsequently washed by distilled water until neutral. The silica precursor solution was prepared from tetra-ethyl orthosilicate (TEOS), ethanol (EtOH) and H_2O (molar ratio = 1:4:4).

The wood flour–SiO_2 composite (SiO_2 content of 50 wt. %) was prepared by subjecting 8.0 g of NaOH-treated wood flour with 50 mL of silica precursor solution at 150 °C for 48 h in a self-made sealed infiltration vessel. Then after subsequent extraction, the infiltrated wood flower was dried in air at 130 °C overnight. Then, 10.0 g of wood flour–SiO_2 composite was impregnated with 20.0 g of phenolic resin (solid content of 50 wt. %) for 12 h, dried and precured at 80 °C for 6 h, and further cured at 130–150 °C for 4 h under a molding pressure of 5 MPa to obtain the wood flour–SiO_2–phenolic composite.

The carbothermal reduction was performed in a horizontally tubular furnace. The wood flour–SiO_2–phenolic composite of size 400 mm×200 mm×50 mm (8.0 g, 26 wt. % SiO_2, 26

wt. % wood flour, 48 wt. % phenolic) in an alumina boat was placed in the middle of a furnace. Then the furnace was respectively heated up to 1350, 1450 and 1550 °C at a rate of 2 °C min^{-1} under a dynamic ultra-high purity N_2 atmosphere at a flow rate of ≈ 3 L h^{-1} and held there for 2 h. Finally, the furnace was allowed to cool naturally to room temperature. In order to remove unreacted carbon, the products as-synthesized at 1550 °C were heated in air at 500 °C for 4 h to obtain the purified SiC ceramics coated by a large number of light-green whiskers on the surface.

Characterization

The crystalline structures of the as-synthesized products were investigated by X-ray diffraction analysis using CuKα radiation (XRD, Rigaku, D/MAX-rB, Japan). The possible chemical composition was investigated by Fourier transform infrared spectroscopy (FTIR, PerkinElmer, Spectrum 100, USA) and field-emission scanning electron microscopy (FESEM, FEI Sirion 200, The Netherlands), with energy-dispersive X-ray spectroscopy (EDS). The samples for FESEM were pre-sputtered with a conducting layer of Au for 1 min at 10 kV. High-resolution field emission transmission electron microscopy (HRTEM, JEOL 2010, Japan) at an acceleration voltage of 200 kV was performed to observe the morphology and the crystal lattice of the samples.

RESULTS AND DISCUSSION

XRD Analysis

The XRD patterns of the wood flour–SiO_2–phenolic composite and the as-obtained products after sintering at different temperatures for 2 h are shown in Fig. 1. It can be seen that the broad peak centered at around 2θ = 23.4° is due to the overlap of the characteristic peak of cellulose centered at 2θ = 22.3° and the characteristic peak of amorphous SiO_2 centered at 2θ = 23.8°.[18] After thermal

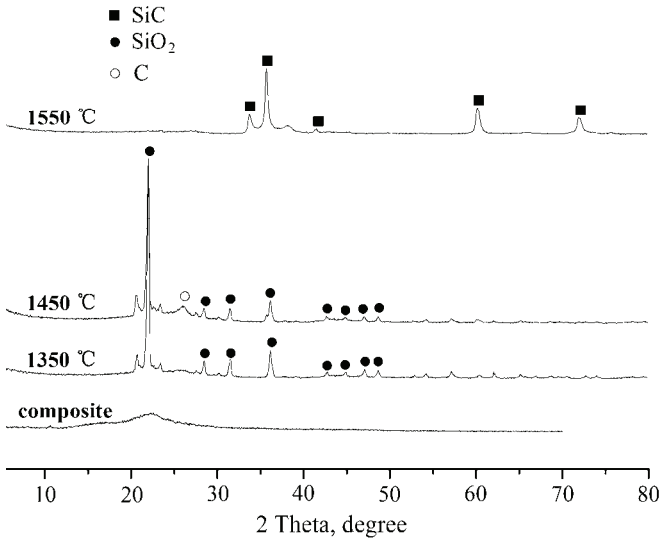

Fig. 1. XRD Patterns of the wood flour–SiO_2–phenolic composite and its corresponding products obtained by sintering at 1350, 1450 and 1550 °C for 2 h.

treatment of wood flour–SiO_2–phenolic composite at 1350 °C, no diffraction peaks due to an SiC phase appeared, but many peaks of cristobalite were observed. Simultaneously, the high baseline suggests that a great deal of amorphous carbon was present.[15] After sintering at 1450 °C, the peak for graphite phases at 2θ = 26.4° was observed together with the peaks of cristobalite. On further increasing the sintering temperature to 1550 °C, the peaks of β-SiC at 2θ 35.3, 60.2 and 71.9° were observed in the diffraction pattern.[19] In contrast, the peaks due to cristobalite had nearly completely disappeared, indicating that the carbothermal reduction had occurred to form SiC.

FTIR Analysis

FTIR Spectra of the wood flour–SiO_2–phenolic composite and its corresponding products obtained at different sintering temperatures for 2 h are shown in Fig. 2. The absorption peak at 3420 cm^{-1} in the FTIR spectrum of wood flour––SiO_2–phenolic composite is attributed to stretching vibrations of OH bonds in the wood flour and the Si–OH bond in SiO_2. The absorption bands at 2928 and 1636 cm^{-1} are attributed to the C–H stretching and C=C bending vibrations in flour, respectively. The absorption band of stretching vibrations of C–O groups in the wood flour is at 1050 cm^{-1}. The peaks at 1090, 790 and 460 cm^{-1} are ascribed to the antisymmetric and symmetric stretching vibrations of Si–O–Si bond.[20] When the composite was sintered at 1350 °C, the above-mentioned peaks for wood significantly decreased or disappeared while the peaks ascribed to the Si–O–Si bond remained, suggesting that the wood was pyrolyzed to carbon, and condensation reaction in SiO_2 was completed after sintering. After

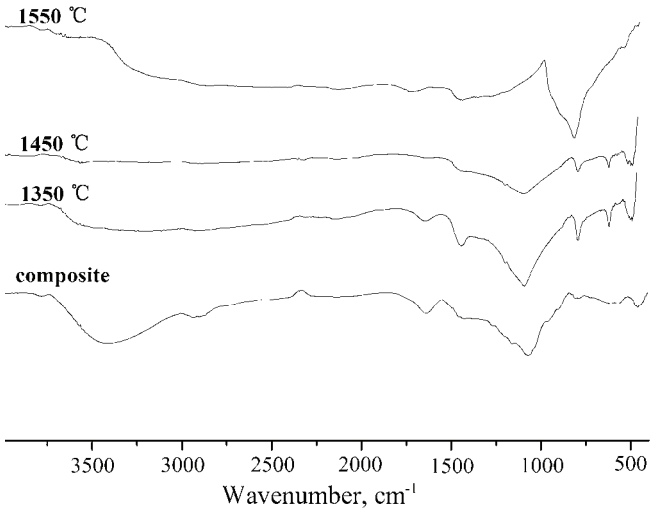

Fig. 2. FTIR Spectra of wood flour–SiO_2–phenolic composite and its corresponding products obtained by sintering at 1350, 1450 and 1550 °C for 2 h.

sintering at 1450 °C, no new absorption peak appeared, indicating that carbothermal reduction still had not occurred. On further increasing the sintering temperature to 1550 °C, the peaks ascribed to Si–O bond disappeared and a new peak appeared at 820 cm^{-1}, which is ascribed to the fundamental stretching vibrations of Si–C, suggesting that carbothermal reduction had occurred.[21,22]

FESEM Analysis

FESEM Images of the NaOH-treated wood flour and the wood flour–SiO_2 composites are presented in Fig. 3. The fir wood, which is a softwood, is composed of unique cross-sectional constructed tracheid cells with bordered pits along their walls, which are channels to connect the different tracheid cells and enhance their connectivity. NaOH treatment can clean the surface of the flour, and enlarge the size of the pit pores. The highly uniform parallel tubular cellular structures and ordered arrays of bordered pits can be clearly observed in Fig. 3a. The pit pores at the tracheid walls are 10–15 μm in diameter. Such hierarchical structures can be maintained upon heating at an inert atmosphere due to the ordered semicrystalline cellulose networks. A wood flour–SiO_2 composite was formed on infiltration of the SiO_2 precursor solution into the wood flour (Fig. 3b). It can be seen in Fig. 3b that the SiO_2 covers the surface of flour and fills almost all the pores of the tracheids and pits, suggesting that the SiO_2 precursor solution penetrated the cell wall structures and condensed around the cellular tissues. As shown in Fig. 3c, the wood flour–SiO_2–phenolic composite is composed of a uniformly continuous matrix of phenolic resin and embedded wood flour–SiO_2 composites, and the fine SiO_2 fibers or rods appear in the tubular pores of the wood flour.

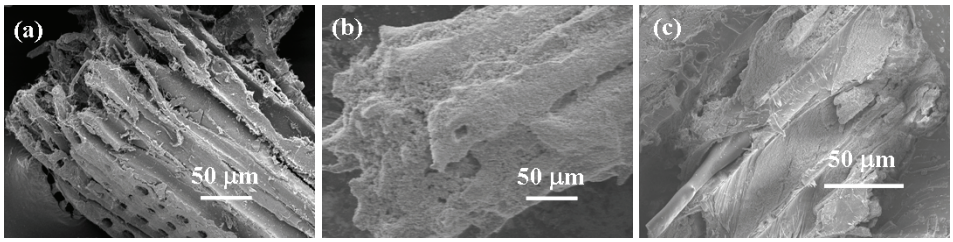

Fig. 3. FESEM Micrographs of a) NaOH treated wood flour, b) wood flour–SiO_2 composite and c) wood flour–SiO_2–phenolic composite.

The FESEM images of the products obtained at different sintering temperatures are presented in Fig. 4. When the composite was sintered at 1350 °C, glassy carbon, which has smooth and glassy fracture surface from the carbonization of phenol resin, was formed in a continuous phase and the wood flour carbon, which maintained the texture and shape of the wood flour, are separated and surrounded by the glassy carbon (Fig. 4a). It can be seen that the wood carbon

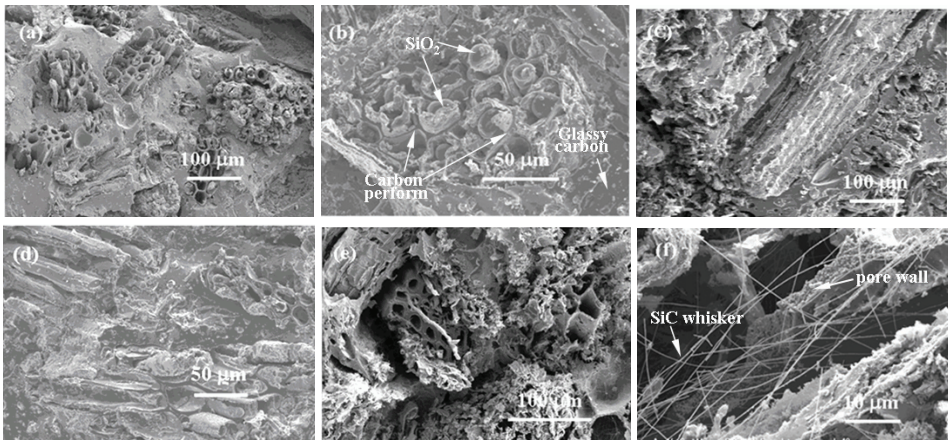

Fig. 4. FESEM Images of the products obtained by sintering the wood flour–SiO_2–phenolic composite at 1350 (a and b), 1450 (c and d) and 1550 °C (e and f) for 2 h.

pores are completely and uniformly filled with SiO_2 (Fig. 4b). By comparing Figs. 4a and 4c, it is evident that they show the same morphological characteristics, suggesting that the carbothermal reduction had still not occurred at 1450 °C, which is in agreement with the results of XRD and FTIR. The FESEM micrograph of porous SiC ceramics prepared at 1550 °C for 2 h is shown in Fig. 4e. It can be seen that the matrix is randomly embedded with tubular interpenetrating pores from the wood flour. Most of the pores show a round or elliptic shape and pore diameters of 10–40 μm. An FESEM micrograph obtained at higher magnification show is shown in Fig. 4f from which it can be seen that the thickness of the tubular pore walls, composed of SiC particles, is less than 5 μm. From the FESEM images, the formation of SiC whiskers in the pores is also observed (Figs. 4e and 4f), which are generally straight, several tens to over 100 μm in length and less than 50 nm in diameter. EDS analyses were used to determine the possible chemical compositions of the wire-like whiskers and the results are shown in Fig. 5a. The observed peaks demonstrate that the whiskers were composed of Si, C and a small amount of O. It is found that the Si:C ratio was about 1:1, suggesting that the wire-like whiskers grown inside the pores consisted of the SiC phase. The small quantity of oxygen may arise from a resident oxide layer. The morphology and crystal structure of the SiC wire-like whiskers were further characterized using TEM. A straight whisker with a uniform diameter of approximately 100 nm was inspected, as shown in Fig. 6a. This whisker was highly uniform over its entire length. From Fig. 6c, it can be seen that the (111) fringes perpendicular to the axis are on average separated by 0.25 nm (marked with the parallel lines in Fig. 6c), which indicates that single crystalline SiC whiskers grew along the [111] direction. Many stacking faults were also found in

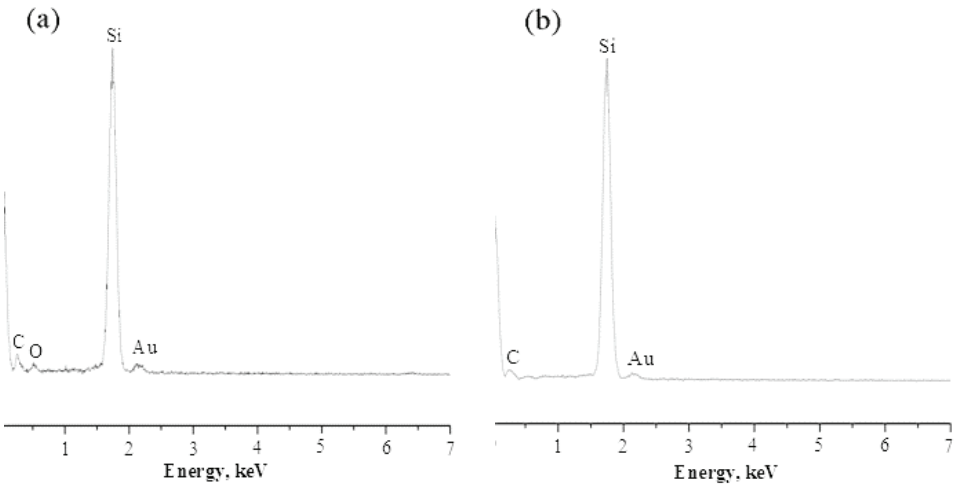

Fig. 5. EDS Spectra of a) the SiC wire-like whisker in the pores of ceramics and b) the SiC necklace-like whiskers on the surface of ceramics (Au element arises from the conducting layer of Au in the FESEM characterization).

the wire-like whiskers.[23,24] The selected-area electron diffraction (SAED) pattern shown in Fig. 6b indicates a high degree of crystallinity (β-SiC).[25]

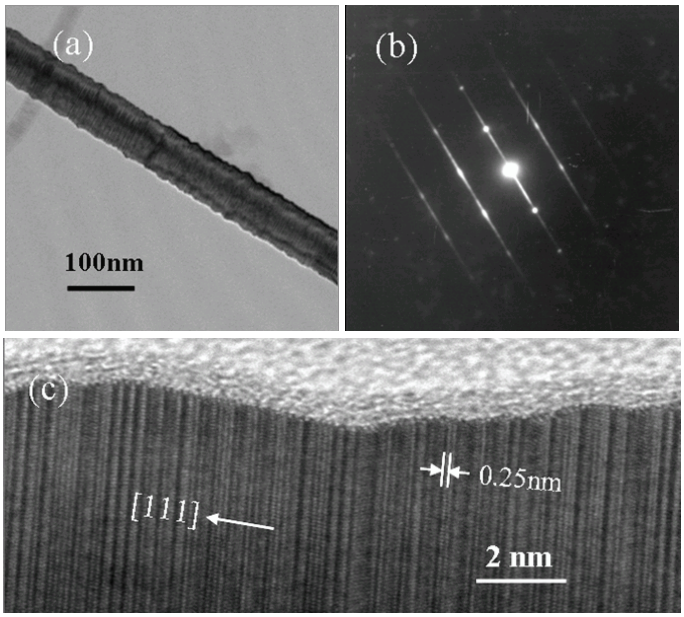

Fig. 6. Typical transmission electron spectroscopy image of a) the SiC wire-like whisker in the pores of ceramics, b) the corresponding SAED pattern and c) the HRTEM image of the wire-like whiskers.

The FESEM images of SiC whiskers grown on the surface of the porous SiC ceramics obtained at 1550 °C for 2 h are shown in Fig. 7. The low magnification SEM image shown in Fig. 7a displays that the most evident characteristic of the whiskers is the unique necklace-like morphology. As indicated by SEM images, most of the necklace-like whiskers are straight, hundreds of micrometers in length. Closer examination (Fig. 7b) of the whiskers indicates that the string of 1–2 μm in diameter is regularly decorated with numerous equally-sized beads. The uniform beads are 3–5 μm in diameter. EDS analysis of the necklace-like whiskers indicated that the synthesized whiskers were composed of the elements Si and C in an atomic ratio close to 1:1, implying standard SiC (Fig. 5b). The structural details and the growth mechanism of the necklace-like SiC whiskers were investigated in a previous study.[26]

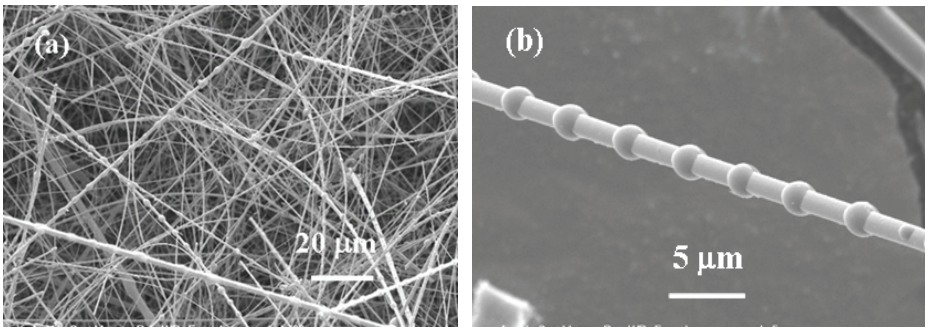

Fig. 7. FESEM Images at different magnifications of the SiC necklace-like whiskers grown on the surface of the porous SiC ceramics obtained at 1550 °C for 2 h.

Mechanism of conversion of wood flour–SiO_2–phenolic composites into SiC ceramics and SiC whiskers

It is well known that the synthesis of *β*-SiC *via* the carbothermal reduction of silica (SiO_2) is a vapor–solid (V–S) growth process, in which the following reaction occurs:[27,28]

$$SiO_2(s,l) + 3C(s) \rightarrow SiC(s) + 2CO(g) \quad (1)$$

The generally accepted mechanism for the overall reaction (1) is a multiple-step process that involves the formation of volatile SiO gas and its subsequent reduction to SiC.[29,30]

$$SiO_2(s,l) + C(s) \rightarrow SiO(g) + CO(g) \quad (2)$$

$$SiO_2(s) + CO(g) \rightarrow SiO(g) + CO_2(g) \quad (3)$$

$$CO_2(g) + C(s) \rightarrow 2CO(g) \quad (4)$$

$$SiO(g) + 2C(s) \rightarrow SiC(s) + CO(g) \quad (5)$$

$$SiO(g) + 3CO(g) \rightarrow SiC(s) + 2CO_2(g) \quad (6)$$

The SiO gas obtained from reactions (2) and (3) reacts with C or CO to yield SiC through reactions (5) and (6). All these reactions can make a circle to continue the synthesis process from the starting steps.

In the present work, at the reaction temperature, the SiO_2 component is first reduced by carbon from the wood flour and phenolic resin to generate gaseous SiO and CO according to reaction (2). Then the gaseous SiO reacts further with C to yield SiC nuclei heterogeneously on the surfaces of carbon through reaction (5). As the SiC nuclei are formed, SiC whiskers grow through the gas–gas reaction between SiO and CO according to reaction (6). In this work, the interconnected porous structures from wood flour after the initial carbothermal reduction could accelerate these reactions because these pores facilitate the diffusion of the formed gaseous SiO, CO and CO_2. This suggests that, as the gaseous diffusion path, the interpenetrating pores play an important role in the SiC synthesis process. As the reactions proceeds, the gaseous SiO molecules diffuse into carbonaceous cell wall and react and the created SiC particles (reaction 5). Meanwhile, SiO and CO generate SiC whiskers in the free space through the gas–gas reaction (6). It should be noted that the wire-like whiskers grew in the pores of the porous SiC ceramics (Fig. 4f), and the necklace-like whiskers grew on the surface of the porous SiC ceramics (Fig. 7a). As is known, the vapor pressure inside the pores is higher than that on the outer surface of ceramic, suggesting that the vapor pressure affects the growth process of whiskers. Further work is required for a full understanding of the pressure effect.

CONCLUSIONS

A porous SiC ceramic with SiC whiskers was successfully synthesized by the carbothermal reduction at 1550 °C using a novel wood flour–SiO_2–phenolic composite as the precursor. The porous ceramic with pore diameters of 10–40 μm consisted of β-SiC located at the position of the former wood cell walls. The wire-like whiskers formed inside the pores showed highly ordered cubic SiC with a less than 50 nm diameter and several tens to over 100 μm in length. The necklace-like whiskers that grew on the surface with a length of up to hundreds of micrometers were composed of uniform β-SiC oriented in the (111) direction and stacking faults perpendicular to the [111] plane. The interconnected porous structures from wood flour after initial carbothermal reduction play an important role in SiC synthesis process because those pores facilitate the diffusion of the gaseous SiO, CO and CO_2.

Acknowledgements. The authors gratefully acknowledge the financial support from the National Natural Science Foundation of China (Grant No. 50973024), the project of Anhui Provincial Education Department (No. KJ2013A090) and the Doctoral Foundation of Anhui University of Science and Technology.

И З В О Д

КОНВЕРЗИЈА ФЕНОЛНОГ КОМПОЗИТА ДРВНИ ПРАХ–SiO_2 У ПОРОЗНУ SiC КЕРАМИКУ СА SiC ВЛАКНИМА

HONG LI[1], TIEJUN SHI[2] и DEXIN TAN[1]

[1]*School of Chemical Engineering, Anhui University of Science & Technology, Huainan 232001, China и* [2]*School of Chemical Engineering, Hefei University of Technology, Hefei 230009, China*

Нови фенолни композит дрвни прах–SiO_2 употребљен је за конверзију у порозну SiC керамику која садржи влакна SiC настала применом поступка карбо-термијске редукције. На температури од 1550 °C композит је конвертован у порозну SiC керамику са порама пречника 10–40 μm, где је SiC у положају изворних зидова ћелија дрвета. Унутар пора се формирају β-SiC влакна облика жице мање од 50 nm у пречнику и дужине од неколико десетина до преко 100 μm. Површина добијене керамике је покривена влакнима пречника 1–2 μm у облику огрлице.

(Примљено 1. децембра 2012, ревидирано 5. фебруара 2013)

REFERENCES

1. P. Greil, T. Lifka, A. Kaindl, *J. Eur. Ceram. Soc.* **18** (1998) 1961
2. T. Ota, M. Imaeda, H. Takase, M. Kobayashi, N. Kinoshita, T. Hirashita, H. Miyazaki, Y. Hikichi, *J. Am. Ceram. Soc.* **83** (2000) 1521
3. A. Egelja, J. Gulicovski, A. Devecerski, B. Babić, M. Miljković, S. Bošković, B. Matović, *J. Serb. Chem. Soc.* **73** (2008) 745
4. G. Bantsis, M. Betsiou, A. Bourliva, T. Yioultsis, C. Sikalidis, *Ceram. Int.* **38** (2012) 721
5. E. Vogli, J. Mukerji, C. Hoffman, R. Kladny, H. Sieber, P. Greil, *J. Am. Ceram. Soc.* **84** (2001) 1236
6. B. H. Sun, T. X. Fan, D. Zhang, *J. Porous Mater.* **9** (2002) 275
7. Z. Li, T. Shi, L. Gao, *J. Serb. Chem. Soc.* **75** (2010) 385
8. R. Dhiman, V. Petrunin, K. Rana, P. Morgen, *Ceram. Int.* **37** (2011) 3281
9. K. Vyshnyakova, G. Yushin, L. Pereselentseva, Y. Gogotsi, *Int. J. Appl. Ceram. Technol.* **3** (2006) 485
10. H. Sieber, C. Hoffmann, A. Kaindl, P. Greil, *Adv. Eng. Mater.* **2** (2000) 105
11. T. Ota, M. Takahashi, T. Hibi, M. Ozawa, S. Suzuki, Y. Hikichi, H. Suzuki, *J. Am. Ceram. Soc.* **78** (1995) 3409
12. L. Esposito, D. Sciti, A. Piancastelli, A. Bellosi, *J. Eur. Ceram. Soc.* **24** (2004) 533
13. Y. S. Shin, C. M. Wang, G. J. Exarhos, *Adv. Mater.* **17** (2005) 73
14. A. Herzog, U. Vogt, O. Kaczmarek, R. Klingner, K. Richter, H. Thoemen, *J. Am. Ceram. Soc.* **89** (2006) 1499
15. J. M. Qian, Z. H. Jin, *J. Eur. Ceram. Soc.* **26** (2006) 1311
16. R. Klingner, J. Sell, T. Zimmermann, A. Herzog, U. Vogt, T. Graule, O. Turner, F. Beckmann, B. Müller, *Holzforschung* **57** (2003) 440
17. T. Hirose, B. Zhao, T. Okabe, M. Yoshimura, *J. Mater. Sci.* **37** (2002) 3453
18. R. Dhiman, E. Johnson, P. Morgen**,** *Ceram. Int.* **37** (2011) 3759
19. J. Locs, L. Berzina-Cimdina, A. Zhurinsh, D. Loca, *J. Eur. Ceram. Soc.* **29** (2009) 1513
20. C. Martos, F. Rubio, J. Rubio, J. L. Oteo, *J. Sol–Gel Sci. Technol.* **26** (2003) 511
21. S. Dhage, H. C. Lee, M. S. Hassan, M. S. Akhtar, C. Y. Kim, J. M. Sohn, K. J. Kim, H. S. Shin, O. B. Yang, *Mater. Lett.* **63** (2009) 174
22. Z. Y. Ryu, J. T. Zheng, M. Z. Wang, B. J. Zhang, *Carbon* **40** (2002) 715
23. S. M. Pickard, B. Derby, *J. Mater. Sci.* **26** (1991) 6207

24. W. S. Seo, K. Koumoto, *J. Am. Ceram. Soc.* **83** (2000) 2584
25. H. J. Choi, J. G. Lee, *Ceram. Int.* **26** (2000) 7
26. Z. Li, T. Shi, D. Tan, *J. Am. Ceram. Soc.* **93** (2010) 3499
27. A. Herzog, R. Klingner, U. Vogt, T. Graule, *J. Am. Ceram. Soc.* **87** (2004) 784
28. G. W. Meng, Z. Cui, L. D. Zhang, F. Phillipp, *J. Cryst. Growth* **209** (2000) 801
29. J. M. Qian, J. P. Wang, Z. H. Jin, *Mater. Sci. Eng., A* **371** (2004) 229
30. C. Zollfrank, H. Sieber, *J. Am. Ceram. Soc.* **88** (2005) 51.

Journal of the Serbian Chemical Society
JSCS-info@shd.org.rs • www.shd.org.rs/JSCS
J. Serb. Chem. Soc. 78 (8) 1225–1240 (2013)
JSCS–4493
UDC 633.71–32+54–145.2+547.288.1+546.11'226:541.25
Original scientific paper

Solution thermodynamics of aqueous nicotinic acid solutions in the presence of tetrabutylammonium hydrogen sulphate

ABHIJIT SARKAR and BISWAJIT SINHA*

Department of Chemistry, University of North Bengal, Darjeeling-734013, India

(Received 12 December 2012, revised 27 February 2013)

Abstract: In this study, we investigated the effects of tetrabutylammonium hydrogen sulphate (Bu_4NHSO_4) on the solute–solute and solute–solvent interactions in the aqueous solutions of nicotinic acid in terms of the apparent molar volumes (φ_V), standard partial molar volumes (φ_V^0) and viscosity *B*-coefficients at 298.15, 308.15 and 318.15 K under ambient pressure. These interactions are further discussed in terms of ion–dipolar, hydrophobic–hydrophobic, hydrophilic–hydrophobic group interactions. The activation parameters of viscous flow for Bu_4NHSO_4 in the aqueous solutions of nicotinic acid are discussed in terms of the transition state theory. The overall results indicated that ion–hydrophilic and hydrophilic–hydrophilic group interactions are predominant in aqueous solutions of nicotinic acid and that Bu_4NHSO_4 has a dehydration effect on hydrated nicotinic acid.

Keywords: Partial molar volumes; viscosity *B*-coefficients; tetrabutylammonium hydrogen sulphate; nicotinic acid.

INTRODUCTION

Nicotinic acid has gained huge attention over the years since it was synthesised in 1867 by Huber.[1] This is because of its versatility in terms of chemical, biochemical and therapeutic applications.[1] This derivative of pyridine has the molecular formula $C_6H_5NO_2$ with a carboxyl group (–COOH) at the 3-position and it is sometimes called niacin or vitamin B_3 in combination with nicotinamide.[2,3] It is a colourless, water-soluble compound and it can be converted to nicotinamide adenine dinucleotide (NAD^+) and nicotinamide adenine dinucleotide phosphate ($NADP^+$) *in vivo* in pharmacological doses. It reverses atherosclerosis by reducing the total cholesterol, triglycerides and lipoproteins. It also plays a crucial role in both repairing DNA and in the production of steroid hormones in the adrenal gland. Hence, it finds widespread application as an additive in food, forage and cosmetics.[4,5]

* Corresponding author. E-mail: biswachem@gmail.com
doi: 10.2298/JSC111212027S

Many effective components of drugs are weak organic electrolytes and their degree of dissociation is determined mainly by the media, especially aqueous medium since biochemical actions generally occur in the aqueous phase. In pharmaceutical techniques, materials of pharmaceutical aids are usually introduced to enhance the bioavailability of the drugs. The effects of the composition of the solvent on the dissociation and diffusion of drugs are therefore crucial. It has also been found that salt concentration has large effects on vitamins, such as on their solubilities, stabilities and biological activities in different manners. The behaviour of vitamins in solution phase is governed by a combination of many specific interactions, namely ion–dipolar, hydrophobic–hydrophobic and hydrophilic––hydrophobic group interactions. Tetra-alkylammonium salts are bulky in nature and are known to orient water molecules around themselves depending on their alkyl chain lengths.[6,7] Therefore, aqueous solutions of symmetrical tetra-alkylammonium cations (R_4N^+) are considered to provide model systems for the study of hydrophobic hydration[8] and salts such as tetrabutylammonium hydrogen sulphate (Bu_4NHSO_4) can provide better information about the effects of electrostatic, hydrophilic and hydrophobic interactions on the stabilities of vitamins, because such salts can influence the macromolecular conformations by affecting inter and intra charge–charge interactions and hydrophobic interactions.

Although extensive studies[9–19] are available on various properties of nicotinic acid in solution phase, a study on solution thermodynamics of aqueous solution of nicotinic acid in presence of Bu_4NHSO_4 is not available in the literature. Hence, in this work, the effects of Bu_4NHSO_4 on the solute–solute, solute–co-solute and solute–solvent or co-solute–solvent interactions in the aqueous solution of nicotinic acid were studied in terms of apparent molar volumes (φ_V), standard partial molar volumes (φ_V^0) and viscosity *B*-coefficients as a function of concentrations of Bu_4NHSO_4 and nicotinic acid in aqueous solution at 298.15, 308.15 and 318.15 K under ambient pressure.

EXPERIMENTAL

Materials

Nicotinic acid (Sigma Aldrich, USA, mass fraction purity > 99.5 %,) and Bu_4NHSO_4 (S. D. Fine Chemicals, India, mass fraction purity > 98.5 %) were used in the present study. Deionized, doubly distilled, degassed water with a specific conductance of 1×10^{-6} S cm^{-1} was used for the preparation of all aqueous solutions. Nicotinic acid was used as received from the vendor and its melting point was found to be 236.5 °C. The physical properties of different aqueous solutions of nicotinic acid are reported in Table S-I of the Supplementary material to this paper. No comparable literature data were found on the densities (ρ_0) and viscosities (η_0) for aqueous solutions of nicotinic acid (used as solvents) in this work. Bu_4NHSO_4 was purified by dissolving it in 1:1 (v/v) mixture of methanol and ethanol and recrystallized from diethyl ether. After filtration, the salt was dried in *vacuo* for few hours and its melting point was measured to be 171.5 °C. Stock solutions of Bu_4NHSO_4 in different aqueous solutions of nicotinic acid were prepared by mass and then further diluted to obtain different working

solutions. The pH of the working solutions decreased from 3.33–2.32 as the concentration of Bu_4NHSO_4 increased from 0.005–0.020 mol dm^{-3}. Molalities (m) were converted into molarities (c) using experimental densities. All solutions are prepared fresh before use and adequate precautions were taken to avoid evaporation losses during the measurements. The uncertainty in the molarity of the Bu_4NHSO_4 solutions was evaluated to be within ±0.0001 mol dm^{-3}.

Methods

The mass measurements were realised on a digital electronic analytical balance (Mettler, AG 285, Switzerland) with a precision of ±0.01 mg. The densities were measured with a vibrating-tube density meter (Anton Paar DMA 4500M), which was maintained at ±0.01 K of the desired temperature and calibrated with doubly distilled water and dry air. The uncertainty in the density was estimated to be ±0.0001 g cm^{-3}. The viscosities were measured by means of a suspended Ubbelohde type viscometer, which was calibrated at the experimental temperature with doubly distilled water and purified methanol. A thoroughly cleaned and perfectly dried viscometer (filled with the experimental solution) was placed vertically in a glass-walled thermostat maintained at ±0.01 K of the desired temperature. After attainment of thermal equilibrium, efflux times of flow were recorded with a digital stopwatch that measured time correct to ±0.01 s. At least three repetitions of each data (reproducible to ±0.02 s) were taken to average the flow times. Based on previous work on several pure liquids, the precision of the viscosity measurements was evaluated to be within ±0.003 mPa s and the total uncertainty in the viscosity measurements was 0.05 %. Details of the methods and techniques of the density and viscosity measurements were described elsewhere.[20–22] The absorption spectra were recorded on JascoV-530 double beam UV–Vis spectrophotometer (coupled with a thermostatic arrangement) at ambient temperature using a quartz cell of 1 cm path length. Doubly distilled water was used as the reference solvent for the spectroscopic measurements. The melting points of the solid solutes were determined by the open capillary method. The pH values of the working solutions were measured with a Systronics MK-VI 5631 digital pH meter, which had been calibrated with a commercially available buffer capsule (Merck, India) of pH 4.00 at 298.15 K before the readings were taken.

RESULTS AND DISCUSSION

The apparent molar volumes (φ_V) of Bu_4NHSO_4 in different aqueous solutions of nicotinic acid were determined from the solution densities using the following equation:[23]

$$\varphi_V = (M / \rho_0) - 1000(\rho - \rho_0) / (c\rho_0) \quad (1)$$

where M and c are the molar mass and molarity of Bu_4NHSO_4 in the aqueous solutions of nicotinic acid; ρ_0 and ρ are the densities of the solvent and the solution, respectively. The experimental densities (ρ), viscosities (η) and derived parameters at 298.15, 308.15 and 318.15 K are reported in Table S-II of the Supplementary material. As the φ_V values are independent of the concentrations of Bu_4NHSO_4 for extremely dilute solutions, it may be assumed that the φ_V values are equal to the partial molar volume (φ_V^0) at infinite dilution. The plots of the φ_V values against the square root of the molar concentrations ($\sqrt{c}$) of Bu_4NHSO_4 were found to be linear. Hence, the partial molar volumes (φ_V^0) at

infinite dilution and the experimental slopes (S_V^*) were determined by using least squares fitting (as shown in Fig. 1) of the φ_V values to the Masson Equation:[24]

$$\varphi_V = \varphi_V^0 + S_V^* \sqrt{c} \quad (2)$$

The φ_V^0 and S_V^* values are reported in Table I, from which it could be seen that the φ_V^0 values are positive and increase with increasing molarity of the nicotinic acid in the mixtures and decrease with increasing temperature of the respective mixtures. This trend in φ_V^0 values indicates the presence of strong solute–solvent interactions and such interactions further strengthen at higher concentrations of nicotinic acid in the ternary solutions and decrease when the temperature increases, probably due to greater thermal agitation leading to disruption of the developing specific interactions between the solute and solvent molecules at higher temperatures. These trends in φ_V^0 values are clear manifestations of the trends in *t*he φ_V values (as listed in Table S-II of the Supplementary material).

The parameter S_V^* is a volumetric viral coefficient and characterizes the pair-wise interactions between solvated species[25–27] in the solution. Its sign is determined by the interactions between solute species. Table I shows that the S_V^* values are positive for all the ternary solutions and such values increase when the experimental temperatures increase but decrease when the nicotinic acid concentration in the ternary solutions increases. For ionic species such as Bu_4NHSO_4 or zwitterionic nicotinic acid, the positive S_V^* values suggest that the pair-wise interactions (between solute–solute or solute–co-solute) were dominated by the charged end groups or ions and the S_V^* values just reciprocate the trends in φ_V^0 values for the studied experimental aqueous solutions.

Apparent molar volumes (φ_V) and densities (ρ) were used to derive the apparent molar expansibilities (φ_E) of nicotinic acid solutions by using the relation:[28]

$$\varphi_E = \alpha\varphi_V + 1000(\alpha - \alpha_0)/(m\rho_0) \quad (3)$$

where α and α_0 are the coefficients of isobaric thermal expansion of the solvent and solution, respectively and the other symbols have their usual significances. The coefficients α and α_0 are defined as: $\alpha = -\rho_0^{-1}(\mathrm{d}\rho_0/\mathrm{d}T)_P$ and $\alpha_0 = -\rho^{-1}(\mathrm{d}\rho/\mathrm{d}T)_P$, respectively.

The uncertainty of α and α_0 values was $\pm 5\times10^{-6}$ K^{-1}. The uncertainty of apparent molar expansibilities (φ_E) was within $\pm 0.001\times10^{-6}$ m^3 mol^{-1} K^{-1}. The partial molar expansibilities (φ_E^0) were derived from the relation:[28]

$$\varphi_E = \varphi_E^0 + S_E \sqrt{m} \quad (4)$$

The φ_E^0 values for the experimental solutions at different temperatures are reported in Table II, from which it could be seen that the φ_E^0 values are negative and further decrease with increasing temperature and nicotinic acid concentration.

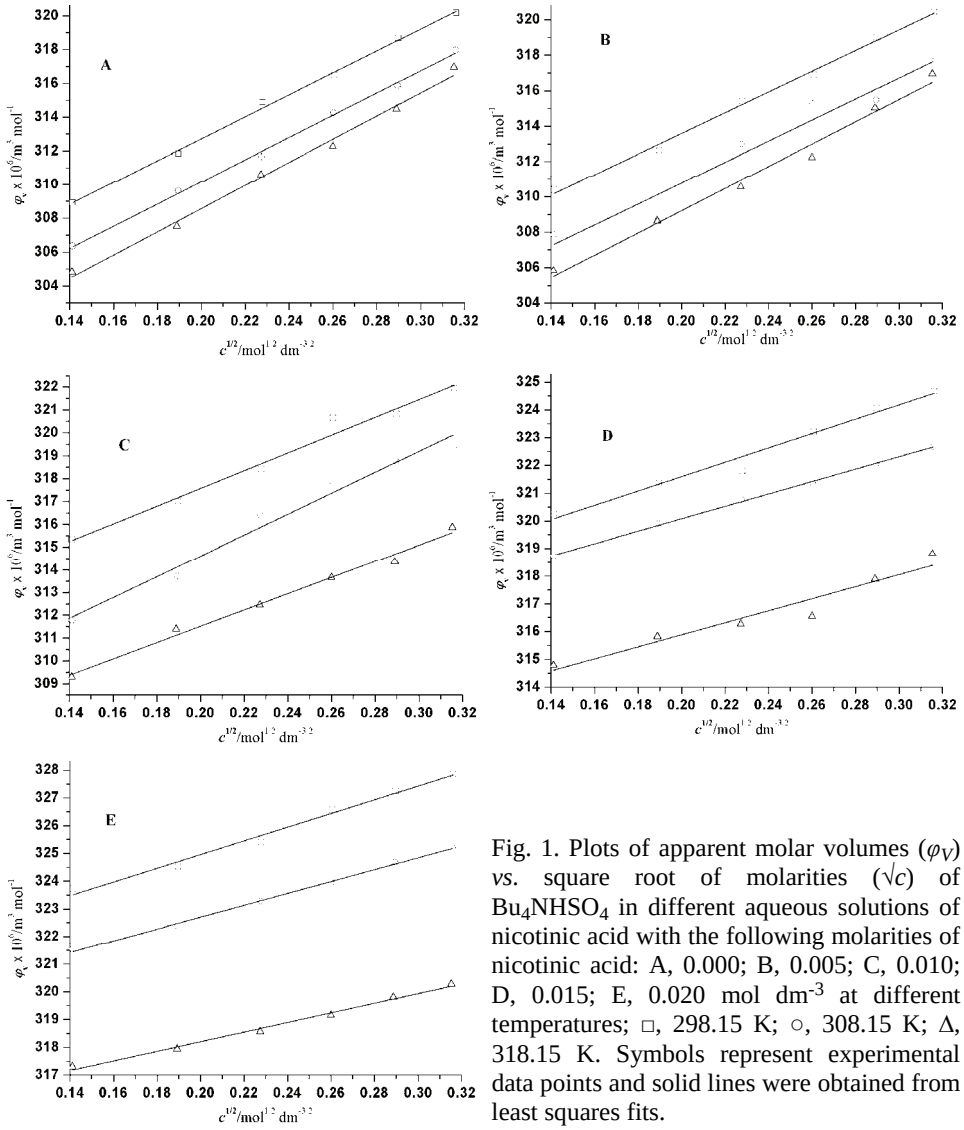

Fig. 1. Plots of apparent molar volumes (φ_V) *vs.* square root of molarities ($\sqrt{c}$) of Bu_4NHSO_4 in different aqueous solutions of nicotinic acid with the following molarities of nicotinic acid: A, 0.000; B, 0.005; C, 0.010; D, 0.015; E, 0.020 mol dm^{-3} at different temperatures; □, 298.15 K; ○, 308.15 K; Δ, 318.15 K. Symbols represent experimental data points and solid lines were obtained from least squares fits.

Such a trend in the φ_E^0 values may be attributed to structural perturbations caused by the addition of nicotinic acid or to the appearance of caging or packing effects.[29,30] However, such effects gradually decrease and lead to the release of solvated H_2O molecules in favour of the bulk water structure. Thus, the volume of the solution decreases and the density increases, as given in Table S-II of the Supplementary material. According to Heplar,[32] the long-range structure making or breaking ability of solutes in solutions can be better characterized by the sign of the $(\mathrm{d}\varphi_E^0/\mathrm{d}T)_P$ terms. If the sign of $(\mathrm{d}\varphi_E^0/\mathrm{d}T)_P$ is slightly negative or posi-

tive, the solute is a structure maker, otherwise it is a structure breaker. The $(\mathrm{d}\varphi_E^0/\mathrm{d}T)_P$ values were obtained from the slopes of linear fits of φ_E^0 values against the experimental temperatures (T), which have coefficient of regression (R^2) values lying within the range of 0.99998–0.99999. From the values of $(\mathrm{d}\varphi_E^0/\mathrm{d}T)_P$ reported in Table II, it is evident that Bu_4NHSO_4 acts as a mild structure maker and its structure making ability decreases to some extent with increasing nicotinic acid concentrations in the studied solutions.

TABLE I. Partial molar volumes (φ_V^0) and the experimental slopes (S_V*) of Eq. (2) for Bu_4NHSO_4 in aqueous solutions of nicotinic acid with corresponding standard deviations (σ) at different temperatures

T / K	$\varphi_V^0 \times 10^6$ / m^3 mol^{-1}	$S_V^* \times 10^6$ / m$^{9/2}$ mol$^{-3/2}$	$\sigma^b \times 10^6$ / m^3 mol^{-1}
		c_{NA}[a] = 0.000	
298.15	299.73 (±0.81)	64.94 (±3.33)	0.09 (0.99755)
308.15	297.02 (±0.80)	65.74 (±3.28)	0.09 (0.99774)
318.15	294.84 (±1.07)	68.64 (±4.40)	0.29 (0.99338)
		c_{NA} = 0.005	
298.15	301.92 (±0.88)	58.39 (±3.63)	0.13 (0.99571)
308.15	298.94 (±1.66)	59.24 (±6.80)	1.68 (0.95124)
318.15	296.62 (±1.21)	62.96 (±4.99)	0.48 (0.98703)
		c_{NA} = 0.010	
298.15	309.80 (±1.07)	38.85 (±4.40)	0.29 (0.98703)
308.15	305.45(±1.20)	45.77 (±4.90)	0.45 (0.97948)
318.15	304.38 (±0.84)	35.69 (±3.44)	0.11 (0.99085)
		c_{NA} = 0.015	
298.15	316.42 (±0.91)	25.88 (±3.70)	0.15 (0.97684)
308.15	315.61 (±0.44)	22.33 (±1.80)	0.01 (0.99822)
318.15	311.55 (±1.08)	21.67 (±4.45)	0.01 (0.93418)
		c_{NA} = 0.020	
298.15	320.03 (±0.75)	24.66 (±3.06)	0.07 (0.98794)
308.15	318.43 (±0.45)	21.39 (±1.84)	0.01 (0.99788)
318.15	314.73 (±0.56)	17.53(±2.31)	0.02 (0.99205)

[a]Molarity of nicotinic acid in water; [b]values of coefficient of regression (R^2) in parentheses

The partial molar volumes of transfer $(\Delta\varphi_V^0)$ from water to an aqueous solution of nicotinic acid were determined from the relation:[27,33]

$$\Delta\varphi_V^0 = \varphi_V^0[\text{Aqueous solution of nicotinic acid}] - \varphi_V^0[\text{Water}] \quad (5)$$

The $\Delta\varphi_V^0$ values are depicted in Fig. 2 as a function of the molarity of the aqueous nicotinic acid solutions. The $\Delta\varphi_V^0$ values are free from solute–solute interactions and, therefore, provide valuable information about solute–co-solute interactions.[33] Figure 2 shows that the $\Delta\varphi_V^0$ values were positive at all the experimental temperatures and increase monotonically with increasing nicotinic acid concentration in the ternary solutions. According to the co-sphere model,[34]

while the overlap of hydration co-spheres of two ionic species results in a volume increase, those of hydration co-spheres of hydrophobic–hydrophobic and ion–hydrophobic groups result in a net volume decrease. The positive $\Delta\varphi_V^0$ values indicate that ion–hydrophilic and hydrophilic–hydrophilic group interactions are predominant over ion–hydrophobic, hydrophobic–hydrophobic and hydrophilic–hydrophobic interactions and the overall effect of the overlap of the hydration co-spheres of Bu_4NHSO_4 and zwitterionic nicotinic acid reduces the electrostriction of water by Bu_4NHSO_4. Such reduced electrostriction results in a concomitant increase in volume and this effect increases further with increasing molarities of nicotinic acid in the ternary solutions.

TABLE II. Limiting partial molar expansibilities (φ_E^0) for Bu_4NHSO_4 in aqueous solutions of nicotinic acid at different temperatures; standard errors are given in parentheses

c_{NA}[a]	$\varphi_E^0 \times 10^4$ / m^3 mol^{-1} K^{-1}			$S_E \times 10^4$) / m^3 mol^{-1} K^{-1}			$(d\varphi_E^0 / dT)_P \times 10^6$
mol dm^{-3}	298.15 K	308.15 K	318.15 K	298.15 K	308.15 K	318.15 K	m^3 mol^{-1} K^{-2}
0	–3.458	–3.480	–3.351	1.572	1.543	1.612	–0.363
	(±0.001)	(±0.001)	(±0.001)	(±0.001)	(±0.001)	(±0.001)	(±0.001)
0.005	–6.676	–6.740	–6.817	11.773	11.877	12.025	–0.700
	(±0.001)	(±0.001)	(±0.001)	(±0.001)	(±0.001)	(±0.001)	(±0.001)
0.010	–8.058	–8.153	–8.231	11.873	12.062	12.141	–0.863
	(±0.001)	(±0.001)	(±0.001)	(±0.001)	(±0.001)	(±0.001)	(±0.001)
0.015	–5.362	–5.378	–5.439	4.139	4.203	4.242	–0.567
	(±0.001)	(±0.001)	(±0.002)	(±0.001)	(±0.002)	(±0.001)	(±0.001)
0.020	–5.326	–5.384	–5.444	1.027	1.089	1.073	–0.589
	(±0.001)	(±0.002)	(±0.001)	(±0.002)	(±0.001)	(±0.001)	(±0.002)

[a]Molarity of nicotinic acid in aqueous solutions

The partial molar volumes (φ_V^0) of a solute can also be explained by the simple model[25,35] given by the relation:

$$\varphi_V^0 = \varphi_{vw} + \varphi_{void} - \varphi_S \quad (6)$$

where φ_{vw}, φ_{void} and φ_S are the van der Waals volumes, the volumes associated with voids or empty spaces and the shrinkage volumes due to electrostriction, respectively. Assuming the values of φ_{vw} and φ_{void} are of same magnitude in water and in aqueous nicotinic acid solutions of for the same solute, the increase in the φ_V^0 values and the concomitant positive $\Delta\varphi_V^0$ values can be attributed to decreases in the shrinkage volumes (φ_S) of water by Bu_4NHSO_4 in presence of nicotinic acid. This fact suggests that Bu_4NHSO_4 has a dehydration effect on hydrated nicotinic acid. It was already reported in the literature[36–38] that HSO_4^- readily achieves the equilibrium: $HSO_4^- \leftrightarrows H^+ + SO_4^{2-}$ in aqueous solution at low temperatures (<100 °C) under ambient pressure. According to Sharnin *et al.*[39] nicotinic acid exists in the zwitterionic form in aqueous solution and within the pH range of the experimental aqueous solutions, nicotinic acid remains in equi-

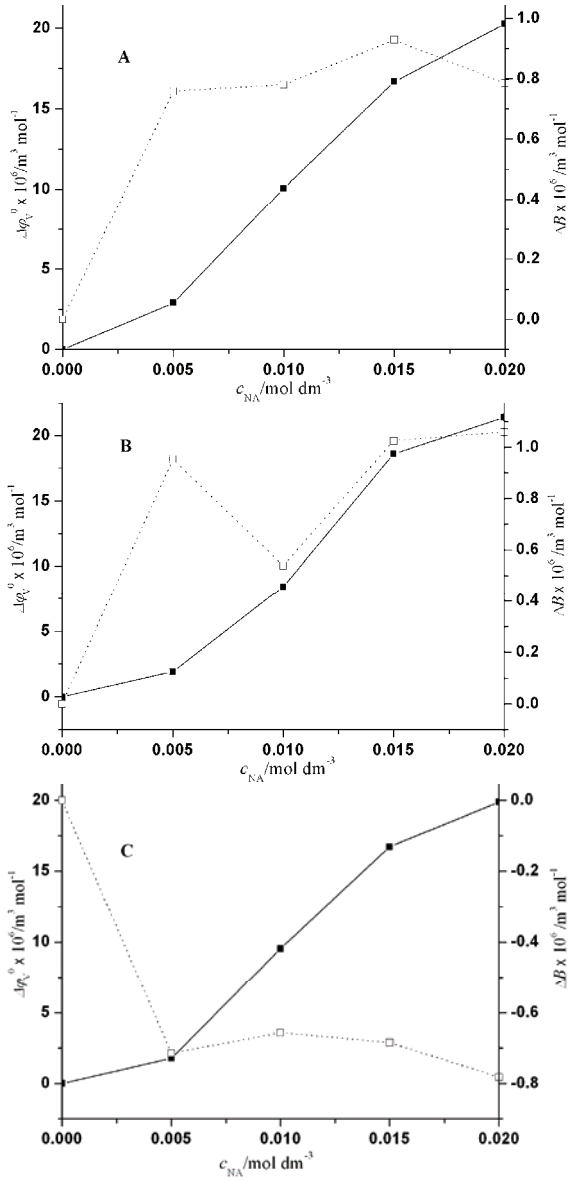

Fig. 2. Plots of partial molar volumes of transfer ($\Delta\varphi_V^0$) and viscosity *B*-coefficients of transfer (ΔB) from water to aqueous solutions of nicotinic acid for Bu_4NHSO_4 at different temperatures: A, 298.15 K; B, 308.15 K; C, 318.15 K; –■–. $\Delta\varphi_V^0$; ···□···, ΔB.

librium with its four possible forms:[40] a positively charged form (AH_2^+), two isoelectric forms ($AH^{\pm}$ and AH^0) and a negatively charged form (A^-). Changes in UV–Vis absorption spectra of nicotinic acid (4.0×10^{-5} mol dm^{-3}) in different aqueous solutions of Bu_4NHSO_4 and of nicotinic acid as a function of its concentration in aqueous solution of Bu_4NHSO_4 (4.0×10^{-5} mol dm^{-3}) at 298.15 K are shown in Figs. 3 and 4, respectively. The UV–Vis absorption spectra show

only one peak at 260 nm corresponding to an n→π* transition that involves the molecular orbitals of ≡N: and the pyridine ring. The UV–Vis absorption spectra also show that the intensity of this peak increases with increasing nicotinic acid concentration and decreases with increasing Bu_4NHSO_4 concentration. Hence it could be assumed that nicotinic acid exists in a zwitterionic form and limits the possible interactions involving: *i*) polar $–NH^+$ group of zwitterionic nicotinic acid and HSO_4^-, SO_4^{2-} and HO^-, *ii*) polar $–COO^-$ group (through both the O-atoms) of zwitterionic nicotinic acid and Bu_4N^+ and H^+ ions and *iii*) ionic––hydrophobic interaction between ions of Bu_4NHSO_4 and the non polar part of zwitterionic nicotinic acid molecules. While type *i*) and *ii*) interactions impart positive contributions, type *iii*) interactions impart negative contributions to φ_V^0 values. Therefore the overall positive φ_V^0 values indicate that ionic group interactions (depicted in Fig. 5) predominate over ionic–hydrophobic interactions. This predominance of ionic group interactions reduces the electrostriction of water by Bu_4NHSO_4 and imparts positive contributions to the $\Delta\varphi_V^0$ values.

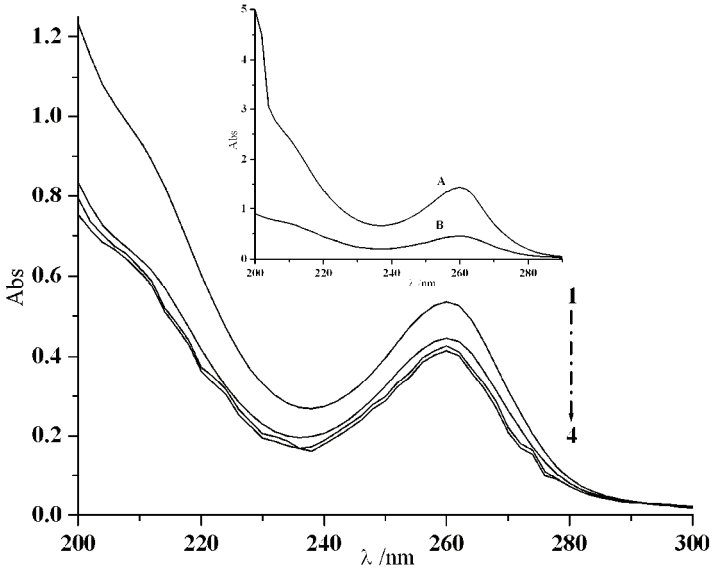

Fig. 3. Changes in the UV–Vis absorption spectra of 4.0×10^{-5} mol dm^{-3} nicotinic acid in ternary solutions (Bu_4NHSO_4 + nicotinic acid + H_2O) with the following molarities of Bu_4NHSO_4: 1, 2.0×10^{-5} mol dm^{-3}; 2, 4.0×10^{-5} mol dm^{-3}; 3, 6.0×10^{-5} mol dm^{-3} and 4, 8.0×10^{-5} mol dm^{-3}. Inset: A, 4.0×10^{-5} mol dm^{-3} nicotinic acid in aqueous solution; B, average spectrum of 1–4.

The viscosities (η) of the different experimental aqueous solutions were analyzed by the Jones–Dole Equation: [41]

$$(\eta/\eta_0 - 1)/\sqrt{c} = (\eta_r - 1)/\sqrt{c} = A + B\sqrt{c} \quad (7)$$

where $\eta_r = \eta/\eta_0$ is the relative viscosity; η_0 and η are the viscosities of solvent and solution, respectively. *A* and *B* are two adjustable parameters that are obtained by a least squares analysis and are reported in Table III. The viscosity *B*-coefficient[42] reflects the effects of solute–solvent interactions on the solution viscosity and provides information about the solvation of a solute and the structure of the solvent in the local vicinity of the solute molecules. Table III shows that the viscosity *B*-coefficients for Bu_4NHSO_4 in the studied solvent systems were positive and thus suggest the presence of strong solute–solvent interactions in the studies solutions. These interactions further increase when both the molarity of Bu_4NHSO_4 in the ternary solutions and the temperature increase. The *A*-coefficients values are indicative of solute–solute or ion–ion interactions and in the present study their values support the results obtained from viscosity *B*-coefficients discussed earlier. Viscosity *B*-coefficients of transfer (ΔB) from water to aqueous solutions of nicotinic acid were determined by using the relation:[27,33]

$$\Delta B = B\,[\text{Aqueous solution of nicotinic acid}] - B\,[\text{Water}] \quad (8)$$

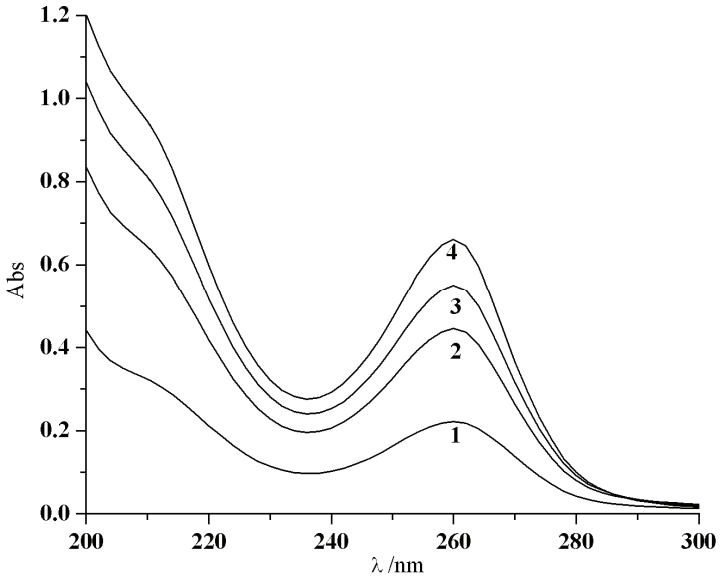

Fig. 4. Changes in the UV–Vis absorption spectra of nicotinic acid (4.0×10^{-5} mol dm^{-3}) in ternary solutions (Bu_4NHSO_4 + nicotinic acid + H_2O) with the following molarities of nicotinic acid: 1, 2.0×10^{-5} mol dm^{-3}; 2, 4.0×10^{-5} mol dm^{-3}; 3, 6.0×10^{-5} mol dm^{-3} and 4, 8.0×10^{-5} mol dm^{-3}.

The ΔB values are depicted in Fig. 2 as a function of the molarity of nicotinic acid in the aqueous solutions and they support the results obtained from the $\Delta\varphi_V^0$ values discussed earlier.

According to transition state theory of relative viscosity,[43] the contribution per mole of a solute to the free energy of activation for viscous flow of the solution ($\Delta\mu_2^{\ominus *}$) is related to the viscosity *B*-coefficients by the following relation:

$$\Delta\mu_2^{\ominus *} = \Delta\mu_1^{\ominus *} + RT\,(1000B + \varphi_{V,2}^0 - \varphi_{V,1}^0)/\varphi_{V,1}^0 \quad (9)$$

where $\varphi_{V,1}^0$ and $\varphi_{V,2}^0$ are the partial molar volumes of the solvent and solute, respectively. The free energy of activation of viscous flow per mole of the pure solvent or solvent mixture ($\Delta\mu_1^{\ominus *}$) is given by the relation:[43,44]

$$\Delta\mu_1^{\ominus *} = \Delta G_1^{\ominus *} = RT \ln (\eta_0 \varphi_{V,1}^0)/hN_A \quad (10)$$

where N_A is the Avogadro number and the other symbols have their usual significances.[43]

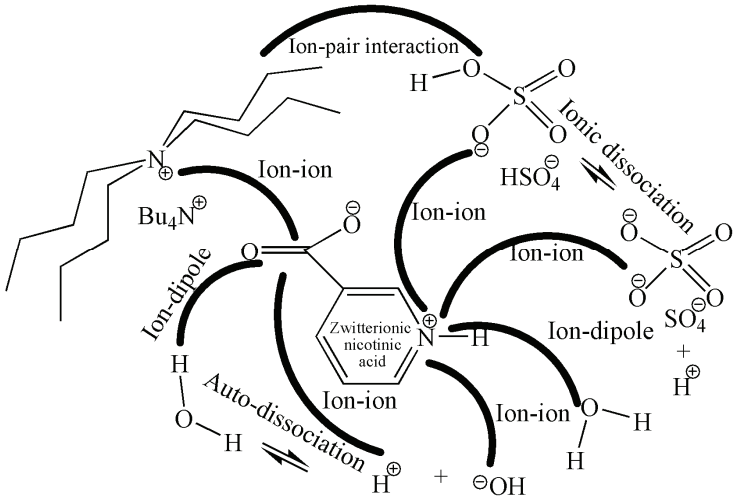

Fig. 5. Different possible ionic group interactions in aqueous solutions of nicotinic acid in presence of Bu_4NHSO_4.

The entropy of activation for viscous flow per mole of the solute in the ternary solutions ($\Delta S_2^{\ominus *}$) can be obtained from the negative slope of the plots of $\Delta\mu_2^{\ominus *}$ against *T*:

$$\Delta S_2^{\ominus *} = -\mathrm{d}(\Delta\mu_2^{\ominus *})/\mathrm{d}T \quad (11)$$

and the activation enthalpy for viscous flow ($\Delta H_2^{\ominus *}$) can be obtained from the relation:

$$\Delta H_2^{\ominus *} = \Delta\mu_2^{\ominus *} + T\Delta S_2^{\ominus *} \quad (12)$$

TABLE III. Values of viscosity *A*- and *B*-coefficients for Bu_4NHSO_4 in aqueous solutions of nicotinic acid at different temperatures

Viscosity coefficients	*T* / K		
	298.15	308.15	318.15
	c_{NA}[a] = 0.000		
$A\times10^{-6}$ / $m^{3/2}$ $mol^{-1/2}$	–0.145	–0.087	–0.142
$B\times10^{-6}$ / m^3 mol^{-1}	1.004	1.248	1.446
$\sigma\times10^{-6}$ / $m^{3/2}$ $mol^{-1/2}$	0.001	0.001	0.002
	c_{NA}= 0.005		
$A\times10^{-6}$ / $m^{3/2}$ $mol^{-1/2}$	–0.096	–0.087	0.212
$B\times10^{-6}$ / m^3 mol^{-1}	1.762	2.201	0.731
$\sigma\times10^{-6}$ / $m^{3/2}$ $mol^{-1/2}$	0.002	0.001	0.001
	c_{NA} = 0.010		
$A\times10^{-6}$ / $m^{3/2}$ $mol^{-1/2}$	–0.092	–0.017	0.287
$B\times10^{-6}$ / m^3 mol^{-1}	1.784	1.787	0.789
$\sigma\times10^{-6}$ / $m^{3/2}$ $mol^{-1/2}$	0.001	0.001	0.002
	c_{NA}= 0.015		
$A\times10^{-6}$ / $m^{3/2}$ $mol^{-1/2}$	–0.099	–0.238	0.132
$B\times10^{-6}$ / m^3 mol^{-1}	1.933	2.273	0.761
$\sigma\times10^{-6}$ / $m^{3/2}$ $mol^{-1/2}$	0.001	0.004	0.001
	c_{NA}= 0.020		
$A\times10^{-6}$ / $m^{3/2}$ $mol^{-1/2}$	–0.078	–0.179	0.189
$B\times10^{-6}$ / m^3 mol^{-1}	1.778	2.307	0.664
$\sigma\times10^{-6}$ / $m^{3/2}$ $mol^{-1/2}$	0.001	0.001	0.001

[a]Molarity of nicotinic acid in water

The parameters $(\varphi_{V,2}^0 - \varphi_{V,1}^0)$, $\Delta\mu_1^{\ominus *}$, $\Delta\mu_2^{\ominus *}$, $\Delta H_2^{\ominus *}$ and $T\Delta S_2^{\ominus *}$ are reported in Table IV, from which it can be seen that the $\Delta\mu_1^{\ominus *}$ values are almost invariant of the solvent composition and temperature, implying also that the $\Delta\mu_2^{\ominus *}$ values are dependent mainly on the viscosity *B*-coefficient and the $(\varphi_{V,2}^0 - -\varphi_{V,1}^0)$ deviations. The $\Delta\mu_2^{\ominus *}$ values contain the change in the free energy of activation of the solute in presence of solvent as well as contributions from the movement of the solute molecules. The $\Delta\mu_2^{\ominus *}$ values were found to be positive at all the experimental temperatures and decreased with increasing temperature and increased with increasing nicotinic acid concentration in the ternary solutions. Such trends suggest that the viscous flow process becomes more difficult with increasing nicotinic acid concentration in the solutions but becomes favourable at higher temperatures. Hence the formation of the transition state becomes less favourable in the presence of nicotinic acid but becomes somewhat more favourable at higher temperatures. The $(\Delta\mu_2^{\ominus *} - \Delta\mu_1^{\ominus *})$ deviations reflect the change in the activation energy per mole of solute when one mole of the solvent is replaced by one mole of the solute at infinite dilution. Hence according to Feakins *et al.*,[43] for solutes with positive $\Delta S_2^{\ominus *}$, $\Delta H_2^{\ominus *}$ and viscosity *B*-coefficients, $\Delta\mu_2^{\ominus *} > \Delta\mu_1^{\ominus *}$ indicates stronger solute–solvent interactions and thus

suggests that the formation of the transition state is accompanied by the rupture and distortion of the intermolecular forces in the solvent structure.[43] The greater the value of $\Delta\mu_2^{\ominus *}$, the greater is the structure-promoting tendency of a solute and the higher values of $\Delta\mu_2^{\ominus *}$ for Bu_4NHSO_4 in the ternary solutions when compared to those in the aqueous binary solutions suggest that Bu_4NHSO_4 is a better structure promoter for the ternary mixtures than for aqueous binary solutions. Although a detailed mechanism for the formation of such a transition state cannot be easily advanced, it may be suggested that the viscous process is endothermic (positive $\Delta H_2^{\ominus *}$ values) and the slip-plane is in an ordered state (positive $\Delta S_2^{\ominus *}$ values) and involves a centro-symmetric region.[43,44]

TABLE IV. Values of $(\varphi_{V,2}^0 - \varphi_{V,1}^0)$, $\Delta\mu_1^{\ominus *}$, $\Delta\mu_2^{\ominus *}$, $\Delta H_2^{\ominus *}$ and $T\Delta S_2^{\ominus *}$ for Bu_4NHSO_4 in different aqueous solutions of nicotinic acid at different temperatures

Parameters	T / K		
	298.15	308.15	318.15
	c_{NA}[a] = 0.000		
$(\varphi_{V,2}^0 - \varphi_{V,1}^0)\times10^6$ / m^3 mol^{-1}	281.61	278.79	276.47
$\Delta\mu_1^{\ominus *}$ / kJ mol^{-1}	9.17	8.95	8.76
$\Delta\mu_2^{\ominus *}$ / kJ mol^{-1}	185.01	223.53	256.79
$T\Delta S^{\ominus *}$ / kJ mol^{-1}	–1070.04	–1105.93	–1141.82
$\Delta H^{\ominus *}$ / kJ mol^{-1}	–885.03	–882.40	–885.03
	c_{NA} = 0.005		
$(\varphi_{V,2}^0 - \varphi_{V,1}^0)\times10^6$ / m^3 mol^{-1}	283.77	280.73	278.24
$\Delta\mu_1^{\ominus *}$ / kJ mol^{-1}	9.14	8.93	8.68
$\Delta\mu_2^{\ominus *}$ / kJ mol^{-1}	288.54	358.15	153.94
$T\Delta S^{\ominus *}$ / kJ mol^{-1}	2006.50	2073.80	2141.10
$\Delta H^{\ominus *}$ / kJ mol^{-1}	2295.04	2431.95	2295.04
	c_{NA} = 0.010		
$(\varphi_{V,2}^0 - \varphi_{V,1}^0)\times10^6$ / m^3 mol^{-1}	291.65	287.25	286.01
$\Delta\mu_1^{\ominus *}$ / kJ mol^{-1}	9.24	8.98	8.72
$\Delta\mu_2^{\ominus *}$ / kJ mol^{-1}	292.77	300.94	163.48
$T\Delta S^{\ominus *}$ / kJ mol^{-1}	1927.46	1992.11	2056.76
$\Delta H^{\ominus *}$ / kJ mol^{-1}	2220.24	2293.05	2220.24
	c_{NA} = 0.015		
$(\varphi_{V,2}^0 - \varphi_{V,1}^0)\times10^6$ / m^3 mol^{-1}	298.28	297.41	293.18
$\Delta\mu_1^{\ominus *}$ / kJ mol^{-1}	9.28	9.06	8.82
$\Delta\mu_2^{\ominus *}$ / kJ mol^{-1}	314.16	370.98	160.62
$T\Delta S^{\ominus *}$ / kJ mol^{-1}	2288.89	2365.67	2442.44
$\Delta H^{\ominus *}$ / kJ mol^{-1}	2603.06	2736.65	2603.06
	c_{NA} = 0.020		
$(\varphi_{V,2}^0 - \varphi_{V,1}^0)\times10^6$ / m^3 mol^{-1}	301.89	300.24	296.37
$\Delta\mu_1^{\ominus *}$ / kJ mol^{-1}	9.31	9.15	8.89
$\Delta\mu_2^{\ominus *}$ / kJ mol^{-1}	293.64	376.45	147.23
$T\Delta S^{\ominus *}$ / kJ mol^{-1}	2182.68	2255.89	2329.09
$\Delta H^{\ominus *}$ / kJ mol^{-1}	2476.33	2632.34	2476.33

[a]Molarity of nicotinic acid in water

CONCLUSIONS

In summary, the partial molar volumes (φ_V^0) and viscosity *B*-coefficients of Bu_4NHSO_4 in aqueous solutions of nicotinic acid indicate the presence of strong solute–solvent interactions and such interactions further strengthen at higher nicotinic acid concentrations but decrease at higher temperatures. These facts may be attributed to the predominance of ion–hydrophilic and hydrophilic–hydrophilic group interactions over ion–hydrophobic, hydrophobic–hydrophobic and hydrophilic–hydrophobic interactions. Moreover, the trends in $(\mathrm{d}\varphi_E^0/\mathrm{d}T)_P$ and $\Delta\mu_2^{\ominus *}$ for Bu_4NHSO_4 in aqueous solutions of nicotinic acid suggest that Bu_4NHSO_4 is a net structure promoter in the studied aqueous solutions and it has a dehydration effect on hydrated nicotinic acid.

SUPPLEMENTARY MATERIAL

The physical properties of different aqueous solutions of nicotinic acid and experimental densities, viscosities along with derived parameters at the experimental temperatures (listed in Tables S-I and S-II) are available electronically from http://www.shd.org.rs/JSCS/ or from the author on request.

Acknowledgement. The authors are grateful to the Departmental Special Assistance Scheme under the University Grants Commission, New Delhi (No. F540/27/DRS/2007, SAP-1) for financial support.

ИЗВОД

ТЕРМОДИНАМИКА ВОДЕНОГ РАСТВОРА НИКОТИНСКЕ КИСЕЛИНЕ У ПРИСУСТВУ ТЕТРАБУТИЛАМОНИЈУМ-ХИДРОГЕН-СУЛФАТА

ABHIJIT SARKAR and BISWAJIT SINHA

Department of Chemistry, University of North Bengal, Darjeeling-734013, India

У овом раду истражен је утицај тетрабутиламонијум-хидроген-сулфата (Bu_4NHSO_4) на интеракције растворена супстанца–растворена супстанца и растворена супстанца––растварач у воденим растворима никотинске киселине, користећи привидне моларне запремине (φ_B), стандардне парцијалне моларне запремине (φ_B^0) и *B*-коефицијенте на 298,15, 308,15 и 318,15 K и на атмосферском притиску. Ове интеракције су додатно дискутоване преко јон–дипол, хидрофобно–хидрофобних и хидрофилно–хидрофобних група интеракција. Активациони параметри вискозног тока за Bu_4NHSO_4 у воденим растворима никотинске киселине дискутовани су користећи теорију прелазног стања. Укупни резултати су показали да су јон–хидрофилне и хидрофилно–хидрофилне групе интеракција доминантне у воденим растворима никотинске киселине и да Bu_4NHSO_4 има дехидратациони ефекат на хидратисану никотинску киселину.

(Примљено 12. децембра 2012, ревидирано 27. фебруара 2013)

REFERENCES

1. C. A. Elvehjem, L. J. Teply, *Chem. Rev.* **33** (1943) 185
2. A. N. Nesmeyanov, N. A. Nesmeyanov, *Fundamentals of Organic Chemistry*, Vol. 3, Mir Pub., Moscow, 1981, p. 393

3. A. S. Fauci, E. Braunwald, K. J. Isselbacher, J. D. Wilson, J. B. Martin, D. L. Kasper, S. L. Hauser, D. L. Long, *Harrison's Principles of Internal Medicine*, Vol. 1, 14th ed., McGraw-Hill, New York, 1998
4. J. Block, *Vitamins*, in *Kirk-Othmer Encyclopedia of Chemical Technology*, Vol. 25, 5th ed., S. Seidel, Ed., Wiley, Hoboken, NJ, 1996, p. 797
5. L. A. Carlson, *J. Int. Med.* **258** (2005) 94
6. M. N. Roy, B. Sinha, V. K. Dakua, *Pak. J. Sci. Ind. Res.* **49** (2006) 153
7. L. H. Blanco, E. F. Vargas, *J. Solution. Chem.* **35** (2006) 21
8. W.-Y. Wen, in *Water and Aqueous Solutions: Structure, Thermodynamics, and Transport Processes*, R. A. Horne, Ed., Wiley-Interscience, New York, 1972, p. 613
9. D. Cacaval, A. C. Blaga, M. Camarup, A. I. Galaction, *Sep. Sci. Tech.* **42** (2007) 389
10. H. H. Loh, C. P. Berg, *J. Nutr.* **101** (1971) 1601
11. C. Yiyun, X. Tongwen, *Eur. J. Med. Chem.* **40** (2005) 1384
12. L. Tsai, I. Pastan, E. R. Stadtman, *J. Biol. Chem.* **241** (1966) 1807
13. P. K. Mandal, D. K. Chatterjee, B. K. Seal, A. K. Basu, *J. Solution Chem.* **7** (1978) 57
14. A. G. Kharitonova, O. K. Krasilnikova, R. S. Vastapetyan, A. V. Bulanova, *Colloid J.* **67** (2005) 375
15. I. V. Terekhova, N. A. Obukhova, *J. Solution Chem.* **34** (2005) 1273
16. H.-P. Pan, T.-C. Bai, X.-D. Wang, *J. Chem. Eng. Data* **55** (2010) 2257
17. M. Chatterjee, R. Basu, P. Nandy, *J. Biosci.* **15** (1990) 145
18. M. N. Roy, L. Sarkar, B. K. Sarkar, *J. Serb. Chem. Soc.* **73** (2008) 1235
19. Y. Cheng, X. Tongwen, *Eur. J. Med. Chem.* **40** (2005) 1384
20. D. Brahman, B. Sinha, *J. Chem. Eng. Data* **56** (2011) 3073
21. M. N. Roy, B. Sinha, V. K. Dakua, *J. Chem. Eng. Data* **51** (2006) 590
22. M. N. Roy, B. Sinha, *J. Mol. Liq.* **133** (2007) 89
23. B. Sinha, V. K. Dakua, M. N. Roy, *J. Chem. Eng. Data* **52** (2007) 1768
24. D. O. Masson, *Philos. Mag.* **8** (1929) 218
25. R. K. Wadi, P. Ramasami, *J. Chem. Soc., Faraday Trans.* **93** (1997) 243
26. T. S. Banipal, D. Kaur, P. K. Banipal, *J. Chem. Eng. Data* **49** (2004) 1236
27. K. Belibagli, E. Agranci, *J. Solution Chem.* **19** (1990) 867
28. H. S. Harned, B. B. Owen, *The physical chemistry of electrolytic solutions*, 3rd Ed., Reinhold Pub., New York, 1964
29. F. J. Millero, in *Water and Aqueous Solutions: Structure, Thermodynamics, and Transport Processes*, R. A. Horne, Ed., Wiley-Interscience, New York, 1972
30. M. L. Parmar, D. S. Banyal, *Indian J. Chem., A* **44** (2005) 1582
31. A. K. Covington, T. Dickinson, *Physical chemistry of organic solvent systems*, Plenum, New York, 1973
32. L. G. Hepler, *Can. J. Chem.* **47** (1969) 4617
33. C. Zhao, P. Ma, J. Li, *J. Chem. Thermodyn.* **37** (2005) 37
34. H. L. Friedman, C. V. Krishnan, in *Water: A comprehensive Treatise*, F. Franks, Ed., Vol. 3, Ch. 1, Plenum Press, New York, 1973
35. R. Bhatt, J. C. Ahlluwalia, *J. Phys. Chem.* **89** (1985) 1099
36. P. R. Mussini, P. Longhi, T. Mussini, S. Rondinini, *J. Chem. Thermodyn.* **21** (1989) 625
37. K. S. Pitzer, R. N. Roy, L. F. Silvester, *J. Am. Chem. Soc.* **99** (1977) 4930
38. A. G. Dickson, D. J. Wesolowski, D. A. Palmer, R. E. Mesmer, *J. Phys. Chem.* **94** (1990) 7978
39. N. N. Kuranova, S. V. Dushina, V. A. Sharnin, *Russ. J. Inorg. Chem.* **53** (2008) 1943
40. I. V. Terekhova1, N. A. Obukhova1, *J. Solution Chem.* **34** (2005) 1273

41. G. Jones, M. Dole, *J. Am. Chem. Soc.* **51** (1929) 2950
42. B. Sinha, P. K. Roy, B. K. Sarkar, D. Brahman, M. N. Roy, *J. Chem. Thermodyn.* **42** (2010) 380
43. D. Feakins, D. J. Freemantle, K. J. Lawrence, *J. Chem. Soc., Faraday Trans.* **70** (1974) 795
44. S. Glasstone, K. Laidler, H. Eyring, *The Theory of Rate Processes*, McGraw-Hill, New York, 1941.

Journal of the Serbian Chemical Society
JSCS@tmf.bg.ac.rs • www.shd.org.rs/JSCS
J. Serb. Chem. Soc. 78 (8) S95–S98 (2013) *Supplementary material*

SUPPLEMENTARY MATERIAL TO

Solution thermodynamics of aqueous nicotinic acid solutions in the presence of tetrabutylammonium hydrogen sulphate

ABHIJIT SARKAR and BISWAJIT SINHA*

Department of Chemistry, University of North Bengal, Darjeeling-734013, India

J. Serb. Chem. Soc. 78 (8) (2013) 1125–1240

TABLE S-I. Density (ρ) and viscosity (η) for aqueous solutions of nicotinic acid of different concentrations (c_{NA}) different at different temperatures

c_{NA} / mol dm^{-3}	T / K	$\rho\times10^{-3}$ / kg m^{-3}	η / mPa s
0.005	298.15	0.9972	0.879
	308.15	0.9941	0.717
	318.15	0.9903	0.578
0.010	298.15	0.9975	0.913
	308.15	0.9944	0.731
	318.15	0.9905	0.587
0.015	298.15	0.9977	0.929
	308.15	0.9947	0.754
	318.15	0.9908	0.609
0.020	298.15	0.9982	0.941
	308.15	0.9953	0.782
	318.15	0.9911	0.627

TABLE S-II. Molarities (c), densities (ρ), viscosities (η), apparent molar volumes (φ_V) and $(\eta_r - 1)/\sqrt{c}$ for Bu_4NHSO_4 in aqueous solutions of nicotinic acid of different concentrations (c_{NA})

c / mol dm^{-3}	$\rho\times10^{-3}$ / kg m^{-3}	η / mPa s	$\varphi_V^0\times10^6$ / m^3 mol^{-1}	$(\eta_r - 1)/\sqrt{c}$ / mol$^{-1/2}$ dm$^{3/2}$
c_{NA} = 0.000 mol dm^{-3}				
T = 298.15 K				
0.0200	0.9977	0.884	308.94	0.0048
0.0360	0.9981	0.896	311.84	0.0331
0.0520	0.9984	0.907	314.88	0.0817
0.0680	0.9987	0.919	316.49	0.1232
0.0840	0.9989	0.928	318.68	0.1457
0.1000	0.9991	0.939	320.18	0.1726

* Corresponding author. E-mail: biswachem@gmail.com

TABLE S-II. Continued

c / mol dm^{-3}	$\rho\times10^{-3}$ / kg m^{-3}	η / mPa s	$\varphi_V^0\times10^6$ / m^3 mol^{-1}	$(\eta_r-1)/\sqrt{c}$ / mol$^{-1/2}$ dm$^{3/2}$
c_{NA} = 0.000 mol dm^{-3}				
T = 308.15 K				
0.0200	0.9947	0.729	306.36	0.0943
0.0359	0.9952	0.739	309.62	0.1438
0.0518	0.9956	0.751	311.66	0.1930
0.0678	0.9959	0.764	314.27	0.2381
0.0838	0.9962	0.776	315.88	0.2718
0.0997	0.9964	0.790	317.96	0.3108
T = 318.15 K				
0.0199	0.9910	0.600	304.82	0.0476
0.0357	0.9915	0.612	307.52	0.1421
0.0516	0.9919	0.623	310.59	0.1994
0.0676	0.9923	0.633	312.26	0.2388
0.0835	0.9926	0.642	314.46	0.2671
0.0993	0.9928	0.654	316.95	0.3088
c_{NA} = 0.005 mol dm^{-3}				
T = 298.15 K				
0.0200	0.9978	0.902	310.41	0.1850
0.0360	0.9982	0.916	312.64	0.2218
0.0520	0.9985	0.935	315.42	0.2794
0.0680	0.9988	0.957	316.89	0.3403
0.0840	0.9990	0.985	319.00	0.4161
0.1000	0.9992	1.016	320.44	0.4929
T = 308.15 K				
0.0200	0.9948	0.741	307.85	0.2367
0.0359	0.9953	0.760	308.76	0.3165
0.0518	0.9956	0.783	312.99	0.4044
0.0678	0.9959	0.808	315.28	0.4874
0.0838	0.9963	0.831	315.49	0.5492
0.0997	0.9965	0.856	317.63	0.6139
T = 318.15 K				
0.0199	0.9911	0.604	305.81	0.3188
0.0357	0.9916	0.616	308.62	0.3479
0.0516	0.9920	0.628	310.56	0.3808
0.0676	0.9924	0.637	312.23	0.3926
0.0835	0.9926	0.647	315.03	0.4131
0.0994	0.9929	0.661	316.94	0.4555
c_{NA} = 0.010 mol dm^{-3}				
T = 298.15 K				
0.0200	0.9979	0.932	315.34	0.1471
0.0360	0.9983	0.957	317.01	0.2539
0.0520	0.9986	0.982	318.43	0.3314
0.0680	0.9988	1.003	320.65	0.3780

TABLE S-II. Continued

c / mol dm^{-3}	$\rho\times10^{-3}$ / kg m^{-3}	η / mPa s	$\varphi_V^0\times10^6$ / m^3 mol^{-1}	$(\eta_r-1)/\sqrt{c}$ / mol$^{-1/2}$ dm$^{3/2}$
c_{NA} = 0.010 mol dm^{-3}				
T = 298.15 K				
0.0840	0.9991	1.023	320.83	0.4157
0.1000	0.9993	1.048	321.96	0.4676
T = 308.15 K				
0.0200	0.9950	0.755	311.78	0.2321
0.0359	0.9954	0.775	313.72	0.3178
0.0518	0.9957	0.796	316.40	0.3907
0.0678	0.9960	0.819	317.87	0.4623
0.0838	0.9963	0.838	318.77	0.5056
0.0997	0.9966	0.854	319.36	0.5329
T = 318.15 K				
0.0199	0.9912	0.623	309.29	0.4347
0.0357	0.9916	0.633	311.39	0.4147
0.0516	0.9921	0.644	312.45	0.4275
0.0676	0.9925	0.661	313.66	0.4849
0.0835	0.9929	0.675	314.37	0.5188
0.0994	0.9932	0.691	315.86	0.5619
c_{NA} = 0.015 mol dm^{-3}				
T = 298.15 K				
0.0200	0.9981	0.950	320.26	0.1598
0.0360	0.9984	0.978	321.38	0.2779
0.0520	0.9987	1.005	321.81	0.3587
0.0680	0.9989	1.027	323.21	0.4045
0.0840	0.9991	1.050	324.08	0.4494
0.1000	0.9993	1.079	324.67	0.5106
T = 308.15 K				
0.0200	0.9952	0.769	318.71	0.1407
0.0359	0.9955	0.773	319.91	0.1329
0.0518	0.9958	0.796	320.77	0.2447
0.0678	0.9961	0.824	321.37	0.3565
0.0838	0.9963	0.847	322.04	0.4261
0.0997	0.9966	0.874	322.68	0.5040
T = 318.15 K				
0.0199	0.9914	0.630	314.78	0.2444
0.0357	0.9918	0.642	315.82	0.2868
0.0516	0.9922	0.649	316.27	0.2891
0.0676	0.9926	0.659	316.55	0.3158
0.0835	0.9929	0.670	317.89	0.3466
0.0994	0.9932	0.684	318.81	0.3906

TABLE S-II. Continued

c / mol dm^{-3}	$\rho\times10^{-3}$ / kg m^{-3}	η / mPa s	$\varphi_V^0\times10^6$ / m^3 mol^{-1}	$(\eta_r-1)/\sqrt{c}$ / mol$^{-1/2}$ dm$^{3/2}$
c_{NA} = 0.020 mol dm^{-3}				
T = 298.15 K				
0.0200	0.9985	0.964	323.72	0.1728
0.0360	0.9987	0.987	324.53	0.2576
0.0520	0.9989	1.014	325.4	0.3402
0.0680	0.9991	1.034	326.57	0.3789
0.0840	0.9992	1.057	327.26	0.4253
0.1000	0.9994	1.088	327.85	0.4940
T = 308.15 K				
0.02	0.9957	0.796	321.53	0.1266
0.0359	0.9960	0.822	322.40	0.2699
0.0518	0.9962	0.847	323.27	0.3652
0.0678	0.9964	0.870	323.94	0.4322
0.0838	0.9966	0.890	324.68	0.4771
0.0997	0.9968	0.915	325.20	0.5386
T = 318.15 K				
0.0199	0.9916	0.653	317.30	0.2939
0.0358	0.9920	0.663	317.94	0.3034
0.0517	0.9923	0.675	318.56	0.3367
0.0676	0.9926	0.686	319.15	0.3619
0.0834	0.9930	0.696	319.80	0.3811
0.0994	0.9933	0.707	320.27	0.4047

Journal of the Serbian Chemical Society
JSCS-info@shd.org.rs • www.shd.org.rs/JSCS
J. Serb. Chem. Soc. 78 (8) 1241–1258 (2013)
JSCS–4494
UDC **Phragmites australis*+546.47/.49'56'815:627.81.000.57:581.9(497.16)
Original scientific paper

Seasonal changes in metal accumulation and distribution in the organs of *Phragmites australis* (common reed) from Lake Skadar, Montenegro

VLATKO KASTRATOVIĆ[1]*, SLAĐANA KRIVOKAPIĆ[1], DIJANA ĐUROVIĆ[2#] and NADA BLAGOJEVIĆ[3]

[1]*Faculty of Natural Sciences and Mathematics, University of Montenegro, G. Washington Street, P. O. Box 5455, 81000 Podgorica, Montenegro,* [2]*Institute of Public Health of Montenegro, Ljubljanska bb, 81000 Podgorica, Montenegro and* [3]*Faculty of Metallurgy and Technology, University of Montenegro, G. Washington Street, P. O. Box 5455, 81000 Podgorica, Montenegro*

(Received 16 October, revised 8 December 2012)

Abstract: Due to its ability to accumulate metals, availability throughout the year and large biomass, *Phragmites australis* (common reed) is suitable for biomonitoring studies for the evaluation of load levels of trace metals in aqueous ecosystems. The heavy metals concentration in *P. australis* tissue can be several ten to several thousand times higher than those in the surrounding water. In this study, the content of heavy metals (Cd, Co, Cr, Cu, Mn, Ni, Pb, Zn, Sr and V) in sediment, water and different organs of *Phragmites australis* collected from Lake Skadar, Montenegro, during different seasons of the year 2011, were examined. The highest concentrations of Sr were found in the leaves, while the other studied metals showed their highest concentrations in the roots. Thus, *P. australis* is considered a root bioaccumulation species. For most metals, the concentrations in the roots and stems increased over time until the end of the growing season and then decreased, while the concentrations in the leaves increased even after the growing season of the plant. If *P. australis* is used for phytoremediation purposes, then it should be harvested after the growing season because then the concentrations of metals in the above-ground parts are maximal.

Keywords: phragmites australis; heavy metals; Lake Skadar; bioaccumulation; phytoremediation.

* Corresponding author. E-mail: vlatkok@ac.me
# Serbian Chemical Society member.
doi: 10.2298/JSC121026153K

INTRODUCTION

Water systems are the main destination of pollutants, directly or indirectly, and heavy metals are certainly the most important contaminants.[1] The ability of aquatic plants to accumulate heavy metals is being increasingly used for the evaluation of changes in aqueous systems resulting from environmental pollution.[2] The important role of aquatic flora results from the fact that the concentrations of metals in the macrophyte tissues can be 10^5 times higher than their concentration in the surrounding water.[3]

Chemical absorption and distribution of metals in plants depend on many factors: the plant species and its characteristics, the type of metal and its physical and chemical properties and ecological environmental factors.[4–8]

Unlike water and sediments, plants show significant changes in metal concentration over time. For phytomanagement, it is necessary to take into consideration seasonal and annual concentration changes in plants.[9–11] The use of macrophytes provides a relatively quick way to determine the space and time variations of the bioavailability of heavy metals, which makes plants superior compared to water or sediment samples.[12]

Immersed plants take up metals mainly by roots from the sediment, and considerably less by stem and the leaves from the water and air.[13] Based on a variety of trace metals translocation from roots to shoots, macrophytes form three groups:[14] 1) somewhat uniformly distributed between roots and shoots, *e.g.*, Zn, Mn, Ni and B; 2) usually more in the roots than in the shoots with moderate to sometimes large quantities in the shoots, *e.g.*, Cu, Cd, Co and Mo; 3) mostly in roots with very little in the shoots, *e.g.*, Pb, Sn, Ti, Ag and V. This groupation however may change with plant species, high levels of element in the sediment, location and testing season. The identification of the time that corresponds to maximum accumulation of heavy metals in the above-ground parts of plants is of importance for the optimization of the potential of plants for metal removal.

Phragmites sp. is one of the most widely distributed species in the world. It grows fast, is easy to collect and find on the ground, and it can withstand extreme environmental conditions, including the presence of heavy metals.[15] It accumulates heavy metals both from sediment and water, concentrating them in its tissues and thus reflecting the degree of environmental pollution. It is a continually good bio-indicator over a longer investigation period. The biomass of the above-ground part is 700–4000 g m^{-2},[16] which makes it suitable for potential phytoremediation. Over the past two decades *P. australis* has been widely used in constructed wetlands for the treatment of industrial wastewaters containing metals.[17]

There are only a small number of studies concerning the concentration of trace metals in plant species of Lake Skadar,[18–20] and especially little data on their concentration in different parts of aquatic macrophytes and their seasonal variations.

In this study, the content of heavy metals (Cd, Co, Cr, Cu, Mn, Ni, Pb, Zn, Sr and V) in sediment, water and different organs of *P. australis* collected from Lake Skadar, Montenegro, during the different seasons of the year 2011 were investigated.

The aim of this study was to determine the dynamics of the distribution of metals in different organs of the plant *P. australis*, and particularly to determine the time of maximum accumulation in the above-ground tissue. Another aim was to use the chemical composition (heavy metals content) of the dominant plant species as an indicator of the degree of the metal load of water and lake sediment over a longer period.

EXPERIMENTAL

Study area

Lake Skadar (19°03′–19°30′E, 42°03′–42°21′N) is the largest lake on the Balkan Peninsula. It is located on the border between Montenegro and Albania. Two-thirds of the lake lies in Montenegro. During the summer, Lake Skadar has a surface of 370 km^2, which expands to 540 km^2 in the winter. The lake is 44 km long and 13 km wide.

Sediment samples from Lake Skadar were collected at 6 locations (Fig. 1): 1 – Raduš, 2 – Right estuary of Morača, 3 – Left estuary Morača, 4 – Plavnica, 5 – Crni Zar and 6 – Crnojevića River. The right and left estuaries of the Morača and the Plavnica and Crnojevića Rivers feed the Lake. The Plavnica and Crnojevića Rivers are popular tourist destinations, especially in the last few years. Raduš is the deepest of many underwater springs of the Lake, while Crni Zar is a special nature reservation.

Fig. 1. Location of the sampling station in Lake Skadar.

Sampling collection

The samples of sediments, water and *P. australis* were taken four times during 2011, from early April to late October, every 60 to 70 days, from 6 locations on Lake Skadar.

P. australis was sampled at locations with a high density and coverage of the plant under a clear sky with no wind. At each location of about 25 m^2, 3–4 whole healthy plants of similar size, shape and weight were sampled manually in order to repeat the results for each site.

Sediment and water samples were also taken from the same locations as *P. australis.* Sediment sampling was realize with an Ekman dredge from the depth of 0–20 cm. Water samples were collected from the depth of 0.5–1 m using 1.5 L PET bottles. The samples were stored in a refrigerator (5±2 °C).

Data analyzes

The sampled plant material was washed in the laboratory first with tap water, and then twice with deionized water. The plant parts were cut with stainless scissors into roots, stems and leaves of *P. australis*, for determination of the bioaccumulation diversity of the plant organs. The plant material was subsequently dried at 75 °C for 48 h and then ground into a fine powder and homogenized. In order to avoid the influence of the matrix, the samples were mineralized. Thus, the prepared samples (0.5±0.0001 g) were mineralized with a mixture of 5 mL HNO_3 and 2 mL H_2O_2 in a Milestone Ethos 1 Microwave digestion system. After digestion, the solutions were diluted with deionized water to a final volume of 25.0 mL.

Sediment samples were dried at 75 °C for 48 h under air in a dryer. The dried sediment samples were ground in an agate mortar and sieved to <1.5 mm. The sediment samples (0.5±0.0001 g) were mineralized under pressure and high temperature using a mixture of HCl:HNO_3:HF (6 mL:2 mL:1 mL). After mineralization, the solutions were diluted with deionized water to a final volume of 25.0 mL.

Water samples were filtered through a 0.45 μm Millipore filter and stored in 1 L plastic bottles after addition of 2 mL HNO_3.

All samples of plants parts, sediments and water were prepared three times. In each batch of ten samples, a blank solution was included. The concentrations of heavy metals (Cd, Cu, Co, Cr, Mn, Ni, Pb, Zn, Sr and V) were determined using the ICP-OES technique on a Spectro Arcos instrument. The analytical accuracy was determined using certified reference materials from the National Institute of Standards and Technology (USA), a standard for trace elements in lake sediments (SRM 2709) and for plants, Tea Leaves (INCT-TL-1). The recoveries were within 10 % of the certified values.

Statistical analysis

The Microsoft Excel 2000 package was used for the calculation of the mean, standard deviation and variation coefficient. One-way ANOVA with the value of $p < 0.05$ was performed between the content of each metal in roots, stems and leaves and between the content of each metal in some parts of *P. australis* with regard to the sampling season. If the differences between the mean values were significant at the 5 % level, the post hoc Duncan test was used to determine the minimum allowable differences between particular result groups. All calculations were performed using the SPSS (version 11.5) software package (SPSS Inc., Chicago, USA).

The ability of plants to absorb and accumulate metals from the growth media was evaluated using the bioconcentration factor (*BCF*). The *BCF* value was calculated as the ratio of the concentrations of metals in plants and sediments:

$$BCF = [\text{Metal}]_{\text{plant}}/[\text{Metal}]_{\text{sediment}}.$$

A higher *BCF* implies a greater phyto-accumulation ability of the plant.

The possibility of plants to transport metals from the roots to the above-ground organs was estimated using the translocation ability (*TA*). The value of the translocation ability was calculated as the ratio of the concentrations of metals in roots and a part of the plant:

$$TA = [\text{Metal}]_{\text{root}}/[\text{Metal}]_{\text{part of the plant}}.$$

A higher *TA* means a smaller translocation ability.

RESULTS

The determined values of the metal concentrations in water and sediment are given in Table I, respectively.

TABLE I. Seasonal minimal, maximal and average concentrations ± standard deviation (*SD*) of metals in water (mg L^{-1}) and sediment (mg kg^{-1})

Metal	Concentration type	Month			
		April	June	August	October
		Water			
Cd	–	<0.001	<0.001	<0.001	<0.001
Cu	Min.–max.	0.003–0.012	0.002–0.012	0.002–0.013	0.002–0.014
	Average ± *SD*	0.007±0.004	0.007±0.004	0.007±0.004	0.007±0.004
Co	–	<0.001	<0.001	<0.001	<0.001
Cr	–	<0.002	<0.002	<0.002	<0.002
Mn	Min.–max.	0.006–0.013	0.005–0.013	0.007–0.014	0.006–0.014
	Average ± *SD*	0.009±0.003	0.010±0.003	0.011±0.003	0.010±0.003
Ni	–	<0.001	<0.001	<0.001	<0.001
Pb	–	<0.005	<0.005	<0.005	<0.005
Zn	Min.–max.	0.002–0.008	0.002–0.007	0.003–0.008	0.003–0.008
	Average ± *SD*	0.005±0.002	0.005±0.002	0.005±0.002	0.005±0.002
V	Min.–max.	0.002–0.007	0.002–0.007	0.002–0.006	0.002–0.005
	Average ± *SD*	0.004±0.002	0.004±0.002	0.004±0.002	0.004±0.001
Sr	Min.–max.	0.023–0.047	0.019–0.046	0.020–0.052	0.020–0.051
	Average ± *SD*	0.035±0.009	0.034±0.010	0.035±0.011	0.037±0.012
		Sediment			
Cd	Min.–max.	0.27–0.66	0.29–0.63	0.28–0.65	0.28–0.65
	Average ± *SD*	0.40±0.15	0.41±0.14	0.41±0.14	0.40±0.15
Cu	Min.–max.	27.2–50.4	25.5–46.9	25.5–52.1	23.9–54.4
	Average ± *SD*	34.5±8.84	33.1±7.81	33.3±10.2	34.0±11.1
Co	Min.–max.	6.31–10.1	5.73–12.9	5.28–13.2	5.12–12.6
	Average ± *SD*	8.96±2.52	9.02±2.94	8.76±3.13	9.18±3.08
Cr	Min.–max.	42.4–127	42.3–117	39.8–122	35.6–126
	Average ± *SD*	69.7±31.4	67.0±27.6	68.7±30.2	68.2±32.0
Mn	Min.–max.	99.0–424	120–357	118–379	95.4–419
	Average ± *SD*	232±122	221±91.4	223±101	239±128
Ni	Min.–max.	29.3–131	34.8–110	30.1–113	34.6–125
	Average ± *SD*	79.0±44.3	73.1±36.3	74.5±40.6	83.4±47.6
Pb	Min.–max.	19.1–43.2	16.6–37.6	19.4–43.5	17.6–46.2
	Average ± *SD*	29.0±10.2	25.7±9.39	27.6±9.85	30.2±12.1

TABLE I. Continued

Metal	Concentration type	Month			
		April	June	August	October
		Sediment			
Zn	Min.–max.	47.6–117	56.1–135	59.1–128	53.2–108
	Average ± *SD*	75.4±24.0	79.1±29.7	76.2±26.1	73.8±19.7
V	Min.–max.	20.4–46.7	20.1–45.3	18.8–49.5	18.1–45.5
	Average ± *SD*	29.4±9.93	28.9±10.6	27.9±11.7	26.9±9.92
Sr	Min.–max.	17.7–101	20.4–101	18.2–113	16.8–105
	Average ± *SD*	55.1±30.6	55.8±30.7	56.2±34.2	57.6±32.3

Based on the results given in Table I, it could be concluded that there were no time variations of the results in the water and sediments, at the 95 % level of confidence. There were considerable space variations of the results, reflected in high standard deviation and variation coefficient, sometimes over 50 %. Low concentrations of metals were registered in the water samples. Cd, Co and Pb were below the *LOQ* value at all sampling locations, Cr at one location and Ni at three of the six sampling locations. The results for the individual parts of *P. australis* per season are given in Table II. It could be concluded that the concentrations of metals in water, sediment and the organs of *P. australis* differed significantly. Depending on the type of the sample, different trends of metal concentration reductions were registered:

- in water: Sr > Mn > Cu > Zn > V > Pb, Cr, Ni, Co, Cd
- in sediment: Mn > Ni ≈ Zn > Cr > Sr > Cu > Pb ≈ V > Co > Cd
- in root: Mn > Zn > Cu > Pb ≈ Ni > Cr > Sr > V > Co > Cd
- in stem: Mn > Zn > Cu > Pb > Sr > Cr ≈ Ni > V > Co > Cd
- in leaves: Mn > Zn> Sr > Cu > Pb > Ni > Cr > Co > V > Cd

In sediments and some parts of *P. australis*, the highest concentrations of Mn and Zn were found, the concentrations of which in the sediments did not differ statistically from those of Ni. Vanadium, Co and Cd showed the lowest concentrations in sediment and some parts of *P. australis* (Tables I and II).

Regardless of the sampling period, Zn, Cd and Co followed the concentration trend: root > leaf > stem (Table II). Ni, Pb, Mn and Cr in the first three sampling periods followed the trend: root > stem > leaf. After the vegetation period, their concentrations in leaves were higher than those in the stems. By the end of vegetation period, the highest concentrations of Cu were found in the roots, but at the end of October, the highest concentrations were registered in the leaves. Regardless of the sampling period, the highest concentrations of Sr were registered in leaves, then in the roots and finally in stems of *P. australis*. Almost all the V during the entire investigation period was stored in roots of the plant (Table II).

The seasonal changes in the bioconcentration factors (*BCF*) for the roots, stems and leaves are shown in Fig. 2. The BCF_{root} for all the studied metals increased until the end of the growing season and then decreased, except for Cd and Pb, which slightly increased even after completion of vegetation. The accumulation of metals by roots from the sediment follows the order: Mn > Zn > Cd > Cu > Co > Pb > V > Sr > Cr > Ni. The order is somewhat similar even considering the overall bioaccumulation for all plant parts, *i.e.*, average during the investigation period: Mn ≈ Zn ≈ Cu > Cd > Sr > Pb > Ni ≈ V ≈ Cr. Similarly, to root bioaccumulation, the BCF_{stem} increased from April to August, while it decreased in October. The BCF_{leaf} constantly increased during and after the vegetation period.

TABLE II. Seasonal changes in metal concentrations (min.–max., average ± *SD*, mg per kg of dry weight) in the parts of *P. australis*; minimal and maximal concentrations and average concentrations ± standard deviation (*SD*)

Metal	Part	Month			
		April	June	August	October
Cd	Root	0.05–0.11	0.07–0.24	0.11–0.35	0.12–0.39
		0.08±0.02 a[a] (b)[b]	0.13±0.06 a (ab)	0.22±0.08 a (ab)	0.24±0.10 a (ab)
	Stem	0.02–0.08	0.03–0.11	0.04–0.12	0.04–0.14
		0.06±0.02 a (a)	0.07±0.03 b (a)	0.09±0.03 b (a)	0.10±0.03 b (a)
	Leaf	0.02–0.09	0.04–0.10	0.07–0.13	0.09–0.17
		0.06±0.03 a (b)	0.08±0.02 b (b)	0.10±0.03 b (a)	0.12±0.03 b (a)
Cu	Root	6.68–14.5	9.00–17.7	16.9–23.0	12.4–20.5
		8.92±2.89 a (c)	12.3±3.91 a (bc)	19.3±2.04 a (a)	16.9±3.53 a (ab)
	Stem	3.46–13.4	8.45–15.5	8.60–17.7	7.13–16.1
		6.95±3.61 a (b)	11.2±3.03 a (a)	11.5±3.41 b (a)	10.6±2.95 b (a)
	Leaf	4.75–13.6	4.21–16.4	6.79–20.7	14.9–28.7
		8.72±3.44 a (b)	10.1±4.98 a (b)	12.4±5.99 b (ab)	20.6±5.38 a (a)
Co	Root	0.40–0.90	0.20–2.96	3.86–8.20	2.58–5.40
		0.60±0.19 a (c)	1.34±1.03 a (bc)	5.57±1.98 a (a)	3.71±1.03 a (ab)
	Stem	0.04–0.09	0.05–0.13	0.07–0.29	0.04–0.24
		0.06±0.02 b (c)	0.09±0.04 b (bc)	0.16±0.09 b (a)	0.14±0.08 b (ab)
	Leaf	0.08–0.24	0.12–0.40	0.19–0.92	0.18–0.98
		0.14±0.06 b (a)	0.20±0.10 b (a)	0.41±0.26 b (a)	0.46±0.28 b (a)
Cr	Root	1.25–4.73	3.27–19.1	4.00–12.4	2.37–10.7
		3.32±1.21 a (c)	10.3±6.31 a (a)	7.98±2.80 a (ab)	5.90±2.32 a (bc)
	Stem	0.49–1.77	1.28–6.16	0.80–3.75	0.40–3.20
		1.05±0.52 b (b)	2.68±1.76 b (a)	2.09±1.22 b (ab)	1.26±1.03 b (b)
	Leaf	0.21–0.38	0.28–0.88	0.41–1.09	0.70–1.99
		0.28±0.06 b (b)	0.48±0.22 b (ab)	0.66±0.24 b (ab)	1.24±0.43 b (a)
Mn	Root	66.1–143	52.4–279	117–239	61.4–176
		95.8±37.1 a (b)	148±84.9 a (ab)	181±52.4 a (a)	95.8±42.7 a (b)
	Stem	11.6–47.1	27.4–76.0	33.9–90.9	23.8–94.8
		30.2±12.3 b (b)	40.6±18.5 b (ab)	54.4±20.0 b (a)	47.3±27.4 a (ab)

TABLE II. Continued

Metal	Part	Month			
		April	June	August	October
Mn	Leaf	11.0–22.1	16.9–33.5	23.4–83.5	45.1–169
		16.5±4.49 b (c)	23.8±7.47 b (bc)	43.4±21.6 b (b)	86.1±46.0 a (a)
Ni	Root	0.89–7.79	3.54–9.19	5.02–13.5	3.78–10.7
		4.38±2.91 b (d)	6.50±2.59 a (c)	9.81±3.32 a (a)	8.00±3.00 a (b)
	Stem	0.49–2.28	1.09–2.29	1.49–3.58	1.28–2.20
		1.02±0.68 b (b)	1.81±0.48 b (ab)	2.42±0.74 b (a)	1.72±0.35 b (ab)
	Leaf	0.30–2.16	0.50–2.39	1.09–2.96	1.96–4.46
		1.31±0.65 b (b)	1.52±0.72 b (b)	2.11±0.61 b (ab)	3.00±1.08 b (a)
Pb	Root	1.47–6.46	3.90–9.01	4.64–13.1	4.36–14.8
		3.68±1.84 a (c)	6.30±1.79 a (bc)	8.94±2.98 a (ab)	10.1±4.46 a (a)
	Stem	0.58–4.26	3.09–6.26	4.48–9.18	3.54–9.93
		2.04±1.71 ab (c)	4.22±1.15 ab (b)	6.75±1.69 a (a)	6.64±2.50 a (a)
	Leaf	0.32–1.67	0.20–6.05	1.38–9.76	5.43–11.4
		0.88±0.45 b (b)	2.63±2.18 b (b)	6.57±3.07 a (a)	9.67±2.15 a (a)
Zn	Root	18.4–40.2	25.3–49.1	36.3–72.9	21.1–79.4
		28.4±8.33 a (c)	37.5±9.15 a (b)	52.1±15.8 a (a)	45.8±21.6 a (ab)
	Stem	5.34–22.5	17.1–29.1	13.0–31.7	8.28–33.4
		14.8±5.68 b (b)	24.4±4.21 b (a)	22.0±7.67 b (a)	16.3±9.68 b (b)
	Leaf	12.8–31.7	13.1–44.8	17.4–48.4	9.42–48.3
		22.4±6.86 ab (b)	29.0±11.1 ab (a)	30.7±11.1 b (a)	25.2±12.9 ab (ab)
V	Root	0.29–2.19	1.58–4.05	6.91–9.24	2.66–8.12
		1.28±0.66 a (c)	2.62±0.84 a (c)	8.15±0.95 a (a)	4.50±2.04 a (b)
	Stem	0–0.18	0.13–0.32	0.18–0.69	0.10–0.23
		0.12±0.07 b (b)	0.22±0.07 b (ab)	0.30±0.19 b (a)	0.16±0.04 b (b)
	Leaf	0–0.20	0.15–0.37	0.04–0.31	0.02–0.12
		0.09±0.07 b (c)	0.23±0.08 b (a)	0.15±0.10 b (b)	0.05±0.04 b (d)
Sr	Root	1.87–5.62	3.69–6.53	4.76–13.7	3.14–10.8
		3.80±1.30 a (b)	5.28±1.13 b (ab)	8.86±3.51 b (a)	5.93±2.71 b (ab)
	Stem	0.77–4.13	1.87–5.81	1.97–5.14	1.99–9.28
		2.78±1.19 a (b)	3.41±1.54 b (ab)	3.62±1.34 b (ab)	5.54±2.50 b (a)
	Leaf	0.58–11.7	5.56–26.9	21.5–34.9	25.5–50.8
		6.45±4.13 a (c)	14.4±8.12 a (bc)	27.9±5.79 a (ab)	35.8±9.14 a (a)

[a]The values of individual metals with the same first letter(s) are not significantly different at $p = 0.05$ in the column (*i.e.*, between the different parts of the plant); [b]the values in individual parts of the plant with the same letter(s) in parentheses are not significantly different at $p = 0.05$ in the row (*i.e.*, between seasons)

The values of metal translocation ability are given in Table III. Translocation between different parts of *P. australis* depended on the type of metal and the sampling period. All the investigated metals showed the highest translocation from the stem to the leaves, particularly in the post-growing season. From the root to the above-ground organs, the most mobile metals were Sr and Cu, while Cr, V and Co showed the lowest mobilities.

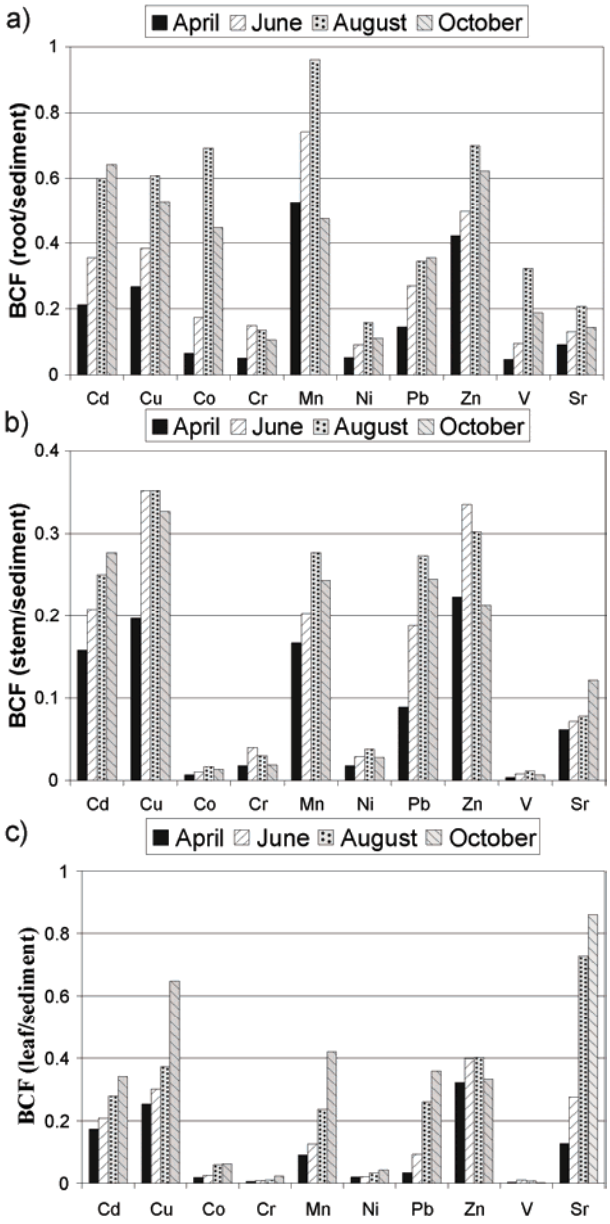

Fig. 2. Seasonal changes in the bioconcentration factor (*BCF*): a) root, b) stem and c) leaf.

DISCUSSION

Cd is a toxic element. In sediment, water and plants it comes mainly from natural sources. Possible anthropogenic input of Cd to the ecosystem of Lake Skadar comes from a metal industry located in the surroundings of the lake, as well

as from the use of agricultural fertilizers, pesticides and combustion of fossil fertilizers. The Cd contents in the sediment and parts of the plant were the lowest of all the investigated elements. Except in April, statistically the content of Cd in roots was significantly higher than in the above-ground parts of *P. australis*. Scierup and Larsen[21] reached a similar conclusion, as did Bonanno and Guidice.[22] Fediuc and Erdei[23] found higher Cd concentration in the shoots of *P. australis*.

TABLE III. Seasonal changes in the translocation ability (TA)

Metal	Part	Month			
		April	June	August	October
Cd	Root/stem	1.53	2.01	2.51	2.60
	Root/leaf	1.74	2.09	2.21	1.89
	Stem/leaf	1.14	1.04	0.88	0.73
Cu	Root/stem	1.58	1.18	1.76	1.68
	Root/leaf	1.15	1.55	1.82	0.86
	Stem/leaf	0.73	1.31	1.03	0.51
Co	Root/stem	10.1	18.0	41.4	37.1
	Root/leaf	4.94	7.17	18.1	11.2
	Stem/leaf	0.49	0.40	0.44	0.30
Cr	Root/stem	4.10	4.64	5.28	6.39
	Root/leaf	12.1	25.8	12.8	5.34
	Stem/leaf	2.95	5.56	2.42	0.84
Mn	Root/stem	3.49	4.08	3.81	2.28
	Root/leaf	6.00	6.07	5.03	1.16
	Stem/leaf	1.72	1.48	1.32	0.51
Ni	Root/stem	5.32	3.69	4.11	4.65
	Root/leaf	3.42	4.74	4.88	2.80
	Stem/leaf	0.64	1.28	1.19	0.60
Pb	Root/stem	2.74	1.52	1.38	1.63
	Root/leaf	6.22	7.52	1.93	1.18
	Stem/leaf	2.27	4.95	1.40	0.72
Zn	Root/stem	2.13	1.60	2.50	3.36
	Root/leaf	1.36	1.42	1.75	1.93
	Stem/leaf	0.64	0.88	0.7	0.57
V	Root/stem	8.98	12.3	33.0	31.8
	Root/leaf	16.7	12.6	95	165
	Stem/leaf	1.86	1.02	2.88	5.19
Sr	Root/stem	1.51	1.73	2.51	1.24
	Root/leaf	1.13	0.54	0.32	0.16
	Stem/leaf	0.75	0.31	0.13	0.13

There were no significant seasonal changes in the Cd concentrations in the stems and leaves of *P. australis*, while the concentration of Cd in the roots increased until the end of the vegetation period (Table II). The accumulation factor showed a similar trend (Fig. 2). The accumulation at the end of the exa-

mination period was higher probably due to decreased metabolic processes and smaller changes in plant biomass. Thus, with a similar absorption or translocation and bioavailability of metals, the concentrations changed significantly.

Cu is an important essential microelement for plants, but it can be toxic at higher concentrations. Cu contributes to several physiological processes in plants.[24]

In the investigated samples of *P. australis*, the lowest average concentration of Cu was recorded in the stems in April and the highest in the leaves in October (Table II). Numerous studies agreed on Cu accumulation in the root of *P. australis.* However, the conclusions about the further fate of Cu, *i.e.*, about its translocation through the plant, were different. The values of Cu accumulation in roots and above-ground parts of *P. australis* taken from Lake Skadar were similar in April and June. Sampling in August showed greater accumulation in roots, while the concentrations in stems and leaves were similar (Table II). In October, the concentration of Cu in the leaves was higher than in the roots and stems, which is in agreement with the statement of Windham *et al.*[25] Yongxia *et al.*[26] found the following Cu trend: sediment > above-ground part > underground part in *P. australis*. Fitzgerald *et al.*[27] found that *P. australis* translocated Cu more to the shoots. Bragato *et al.*[6] found that the accumulation of Cu in the leaves of *P. australis* was comparable to those measured in the stems and rhizome from July to October.

It can be assumed that the plant has an effective translocation root–shoots system, which is activated at the end of the growing season, allowing a higher concentration of elements in the aging tissues. In this way, plants can eliminate heavy metals through phonem during the winter.[28]

Co, after Cd, is the least present of the examined elements in the sediment of Lake Skadar, in roots and stems of *P. australis*, and after V in the leaves. Co showed relatively high root/sediment mobility in August and October (Fig. 2a). A similar mobility Co from sediment to roots was found by Bonanno[29] in Italy and Kumar *et al.*[30] in India.

However, the translocation of Co within *P. australis* was low (Table III). Co has the lowest root/stem translocation of the analyzed elements throughout the whole investigation period. Bonanno[29] also found relatively low translocation of Co through the organs of *P. australis*.

It is not completely clear if Co is essential for higher plants, although there is some evidence that it favorably effects plant growth.[31] However, Co is one of the most important toxic metals, and the fact that Co was mostly absorbed by the roots might mean that the root acted as a filter for undesirable effects on other organs of the plant. The high accumulation in the roots could be a reaction of the plant to the toxicity of metals, which are immobilized in the vacuoles of the roots.[32]

Cr is not essential for plants and it is toxic even at low concentrations.[33] In these investigations, Cr had the lowest bioaccumulation capacity of the examined elements (Fig. 2) in April, August and October. The average values of the *BCF* for Cr during the entire investigation period, together with Ni and V (Fig. 2), also were the lowest. The results of this study show that most of the adopted Cr was found in the roots (Table II). The highest root and stem accumulation was recorded in June, and then decreased. The Cr concentration in the leaves of *P. australis* increased slightly during the entire investigation period.

Bragato *et al.*[6] found Cr was accumulated in the stems and rhizome of *P. australis* mostly in July, and then decreased and became constant from August to December.

In addition to its lower bioaccumulation compared to the other elements, Cr also showed low mobility, as did Co and V (Table III). During the growing season, the translocation ratio decreased (Table III), indicating limited transport of toxic metals from the roots to the shoots. Some authors[34–36] indicated low mobility of Cr from roots to shoots and leaves. It is obvious that there is a physiological barrier, *i.e.*, the absence of a transport mechanism of this element from roots to the green parts of the plant. Relatively low concentration of Cr in foliar tissues during all the sampling period is probably the result of the need of the plant to prevent pollution of its photosynthetic apparatus, as suggested by other authors.[37,38]

Mn is an essential nutrient for plants. It is a functional component of nitrate assimilation and indispensable element of many enzyme systems in plants.

Mn is the most abundant of all the investigated elements in the sediment of Lake Skadar and in all parts of *P. australis* (Tables II and III). After Zn, together with Cu, it has the highest bioaccumulation capacity, as well as the average value for the entire investigation period (Table II). The largest amount of accumulated Mn is in the roots, but a significant part is translocated to the stems and leaves. Both, space and time variations of Mn content are present, except between some organs of *P. australis.* Duman *et al.*,[39] of the seven investigated metals, also found the highest concentration of Mn in the sediment and some parts of *P. australis.* During all the sampling period, the Mn concentration in the roots of *P. australis* was higher than in the sediment. Bonanno and LoGiudice,[22] of the eight examined elements, also found the highest concentration of Mn in each organ of *P. australis.*

There is a tendency of many elements to show their highest concentration at the end of the growing season due to continuous accumulation during vegetation. Nikolaidis *et al.*[9] reported that heavy metals showed increased accumulation in *P. australis* during the growing season, with the maximum values in August and September, and then continuously decrease. Marchand *et al.*[17] evidenced more active metabolism of the plants in the summer than in the winter.

Although Khan and Moheman[40] were of the opinion that Ni was not necessary for healthy plant growth, recent research suggests that Ni is an essential element in many plant species.[41] It helps in the transport of oxygen, stimulates metabolism and it is a key metal for some enzymatic systems of some plants.[42]

According to these studies, Ni is a poorly accumulated element of sediment and, together with Cr and V, has the lowest bioconcentration ratio. The *BCF* for Ni had a maximum value in August, and as the sum of the three *BFC*s (Fig. 2) its value was 0.23. Kumar *et al.*[30] gave a value of *BCF* = 1.17 for *P. australis.* Duman *et al.*[39] found in spring and summer the *BCF* was less than 1, while it was greater than 1 in autumn and winter.

These results show an increase in the concentration of Ni in the plant during the growing season, while the concentration decreased in October (Table II). Most of accumulated Ni was found in the root. The concentrations in the stems and leaves were similar during season, with slightly higher content found in the leaves in October. Bragato *et al.*[6] examined *P. australis* from July to December and reported low Ni contents in leaves from July to October, while in December, the content was 10 times higher.

The mobility of Ni in plants varies among the species, from mobile[43,44] in some plants to immobile[45] in others. In the present investigation, the ratio root/ /leaf and root/stem varied depending on the season (Table III).

Pb is a potentially dangerous and toxic metal for most forms of life, and it is relatively accessible to aquatic organisms. Pb is particularly present in aquatic environments in areas with heavy traffic and neighboring cities.

In these tests, bioaccumulation ability of three investigated organs of *P. australis* for Pb increased during the whole investigation period (Fig. 2) and the sum of all three *BCF* values (Fig. 2) reached a value close to 1 in August and October. The average *BCF* value was 0.66 during the whole investigation period. Kumar *et al.*[30] found *BCF* = 0.59.

Most of the absorbed Pb was in the roots and the amount significantly increased during the season (Table II). The concentration in the stems increased significantly until August but thereafter remained almost constant until October. The concentration of Pb in the leaves increased significantly from April to October.

The absorbed Pb, mainly from sediment, was mostly translocated to the stems during the investigation period with the highest *TA* in August (Table III). The translocation from roots to leaves was low during April and June, while in August and October, it is significantly higher. Several papers[27,46,47] indicate great mobility of Pb through the organs of *P. australis* and its translocation to the shoots. On the contrary, other papers[34,35,48] evidenced the highest concentration of Pb in the roots, while only small amounts were transported to other parts of *P. australis*.

The significantly increased concentration ratios leaf/root in August and October were mainly caused by the increased mobility in the plant, but it could also be the result of foliar adsorption of the metal during the peak tourist season on Lake Skadar and usage of leaded gasoline by small boats and boats.

Zn is an essential and useful element for plants, mainly as a part of various metallo-enzymes. In most aquatic ecosystems, Zn^{2+} can be toxic for the organisms.

Among the examined elements, Zn was the most abundant element after Mn, in sediment and some parts of *P. australis* (Tables II and III). According to the present study, the roots of *P. australis* actively adsorbed Zn, which contained the most Zn during all the sampling period. The sum of the bioconcentration factors for Zn was the highest of all the investigated elements during April and June (Fig. 2) and the average values were the highest during the whole investigation period. Apart from April, when the value was ≈1, in the other seasons the *BCF* value was > 1. The greatest bioaccumulation was noticed at the end of the growing season. Kumar *et al.*[30] reported a *BCF* value of 1.79.

A significant translocation of Zn from the roots to the above-ground organs was registered. The average seasonal ratio root/stem was 2.39, while root/leaf ratio was 1.61 (Table III). Baldantoni *et al.*[35] found a root/leaf ratio of 4.2, while the root/shoot ratio was 1.6. Świerk Szpakowska[46] reported low Zn mobility, with a rhizome/leaf ratio of 3.7.

The distribution of metals in some parts of the plant is the result of differences in the amount and rate of metals input, primarily by root pressure and their release into the environment, mainly through the transpiration of the leaves.[49,50] Some metals are accumulated in roots, probably because of some physiological barriers for the transport of toxic elements in traces. The metals essential for metabolic needs are easily transported to the above-ground parts of the plant.

In recent years, V, together with some other metals, has become a point of increased interest due to its negative impact on the environment.[31]

The bioaccumulation of V, together with Ni and Cr, was the lowest during the investigated period (Fig. 2). The average *BCF* value of during the season was 0.18, almost identical to the value reported by Bonanno.[29] Almost whole amount of the accumulated V was found in roots of *P. australis* and significantly highest concentration was recorded in August (Table II). The phytotoxic level of V in roots in August and low mobility indicate that the root is tolerant to this metal and acts as a filter for the prevention of its toxic distribution in the plant. The translocation of V from roots to stems was, after Co, the lowest among the investigated elements, (Table III). The translocation of V from the underground part to leaves was the lowest among the studied metals. Variations in concentrations during the season in the stems and leaves, as well as of the maximum values during and at the end of the growing season, were noticed.

Bonanno[29] found V only in the underground organs of *P. australis* so that roots disabled its transport to other organs. Soluble forms of V in the sediment are quickly taken up by the roots, and, as well as some other plants, P. *australis* showed great ability to accumulate this metal in the roots.[24]

The absorption of Sr from sediment by *P. australis* in April and June was insignificant, while the sum of the three *BCF* values (Fig. 2) was ≥ 1 in August and October. The highest concentration of Sr was registered in October in the leaves (Table II). The concentrations of Sr in the parts of *P. australis* in April were similar, while from June to October, they were much higher in the leaves compared to in the stems and roots (Table II). The translocation of Sr from the roots to the stems was the highest among the analyzed elements in April and October, while it was highest from the roots to leaves and from stems to leaves from June to October (Table III). Bonanno[29] found the lowest bioaccumulation of Sr among the investigated metals. At the same time, Sr showed great mobility within the plant, which is consistent with the results of this study, taking in consideration the mean values during the season.

Underground organs, especially the roots, are mostly places for the storage of excess trace metals, but it is known that various trace metals are deposited even in the leaves.[51] The highest concentrations of Sr are common at the tops of the plants.[24]

CONCLUSIONS

The concentration of metals in various organs of *P. australis* varies depending on the location and time of sampling. For most metals, the concentrations in the roots and stems increased over time until the end of the growing season and then decreased, while the concentrations in leaves increased even after the period of plant growth. The results of this study showed that the concentrations of five (Cd, Cu, Mn, Zn and Sr) of the ten studied metals were higher in the plant than in sediment during and after the growing season. At the same time, the concentrations of metals in the plants were much higher than those in the water, which indicates sediment as the major source of the metals absorbed by the plant roots. The highest concentrations of Sr were found in leaves, while all other studied metals, the highest concentrations were found in the roots. Thus, *P. australis* could be considered a root bioaccumulation species. However, significant concentrations of the metals were found in both the stems and leaves. Thus, in addition to the absorption mechanism by root, transfer to the shoots must be taken into consideration. Generally, metal mobility through the plant, from roots to leaves, is generally higher than from sediment to the plant.

Due to its ability to accumulate metals, availability throughout the year and its large biomass, *P. australis* is suitable for biomonitoring studies for the evaluation of contamination of the lake with trace metals. If *P. australis* is used for

phytoremediation purposes, then it should be harvested after the growing season because the concentration of metals in the above-ground parts is then maximal.

Although the results show that the toxic values of the investigated heavy metals in Lake Skadar are not alarming at present, the control of possible anthropogenic inputs is recommended. For several years, the surrounding factories have not been working or have been working at reduced capacity; hence, the greatest attention should be paid to the prevention, control and drainage of the metal load from surrounding farms and municipal water utilities.

И З В О Д

СЕЗОНСКЕ ПРОМЕНЕ АКУМУЛАЦИЈЕ И ТРАНСЛОКАЦИЈЕ МЕТАЛА У ОРГАНИМА *Phragmites australis* (ТРСКА) ИЗ СКАДАРСКОГ ЈЕЗЕРА, ЦРНА ГОРА

ВЛАТКО КАСТРАТОВИЋ[1], СЛАЂАНА КРИВОКАПИЋ[1], ДИЈАНА ЂУРОВИЋ[2] и НАДА БЛАГОЈЕВИЋ[3]

[1]Природно–математички-факултет, Универзитет Црне Горе, Ц. Вашингтона, п. пр. 5455, 81000 Подгорица, Црна Гора, [2]Институт за јавно здравље Црне Горе, Љубљанска бб, 81000 Подгорица, Црна Гора и [3]Металуршко–технолошки факултет, Универзитет Црне Горе, Ц. Вашингтона, п. пр. 5455, 81000 Подгорица, Црна Гора

Phragmites australis (трска) је због способности акумулације метала, доступности током целе године и велике биомасе подесан у студијама биомониторинга за процену оптерећења воденог еко-система траговима метала. Концентрација тешких метала у ткиву *P. australis* може бити неколико десетина до неколико хиљада пута већа него у околној води. У овој студији испитиван је садржај тешких метала (Cd, Co, Cr, Cu, Mn, Ni, Pb, Zn, Sr и V) у седименту, води и различитим органима *Phragmites australis* сакупљеним из Скадарског језера, Црна Гора, током различитих сезона 2011. године. Највеће концентрације Sr нађене су у листу а сви остали испитивани метали имају највећу концентрацију у корену што истиче *P. australis* као корен биоакумулаторску врсту. Код већине метала концентрација у корену и стаблу се повећава током времена до краја вегетационог периода а након тога опада, док се концентрација у лишћу повећава и након периода раста биљке. Уколико се *P. australis* користи и у фиторемедијационе сврхе, онда жетву треба извршити након сезоне раста јер је тада максимална концентрација метала у надземним деловима.

(Примљено 16. октобра, ревидирано 8 децембра 2012)

REFERENCES

1. S. Dhote, S. Dixit, *Environ. Monit. Assess.* **152** (2009) 149
2. M. Jastrzębska, P. Cwynar, R. Polechoński, T. Skwara, *Pol. J. Environ. Stud.* **19** (2010) 243
3. P. H. Albers, M. B. Camardese, *Environ. Toxicol. Chem.* **12** (1993) 959
4. T. Sawidis, J. Stratis, G. Zachariadis, *Sci. Total Environ.* **102** (1991) 261
5. S. Susarla, V. F. Medina, S. C. McCutcheon, *Ecol. Eng.* **18** (2002) 647
6. C. Bragato, M. Schiavon, R. Polese, A. Ertani, M. Pittarello, M. Malagoli, *Desalination* **246** (2009) 35
7. D. Demirezen, A. Aksoy, *Ecol. Indic.* **6** (2006) 388
8. P. R. Kumar, *Environ. Sci. Technol.* **39** (2009) 697

9. N. P. Nikolaidis, T. Koussouris, T. E. Murria, I. Bertahas, A. Diapoulus, A. G. Konstantinos, *Lake Reservoir Manage*. **12** (1996) 364
10. G. Bidar, C. Pruvot, G. Garçon, A. Verdun, P. Shirali, F. Douay, *Environ. Sci. Pollut. Res. Int*. **16** (2009) 42
11. M. N. Al-Yemni, H. Sher, M. A. El-Sheikh, M. Eid Ebrahem, *Sci. Res. Essays* **6** (2011) 966
12. P.S. Rainbow, *Mar. Pollut. Bull.* **31** (1995) 183
13. E. Chmielewská, M. Ursinyová, *Pet. Coal* **48** (2006) 44
14. A. Assia El Falaky , S. A. Aboulroos, A. A. Saoud, M. A. Ali, *Aquatic Plants for Bio-remediation of Waste Water*, 8th International Water Technology Conference, IWTC8 2004, Alexandria, 2004, p. 361
15. B. H. Lee, M. Scholz, *Ecol. Eng.*, **29** (2007) 87
16. L. A. Meyerson, K. Saltonstall, L. Windham, E. Kiviat, S. Findlay, *Wetlands Ecol. Manag.* **8** (2000) 89
17. L. Marchand, M. Mench, D. L. Jacob, M. L. Otte, *Environ. Pollut.* **158** (2010) 3447
18. S. Filipović, *PhD Thesis*, Faculty of Chemistry, University of Belgrade, Belgrade, Serbia, 1983
19. D. Purić, *Master Thesis*, Faculty of Biology, University of Belgrade, Belgrade, Serbia, 2006
20. M. Talevska, D. Petrovic, T. Talevski, D. Maric, A. Talevska, in *Proceedings of International Conference on "Lakes and nutrient loads" Alblakes09*, Tirana, Albania, 2009, p. 362
21. H. H. Schierup, V. J. Larsen, *Aquat. Bot.* **11** (1981) 197
22. G. Bonanno, R. LoGiudice, *Ecol. Indic.* **10** (2010) 639
23. E. Fediuc, L. Erdei, *J. Plant Physiol.* **159** (2002) 265
24. A. Kabata-Pendias, A. Kabata Pendias, K. A. Pendias Alina, *Trace Elements in Soils and Plants*, 3rd ed., CRC Press, Boca Raton, FL, 2001, p. 413
25. L. Windham, J. S. Weis, P. Weis, *Estuarine Coastal Shelf Sci*. **56** (2003) 63
26. H. Yongxia, W. Yan, L. Huiying, L. Xinxin, H. Z. Xiaojun, *Adv. Mat. Res.* **356** (2011) 994
27. E. J. Fitzgerald, J. M. Caffrey, S. T. Nesaratnam, P. McLoughlin, *Environ. Pollut.* **123** (2003) 67
28. Z. H. Ye, A. J. M. Baker, M. H. Wong, A. J. Willis, *Ann. Bot.* **80** (1997) 363
29. G. Bonanno, *Ecotoxicol. Environ. Saf.* **74** (2011) 1057
30. J. I. N. Kumar, H. Soni, R. N. Kumar, *J. Limnol*. **65** (2006) 9
31. A. Kabata-Pendias, A. B. Mukherjee, *Trace Elements from Soil to Human*, Springer, Heidelberg, 2007
32. A. K. Shankers, C. Cervantes, H. Losa-Tavera, S. Avdainayagam, *Environ. Int.* **31** (2005) 739
33. A. M. Zayed, N. Terry, *Plant Soil Environ.* **249** (2003) 139
34. B. Keller, K. Lajtha, S. Cristofor, *Wetlands* **18** (1998) 42
35. D. Baldantoni, A. Alfani, P. D. Tommasi, G. Bartoli, A. V. De Santo, *Environ. Pollut.* **130** (2004) 149
36. J. Vymazal, J. Švehla, L. Kröpfelová, V. Chrastný, *Sci. Total Environ.* **380** (2007) 154
37. E. Stoltz, M. Greger, *Environ. Exp. Bot.* **47** (2002) 271
38. C. Bragato, H. Brix, M. Malagoli, *Environ. Poll.* **144** (2006) 967
39. F. Duman, M. Cicek, G. Sezen, *Ecotoxicology* **16** (2007) 457

40. S. U. Khan, A. Moheman, *Poll. Res.* **25** (2006) 99
41. D. M. Hammad, *Aust. J. Basic Appl. Sci.* **5** (2011) 11
42. C. D. Jadia, M. H. Fulekar, *Afr. J. Biotechnol.* **8** (2009) 921
43. L. O. Tiffin, *Plant Physiol.* **48** (1971) 273
44. M. O. Thiesen, C. Blincoe, *Biol. Trace Elem. Res.* **16** (1988) 239
45. K. S. Sajwan, W. H. Ornes, T. V. Youngblood, A. K. Alva, *Water Air Soil Poll.* **91** (1996) 209
46. D. Świerk, B. Szpakowska, *Ecol. Chem. Eng.***18** (2011) 3
47. B. Szpakowska, B. Karlik, P. Goliński, Z. Kaczmarek, D. Świerk, *Pol. J. Environ. Stud.* **18** (2009) 436
48. S. Verma, R. S. Dubey, *Plant Sci.* **164** (2003) 645
49. M. M. Lasat, *J. Hazard. Subs. Res.* **2** (2000) 1
50. O. Ravera, *J. Limnol.* **60** (2001) 63
51. S. Clemens, M. G. Plamgren, U. Kramer, *Trends Plant Sci.* **7** (2002) 309.

Journal of the Serbian Chemical Society
JSCS-info@shd.org.rs • www.shd.org.rs/JSCS
J. Serb. Chem. Soc. 78 (8) 1259–1268 (2013)
JSCS–4495
UDC 639.64+581.463+556.56:631.413.3+504.53
Original scientific paper

Halophytes relations to soil ionic composition

DUBRAVKA MILIĆ[1]*, JADRANKA LUKOVIĆ[1], LANA ZORIĆ[1], JOVICA VASIN[2], JORDANA NINKOV[2#], TIJANA ZEREMSKI[2] and STANKO MILIĆ[2]

[1]*Department of Biology and Ecology, Faculty of Sciences, University of Novi Sad, Novi Sad, Serbia and* [2]*Institute of Field and Vegetable Crops, Novi Sad, Serbia*

(Received 2 November, revised 27 December 2012)

Abstract: The concentration of Na^+, K^+, Ca^{2+} and Mg^{2+} in the root and above-ground organs of three halophyte species (*Salicornia europaea*, *Suaeda maritima* and *Salsola soda*) as well as in the soil where they grew from maritime and inland saline areas were investigated. The aim of the research was to evaluate the capability of some halophyte species to absorb different cations and to find if a differentiation of salt accumulation between the populations from inland and maritime saline areas exists. In five analyzed localities (Tivatska solila, Ulcinj salina, Slano Kopovo, Melenci and Okanj), the external Na^+ concentrations exceeded those of the other investigated cations. The investigated halophytes accumulated more Na^+ than Mg^{2+}, Ca^{2+} and K^+ and more cations were recorded in the above-ground organs than in the root. The populations from maritime saline areas generally had higher cation concentrations than plants from inland saline areas.

Keywords: salt accumulation; *Salicornia europaea*; *Suaeda maritima*; *Salsola soda*.

INTRODUCTION

Soil salinization is considered one of the most important factors in land degradation.[1] Today, 20 % of the world's cultivated land and nearly half of all irrigated lands are affected by salinity.[2] NaCl is the major component of most saline soils.[3]

Generally, if a soil has a shallow water table then the salinity of the soil solution will be strongly affected by the salinity of the groundwater. Thus, in the main, the suitability of sites for plants may be based partly on whether the groundwater is too saline or toxic (*e.g.*, with a too low pH).[4]

* Corresponding author. E-mail: dubravka.milic@dbe.uns.ac.rs
# Serbian Chemical Society member.
doi: 10.2298/JSC121102159M

Land reclamation and rehabilitation could be achieved using salt tolerant species.[5] Halophytes generally use similar salt tolerance effectors and regulatory pathways that have been found in glycophytes, but that subtle differences in regulation account for large variations in tolerance or sensitivity.[6] Perennial deep-rooted plants in saline landscapes tend to access water mostly from the regions of the root-zone where the salinity of the soil solution is the lowest. Deep-rooted perennials are able to access water deeper in the soil profile during the dryer summer months, thus avoiding the highly saline soil solution near the surface, whereas more shallow-rooted annuals complete their lifecycle during periods when the salinity of the soil solution near the surface is lower than in the subsoil.[4]

Various halophytes are sensitive to various amounts of different ions. Generally speaking, Na^+ is more effective than K^+ and Cl^- more than SO_4^{2-} in promoting succulence. Many dicotyledonous halophytes are reported to grow optimally in NaCl concentrations ranging from 50 to 250 mM NaCl, while monocotyledonous halophytes grow optimally in the absence of salinity or sometimes in low (<50 mM) concentration of NaCl.[7] The most salt resistant plants are the salt accumulating halophytes, such as *Salicornia*, *Salsola* and *Suaeda*, that have a succulent structure.[8] In succulent halophytes, the vacuolar concentrations of Na^+ and Cl^- generally exceed the external concentrations. This appears to reflect a constitutive ability of halophytes to accumulate high ion concentrations.[9] Another group consists of the salt-localizing halophytes, including *Atriplex* and *Halimione*, in which the salt is localized in special hairs covering the stem and the leaves.[8] Halophytes are of great economic value and can fulfill almost every requirement of human beings, especially those related to food, fodder, fuel and medicines.[10] Moreover, halophytes are potentially ideal plants for phyto-extraction or phytostabilization applications of heavy metal polluted soils and of heavy metal polluted soils affected by salinity.[11,12]

The objective of this study was to determine the capability of halophyte species *Salicornia europaea* L., *Suaeda maritima* (L.) Dumort. *and Salsola soda* L. to absorb different cations and to determine if differentiation according to cation accumulation exists between the populations from maritime and inland saline areas.

EXPERIMENTAL

Soil and plant analyses were performed on samples from five localities: two from Montenegro (Tivatska solila and Ulcinj salina) and three from inland saline areas in the Pannonian plane in Serbia (Slano Kopovo, Melenci and Okanj) (Fig. 1). Ulcinj salina is the greatest saltern in Montenegro and Tivatska solila was previously a saltern, while the three localities in Pannonian plane are situated within the greatest agricultural area of Serbia.

Salicornia europaea, *Suaeda maritima* and *Salsola soda* were harvested in October 2006 and 2007. Simultaneously, soil samples were collected from the five analyzed localities. The plants were determined at the Department of Biology and Ecology, University of Novi Sad.

The content of water soluble salts, the soil pH value in suspension with water and conductivity (*EC*) in the soil were determined in accordance with ISO methods for soil quality.[13] The particle size distribution was determined in the < 2 mm fraction by the internationally recognized pipette method with Na-pyrophosphate preparation of the samples and a combination of sieving and the sedimentation fractionation model.[14]

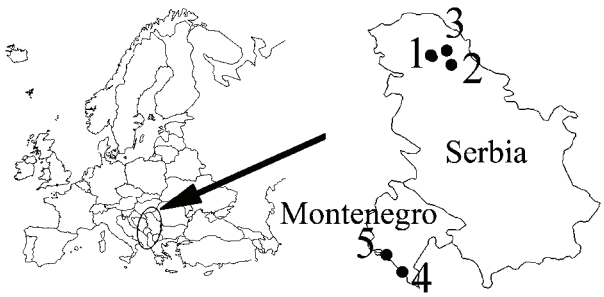

Fig. 1. Localities of the analyzed populations: 1 – Slano Kopovo, 2 – Melenci, 3 – Okanj, 4 – Ulcinj, 5 – Tivat.

The concentration of water soluble salts in soil was determined in soil water extract obtained by filtering soil suspension (soil paste) prepared by mixing 300 g of soil with 130––300 mL of deionized water in dependence on the water capacity of the soil sample. Analysis was subsequently performed by inductively coupled plasma–optical emission spectrometry, ICP-OES, (Varian Vista Pro-axial).

The plant roots were separated from the soil. The roots and the above-ground organs were washed three times with deionized water, oven-dried at 60 °C to constant mass and weighed. The concentrations of the cations in the plant tissues were determined by ICP-OES (Varian, Vista-Pro) after digestion in a mixture of 10 mL of HNO_3 (65 %) and 2 mL of H_2O_2 (30 %) using the microwave technique.

To avoid interferences and signal reductions due to ionization of Na and K, a Cs ionization buffer was used. A solution containing 2 % CsCl was added online to all solutions introduced into the ICP by pumping the solution into a "T" piece just before the nebulizer.

Data were statistically processed by analysis of the variance and means, standard errors and coefficients of variation, calculated using Statistica for Windows, version 10.0.[15] The significance of the differences in the measured parameters between the soil samples were determined using the Duncan test ($p \leq 0.05$), while the significance of differences in the cation concentrations in the plant organs from the inland and maritime saline areas were determined according to the *t*-test ($p \leq 0.05$). The general structure of the variability of the sample was established by principal component analysis (PCA), based on a correlation matrix. The overall differences between the compared groups are presented by Euclidian distances.

RESULTS

The texture characteristics of soil are presented in Table I. In all localities, except Tivat, clay was dominant and ranged from 28.6 to 52.6 %. The proportion

of coarse sand was significantly higher in the Ulcinj locality, fine sand in the inland saline area Melenci and silt in Tivat.

TABLE I. Soil texture, mass %; different superscript letters, a–e indicate that the differences between the localities are significant according to the Duncan test ($p \leq 0.05$); the letter "a" represents the highest value, while the letter "e" the lowest; coefficients of variation are given in brackets

Soil component	Locality				
	Ulcinj saline	Tivatska solila	Okanj	Slano Kopovo	Melenci
Coarse sand	23.9±0.06^{a} (0.42)	3.7±0.01^{b} (0.03)	2.8±0.1^{c} (0.04)	3.7±0.1^{b} (0.03)	1.2±0.1^{d} (0.08)
Fine sand	24.3±0.01^{d} (0.04)	26.8 ±0.01^{b} (0.04)	16.6±0.01^{e} (0.06)	25.4±0.01^{c} (0.04)	37.0 ±0.01^{a} (0.27)
Silt	23.2±0.06^{e} (0.004)	40.4±0.01^{a} (0.02)	28.0±0.01^{b} (0.04)	24.4±0.01^{d} (0.04)	27.0±0.01^{c} (0.04)
Clay	28.6±0.99^{e} (0.06)	29.1±0.01^{d} (0.03)	52.6±0.01^{a} (0.02)	46.7±0.01^{b} (0.02)	34.8±0.01^{c} (0.03)

The soil at the inland saline areas contained small amounts of salts (0.6 mass %), whereas significantly higher amounts were detected in the soils at the maritime areas (0.8–1.5 mass %) (Table II). High *EC* values reflect the existence of an overlying salt crust. The soil at the Ulcinj locality had the highest conductivity (96 mS cm^{-1}). The soils at the localities from the inland saline area had the same *EC* values (6.6 mS cm^{-1}) and between these sites, there were no significant differences. The pH values ranged from 8.1 (Tivat) to 10.6 (Melenci). The Duncan test showed significant differences in the abundance of ions between all the analyzed soils from the five localities. The ion abundances of all the investigated cations were significantly greater in Ulcinj. The quantitative abundance of ions followed the order: sodium > magnesium > calcium > potassium.

Soil separation between analyzed samples was clearly observed based on the overall Euclidian distances, where localities from the inland saline area formed one cluster and were separated from the maritime ones (Fig. 2).

The sodium ion content for all species was higher than the Mg^{2+}, Ca^{2+} and K^{+} content (Fig. 3). A comparison between the three species showed that *Salicornia europaea* and *Suaeda maritima* were richer in Na^{+} and Mg^{2+} than *Salsola soda*. However, *Salsola soda* accumulated more K^{+} and Ca^{2+} than the other two species. The cation content in the above-ground organs of *Salicornia europaea*, *Suaeda maritima* and *Salsola soda* was greater than in the root. The populations from the maritime saline area generally had significantly higher cation concentrations than the plants from the inland saline area.

Principal components analysis (PCA) indicated the presence of three groups of analyzed parameters, which explained 86.2 mass % of the total variation (Table

TABLE II. Soil salinity – Salt composition; different superscript letters, a–e, indicate that the differences between the localities are significant according to the Duncan test ($p \leq 0.05$); the letter "a" represents the highest value, while the letter "e" the lowest

Parameter		Locality				
		Ulcinj saline	Tivatska solila	Okanj	Slano Kopovo	Melenci
Salts concentration, %		0.8±0.06^{b} (0.12)	1.5±0.06^{a} (0.07)	0.6±0.06^{c} (0.02)	0.6±0.06^{c} (0.02)	0.6±0.06^{c} (0.2)
Soil reaction, pH		8.2±0.01^{c} (0.12)	8.1±0.01^{d} (0.12)	9.4±0.01^{b} (0.11)	9.3±0.01^{b} (1.08)	10.6±0.01^{a} (0.09)
Conductivity, mS cm^{-1}		96.0±0.01^{a} (0.10)	46.3±0.01^{b} (0.22)	6.6 ±0.01^{c} (0.15)	6.6 ±0.01^{c} (0.15)	6.6±0.01^{c} (0.15)
Cation concentation, meq L^{-1}	Na^{+}	1031.3±0.1^{a} (0.001)	589.3±0.01^{b} (0.002)	55.5±0.01^{e} (0.02)	123.9±0.01^{d} (0.01)	239.4±0.01^{c} (0.004)
	K^{+}	28.8±0.01^{a} (0.03)	6.5±0.01^{b} (0.15)	0.1±0.01^{e} (8.33)	0.2±0.01^{d} (5.56)	0.6±0.01^{c} (1.53)
	Ca^{2+}	67.1±0.01^{a} (0.01)	42.9±0.01^{b} (0.02)	1.2±0.01^{d} (0.85)	1.9±0.01^{c} (0.53)	1.0±0.01^{e} (0.97)
	Mg^{2+}	201.9±0.01^{a} (0.005)	89.4±0.01^{b} (0.01)	1.2±0.01^{d} (0.84)	3.9±0.01^{c} (0.26)	0.8±0.01^{e} (1.26)

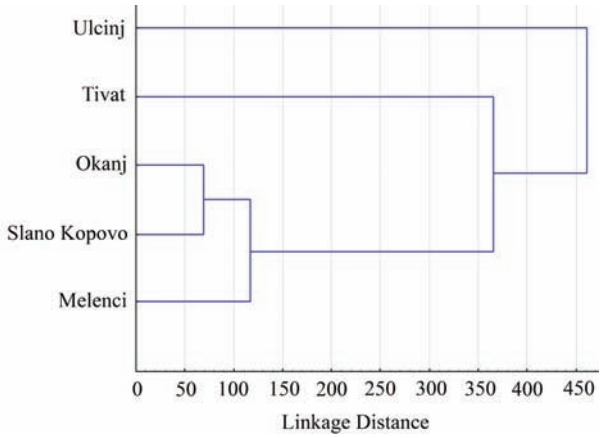

Fig. 2. Euclidian distances between the analyzed soil samples.

III). The most variable were the root and stem concentrations of Ca^{2+}, the Na^{+} concentrations in the stem and Mg^{2+}concentrations in all plant organs. The first principal component explained 46.4 mass % of the variation. The second principal component explained 31.1 mass % of variation due to the variability of the Na^{+} concentrations in the root and K^{+} and Ca^{2+} concentrations in the leaves. The third principal component explained 8.7 mass % of variation. Parameters that did not contribute significantly to the total variation were the accumulations of K^{+} in the root and stem and the Na^{+} concentrations in the leaves. According to the type of variability, the examined populations were grouped by PCA (Fig. 4). The projection of the cases for the first two components showed that populations

from inland and maritime saline areas could be clearly separated according to the type of variation in the accumulation of cations.

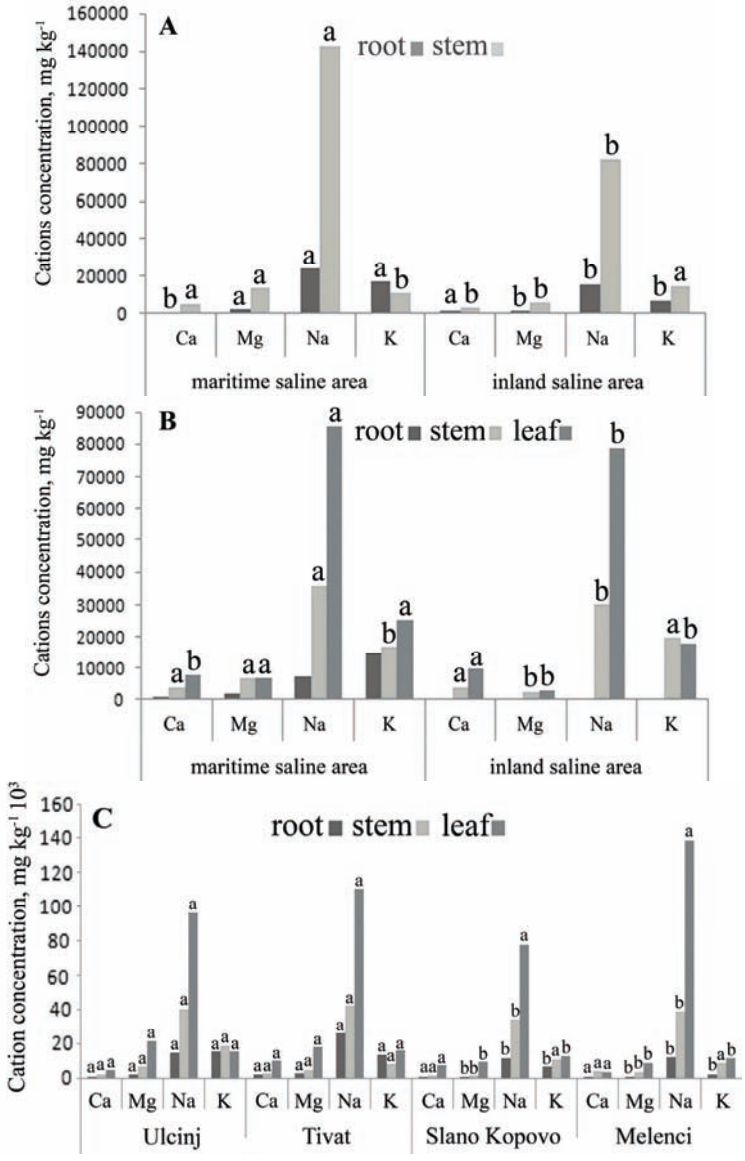

Fig. 3. Mean Na^+, K^+, Ca^{2+} and Mg^{2+} contents in root, stem and leaf of A – *Salicornia europaea*, B – *Salsola soda* and C – *Suaeda maritima* from the inland and maritime saline areas. Letters from "a" to "e" indicate differences in cation concentrations between the plant organs from the inland and maritime saline areas. The same letter means that the differences are not significant according to the *t*-test ($p \leq 0.05$); the letter "a" represents the highest value, while the letter "e" the lowest; MSA – maritime saline area, ISA – inland saline area.

DISCUSSION

Under natural conditions, halophytes accurately reflect the chemical composition of the soil as well as the intensity and type of salinity.[16,17]

TABLE III. Factor analyses of the cation concentrations in the halophytic species from the inland and maritime saline areas; * marked numbers are statistically significant at $p \leq 0.05$

Part	Ion	Factor 1	Factor 2	Factor 3
Root	Na^+	–0.622314	0.733941*	–0.226497
	K^+	–0.685478	0.480832	0.466223
	Ca^{2+}	–0.717438*	0.347608	–0.430767
	Mg^{2+}	–0.825518*	0.483519	0.085686
Stem	Na^+	–0.732384*	0.313893	–0.168400
	K^+	–0.590531	–0.526443	0.540335
	Ca^{2+}	–0.760969*	–0.472099	–0.232195
	Mg^{2+}	–0.898387*	0.173187	0.216213
Leaf	Na^+	–0.523447	–0.681560	–0.282737
	K^+	–0.378400	–0.894610*	0.163398
	Ca^{2+}	–0.327730	–0.814599*	–0.242078
	Mg^{2+}	–0.848353*	–0.221580	0.014006
Cumulative percentages of the vectors		46.41	77.50	86.23

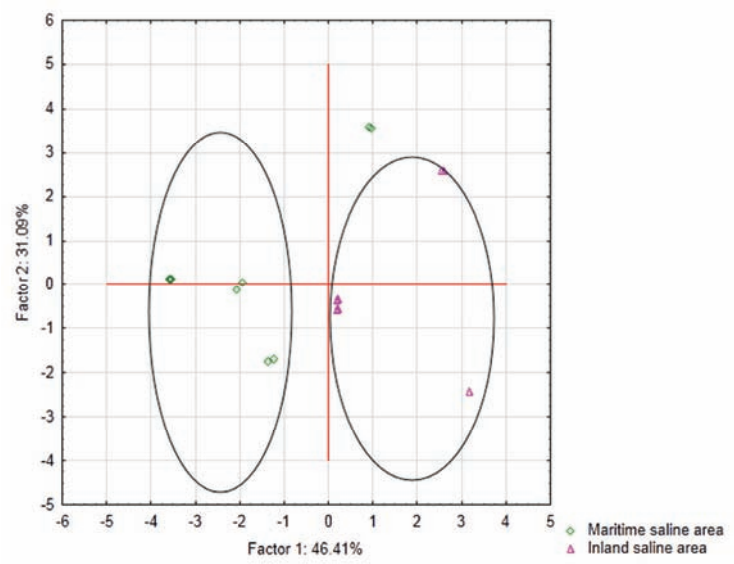

Fig. 4. The projection of the cases of the first two components of the principal component analysis.

In most saline environments,[8] including the five localities analyzed in the present study, the external Na^+ concentrations exceed those of the other investigated cations. Soils are considered to be salinized when a soil saturation extract

has an *EC* value of 4 dS m^{-1} or greater.[18] In the investigated localities, the *EC* values ranged from 6.6–96 dS m^{-1}, which confirmed that the localities were strongly salinized.

Many species of Chenopodiaceae accumulate large amounts of Na^+ and Cl^- when the external salinity is high.[19–21] The investigated halophytes accumulated more Na^+ than Mg^{2+}, Ca^{2+} and K^+. Keiffer and Ungar [22] obtained similar result for *Atriplex prostrara*, *Hordeum jubatum*, *Salicornia europaea* and *Spergulatria marina*. The calcium contents in the plant organs of *Salsola soda* were higher than the magnesium contents, while in *Salicornia europaea* and *Suaeda maritima* the opposite was found. The calcium content decreased as the soil salinity increased, probably because of a competitive effect with sodium.[23] The halophytes investigated in the present research accumulated cations more in aboveground organs than in the root. This feature could be associated with the efficiency of such plants to deliver ions into the vacuoles.[24] Many halophytic species are characterized by their large vacuoles. Vacuoles occupy 77 % of the leaf mesophyll cells of *Suaeda maritima*,[25] and are capable of accumulating salts to concentrations higher than 500 mM.[26]

Principal component analysis showed that the populations from the inland and maritime saline areas had different types of variability in ion accumulation and distribution in their organs, and that they could be clearly separated. These differences were probably also induced by the differences in the soil composition of their sites.

CONCLUSIONS

Soil salinization is considered one of the most important factors in land degradation. The results of this study indicate that halophyte species *Salicornia europaea*, *Suaeda maritima* and *Salsola soda* may accumulate significant amounts of salt from salt-affected soil and therefore remediate land to the point where native plants could invade and become established, or the site could be returned to agricultural productivity. Other important benefits from bioremediation include erosion control, reduced salt in the soil and conservation of wildlife.

Acknowledgement. This work was financially supported by the Ministry of Education, Science and Technological Development of the Republic of Serbia, Grant No. 173002.

И З В О Д

УТИЦАЈ ЈОНСКОГ САСТАВА ЗЕМЉИШТА НА ХАЛОФИТЕ

ДУБРАВКА МИЛИЋ[1], ЈАДРАНКА ЛУКОВИЋ[1], ЛАНА ЗОРИЋ[1], ЈОВИЦА ВАСИН[2], ЈОРДАНА НИНКОВ[2], ТИЈАНА ЗЕРЕМСКИ[2] и СТАНКО МИЛИЋ[2]

[1]*Департман за биологију и екологију, Природно математички факултет, Универзитет у Новом Саду и* [2]*Институт за ратарство и повртарство, Нови Сад*

У овом раду су испитиване концентрације Na^+, K^+, Ca^{2+} и Mg^{2+} у корену и надземним биљним органима код три халофитске врсте (*Salicornia europaea*, *Suaeda maritima* и

Salsola soda), као и састав земљишта на којима ове биљке расту са маритимних и континенталних халобиома. Циљ рада је био да се утврди способност халофитских врста да апсорбују различите катјоне, као и да се испита да ли постоји диференцијација популација са маритимних и континенталних халобиома у односу на способност њихове акумулације соли. У земљишту код пет анализираних локалитета (Тиватска солила, Улцињска солана, Слано Копово, Меленци и Окањ) је констатована већа концентрација Na^+ у односу на друге катјоне. Истраживане халофитске врсте акумулирају више Na^+ него Mg^{2+}, Ca^{2+} и K^+. Такође, већа концентрација катјона забележена је у надземним органима, него у корену. У вегетативним органима популација са маритимних халобиома констатована је већа концентрација катјона у поређењу са биљкама са континенталних халобиома.

(Примљено 2. новембра, ревидирано 27. децембра 2012)

REFERENCES

1. I. Rogel, S. Ortiz, A. Alcaraz, *Geoderma* **99** (2001) 81
2. J. D. Rhoades, J. Loveday, *Salinity in irrigated agriculture*, in *Irrigation of agricultural crops*, B. A. Steward, D. R. Nielsen, Eds., American Society of Agronomists, Madison, WI, 1990, p. 1089
3. P. E. Verslues, M. Agarwal, S. Katiyar-Agarwal, Z. Jianhua, Z. Jian-Kang, *Plant J.* **45** (2006) 523
4. S. J. Bennett, E. G. Barrett-Lennard, T. D. Colmer, *Agric. Ecosyst. Environ.* **129** (2009) 349
5. H. N. Le Houérou, Salt-tolerant plants for the arid regions of the Mediterranean isoclimatic zone, in Towards the rational use of high salinity tolerant plants, Vol. 1, H. Lieth, A. Al Masoom, Eds., Kluwer Academic Publishers, Dordrecht, 1993, p. 403
6. J. K. Zhu, *Plant Physiol*. **124 (**2000) 941
7. T. J. Flowers, T. D. Colmer, *New Phytol*. **179** (2008) 945
8. H. R. Krüger, N. Peinemann, *Vegetation* **122** (1996) 143
9. T. J. Flowers, *Plant Soil* **89** (1985) 41
10. A. Hameed, M. A. Khan, *Karachi Univ. J. Sci*. **39** (2011) 40
11. E. Manousaki, N. Kalogerakis, *Ind. Eng. Chem. Res.* **50** (2011) 656
12. D. Milić, J. Luković, J. Ninkov, T. Zeremski-Škorić, L. Zorić, J. Vasin, S. Milić, *Cent. Eur. J. Biol.* **7** (2012) 307
13. ISO 10390, *Soil quality – Determination of pH*, 1994
14. Handbook of JDPZ research methods, determination of physical soil properties, Novi Sad, 1997, p. 17 (in Serbian)
15. StatSoft, Inc., Statistica (data analysis software system), version 10.0, 2011, www.statsoft.com
16. V. A. Kovda, C. Van den Berg, R. M. Hagan, Eds., *Irrigation, drainage and salinity*, Hutchinson, FAO, Unesco, London, 1973, pp.1–150
17. C. V. Malcolm, in *Biology and utilization of shrubs*, C. M. McKell, Ed., Academic Press, San Diego, CA, 1989, pp. 553–574
18. M. Treshow, *Environment and Plant Response*, McGraw Hill, New York, 1970, p. 345
19. R. Albert, *Oecologia* **21 (**1975) 57
20. I. A. Ungar, *Actualites Botaniques* **125** (1978) 95
21. T. J. Flowers, M. A. Hajibagheri, N. J. W Clipson, *Q. Rev. Biol*. 61 (1986) 313
22. K. H. Keiffer, I. A. Ungar, *Wet Ecol Manag.* **9** (2001) 469

23. W. H. Van der Molen, in *Prognosis of Salinity and Alkalinity*, Report of an Expert Consultation Rome, 1975, FAO, Rome, Italy, 1976, pp. 31–52
24. Z. Dajić, in *Physiology and molecular biology of stress tolerance in plants*, K. V. Madhava Rao, A. S. Raghavendra, K. J. Reddy, Eds., Springer, Dordrecht, 2006, p. 41
25. M. A. Hajibagheri, J. L. Hall, T. J. Flowers, *J. Exp. Bot.* **35** (1984) 1547
26. M. N. H. Dracup, H. Greenway, *Plant Cell Environ.* **8** (1985) 149.